Catalytic Conversion of Biomass-Derived Platform Molecules to Distillate-Range Fuels

By

Nathaniel M. Eagan

A dissertation submitted in partial fulfillment of

the requirements for the degree of

Doctor of Philosophy

(Chemical Engineering)

at the

UNIVERSITY OF WISCONSIN-MADISON

2019

Date of final oral examination: 6/17/2019

This dissertation is approved by the following members of the Final Oral Committee:

George W. Huber, Professor, Chemical and Biological Engineering

James Dumesic, Professor, Chemical and Biological Engineering

Brian Pfleger, Professor, Chemical and Biological Engineering

Ive Hermans, Professor, Chemistry

Abstract

Current trends in resource consumption and environmental degradation inspire research into the benign transformation of renewable feedstocks to transportation fuels with lower net greenhouse gas emissions. Growing demands in heavier middle-distillate fuels such as diesel and jet fuel particularly motivate the use of carbon-containing feedstocks such as biomass in order to produce liquid fuels substantially similar to those already essential to our economy. Such fuels still require carbon chains larger than those of the monomeric sugars comprising cellulose and hemicellulose, however, thus carbon-carbon bond forming technologies have an important place in the overall biomass-to-distillate landscape. These technologies can be utilized to upgrade platform molecules easily obtainable from biomass. The research discussed here focuses on the use of sorbitol and ethanol platforms, providing promising new directions for their utilization.

Sorbitol conversion to distillate fuels first requires a challenging hydrodeoxygenation step focused on producing mono-functional oxygenates. Here this chemistry was promoted by a Co/TiO_2 catalyst at yields (56%) competitive with more costly noble-metal catalysts. FT-ICR-MS provided evidence that oligomeric species produced may also act as intermediates in the process. However, this catalyst suffered from irreversible deactivation via oxygenate-promoted Co leaching and sintering which could not be inhibited by the SMSI-stabilization of the catalyst.

Pathways by which ethanol can be converted into middle-distillate fuels were then extensively evaluated by considering the fundamental chemistries which can be exploited and how they can be most effectively combined. These processes involve integrating dehydration, hydrogen transfer, olefin oligomerization, aldol condensation, and ketonization in a variety of ways which can overcome the limitations of any one particular technology. From these analyses, promising

research directions are recommended. The subsequent focus here is on the use of Guerbet coupling to directly oligomerize ethanol to distillate-range fuels.

Cu-doped AlMgO and AlCaO catalysts were first examined for this purpose, with the importance of operating at elevated pressures to promote selective coupling explained. Selective ethanol oligomerization is still challenging with these catalysts, however, given that alcohol selectivities were limited here to ~55% at 20% conversions, and conversions above 30% were difficult to achieve due to inhibition by products of the reaction (e.g. water). Calcium hydroxyapatite (HAP) was then examined as a more selective catalyst for this transformation, though declining selectivities and reaction rates were observed as conversion increased. However, integration of selective ethanol coupling over HAP with bimolecular dehydration shows promise as a novel method to produce diesel-range ethers from biomass-derived sources. Overall a process was developed which can produce these ethers in addition to jet-range paraffins at theoretical yields above 80%. Lastly kinetic modeling was utilized to better understand the limitations and potential of using Guerbet coupling to oligomerize ethanol to distillate-range alcohols. Inhibition effects by water rationalize the aforementioned declining rates and selectivities observed with increasing conversion. In the absence of these phenomena, however, the production of distillate-range alcohols is limited by the underlying kinetics which resemble step-growth oligomerization with the additional stipulation that branched alcohols cannot couple as nucleophiles. The model discussed here suggests that catalysts which promote the electrophilic action of higher alcohols over that of ethanol are promising for promoting linear alcohol formation that cascades into the distillate-range.

Acknowledgements

I would like to thank everyone who has helped me along my academic journey to get me where I am today. First, I would like to thank my PhD advisor Professor George Huber. George has taught me how to approach scientific problems from a rational perspective, ensuring that I always aim to impact both the scientific community and the world around us with my work. He has allowed me to grow into the researcher I want to be, supporting new research directions I wanted to pursue whether they wound up leading to something interesting or ultimately falling flat. I will always be thankful of his support and would not be the researcher I am without him. Second, I would like to thank Professor James Dumesic, Professor Regina Murphy, and Professor Reid Van Lehn who have all impacted me in different ways in my academic journey. The elegance with which Professor Dumesic introduces challenges and methods to solve them is inspiring. Prof. Murphy and Prof. Van Lehn helped me to find myself as a teacher and have provided a strong example for me to follow when I hopefully one day lead classrooms of my own. Third, I would like to thank the other members of my committee (Professor Brian Pfleger and Professor Ive Hermans) both for their service in this regard and for more generally serving as sources of academic inspiration. Fourth, I would like to thank the academic staff in the Chemical Engineering department who have helped me over these years. I appreciate all of their efforts (which I have too often taken for granted) in directly helping me and for supporting the department in general. Fifth, I would like to thank my collaborators at ExxonMobil who have been with me throughout my entire PhD, namely J. Scott Buchanan, Ashley Wittrig, and Michael Lanci. The last four years of our monthly meetings have helped me to be clearer and more concise in my communication (though it might not seem so given the length of this dissertation), and their technical insights have been critical to my work. Sixth, I would like to thank the various Huber group members and other

catalysis researchers who have helped me over the years. Pranav Karanjkar, Mrunmayi Kumbhalkar (from the Dumesic group), Insoo Ro, Zhuoran Xu, Joe Chada, Kevin Barnett, and Dan McClelland were all mentors to me in one way or another, and every single one of them was willing to help whenever I needed it. Siddarth Krishna, Juan Venegas, Maddie Ball, Sean Tacey, and Hugh Purdy have all helped me to think over my ideas and to keep me level during my time here while constantly inspiring by the examples they set in their own rights. I look forward to seeing what they achieve in the years to come. In the cohorts immediately below me, I would like to specifically thank Peter Galebach, Ted Walker, Anthony Anderson, Mark Lindsay, Keishla Rivera-Donnes, and Elise Gilcher. Looking forward, I also want to thank Alvin Jonathan and Paolo Cuello Penaloza for working directly with me and moving forward with the thoughts and ideas I did not have the time to follow through with in my time in Wisconsin. Seventh, I would like to thank my family for the support they have given me and the inspiring examples they have always set. My mother (Denise) and father (Tom) instilled in me the importance of finding what you love and giving it everything you have while still taking the time to appreciate the world and the people around you. I only hope that when I have children of my own I will be even half as good of a parent as they were to me. My brother (Sean) has also always been there to set an example for me, challenge me, and support me. While it frustrated me when I was younger that he would never let me win, today I could not be more appreciative that he will never let me win again, as he has proven by earning his law degree just weeks before I defend this dissertation. Finally, I would like to thank Kayla Pelland, my fiancé who has been with me for the last ten years and not only supported me in my academic endeavors but also helped shape who I am. I am a better researcher, a better teacher, and a better person because of her and cannot wait to spend the rest of my life with her.

Table of Contents

List of Figures

List of Tables

Chapter 1. Introduction

1.1 Distillate fuel market expansion: motivations for biomass valorization technologies

Our societal dependence on the exploitation of fossil fuels has long raised concerns regarding resource sustainability, economic security, and environmental health. Recent years have seen increased attention drawn to climate change issues, with the United Nations recently reporting that the global temperature is on track to rise a critical 1.5°C above pre-industrial levels in as few as 12 years.[1] Simultaneously, increasing global prosperity and demands for goods and services lead to increasing energy needs to power our society.[2] This in turn leads to growing transportation fuel demands. While the growing fuel efficiency of light-duty vehicles is projected to over-compensate for this and lead to decreasing gasoline demands, the need for heavier C_8-C_{22} middle-distillate fuels such as jet and diesel will continue to grow. Looking forward, it is therefore imperative that new technologies are developed which enable the environmentally benign conversion of alternative feedstocks to heavy-duty fuels which can be employed with lower net greenhouse gas emissions. Global pressures to decrease sulfur emissions from marine diesel combustion additional provide economic incentives for such technological developments.[3] The aviation industry has also explicitly committed to increasing alternative fuel usage in order to lower its net carbon emissions.[4-9] In order to operate within the current fuel infrastructure, such alternative fuels should ideally resemble petroleum-derived fuels, consisting primarily of long-chain hydrocarbons.

Lignocellulosic biomass is an abundant, low-cost carbonaceous feedstock well-suited for this purpose.[10] The carbon dioxide released during the combustion of these fuels can be partially captured in the growth of the biomass feedstock, potentially leading to reduced net greenhouse gas emissions compared to fossil fuel utilization. The United States Energy Policy Act of 2005

introduced Renewable Fuel Standards to regulate and promote the use of biofuels, imposing minimum volume standards for biofuel consumption in the US.[11] In 2007, the Energy Independence and Security Act expanded the Renewable Fuel Standards to further increase volume requirements to a goal of producing 36 billion gallons of renewable fuel per year by 2022.[12] Annual targets have been updated more frequently in recent years. In 2018, the 2019 requirement was set to be 19 billion gallons — below the 28 billion gallons originally targeted a decade ago.[513] Ethanol (EtOH) used in gasoline blending makes up approximately 85% of the biofuels utilized in the US, while the remaining 15% is predominantly biodiesel derived from oils and waste fats.[14] The potential for expanding biofuels into the distillate fuel market is therefore clear.

1.2 Biomass to distillate fuel conversion through platform molecules

Lignocellulosic biomass predominantly consists of three components: cellulose, hemicellulose, and lignin. The former two, which together make up the majority of the weight, are fundamentally built from ether-linked C_5 and C_6 sugar units and are therefore roughly 50 wt% oxygen. Conventionally, high oxygen contents are undesirable for fuels since they reduce energy density and increase water solubility.[15] While oxygenates have been used in gasoline (e.g. EtOH, methyl *tert*-butyl ether) and diesel (e.g. the fatty acid methyl esters which constitute biodiesel), none have yet been approved for use in aviation fuels. Full deoxygenation of cellulose/hemiceullulose would theoretically lead to C_5-C_6 hydrocarbons, which are too light for middle-distillate fuels. C-C bond formation is therefore required to produce distillate-range molecules. As a result, biomass-to-distillate processes must rely upon three general steps: deconstruction, deoxygenation, and coupling. These typically have very different technological, thermodynamic, and catalytic requirements and therefore cannot be generally performed in a single reactor.

The notion of first selectively converting biomass to a single "platform chemical" has therefore received considerable attention. This concept, which is not exclusively intended for fuel applications, allows for upstream adaptability by enabling the input of a diverse set of feedstocks and taking advantage of natural catalytic tendencies to converge on the formation of a specific compound or class of compounds. This also allows for downstream adaptability, since an ideal platform molecule can be readily converted into a variety of different fuels or chemicals. Promising platform chemical classes include mono-alcohols (e.g. EtOH), polyols (e.g. sorbitol), multi-functional acids (e.g. levulinic acid, 2,5-furan dicarboxylic acid), lactones (e.g. γ-valerolactone), and furans (e.g. 5-hydroxymethylfurfural).[10,16-19] In the context of distillate fuel synthesis, a general requirement for these molecules is that they can be linked together to form larger molecules. Such C-C bond formation chemistries include aldol condensation, olefin oligomerization, and ketonization.[20,21] These chemistries will be discussed in further detail in Chapter 3 in the context of EtOH-to-distillate conversion.

Several biomass-to-distillate process have been proposed previously. C_6 sugars can be dehydrated to 5-hydroxymethylfurfural, coupled via aldol crossed-condensation with acetone, and finally hydrodeoxygenated to produce C_7-C_{15} alkanes.[22] Another process involves the hydroxyalkylation-alkylation of mixtures of furfural and 2-methylfuran followed by hydrodeoxygenation to yield C_{15+} hydrocarbons.[17,18] Furfural can be produced via the hydrolysis/dehydration of the hemicellulose fraction of biomass, and 2-methylfuran can be obtained via the subsequent hydrogenation of furfural. Biomass can also be hydrolyzed to levulinic acid, hydrogenated to γ-valerolactone and valeric acid, and finally coupled through esterification reactions to produce "valeric biofuels," of which pentyl valerate has notably favorable properties for use as a diesel fuel.[19] Liquid alkenes can be produced via decarboxylation of γ-valerolactone

to butene followed by acid-catalyzed oligomerization.[23] The general challenge with these processes is obtaining high selectivities for specific molecules at various stages.

1.3 Overview of the dissertation

This dissertation discusses two general platforms for distillate fuel synthesis: sorbitol-derived mono-functional oxygenates and EtOH. In Chapter 2, the conversion of sorbitol to monofunctional intermediates which can be sequentially upgraded to distillate fuels is discussed.[24] Here a low-cost Co/TiO_2 catalyst is shown to produce these monofunctional intermediates at selectivities up to 56%, competitive with those achieved using more costly Pt- and Pd-based catalysts. Irreversible deactivation is observed, however, which can be attributed to sintering and leaching promoted by chelating oxygenates produced during the reaction. Chapter 3 then describes the use of EtOH as a platform molecule,[21] which in turn motivates the following chapters. First the properties of distillate-range fuels are discussed to more clearly present targets for EtOH-to-distillate technologies. Possible chemistries and processes are then critically assessed to clarify the key challenges and new opportunities for EtOH-to-distillate conversion. Novel perspectives introduced here help guide future research in the area. The remainder of the dissertation is focused on understanding how Guerbet coupling can be utilized to oligomerize EtOH to produce diesel and jet fuels. Chapter 4 discusses the potential use of Cu-doped AlMgO and AlCaO catalysts for EtOH coupling at elevated pressures.[25] All prior studies employing Cu to promote H-transfer reactions have operated at these elevated pressures without rationale, thus a connection between these elevated pressures and the benefits on alcohol selectivity is drawn here. Selective EtOH oligomerization is challenging with these catalysts given that alcohol selectivities are limited to ~55% at 20% conversions and conversions above 30% are difficult to achieve due to inhibition by products of the reaction (e.g. water). Chapter 5 explores the potential of using calcium

hydroxyapatite (HAP) for using EtOH oligomerization to produce distillate fuels.[26] Here an analysis of product distributions at various contact times and temperatures demonstrates a decline in selectivity at elevated conversions which leads to a general drop below an ideal 80% alcohol selectivity at around 40% conversion. This motivated the second portion of this chapter, which proposes the use of etherification to convert the C_{4+} alcohols produced selectively from EtOH at moderate conversions to C_{8+} ethers. These are expected to have improved diesel combustion engines relative to conventional diesel (due to the high cetane numbers of ethers) along with suitable volatilities and energy densities which light ethers (e.g. diethyl ether) do not. A process is proposed which allows for EtOH to be converted to diesel-range ethers as well as jet-range olefins at yields above 70%. Chapter 6 then details the use of kinetic modeling to clarify the limitations experienced and anticipated in using HAP to oligomerize EtOH to distillate-range alcohols. These findings clarify how the competitive adsorption of water alters rates and selectivities with increasing EtOH conversion. This model additionally shows that alcohol chain length and branching are generally consistent with modified step-growth kinetics wherein branched alcohols cannot serve in a nucleophilic role. These kinetics make obtaining distillate-range alcohols challenging, since coupling is essentially terminated when a branched alcohol is formed. Finally, these results are discussed together to provide unique perspectives on the use of monofunctional oxygenate and EtOH platforms for biomass-to-distillate conversion.

1.4 References

1 Global Warming of 1.5°C. *IPCC Geneva, Switzerland* (2018).
2 2017 Outlook for energy: A view to 2040. (ExxonMobil, Irving, 2017).
3 Rapier, R. *Why Diesel Prices Are Set to Soar*, <https://www.forbes.com/sites/rrapier/2018/08/26/why-diesel-prices-are-set-to-soar/#5b7bf1ad1f0c> (2018).
4 Radich, T. The flight paths for biojet fuel. *U.S. Energy Information Administration* (2015).
5 World energy resources: Bioenergy 2016. *World Energy Council* (2016).
6 Mawhood, R., Gazis, E., de Jong, S., Hoefnagels, R. & Slade, R. Production pathways for renewable jet fuel: a review of commercialization status and future prospects. *Biofuel. Bioprod. Bior.* **10**, 462-484, (2016).

7 Wang, W.-C., Tao, L., Markham, J., Zhang, Y., Tan, E., Batan, L., Warner, E. & Biddy, M. Review of biojet fuel conversion technologies. *National Renewable Energy Laboratory* (2016).

8 Fellet, M. Now boarding: commercial planes take flight with biobased jet fuel. *Journal* **94**, 16-18, (2016). >https://cen.acs.org/articles/94/i37/boarding-Commercial-planes-take-flight.html>.

9 Schäfer, A. in *Biofuels for Aviation* (ed Christopher J. Chuck) 3-16 (Academic Press, 2016).

10 Huber, G. W., Iborra, S. & Corma, A. Synthesis of transportation fuels from biomass: chemistry, catalysts, and engineering. *Chem. Rev.* **106**, 4044-4098, (2006).

11 U. S. Department of Energy. Energy policy act of 2005 (2005).

12 U. S. Department of Energy. Energy independence and security act of 2007 (2007).

13 U. S. Environmental Protection Agency. Renewable fuel standard program: standards for 2016 and biomass-based diesel volume for 2018 (2016).

14 Annual energy outlook 2019. (U.S. Energy Information Administration, 2019).

15 Jenkins, R. W., Moore, C. M., Semelsberger, T. A., Chuck, C. J., Gordon, J. C. & Sutton, A. D. The effect of functional groups in bio-derived fuel candidates. *ChemSusChem* **9**, 922-931, (2016).

16 Climent, M. J., Corma, A. & Iborra, S. Conversion of biomass platform molecules into fuel additives and liquid hydrocarbon fuels. *Green Chem.* **16**, 516-547, (2014).

17 Corma, A., de la Torre, O., Renz, M. & Villandier, N. Production of high-quality diesel from biomass waste products. *Angew. Chem.* **123**, 2423-2426, (2011).

18 Li, G. Y., Li, N., Wang, Z. Q., Li, C. Z., Wang, A. Q., Wang, X. D., Cong, Y. & Zhang, T. Synthesis of high-quality diesel with furfural and 2-methylfuran from hemicellulose. *ChemSusChem* **5**, 1958-1966, (2012).

19 Lange, J. P., Price, R., Ayoub, P. M., Louis, J., Petrus, L., Clarke, L. & Gosselink, H. Valeric biofuels: a platform of cellulosic transportation fuels. *Angew. Chem. Int. Ed.* **49**, 4479-4483, (2010).

20 Wu, L., Moteki, T., Gokhale, Amit A., Flaherty, David W. & Toste, F. D. Production of Fuels and Chemicals from Biomass: Condensation Reactions and Beyond. *Chem* **1**, 32-58, (2016).

21 Eagan, N. M., Kumbhalkar, M. D., Buchanan, J. S., Dumesic, J. A. & Huber, G. W. Chemistries and processes for the conversion of ethanol into middle-distillate fuels. *Nature Reviews Chemistry* **3**, 223-249, (2019).

22 Huber, G. W., Chheda, J. N., Barrett, C. J. & Dumesic, J. A. Production of liquid alkanes by aqueous-phase processing of biomass-derived carbohydrates. *Science* **308**, 1446-1450, (2005).

23 Bond, J. Q., Alonso, D. M., Wang, D., West, R. M. & Dumesic, J. A. Integrated catalytic conversion of γ-valerolactone to liquid alkenes for transportation fuels. *Science* **327**, 1110-1114, (2010).

24 Eagan, N. M., Chada, J. P., Wittrig, A. M., Buchanan, J. S., Dumesic, J. A. & Huber, G. W. Hydrodeoxygenation of Sorbitol to Monofunctional Fuel Precursors over Co/TiO2. *Joule* **1**, 178-199, (2017).

25 Petrolini[†], D. D., Eagan[†], N., Ball, M. R., Burt, S. P., Hermans, I., Huber, G. W., Dumesic, J. A. & Martins, L. Ethanol condensation at elevated pressure over copper on AlMgO and AlCaO porous mixed-oxide supports. *Catal. Sci. Technol.* **9**, 2032-2042, (2019).

26 Eagan, N. M., Moore, B. M., McClelland, D. J., Wittrig, A. M., Canales, E., Lanci, M. P. & Huber, G. W. Catalytic synthesis of distillate-range ethers and olefins from ethanol through Guerbet coupling and etherification. *Green Chem.* **21**, 3300-3318, (2019).

Chapter 2. Hydrodeoxygenation of Sorbitol to Monofunctional Fuel Precursors over Co/TiO_2

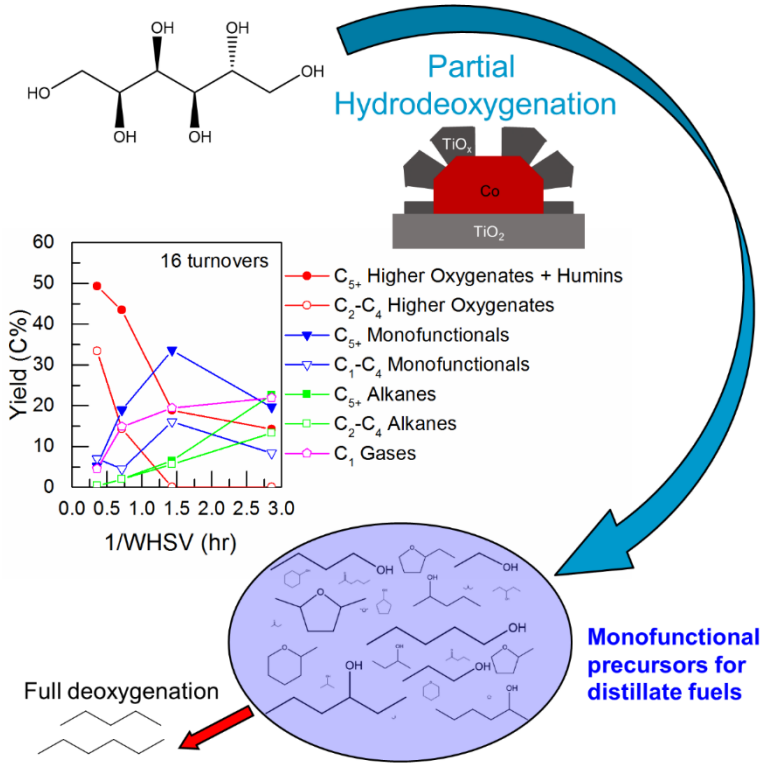

Figure 2.1 | **Hydrodeoxygenation of sorbitol to monofunctional fuel precursors over Co/TiO_2.**[1] Low-cost Co/TiO_2 enables the highest monofunctional yield from sorbitol reported in literature (56.2%) afforded by operating at a moderate weight-hourly space velocity (1.4 h^{-1}) where deoxygenation is appropriately balanced. Chapter adapted from Ref 1.

2.2 Introduction

One of the key challenges associated with using a platform molecule in distillate fuel synthesis is its initial production from biomass. Production of sugars and sugar alcohols from starches is a well-established commercial process, however,[2] thus glucose and sorbitol may be viable substrates for upgrading to fuels. In order to remove oxygen to achieve a low O:C ratio more suitable for fuels (nearly 0), aqueous feeds containing these compounds can be simultaneously dehydrated and hydrogenated in a process known as aqueous-phase hydrodeoxygenation, or APHDO. This typically involves the conversion of aqueous feeds with as

much as 60 wt% sugars or sugar alcohols over bifunctional catalyst beds along with hydrogen at high pressures (~6 MPa) and moderate temperatures (~500 K).[3-5] The majority of these studies have focused on the production of alkanes for use as gasoline blendstocks. Pt-based catalysts utilizing various common acidic supports (e.g. SiO_2-Al_2O_3, H-ZSM-5, WO_x-ZrO_2, Nb_2O_5, Zr-P) have been compared for the production of pentane and hexane, with Zr-P shown to be highly active, selective, and stable under the conditions tested.[6] ZrO_2-supported metals physically mixed with various WO_x-based solid acids have been exploited to tune sorbitol APHDO toward the production of C_5-C_6 alkanes.[7,8] Ultimately, however, these alkanes are not sufficiently heavy for distillate-range fuels.

Alternatively, APHDO can also be tuned to produce species which possess a single oxygen functionality, termed "monofunctional intermediates" or "monofunctionals" (MFs).[9,10] These MFs will spontaneously separate from the aqueous phase if large enough (>C_4). Subsequently, these species can be coupled via a variety of technologies (e.g. dehydration/oligomerization, aldol condensation/dehydration) to produce C_{8+} alkenes which subsequently can be hydrogenated to alkanes for use in jet or diesel blends. The conditions utilized in APHDO are chosen to promote C–O cleavage reactions and simultaneously limit degradation of the substrate and unfavorable C–C cleavage reactions. APHDO catalysts possess both acidic and metallic functionalities which together catalyze a variety of reaction types including hydrogenation, dehydrogenation, retro-aldol condensation, dehydration, decarbonylation, and ring-rearrangement. A generalized pathway for the APHDO of sorbitol is shown in Figure 2.2. Initially, sorbitol either dehydrates to anhydrosorbitol species (mainly 1,4-sorbitan, shown in the C_{5+} higher oxygenates) via acid catalysis or dehydrogenates over metal sites and subsequently undergoes retro-aldol condensation to form two smaller polyoxygenates (primarily either two C_3 or one C_2 and one C_4). The former

dehydration route is preferred for producing liquid fuels, for which preserving energy density is essential. Higher oxygenates then undergo further hydrodeoxygenation reactions to produce monofunctionals and subsequently alkanes, though decarbonylation of aldehydes produces CO which can subsequently react further to form CO_2 (water-gas shift) or CH_4 (methanation). In this study, the coupling of higher oxygenates is also investigated and suggested as a route for generation of MFs. Regardless of the route, production of these MFs requires a balance of acidic and metallic catalyst functionalities such that the dehydration route dominates over retro-aldol condensation in order to preserve energy content while the deoxygenation of MFs (primarily via acid-catalyzed dehydration or metal-catalyzed decarbonylation) does not outcompete their formation. It is important to note that for many catalytic systems used in sorbitol APHDO the sequential deoxygenation reactions proceed slowly such that MFs are not produced at appreciable levels until far past the full conversion of sorbitol. APHDO studies therefore often run at very high sorbitol conversions—often above 100%.

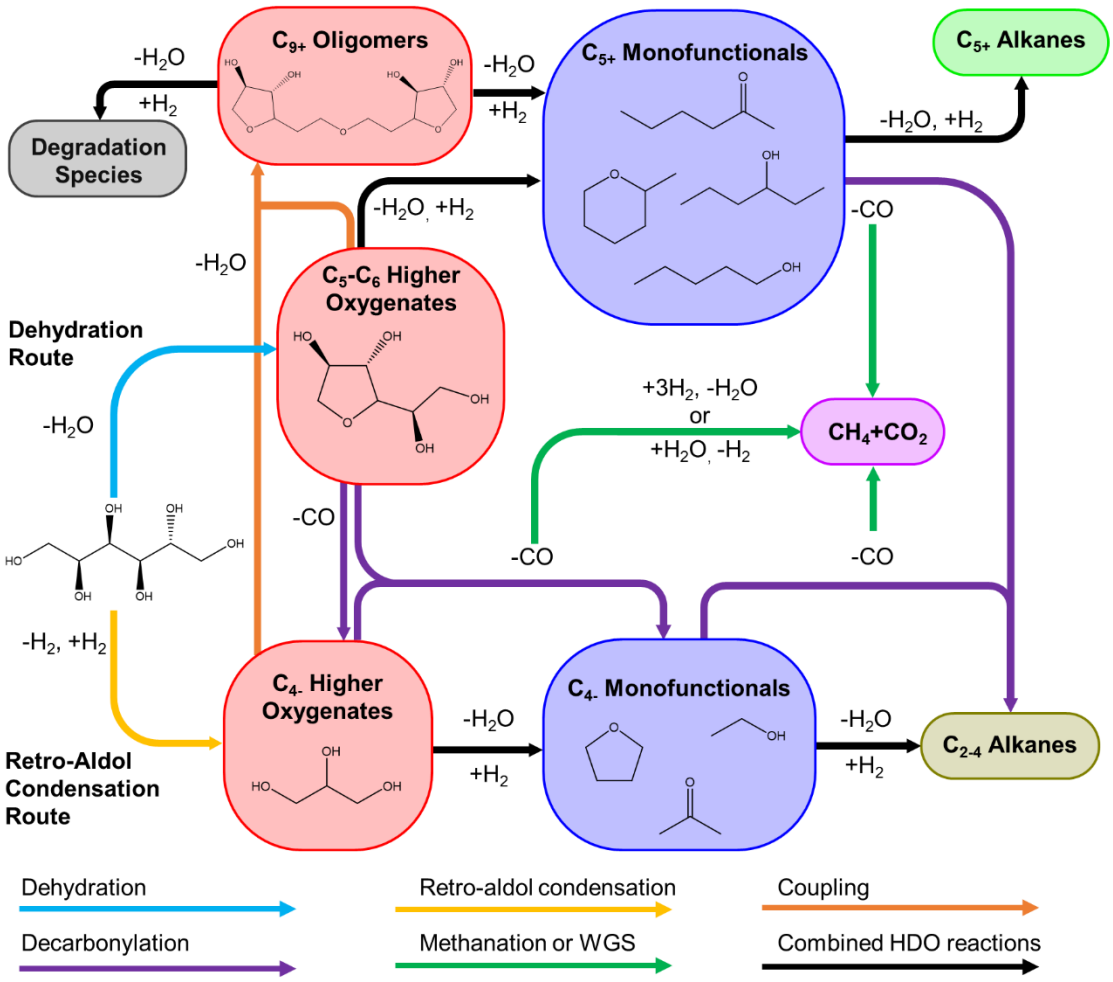

Figure 2.2 | **Generalized pathway for the production of monofunctional species from sorbitol APHDO.** Sorbitol is initially converted to higher oxygenates either through acid-catalyzed dehydrations or metal-promoted retro-aldol condensation. Subsequently these species are deoxygenated via a combination of several reactions including hydrogenation, dehydrogenation, dehydration, ring-rearrangement reactions, and decarbonylation which require both metal and acid functionalities. CO is converted to CO2 via water-gas shift (WGS) or reduced to CH4. The present study additionally provides evidence for the coupling of higher oxygenates to oligomers which may then either degrade to humins and coke or fragment into monofunctionals. Controlled deoxygenation of higher oxygenates produces monofunctional species prior to full deoxygenation to alkanes.

Currently APHDO technology is both limited by the moderately low yields of MFs from sorbitol demonstrated in the literature (below 50% on a carbon basis) and the costly noble metal catalysts used (Pt cost >$34,000 per kg in 2015).[3,5,11,12] The use of low-cost base metals such as Co ($30 per kg in 2015) for APHDO has been limited due to sintering and leaching of the metal.[13-

[17] Recently, the Huber group presented a simple, low-cost method for the stabilization of cobalt catalysts for aqueous-phase hydrogenation reactions via exploitation of the strong metal-support interaction (SMSI).[18] After high-temperature oxidation followed by high-temperature reduction (both at 873 K), the extent of Co leaching from a Co/TiO_2 catalyst was reduced from 44.6% to 0% over 42 hr for the hydrogenation of furfuryl alcohol ($C_5H_6O_2$) in a fixed-bed reactor at 413 K. These pretreatments were shown to promote the migration of partially-reduced TiO_x ($0<x<2$) species over Co nanoparticles such that leaching was inhibited while a sufficient fraction of surface sites remained available to maintain exceptional reaction rates. Additionally, the ring-opening of furfuryl alcohol was attributed to the formation of new Co-TiO_x sites, which may enhance reactivity in sorbitol APHDO as well due to the high frequency of ring-forming and ring-opening reactions which occur throughout the pathway. The purpose of this study is therefore to investigate the potential use of SMSI-stabilized Co/TiO_2 catalysts for the APHDO of sorbitol to produce monofunctional intermediates.

2.3 Experimental methods

2.3.1 Catalyst preparation

Commercial P25 TiO_2 (surface area 51 $m^2\ g^{-1}$, Aldrich) was first calcined in static air to 1023 K (4 K min^{-1}) for 4 hr, denoted in this study as "T." Cobalt(II) nitrate hexahydrate was dissolved in HPLC-grade water and added to the TiO_2 via the incipient wetness impregnation technique to a nominal cobalt loading of 5 wt%. The catalyst was then dried at 383 K in air overnight prior to calcination in static air at 573 K (1 K min^{-1}) for 2 hr. The resulting catalyst is referred to throughout the study as fresh Co/TiO_2, denoted as "F."

2.3.2 Catalyst characterization

Fresh and spent Co/TiO_2 catalysts were characterized after no treatment, after calcination in flowing air (100 mL min^{-1}) to 873 K (5 K min^{-1}, 2 hr), after calcination and subsequent reduction in flowing hydrogen (100 mL min^{-1}) to 873 K (1 K min^{-1}, 2 hr), or after calcination/reduction followed by passivation in 1% oxygen in helium at room temperature. The nomenclature used throughout the study is specified in Table 2.

Brunauer-Emmett-Teller (BET) surface areas were calculated from nitrogen adsorption isotherms collected using a Micromeritics ASAP 2020 automated gas sorption instrument. Isotherms were obtained at 77 K in the range of 0.05-0.30 relative pressure. The cobalt content was measured using inductively-coupled plasma atomic emission spectroscopy (ICP-AES, Perkin-Elmer Plasma 400) on catalysts after dissolution in a mixture of HNO_3, HCl, and HF at 383 K followed by evaporation and dilution. Co and Ti were quantified using external calibration curves at wavelengths of 238.892 nm and 336.121 nm, respectively. Catalyst Co content was determined from the calculated Co:Ti ratio assuming Ti exists primarily as TiO_2. X-ray diffraction (XRD) analyses were conducted using a Bruker D8-Discover diffractometer with a Cu Kα source (λ=1.54184 Å). Scans were collected via an area detector with 300 s acquisition time to obtain data from 15 to 65° 2θ. A linear baseline was developed from points between 33 and 43° 2θ about the Co_3O_4 (311) reflection at 36.85° and subtracted from the unprocessed data. Estimation of Co_3O_4 crystallite size was performed via line-broadening analysis. Peak fits were performed by fitting the data to Gaussian peak shapes from 36.6 to 37.4° since fitting software could not consistently locate this peak due to the much higher intensity of the rutile (101) reflection centered at 36.1°. These fits can be seen in Figure 2.11. The Scherrer equation was utilized assuming a shape factor of 0.94 using the full-width of the peak at half of its maximum height as the measure of peak breadth. Scanning transmission electron microscopy (STEM) images were obtained on a FEI Titan

microscope operated at 200 keV with a Cs probe aberration corrector (CEOS, GmbH). High-angle annular dark field (HAADF) images were obtained in the range of 54 to 270 mrad using a 0.8 nm probe and 24.5 mrad probe convergence semi-angle. Catalyst samples were suspended in ethanol with sonication then deposited on a 200 mesh carbon-coated copper grid (EMS). Samples were plasma cleaned for 15 min prior to analysis.

2.3.3 Sorbitol APHDO

Reactions were conducted in stainless-steel tubular flow reactors (61 cm long, 0.46 cm inner diameter) heated with a tube furnace (Lindberg Blue M Mini-Mite) with a 30 cm heated region. The reactor was packed with 3.30 g fresh catalyst (sample F) with quartz beads and quartz wool on either side of the bed. The bed temperature was kept nearly uniform (maximum deviation of 5 K) via an aluminum block wrapped around the reactor to fill the space between the heater coils and reactor. The temperature was measured at the center of this region by the furnace thermocouple and through 3 external thermocouples at the beginning, middle, and end of the reactor. The beginning of the bed was placed at the start of the aluminum block to avoid homogeneous reactions of sorbitol prior to contact with the catalyst. Prior to reaction the catalyst was first calcined in flowing air (100 mL/min) to 873 K (5 K min^{-1}, 2 hr) and subsequently reduced in flowing hydrogen (100 mL/min) to 873 K (1 K min^{-1}, 2 hr). During the reaction, hydrogen was fed upward at 40 mL/min using mass flow controllers (SLA 5850, Brooks Instrument) concurrently with an aqueous solution of 20 wt% sorbitol fed via a high-pressure syringe pump (Teledyne Isco 500D). For this study, the liquid weight-hourly space velocity (WHSV) is defined as the flow rate of the feed (20 wt% sorbitol) divided by the mass of catalyst (3.30 g). The number of turnovers the catalyst has experienced at a given time point is defined as the WHSV multiplied by the time-on-stream (TOS). A back-pressure regulator maintained the reaction pressure at 6.31

MPa. All reactions were run at 541 K as verified via an external thermocouple placed in contact with the reactor at the center of the heated region. Above the reactor, a 300 mL separator was used to hold liquid for collection every 2-12 hours (depending on flow rate) while gas was sent through the back-pressure regulator to an online gas chromatograph (GC, Shimadzu GC-2014) equipped with both a flame-ionization detector (FID) and a thermal conductivity detector (TCD). Gas samples were collected simultaneously with liquid drains. Liquid drains were extracted into cyclohexane to ensure that water-insoluble species could be quantified. Organic-phase and aqueous-phase samples were analyzed using GC-FID (Shimadzu GC-2010) and GC equipped with a mass spectrometer (MS, Shimadzu GCMS-QP2010S) both with Rtx-VMS capillary columns (Restek Catalog No. 19915). Aqueous-phase samples were additionally analyzed via a total organic carbon analyzer (TOC, Shimadzu TOC-V) and high-performance liquid chromatography (HPLC, Waters Alliance e2695) equipped with a Phenomenex RPM column. After the last sample was collected, the catalyst was dried in flowing helium at atmospheric pressure with the temperature kept at 541 K for 10+ hours. The catalyst was then passivated at room temperature in flowing air diluted in helium to obtain a 1% oxygen stream.

Select aqueous samples were additionally analyzed via a Fourier-transform ion cyclotron resonance mass spectrometer (FT-ICR MS). All FT-ICR MS data were acquired with a Bruker solariX with a 15 T actively shielded superconducting magnet. Instrument control, data acquisition, and preliminary processing were performed on Bruker Daltonics ftmsControl 2.1.0 and Bruker Compass DataAnalysis 4.5 softwares. Atmospheric pressure chemical ionization (APCI) was used to investigate each sample. Samples were diluted in LC MS grade methanol prior to analysis. Flow rates for direct infusion into the FT-ICR MS were controlled by the instrument syringe pump at 120-300 μL/hr. The conditions were set to an APCI temperature of 400-450°C,

corona needle current of 800-1150 nA, dry gas flow of 3500-4000 cm^3/min, and dry gas temperature of 200-220°C. Nitrogen was used as the drying gas. The data was processed by using the sine-squared apodization method in magnitude mode. At least 100 scans were averaged for each mass spectrum. After acquisition, elemental formulas for each peak were assigned by commercially available PetroOrg software.

Conversion, yields, and selectivities are defined on a carbon basis, calculated according to Equations 1-3 respectively. In these equations C represents carbon concentration (moles/volume), V represents the volume of a specific phase collected, $\dot{V}$ represents volumetric flow rate, Δt represents the time lapse between this and the previous sample, the subscript $product$ refers to a specific compound (e.g. 1-hexanol), and the subscript $category$ refers to a specific category (e.g. gas products, products of a specific functionality, converted sorbitol).

Equation 2.1 $$Conversion\ (\%) = \frac{C_{sorbitol,feed} \cdot \dot{V}_{feed} - C_{sorbitol,aqueous} \cdot V_{aqueous}/\Delta t}{C_{sorbitol,feed} \cdot \dot{V}_{feed}}$$

Equation 2.2 $$Yield\ (\%) = \frac{C_{product,organic} \cdot V_{organic}/\Delta t + C_{product,aqueous} \cdot V_{aqueous}/\Delta t + C_{product,gas} \cdot \dot{V}_{gas}}{C_{sorbitol,feed} \cdot \dot{V}_{feed}}$$

Equation 2.3 $$Selectivity(\%) = \frac{Yield_{product}}{Yield_{category}}$$

2.4 Results and discussion

2.4.1 Monofunctionals produced from APHDO of sorbitol over Co/TiO_2

Figure 2.3 shows the time-on-stream (TOS) product distribution for APHDO of sorbitol at WHSVs of 0.35 hr^{-1}, 0.70 hr^{-1}, 1.40 hr^{-1}, and 2.80 hr^{-1}, each reported after an initial transient period. The products are divided into four main categories: light gas (LG), C_5-C_6 alkane/heavy gas (HG), monofunctional (MF), and higher oxygenate (HO). LGs consist of CO, CO_2, and C_1-C_4 alkanes. HGs are primarily C_5 and C_6 *n*-alkanes. MF includes all species which contain exactly one oxygen functionality (e.g. mono-alcohols, ketones, aldehydes, heterocycles). HO includes all species with two or more oxygens (e.g. polyols, mixed alcohol-carbonyl compounds, hydroxy-heterocyles,

anhydrosugars, carboxylic acids). Table 1 shows the detailed yields and selectivities after ~34 turnovers at each WHSV. Sorbitol conversion is >98% for all cases. Within this WHSV range, MF production reaches a maximum yield of 56.2% after 53 hr (37 turnovers) at a WHSV of 0.70 hr^{-1}. This is the highest yield demonstrated from sorbitol in the open literature. These species are predominantly primary alcohols, secondary alcohols, or heterocyclic species. At this WHSV, the product distribution appears to be steady over time. However, this is not the case for the other WHSVs where a loss of activity is observed. Deoxygenation activity decreases with time at all WHSV. At 0.35 hr^{-1} the alkane yield decreases with a simultaneous increase in MF yields and very little impact on HO yields. At 0.70 hr^{-1} the MF yields slowly increases with time accompanied by a slight decrease in HG yields. The LG and MF yields decrease at 1.40 hr^{-1} accompanied by an increase in HO yields. Most of the HOs identified are diols, though tetrahydropyran-2-methanol is also observed in relatively high yields. Many C_{5+} higher oxygenates (likely heterocycles) are produced but could not be identified here with certainty either because standards could not be obtained or MS fragmentation patterns were inconclusive. The lower carbon balance could therefore be largely explained by these types of species as well as insoluble degradation products. At 2.80 hr^{-1}, MF yields continue to decrease down to 8.7% while HO yields go through a maximum. This decrease in the HO yields is a result of the inability to identify a large portion of the oxygenates. Early C_{5+} oxygenates such as 1,4-sorbitan and isosorbide are only detected in low yields (0.9% and 0.5%, respectively at 34 turnovers) while the sorbitol conversion remains above 98%. The unidentified species therefore are likely produced from these anhydrosorbitol species either through hydrodeoxygenation reactions to C_5-C_6 species with 2-4 oxygen atoms or through coupling reactions to oligomeric species larger than C_6, as will be addressed in further detail later.

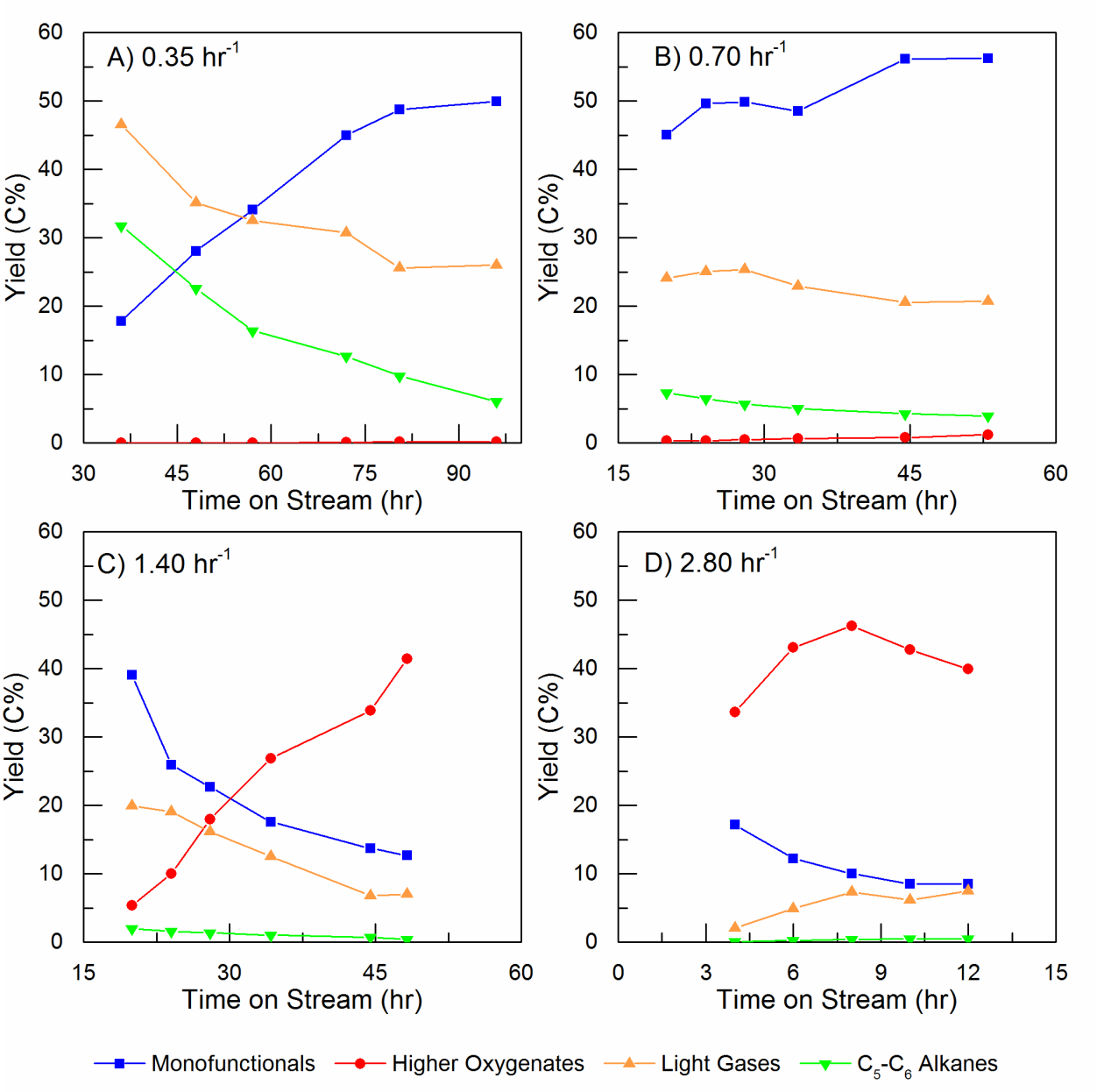

Figure 2.3 | **Production of monofunctional species in the APHDO of sorbitol over Co/TiO$_2$ vs. TOS at multiple WHSVs.** Conditions: 541 K, 6.31 MPa H_2 at 40 mL/min, 3.30 g catalyst, WHSV=0.35-2.80 hr^{-1}.

Table 2.1 | **Product distribution in sorbitol APHDO over Co/TiO_2 at multiple WHSVs.** Conditions: 541 K, 6.31 MPa H_2 at 40 mL/min.

WHSV (hr^{-1})	**0.35**	**0.70**	**1.40**	**2.80**
Conversion (%)	99.9	99.8	99.7	98.9
Gas Yield (%)	**32.0**	**24.6**	**20.7**	**8.0**
Gas Product Selectivity (%)				
CO	0.0	0.0	0.7	5.8
CO_2	10.0	24.5	48.2	45.2
Methane	51.9	48.7	37.0	36.6
Ethane	3.0	2.6	2.4	3.0
Propane	5.9	3.4	2.1	1.6
Butane	10.3	5.0	2.0	1.4
Pentane	12.7	7.4	3.4	2.4
Hexane	6.2	8.4	4.2	3.9
Monofunctional Yield (%)	**49.9**	**56.2**	**25.9**	**8.7**
Monofunctional Selectivity (%)				
Methanol	0.1	0.3	1.9	4.0
Ethanol	4.9	7.5	18.2	13.0
Propanol	7.5	9.8	14.9	10.0
Butanol	11.7	12.2	7.0	4.3
Pentanol	18.2	18.6	13.5	6.3
Hexanol	21.2	20.9	8.9	6.1
Propanal	0.9	0.6	0.9	16.0
Butanal	0.1	0.1	0.3	1.5
Pentanal	0.0	0.0	0.0	0.0
Hexanal	0.0	0.0	0.0	0.0
Acetone	0.5	0.5	3.2	3.3
Butanone	1.1	1.1	3.7	4.9
Pentanone	2.9	2.6	3.4	3.2
Hexanone	2.9	2.6	11.6	18.0
Tetrahydrofuran	0.6	0.6	0.5	1.5
Methyltetrahydrofuran	4.3	3.5	2.9	1.2
Dimethyltetrahydrofuran	8.0	6.7	3.2	4.9
Methylfuran	0.0	0.0	0.0	0.0
Dimethylfuran	0.0	0.6	0.1	0.2
Ethyltetrahydrofuran[a]	5.8	4.3	2.5	1.3
Tetrahydropyran	2.3	2.4	1.9	0.2
Methyltetrahydropyran	6.8	5.0	1.3	0.2
Higher Oxygenate Yield (%)	**0.2**	**1.2**	**9.1**	**39.5**
Higher Oxygenate Selectivity (%)				
Isosorbide	0.0	0.0	0.0	1.4
Isomannide	0.0	0.0	0.0	1.2
1,4-sorbitan	0.0	0.0	0.0	2.2
Glycerol	0.0	0.0	0.0	6.2
1,2,6-hexanetriol	0.0	0.0	0.0	2.6
Hydroxyacetone	0.0	0.0	4.3	4.3
Ethylene glycol	0.0	0.0	3.1	14.5
Propanediol	0.0	0.0	29.0	40.3
Butanediol	0.0	0.0	7.0	10.5
Pentanediol	0.0	0.0	1.5	7.4
Hexanediol	0.0	0.0	5.3	5.7
Hexanedione	0.0	0.0	0.8	1.3
Tetrahydrofurfuryl alcohol	100.0	29.5	2.3	0.0
Furfuryl alcohol	0.0	0.0	0.0	0.0
Hydroxytetrahydrofuran	0.0	0.0	1.4	0.4
Hydroxytetrahydropyran	0.0	0.0	0.0	0.0
Tetrahydropyran-2-methanol	0.0	62.2	21.1	1.8
Acetic acid	0.0	0.0	0.0	0.0
Propionic acid	0.0	0.0	13.5	0.1
Butyric acid	0.0	0.0	0.0	0.0
Valeric acid	0.0	8.3	4.0	0.0
Hexanoic acid	0.0	0.0	6.5	0.0
Aqueous Unidentified Carbon[b] (%)	0.0[c]	14.4	23.5	29.5
Total Unidentified Carbon (%)	16.3	18.2	43.5	42.9
TOS (h)	96.0	53.0	24.0	12.0

[a]Confirmed via GC MS only.

[b]From TOC on aqueous fraction.

[c]112% of aqueous carbon identified according to TOC.

To better understand how both C–C and C–O cleavage occurs throughout the pathway, products have been further subdivided in Figure 2.4 to account for chain length and especially differentiate between C_1 gases produced from decarbonylation and C_{2+} alkanes. The loss of carbon balance here is absorbed by the "C_{5+} Higher Oxygenates and Humins" category, as all C_4 and smaller species have been detected via GC+HPLC. Figure 2.4 plots these categories against 1/WHSV at both an early time on stream (near 16 turnovers) and at a later time on stream (near 34 turnovers). C_2-C_4 species come primarily from the retro-aldol condensation route but may also come from dehydration followed by decarbonylation. Since only ~5% of the carbon goes to C_1 species, it is expected that most of the C_2-C_4 species are from the former, therefore a large fraction of sorbitol (>30%) is converted through the retro-aldol condensation route over Co/TiO_2. Higher residence times show both C_{5+} and C_2-C_4 higher oxygenates converting to MFs, accompanied by a rise in C_1 gases as well as alkanes. Once the C_2-C_4 higher oxygenates yield decreases to zero the MF yields reach a maximum yield (56.2%) where ~2/3 of the MFs are C_{5+}. Yields to C_1 gases do not markedly increase after C_2-C_4 HO yields go to zero, indicating that a larger fraction of the carbon in the retro-aldol route relative to the dehydration route is converted to C_1 carbon. Further increases in residence time leads to a sharp drop in MFs of all lengths accompanied by an increase in alkanes. At 0.35 hr^{-1} ~20% of the sorbitol is converted to C_1 species. Since the majority of C_1 species are produced during deoxygenation of HOs to MFs, subsequent deoxygenation of MFs mainly occurs via dehydration.

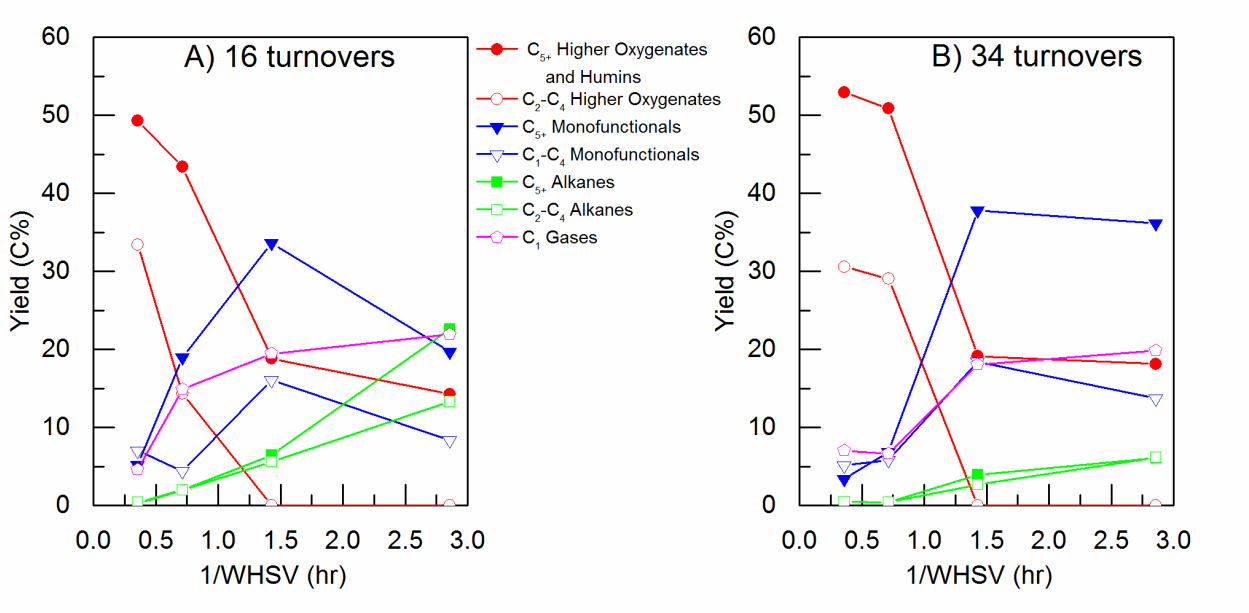

Figure 2.4 | **Production of various categories of species as a function of 1/WHSV.** Yields are reported for each WHSV at (A) an early time on stream (~16 turnovers) and (B) a later time on stream (~34 turnovers). Turnover is calculated as the mass of feed passed over the catalyst per mass of catalyst. Conditions: 541 K, 6.31 MPa H_2 at 40 mL/min, 3.30 g catalyst, WHSV=0.35-2.80 hr^{-1}.

2.4.2 Comparison of monofunctionals produced from Co/TiO₂ versus noble metal catalysts

As demonstrated by Kunkes et al., MFs may be utilized in the production of long-chain alkanes after various coupling reactions.[9] The MF distribution produced via Co/TiO_2 at 0.70 hr^{-1} is compared in Figure 2.5 to the distributions produced using Pt/Zr-P and Pt-Re/C as reported by Kim et al. at the WHSVs that gave the highest MF yields (0.16 hr^{-1}, 42.5% yield and 1.27 hr^{-1}, 32.9% yield, respectively).[3] The study by Kim et al. provides a good comparison since multiple WHSVs were investigated under very similar conditions to those in the current study (20 wt% sorbitol, 6.31 MPa hydrogen at 40 mL/min, 3.30 g catalyst, 523 K). For Co/TiO_2, the majority of MFs produced are alcohols, with primary alcohols making up 37% of the MF carbon and secondary alcohols (including cyclic alcohols) comprising 32%. Heterocycles are also produced in high abundance (23% selective) along with few ketones (7%) and almost no aldehydes (<1%). These trends are the same for the Pt-based catalysts as well, with the exception of primary vs. secondary

alcohol selectivities. Low ketone yields are expected as a result of the high hydrogen pressures. In the case of 2-hexanone, 2-hexanol is favored over 2-hexanone at thermodynamic equilibrium approximately by a ratio of 5:1 (from gas-phase thermodynamic data) while a ratio of 3:1 was observed. Low aldehyde yields can be attributed either to rapid hydrogenation or decarbonylation reactions. In the case of hexanal, the equilibrium ratio of 1-hexanol:hexanal is estimated to be on the order of 10^2 while the equilibrium constant for decarbonylation of hexanal to CO + pentane is on the order of 10^7. Any CO produced undergoes further reaction to produce CO_2 or CH_4 by water-gas shift or methanation. The CO_2:CO thermodynamic equilibrium ratio for water-gas shift under these conditions is estimated to be 10^2 while the CH_4:CO ratio is estimated to be on the order of 10^{11}. No hexanal is observed in these reactions for Co/TiO_2. Decarbonylation is more prevalent with Co/TiO_2 and Pt-Re/C than with Pt/Zr-P, as evidenced by the high selectivities toward C_1 species (73% for Co/TiO_2 and 62% for Pt-Re/C vs. 25% for Pt/Zr-P). This is also reflected in the distribution of primary vs. secondary alcohols among the catalysts. Pt/Zr-P produces almost entirely primary alcohols, while the other catalysts produce primary and secondary alcohols non-selectively. Pt/Zr-P has previously been shown to possess many more Brønsted acid sites than Pt-Re/C (548.1 vs. 36.6 μmol g^{-1}). These are key in the dehydration of the preceding diols and in the opening of heterocycles to form alcohols. All catalysts have a higher selectivity to alcohols than to heterocycles. The reasons for this are much more complex as the balance between the two is dependent upon competition between competing ring-forming, ring-opening, and direct deoxygenation reactions which a hydroxy-heterocycle may undergo to produce MFs. Higher selectivities to alcohols are preferred in the context of this study, since subsequent coupling steps of heterocycles as outlined previously would require an additional ring-opening step.

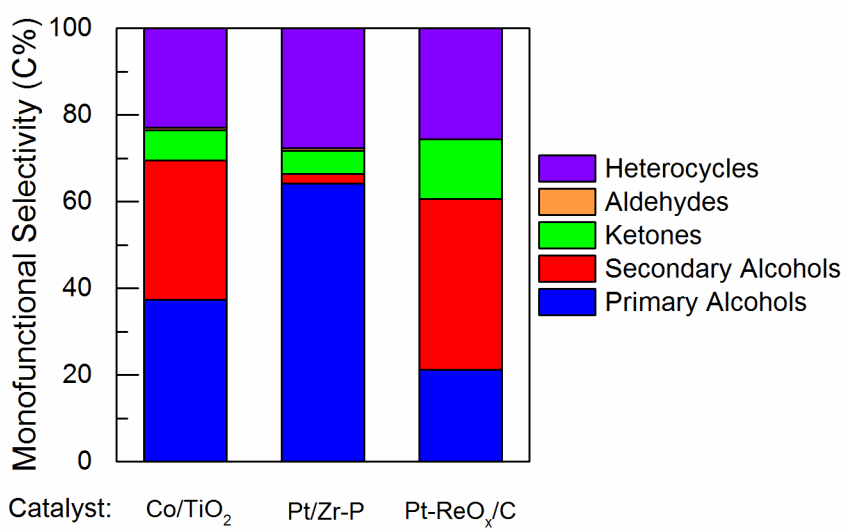

Figure 2.5 | **Distribution of monofunctionals between Co/TiO_2 and catalysts from literature.** Co/TiO_2 data at 0.70 hr^{-1}. Pt/Zr-P and $Pt\text{-}ReO_x/C$ data provided at conditions for maximum MF yield from Kim et al.[3]

Co/TiO_2 and Pt/Zr-P are more selective toward larger species than Pt-Re/C, as shown in Figure 2.6A. Approximately 2/3 of the monofunctionals produced over Co/TiO_2 are C_5-C_6. Several studies have shown that the ratio of acidic to metallic character of catalysts for sorbitol APHDO has a large impact on the size of the species produced.[8,19] Pt/Zr-P likely promotes the dehydration pathway over retro-aldol condensation better than Pt-Re/C due to its higher acid site concentration. In the case of Co/TiO_2, Co may be less active for C–C cleavages than Pt under these conditions. Within the MFs, however, all catalysts demonstrate similar selectivities with a nearly 50:50 split between C_5–C_6 and C_1-C_4 species (Figure 2.6B). Very low C_1 MF yields are likely due to a tendency to form CO instead of methanol or formaldehyde (the only C_1 MFs) from a C_2 oxygenate or fast dehydration/hydrogenation of the MF to form methane.

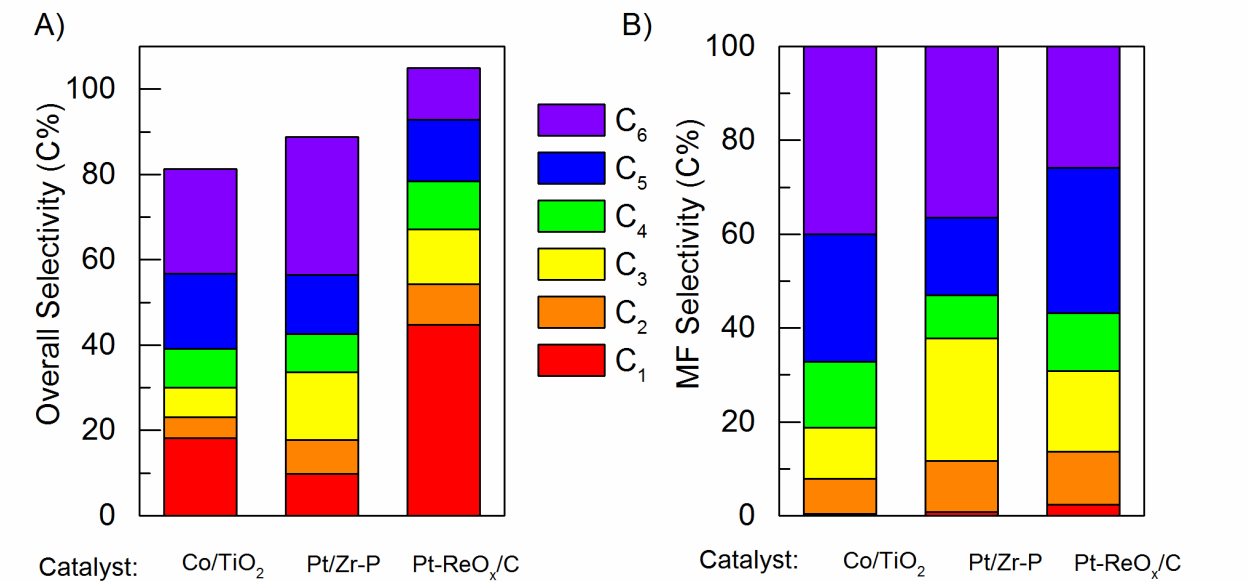

Figure 2.6 | **Selectivity to species of different carbon lengths over Co/TiO_2, Pt/Zr-P, and Pt-ReO_x/C**. (A) Overall product distribution. (B) Selectivity within the monofunctionals produced. Co/TiO_2 data at 0.70 hr^{-1}. Pt/Zr-P and Pt-ReO_x/C data provided at conditions for maximum MF yield from Kim et al.[3]

2.4.3 Evidence of oligomeric species forming and fragmenting to form monofunctionals with increasing residence time

Fourier-transform ion cyclotron resonance mass spectrometry (FT-ICR MS) was performed on select aqueous products to better identify the unknown species produced especially at high WHSV. Oxygen number vs. carbon number is shown in Figure 2.7A while double-bond equivalence (DBE) vs. carbon number is shown in Figure 2.7B for aqueous products produced at 2.80 hr^{-1}. It should first be noted that this technique is low-mass limited such that species below C_5 are not detected. Additionally, the technique is not fully quantitative due to differences in ionization efficiency of different species. However, the $C_6H_{14}O_6$ peak characteristic of sorbitol only accounts for 2.1% of the MS signal despite the fact that only 1.1% of the carbon fed as sorbitol still remains in this sample, suggesting that other species observed are abundant. According to the total organic carbon (TOC) data, 29.5% of the carbon fed was converted to unidentified aqueous species at this WHSV. Oxygenates up to C_{30} are detected via FT-ICR MS, many of which would

not be volatile enough to detect by GC techniques. Signals are concentrated mostly at C_6, C_{12}, and C_{18} with 2-8 oxygens and DBEs of 1-6. The C_{6n} pattern suggests that sorbitol or C_6 derivatives of sorbitol (e.g. anhydrosorbitols) couple early in the reaction network. C_{12} species possess primarily 4 or 6 oxygen atoms, thus a high degree of hydrodeoxygenation occurs either during the oligomerization process or after these oligomers have been formed. DBE likely comes from ether rings which may or may not possess conjugated double bond systems (e.g. furan, tetrahydrofuran), though non-conjugated C–C bonds are expected to readily hydrogenate under the reaction conditions. Ketone groups may also be present, since ketones are observed in low yields at lower WHSVs (e.g. 3.8% yield at 0.70 hr^{-1}). Figure 2.8 shows that the signal intensity gradually decreases with decreasing WHSV. It should be noted that the 2.80 hr^{-1} spectrum was collected separately from the lower WHSV spectra, thus the color scale for Figure 2.8 is different than for Figure 2.7 and intensities are not directly comparable between the two figures (though the maximum intensities are on the same order of magnitude). At 1.40 hr^{-1}, the C_6 and C_{12} signals are still prominent with very low signal from larger species. However, a very strong C_9 signal appears which corresponds to a molecule with 3 oxygen atoms and a DBE of 2. At 2.80 hr^{-1}, low-intensity signals are also evident at C_9, C_{15}, and C_{21}. Such species could be formed either via coupling of C_{6n} species with C_3 oxygenates produced via retro-aldol condensation or through breaking of bonds in the C_{12+6n} oligomers. The former case can be rationalized via consideration of the C_6 signal observed (O=2, DBE~2) and the notable quantities of C_3 oxygenates detected via GC at this WHSV and at 2.80 hr^{-1} (9 and 23% yield, respectively). The C_9 signal could be from a species formed via intermolecular dehydration of the $C_6H_{10}O_2$ species and a C_3 diol. At lower WHSVs, this C_9 signal fades while some C_6 and C_{12} remains at 0.70 hr^{-1}. Very little signal remains at 0.35 hr^{-1}, as is expected since all of the aqueous carbon has been identified according to TOC.

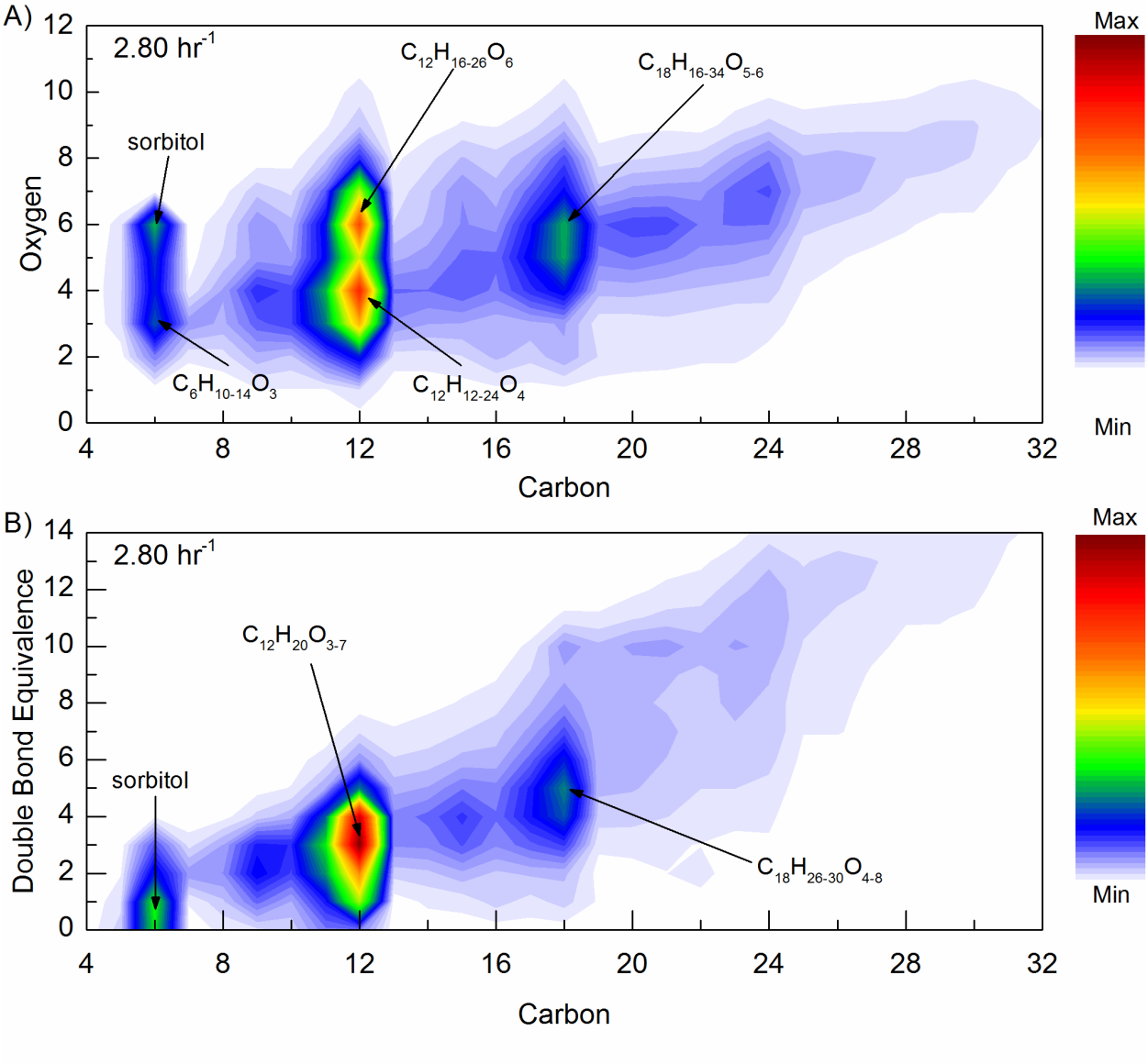

Figure 2.7 | **FT-ICR MS spectra for aqueous fraction of APHDO products at 2.80 hr^{-1} after 34 turnovers.** (A) oxygen number vs. carbon number and (B) double bond equivalence vs. carbon number.

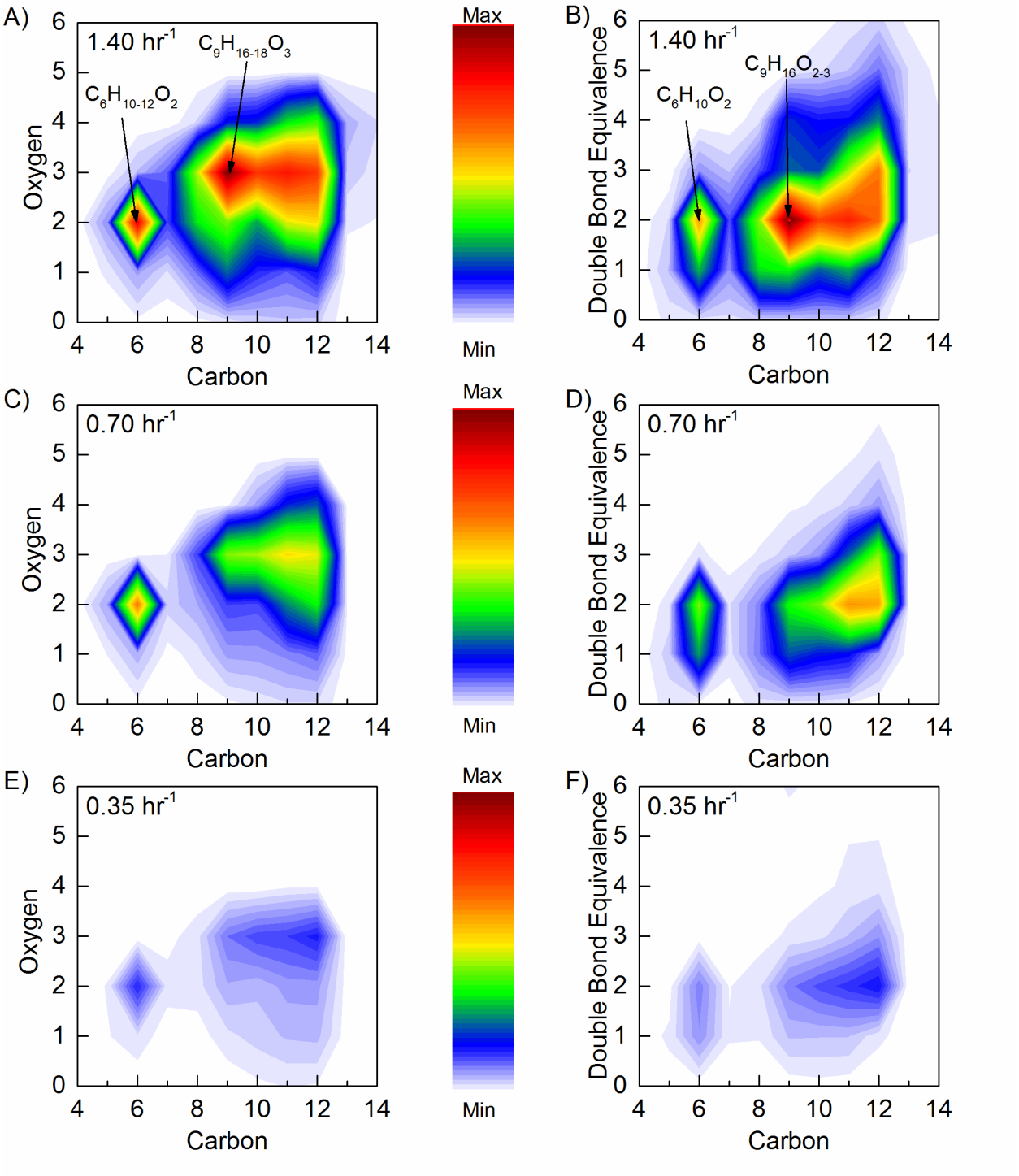

Figure 2.8 | **FT-ICR MS spectra for aqueous fraction of APHDO products.** (A-B) 1.40 hr^{-1}, (C-D) 0.70 hr^{-1}, and (E-D) 0.35 hr^{-1} after ~34 turnovers showing oxygen number and double bond equivalence vs. carbon number. The maximum intensity for these plots is based on the maximum observed at 1.40 hr^{-1}.

The disappearance of C_{9+} species with decreasing WHSV can be explained via two possibilities. These species may polymerize with increasing residence time to form insoluble carbonaceous solids and coke. The maximum amount of carbon deposited is only 1.6% of the carbon fed (at 0.35 hr^{-1}), thus this is not likely the major mechanism by which these oligomers are consumed. Additionally, 96% of the carbon was accounted for as liquid-phase or gas-phase products at 0.70 hr^{-1}. A second possibility is that these oligomers fragment to form MFs and alkanes with increased residence time. C–O–C bonds are less stable under APHDO conditions and therefore can be considered to form reversibly. C–C bonds, however, are more difficult to break unless the proper oxygenated functionalities are maintained (e.g. aldol). It is therefore expected that these oligomers form via ether linkages since oligomer hydrodeoxygenation would yield C_{9+} MFs and alkanes at lower WHSVs if they were linked via C–C bonds. Such species are not detected at any WHSV, though these would certainly be identifiable via GC MS. The combination of FT-ICR MS and GC MS data at varying WHSV therefore provides evidence for a unique pathway for MF and alkane production not discussed prior in the literature. The dehydration route of sorbitol produces C_6 oxygenates which can couple via C–O–C linkages either with each other or with C_3 oxygenates produced via retro-aldol condensation. These oligomers then undergo a series of ether cleavage and formations while deoxygenating. Once a MF is produced, further coupling is less likely due to its lower number of oxygen functionalities. As a result it is either isolated or further deoxygenated to an alkane.

2.4.4 The impact of liquid feed flow rate on the presence of a liquid phase under reaction conditions

In interpreting WHSV trends in aqueous hydrodeoxygenation reactions, the presence of water must also be noted. By definition, it is assumed that the high pressures utilized in APHDO are sufficient to fully inhibit evaporation of water. However, vapor-liquid equilibrium dictates that

total evaporation of water is still possible when a gas is cofed with the liquid feed. This behavior has previously been documented in the case of aqueous butanol dehydration over solid acids where the solute was volatile.[20] The partial pressure of water will be primarily a function of temperature. The molar flow rate of water in the vapor phase can then be calculated from this partial pressure, the system pressure, and the total gas flow rate. The use of a gas cofeed enables large fractions of water to vaporize at lower liquid flow rates, such that 100% will evaporate toward the limit of zero liquid flow. Due to the non-ideality of the mixture in question, ASPEN Plus® software was utilized (with the predictive Soave-Redlich-Kwong property method) to estimate the extent of water evaporation when 20 wt% glucose (as a surrogate for sorbitol) is cofed with hydrogen into a flash tank at various liquid feed flow rates and temperatures. Figure 2.9 shows that the lower flow rates used in this study (at 541 K) allow for nearly complete evaporation of water (98% of water fed) while higher flow rates may still possess modest liquid phases (18% of water fed). At higher flow rates the fraction evaporated is also very strongly dependent on temperature. Between 523 and 541 K, the fraction of water which evaporates almost doubles from 46 to 82%. These values are upper estimates, however, as transient heating and capillary action will restrict the amount that evaporates. As such, "APHDO" is not a sufficient descriptor of this reaction, though it is used throughout this study for historical purposes. Liquid water may introduce a variety of solvent effects that would alter reaction rates compared to the gas phase, thus confounding trends observed with WHSV. While this may be happening here, the general pathway appears to be insensitive to changes in WHSV as well as deactivation since the product distribution from a deactivated catalyst at one WHSV approaches the product distribution of a fresh catalyst at the next higher WHSV (see Figure 2.3). This complexity has not been addressed in past APHDO studies, but could theoretically be corrected for via manipulation of WHSV through adjustment of catalyst loading

rather than liquid flow rate or adjustment of either gas flow rate or pressure to set a constant extent of evaporation. However, these changes may also affect the product distribution by altering reaction rates dependent on gas-phase H_2 pressures, exacerbating the effects of temperature gradients, or altering transport behaviors.

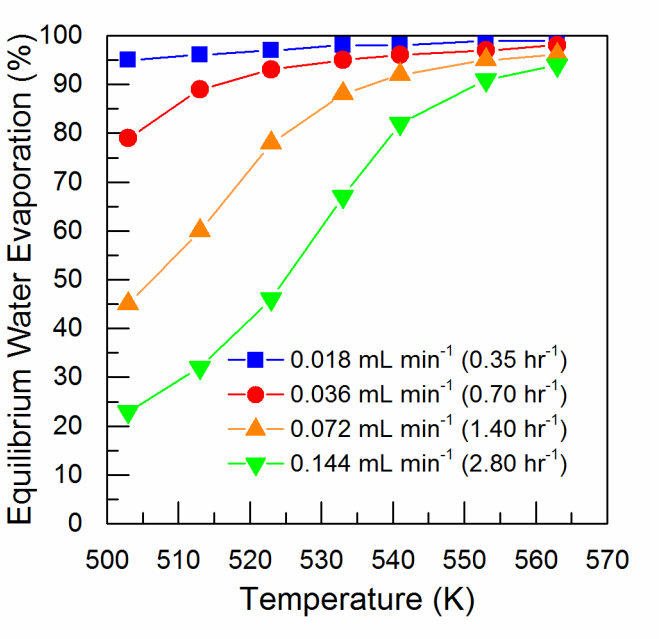

Figure 2.9 | **Equilibrium vaporization of water under APHDO conditions.** Conditions modeled: 20 wt% glucose in water cofed with 40 mL/min (STP) H_2 at 6.31 MPa into a flash tank operating at various temperatures with the liquid flow rates used in this study.

2.4.5 Irreversible deactivation of Co/TiO_2 due to oxygenate-promoted sintering and leaching

In the study of Lee et al., Co/TiO_2 (prepared identically) was shown to be stable in the aqueous-phase hydrogenation of furfuryl alcohol at 413 K with mild deactivation that could be reversed via repetition of the pretreatment calcination and reduction.[18] However, more severe deactivation was observed in the current study on sorbitol APHDO, and this activity could not be recovered after regeneration attempts by repeated calcination and reduction. The present reaction utilizes a much more concentrated feed (20 wt% vs. 2 wt%) which is additionally more highly oxygenated (O:C=1 vs. O:C=0.4) and converted at a much higher temperature (541 K vs. 413 K).

Any of these factors could contribute to this difference in stability. Table 2 summarizes the nomenclature used for catalyst samples, and Table 3 summarizes the characterization results for the fresh and spent catalysts. The 1.40 hr^{-1} sample saw an additional 34 turnovers more than the samples produced at other WHSVs and subsequently 27 more turnovers at lower WHSV and is therefore not directly comparable to the other catalysts. To address the impact of the sorbitol in the feed, the 2.80 hr^{-1} reaction was repeated with a fresh catalyst and a 100% water feed (sample 2.80-WS).

Table 2.2 | **Nomenclature used to describe various catalyst treatments in this study.**

Nomenclature[a]	Treatment Description
T	TiO_2 calcined to 1023 K (4 K min^{-1}, 4 hr).
F	Fresh Co/TiO_2 after static air calcination to 573 K without further treatment.
C	Calcined to 873 K (5 K min^{-1}, 2 hr, 100 mL min^{-1} air).
R	Reduced to 873 K (1 K min^{-1}, 2 hr, 100 mL min^{-1} H_2).
x-S	Co/TiO_2 post reaction. X represents the WHSV of the reaction used to produce this sample. Spent catalysts are additionally treated depending on the characterization technique used.

[a]Catalysts which receive multiple treatments are referred to by combining these nomenclatures in the order in which they occurred. E.g. the catalyst used in reaction is FCR.

Table 2.3 | **Characterization of fresh and spent catalysts.** Nomenclature of samples described in Table 2.2.

Catalyst Treatment	Turnovers (g feed g^{-1} catalyst	Co Content (wt%)	Co_3O_4 Crystallite Size[a] (nm)	BET Surface Area (m^2 g^{-1})	Coke Formation (wt% of C fed)	Coke Formation (mol C mol^{-1} Co)
T	-	-	-	10.3	-	-
F	-	-	37.8	11.3	-	-
FC	-	-	36.2	10.4	-	-
FCR	-	5.10	-	10.7	-	-
FCRC	-	-	22.3	10.4	-	-
2.80-S[b]	33.6	4.46	44.4	9.2	0.30	0.78
1.40-S[b,c]	94.5	4.59	45.2	9.4	1.00	7.33
0.70-S[b]	37.1	4.22	27.1	9.8	1.03	2.98
0.35-S[b]	34.2	4.65	26.5	8.9	1.68	4.37
2.80-WS[d]	33.6	4.97	22.8	11.1	-	-

[a]Estimated from line-broadening analysis in XRD.
[b]Coke formation calculated without further treatment of the sample. Co_3O_4 size and surface area measured after catalyst calcination.
[c]1.40-S underwent additional low WHSV reaction after the data reported, contributing to additional carbon deposition.
[d]2.80-WS produced at identical conditions to 2.80-S without sorbitol in feed.

Cobalt content, particle size, and BET surface area were constant when sorbitol was not present in the feed, thus the presence of oxygenates is critical to catalyst deactivation. The spent catalysts lost between 7 and 16 percent of the cobalt, demonstrating that SMSI did not fully stabilize the catalyst. No systematic trend with deactivation and WHSV was observed. Coke formation is shown to increase with decreasing WHSV from 0.78 to 4.37 moles C per mole of Co, suggesting that carbon deposition occurs more severely deep in the reaction network. This is not the primary mode of deactivation, however, since activity was not restored after burning the carbon off in calcination treatments. Some past studies have suggested that SMSI may be reversed via oxidation by water, eliminating potentially active Co-TiO_x sites.[21,22] While this may be occurring here, it is not the sole cause of deactivation since regeneration would restore the SMSI state. The BET surface area of the catalyst decreases by only 5-15% percent during reaction from 10.7 to a minimum of 8.9 m^2 g^{-1} without any clear trend with WHSV. Restructuring of the support is therefore unlikely to be the cause of deactivation. XRD additionally showed that the rutile phase of TiO_2 induced by the initial calcination did not change (Figure 2.10), which is expected as the transformation from the anatase to rutile is known to be irreversible even after hydrothermal treatments.[11,23] Co crystallite size could not be assessed via XRD line broadening due to the overlap of Co and rutile TiO_2 reflections, as can be seen through comparison of their patterns in the bottom of Figure 2.11. Sintering was therefore evaluated by using the crystallite size of Co_3O_4 (the prominent cobalt oxide phase) in oxidized samples. Spent catalysts were analyzed after calcination at 873 K. This calcination did not affect the crystallite size measured by XRD (samples F vs. FC). The results in Table 3 suggest that reduction of Co/TiO_2 results in a redispersion of the cobalt as the crystallite size decreased from 36.2 to 22.3 nm. It has been proposed that high temperature calcinations of cobalt may form vacancies which decompose upon reduction, resulting in the

formation of smaller particles.[24] While this may be the case, the strong interactions between the nanoparticle and support may instead be limiting the extent to which Co can oxidize, thus the measured Co_3O_4 crystallite size may be smaller than the true CoO_x particle size (where x<4/3). More quantitative comparisons can be drawn through the use of STEM.

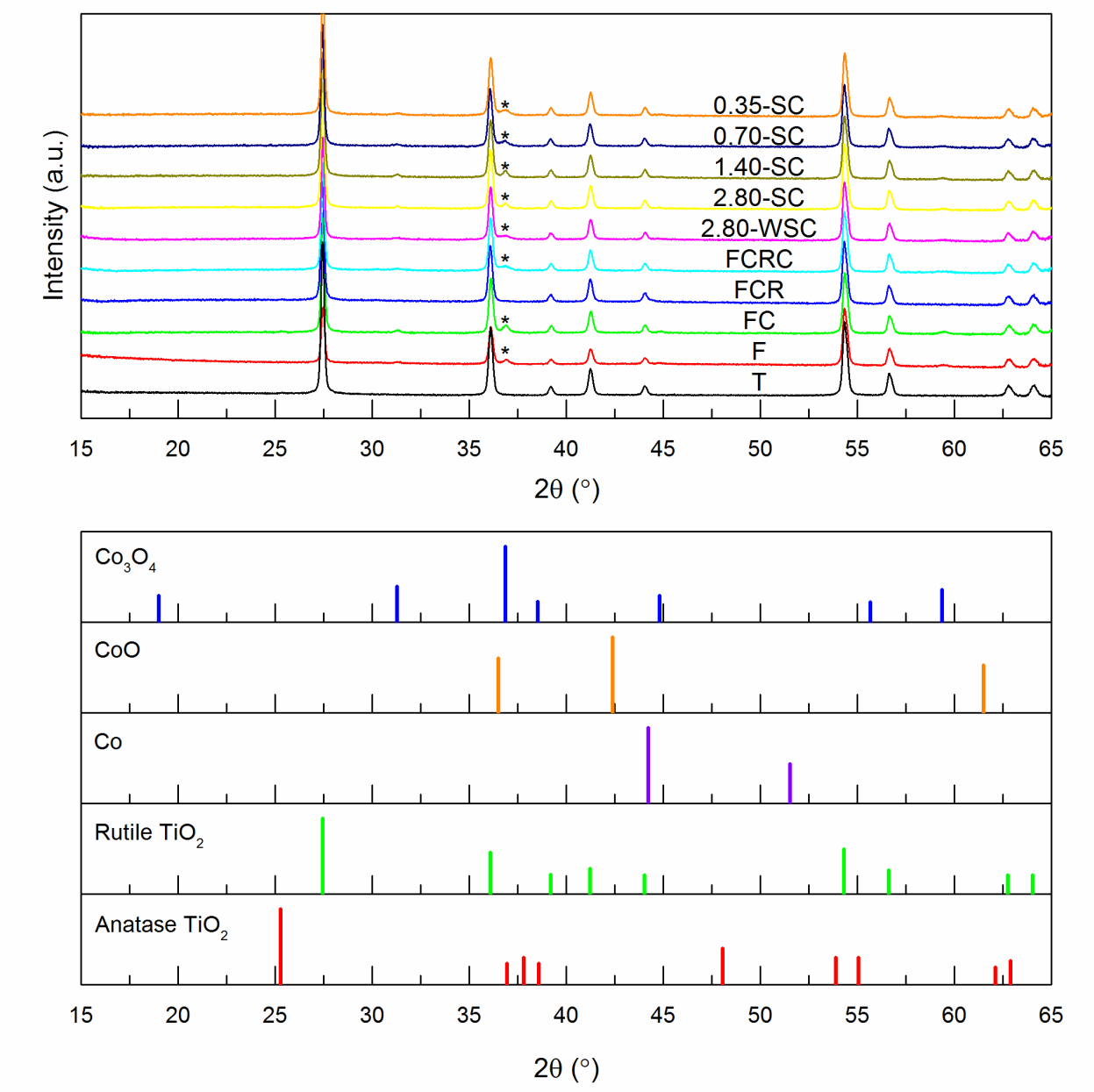

Figure 2.10 | **XRD patterns of support, pretreated catalysts, and spent catalysts.** An asterisk indicates the location of an observable Co_3O_4 peak.

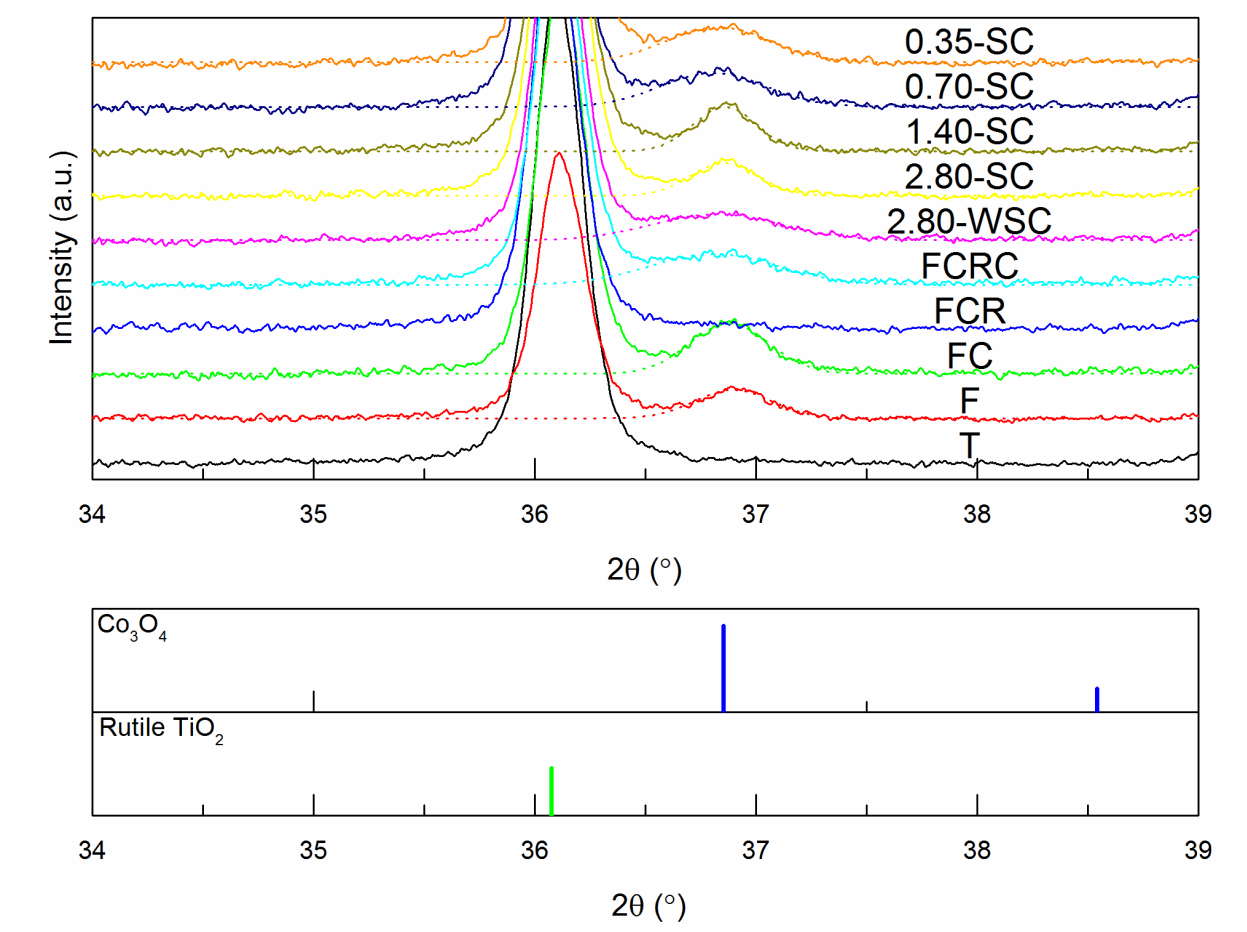

Figure 2.11 | **XRD patterns in Co_3O_4 regime.** Data fits shown with dotted lines.

STEM (Figure 2.12A) shows that the Co particle size in FCR samples (after passivation) is 28.0 +/- 0.6 nm on a number-weighted basis. Using a volume-weighted basis for comparison with XRD, the particle size is ~33 nm, which is more consistent with the Co_3O_4 crystallite size observed in XRD prior to reduction. However, Co_3O_4 particle size is difficult to measure via STEM for these samples due to the similarity in the Co_3O_4 and TiO_2 Z-contrast values. These results do, however, support the hypothesis that the catalyst is not fully oxidized upon calcination, thus Co_3O_4 crystallite sizes can only be used for qualitative comparison, and conclusions should only be drawn with caution. Crystallite sizes are slightly larger (~20%) in catalysts subjected to low WHSV reactions than catalysts which only receive calcination and reduction treatments (sample FCRC),

suggesting that minor sintering may occur during low WHSV reactions. STEM of the spent catalyst at 0.70 hr^{-1} (Figure 2.12B) shows a statistically significant increase in particle size from 28.0 +/- 0.6 nm to 32.2 +/- 0.9 nm. Assuming spherical particles, this corresponds to an approximately 15% reduction in the number of exposed Co atoms (while XRD predicts a 17% reduction). At higher WHSVs, more sintering is apparent as Co_3O_4 crystallite sizes increase to ~44.5 (99% increase) and ~45.2 nm (103% increase) after reactions at 1.40 and 2.80 hr^{-1}, respectively. Due to incomplete oxidation during the calcination post-treatment, these are lower bounds for the size increase, which according to XRD corresponds to an approximate 50% loss in the number of exposed Co atoms. STEM images of 2.80-S (Figure 2.12C) show a clear reduction in the number of observable cobalt particles compared to the fresh catalyst. The particle size was difficult to determine with this sample due to the presence of large Co particles which cannot be easily distinguished from TiO_2. Figure 2.12C shows that Co particles as large as 100 nm may be present after reaction at 2.80 hr^{-1}, as careful contrast analysis of this particle versus similarly sized TiO_2 particles shows that it is unlikely to be TiO_2. The lack of Co particles can therefore be explained by a combination of sintering and leaching. An estimated 11% of the Co leached out over the course of 12 hr at 2.80 hr^{-1} while approximately 15% of Co leached out at 0.70 hr^{-1}, thus the large reduction in particles observed for 2.80-S but not for 0.70-S is likely a result of sintering to form large particles at high WHSV. Assuming spherical Co particles, sintering from 28 to 50 nm would cause a 44% reduction in the number of surface sites and an 82% reduction in the number of particles. Further sintering to 100 nm would cause a net 98% reduction in the number of particles.

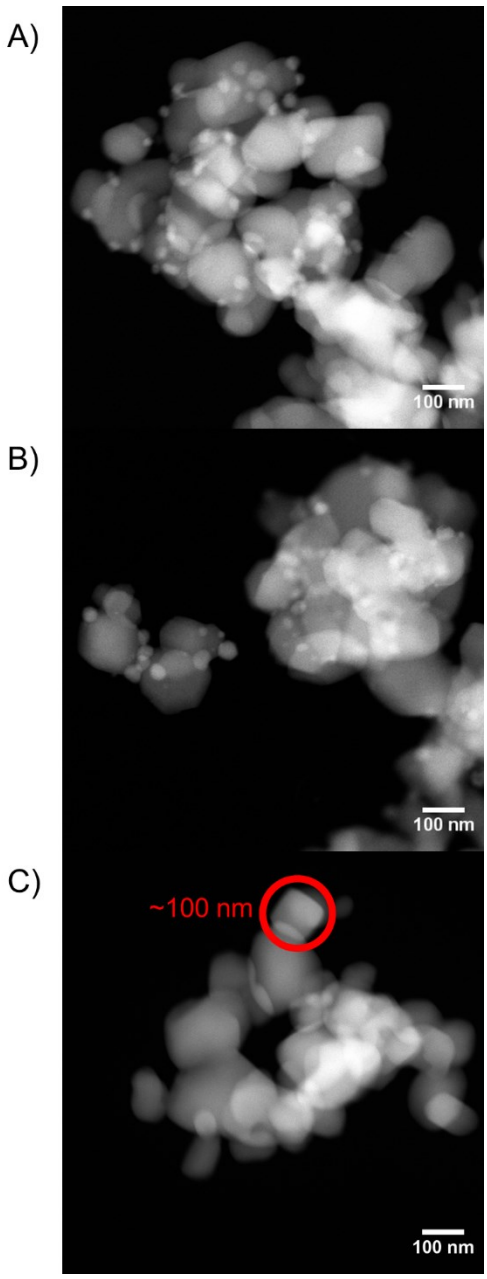

Figure 2.12 | **Representative STEM images of catalysts.** (A) prior to reaction, (B) after reaction at 0.70 hr^{-1}, and (C) after reaction at 2.80 hr^{-1}. The particle circled in (C) appears to be Co due to its higher contrast relative to similarly-sized TiO_2 particles.

The lack of morphological changes from hydrothermal treatments without sorbitol present in addition to the relatively low temperature suggests that catalyst deactivation is caused via a chelation mechanism in combination with Ostwald ripening, by which Co atoms are removed from the catalyst and redeposited to form larger, more thermodynamically stable particles.[14,25]

Thermally-induced sintering via the migration of whole catalyst particles is not likely to occur at these relatively low reaction temperatures.[26] While leaching is not clearly dependent on WHSV, sintering is more significant at higher WHSV. The reasons for this are unclear. Since highly oxygenated species are more prevalent throughout the bed at 2.80 hr^{-1} compared to 0.70

2.4.6 Economic considerations of the monofunctional platform

Figure 2.13 compares Co/TiO_2 against various other catalysts from the literature for the production of MFs. The yields compared here are at conditions where the MF maximum is reported in each study. All catalyst costs reported are estimated assuming the catalyst cost is that of the raw metals used in 2015 dollars.[27] The highest yield to MFs observed in literature is 62% using a Pd-Ag/WO_x-ZrO_2 catalyst with a 60 wt% corn syrup feed.[28] Of the catalysts utilizing a sorbitol feed, Co/TiO_2 produced MFs at the highest yield (56%), with Pt-Nb/ZrCr producing the second most at 55%. Co/TiO_2 is clearly the least expensive catalyst at approximately $2.29 per kg, while the noble-metal catalysts cost 50 to 1,000 times more. Yield, feedstock concentration, catalyst cost, and WHSV were all considered in a simple evaluation of the potential of these catalysts for MF production from an economic standpoint. The potential for hydrodeoxygenation of biomass to MFs can be most appropriately evaluated via comparison to corn fermentation to ethanol (EtOH), since EtOH is currently the most highly commercialized biofuel worldwide. Using a large EtOH plant as a model with 100 million gal/year capacity, the target production capacity for MFs was set to 76.3 million gal/yr utilizing the difference in combustion energy between EtOH and a model MF, 2-pentanol.[29] After these considerations, Co/TiO_2 is still the lowest-cost catalyst with a projected cost of $1.63 million as shown in Figure 2.13. Pd-Ag/WO_x-ZrO_2 is the second least expensive catalyst at $13.5 million due to the low loading of Pd used (0.5 wt%), the high feed concentration (60 wt%), and the higher WHSV (1.17 hr^{-1}). An EtOH plant of this size has a reported capital cost

of $167 million thus the projected cost of Co/TiO_2 is comparatively negligible, while most Pt based catalysts are more expensive than an entire EtOH plant.[29] EtOH plants also require intensive separations to remove water from the EtOH, accounting for approximately 80% of the energy demand of the entire plant.[30] By comparison, separation of C_5-C_6 monofunctionals from water as they are largely insoluble in water, suggesting a lower cost for this separation step.

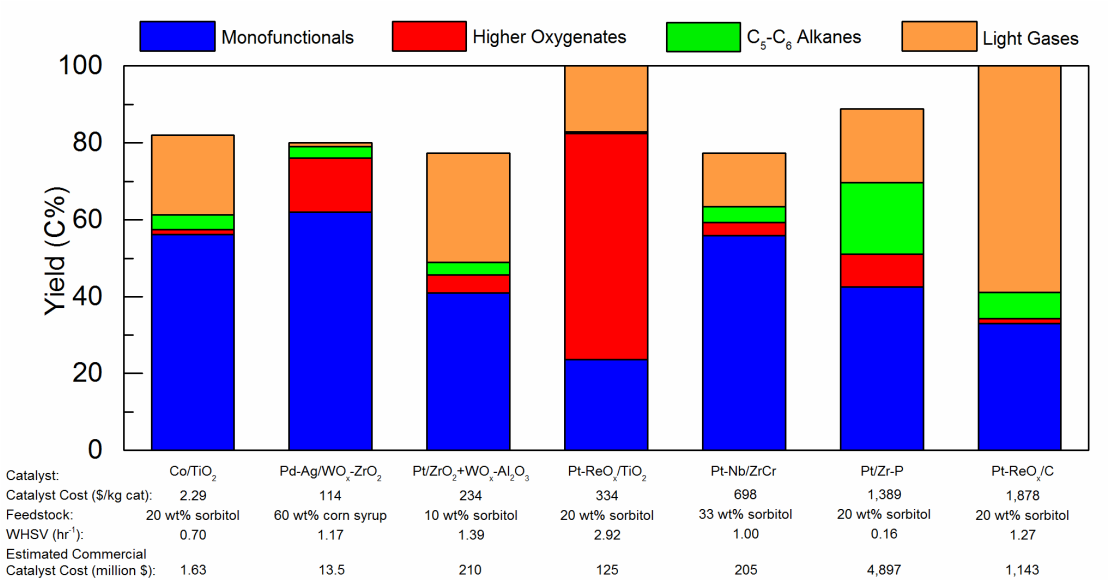

Figure 2.13 | **Comparison of production distribution from APHDO of sorbitol over Co/TiO_2 with catalysts from literature.** Data provided at conditions for maximum MF yield from the following sources: Pd-Ag/WO_x-ZrO_2,[28] Pt/ZrO_2+WO_x/Al_2O,[7] Pt-ReO_x/TiO_2,[11] Pt-Nb/ZrCr,[12] Pt/Zr-P,[3] Pt-ReO_x/C.[3]

2.5 Conclusions

With catalyst cost no longer a concern for this technology, the goals moving forward should be primarily to improve catalyst stability and increase C_{5+} MF yields. At a 60% C yield to MFs, a large portion of carbon is lost to low-value gases. A 2015 study performed by the National Renewable Energy Laboratory (NREL) suggested that low yields were the key limitation in their technoeconomic analysis of a similar process which considered the production of fuels using corn stover as a raw feedstock with multiple pretreatment/hydrolysis steps prior to APHDO.[31] In the NREL study the non-enzymatic conversion cost represented 93% of the overall conversion cost,

thus APHDO efficiency is critical. The NREL study presented a target of 85.6% carbon efficiency in the conversion of hydrolysis products to heavy hydrocarbons (i.e. APHDO followed by coupling chemistries) to obtain a fuel with a minimum selling price below $5/GGE. To reach this goal, a more fundamental understanding of the relative rates of competing reactions in the sorbitol APHDO pathway must be obtained.

2.6 References

1 Eagan, N. M., Chada, J. P., Wittrig, A. M., Buchanan, J. S., Dumesic, J. A. & Huber, G. W. Hydrodeoxygenation of Sorbitol to Monofunctional Fuel Precursors over Co/TiO2. *Joule* **1**, 178-199, (2017).

2 in *Kirk-Othmer Encyclopedia of Chemical Technology*.

3 Kim, Y. T., Dumesic, J. A. & Huber, G. W. Aqueous-phase hydrodeoxygenation of sorbitol: A comparative study of Pt/Zr phosphate and Pt-ReO_x/C. *J. Catal.* **304**, 72-85, (2013).

4 Li, N. & Huber, G. W. Aqueous-phase hydrodeoxygenation of sorbitol with Pt/SiO_2–Al_2O_3: Identification of reaction intermediates. *J. Catal.* **270**, 48-59, (2010).

5 Vilcocq, L., Cabiac, A., Especel, C., Guillon, E. & Duprez, D. Transformation of sorbitol to biofuels by heterogeneous catalysis: Chemical and industrial considerations. *Oil Gas Sci. Technol.* **68**, 841-860, (2013).

6 Li, N., Tompsett, G. A. & Huber, G. W. Renewable high-octane gasoline by aqueous-phase hydrodeoxygenation of C_5 and C_6 carbohydrates over Pt/zirconium phosphate catalysts. *ChemSusChem* **3**, 1154-1157, (2010).

7 Vilcocq, L., Koerin, R., Cabiac, A., Especel, C., Lacombe, S. & Duprez, D. New bifunctional catalytic systems for sorbitol transformation into biofuels. *Applied Catalysis B: Environmental* **148**, 499-508, (2014).

8 Vilcocq, L., Cabiac, A., Especel, C., Lacombe, S. & Duprez, D. Hydrocarbon fuel synthesis from sorbitol over bifunctional catalysts: Association of tungstated titania with platinum, palladium or iridium. *Catal. Today* **242**, 91-100, (2015).

9 Kunkes, E. L., Simonetti, D. A., West, R. M., Serrano-Ruiz, J. C., Gärtner, C. A. & Dumesic, J. A. Catalytic conversion of biomass to monofunctional hydrocarbons and targeted liquid-fuel classes. *Science* **322**, 417-421, (2008).

10 West, R. M., Kunkes, E. L., Simonetti, D. A. & Dumesic, J. A. Catalytic conversion of biomass-derived carbohydrates to fuels and chemicals by formation and upgrading of mono-functional hydrocarbon intermediates. *Catal. Today* **147**, 115-125, (2009).

11 Duan, J., Kim, Y. T., Lou, H. & Huber, G. W. Hydrothermally stable regenerable catalytic supports for aqueous-phase conversion of biomass. *Catal. Today* **234**, 66-74, (2014).

12 Shen, W., Liu, A. & Turbeville, W. Hydrodeoxygenation catalyst. US9278346 B2 (2012).

13 Vilcocq, L., Cabiac, A., Especel, C., Lacombe, S. & Duprez, D. Study of the stability of Pt/SiO_2–Al_2O_3 catalysts in aqueous medium: Application for sorbitol transformation. *Catal. Commun.* **15**, 18-22, (2011).

14 Besson, M. & Gallezot, P. Deactivation of metal catalysts in liquid phase organic reactions. *Catal. Today* **81**, 547-559, (2003).

15 van Haasterecht, T., Ludding, C., de Jong, K. & Bitter, J. Stability and activity of carbon nanofiber-supported catalysts in the aqueous phase reforming of ethylene glycol. *Journal of Energy Chemistry* **22**, 257-269, (2013).

16 Greeley, J. Structural effects on trends in the deposition and dissolution of metal-supported metal adstructures. *Electrochim. Acta* **55**, 5545-5550, (2010).

17 Shabaker, J., Simonetti, D., Cortright, R. & Dumesic, J. Sn-modified Ni catalysts for aqueous-phase reforming: characterization and deactivation studies. *J. Catal.* **231**, 67-76, (2005).

18 Lee, J., Burt, S. P., Carrero, C. A., Alba-Rubio, A. C., Ro, I., O'Neill, B. J., Kim, H. J., Jackson, D. H., Kuech, T. F., Hermans, I., Dumesic, J. A. & Huber, G. W. Stabilizing cobalt catalysts for aqueous-phase reactions by strong metal-support interaction. *J. Catal.* **330**, 19-27, (2015).

19 Huber, G. W., Cortright, R. D. & Dumesic, J. A. Renewable alkanes by aqueous-phase reforming of biomass-derived oxygenates. *Angew. Chem. Int. Ed.* **43**, 1549-1551, (2004).

20 West, R. M., Braden, D. J. & Dumesic, J. A. Dehydration of butanol to butene over solid acid catalysts in high water environments. *J. Catal.* **262**, 134-143, (2009).

21 Baker, R., Prestridge, E. & Garten, R. Electron microscopy of supported metal particles II. Further studies of Pt/TiO_2. *J. Catal.* **59**, 293-302, (1979).

22 Iglesia, E. Design, synthesis, and use of cobalt-based Fischer-Tropsch synthesis catalysts. *Appl. Catal. A-Gen.* **161**, 59-78, (1997).

23 Hanaor, D. A. H. & Sorrell, C. C. Review of the anatase to rutile phase transformation. *J. Mater. Sci.* **46**, 855-874, (2011).

24 Sadasivan, S., Bellabarba, R. M. & Tooze, R. P. Size dependent reduction–oxidation–reduction behaviour of cobalt oxide nanocrystals. *Nanoscale* **5**, 11139-11146, (2013).

25 Voorhees, P. W. The theory of Ostwald ripening. *Journal of Statistical Physics* **38**, 231-252, (1985).

26 Bartholomew, C. H. Mechanisms of catalyst deactivation. *Appl. Catal. A-Gen.* **212**, 17-60, (2001).

27 Mineral commodity summaries 2016. (U. S. Geological Survey, Washington, 2016).

28 Blommel, P., Dally, B., Lyman, W. & Cortright, R. Method and systems for making distillate fuels from biomass. US20120198760 A1 (2012).

29 Drapcho, C. M., Nhuan, N. P. & Walker, T. H. *Biofuels engineering process technology*. 129 (McGraw-Hill New York, NY, USA:, 2008).

30 Mei, F. *Mass and energy balance for a corn-to-ethanol plant* Master of Science thesis, Washington University, (2006).

31 National Renewable Energy Laboratory, U.S. Department of Energy. Dilute-acid and enzymatic deconstruction of biomass to sugars and catalytic conversion of sugars to hydrocarbons (2015).

Chapter 3. Chemistries and Processes for the Conversion of Ethanol to Middle-Distillate Fuels

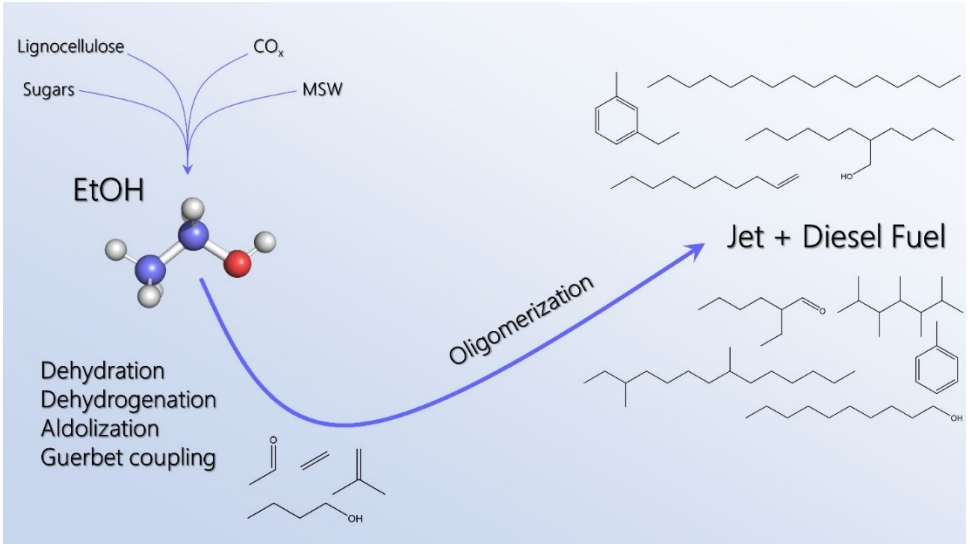

Figure 3.1 | **Conversion of ethanol to distillate-range hydrocarbons and oxygenates.**[1] Ethanol can be sourced from a variety of abundant and renewable feedstocks, suggesting it has potential as a renewable platform molecule for distillate fuel production. After initial functionalization via a combination of dehydration, dehydrogenation, aldolization, or Guerbet coupling, full-range oligomerization can take place to produce hydrocarbons and oxygenates in the middle-distillate range, C_8-C_{22}. Chapter adapted from Ref 1.

3.1 Introduction

The most prominent biofuel in the US and around the world is ethanol (EtOH), accounting for 86% of biofuels produced in the US in 2018.[2,3] Most EtOH is produced by fermenting sugars derived from corn starch or sugar cane, with non-food-lignocelluloses becoming increasingly popular alternative feedstocks. EtOH has also been produced by enzymatic or thermocatalytic upgrading of syngas derived from industrial waste gases (for example, from steel mills) or gasification of municipal solid waste.[4] The status of cellulosic EtOH and suggestions to improve its profitability have been discussed in depth elsewhere.[4-7] Most EtOH currently used in the US is blended with gasoline at levels up to about 10%, which is lower than the levels commonly used in Brazil (near 27%), where pure EtOH and aqueous EtOH (~5% H_2O, near the H_2O–EtOH

azeotrope) are also used.[8] Adding EtOH to gasoline is beneficial in terms of increasing the octane number and decreasing CO and hydrocarbon emissions.[9,10] However, the blend also has a lower energy density, increased H_2O solubility (which can lead to corrosion) and higher CO_2 emissions in spark-ignition engines relative to gasoline. EtOH has also been blended into diesel at levels of 10–20%, but there are problems associated with the constituents being physically very different in several ways such as miscibility and volatility.[10-12]

Given the firm establishment of EtOH production from biomass and continuing commitments to its development, EtOH may be a promising candidate as a platform molecule for distillate fuels if technologies can be developed which enable its conversion to C_8-C_{22} compounds. Such technologies would conceivably rely on one of two C-C bond-forming chemistries: olefin oligomerization (acid- or metal-catalyzed) and aldolization (acid- or base-catalyzed). Figure 3.2 summarizes how these chemistries can be combined with dehydration, hydrogenation/dehydrogenation, and ketonization to convert EtOH to middle-distillate compounds. Some of these processes yield hydrocarbon mixtures similar to conventional fuels, while some yield oxygenates which may require further processing such as hydrodeoxygenation before they can be used in fuels.

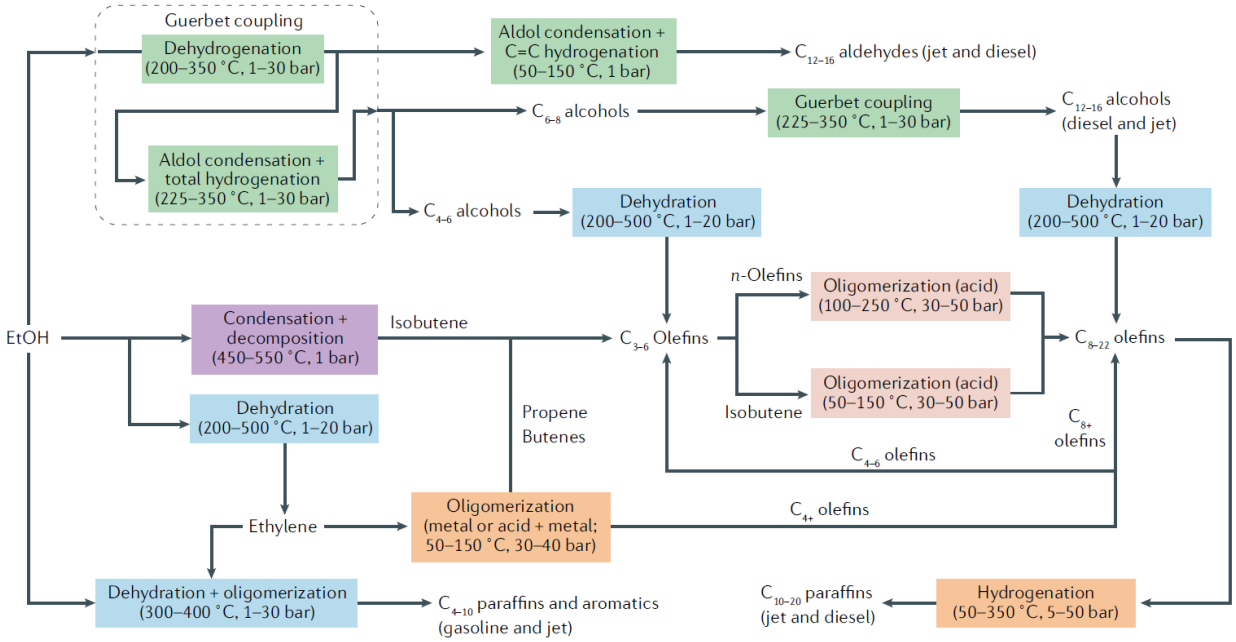

Figure 3.2 | **Pathways for the conversion of EtOH into middle-distillate fuels.** The top pathway involves either dehydration or dehydrogenation. Dehydrogenation affords acetaldehyde, which is used as a reactant in a subsequent reactor or is directly converted through condensation mechanisms, such as in Guerbet coupling to higher alcohols or condensation and decomposition to isobutene. The bottom process — dehydration and olefin oligomerization —affords heavy olefins, paraffins, and aromatics. These reactions can be mediated by metal or acid catalysts, while the aldol condensation typically requires acid or base catalysts. Overall, these pathways here afford hydrocarbons (paraffins and aromatics) and oxygenates (alcohols and aldehydes) in the middle-distillate range (C_8–C_{22}).

In this chapter, these chemistries will be discussed in context to provide a framework for EtOH-to-distillate (ETD) conversion pathways with new guiding insights into promising research areas for the general advancement of the concept. The processes described are in different stages of technological readiness and some have seldom been mentioned prior to the review we have written which this chapter is based upon.[1] In order to provide proper context for these technologies, the general properties of diesel and jet fuels will first be described.

3.2 Properties of middle-distillate fuels and fuel-range oxygenates

Middle distillates represent the fraction of refined petroleum between gasoline and heavy fuel oil and traditionally have little or no O content. Key fuel properties which are dependent on the bulk composition include: density, energy content, cold flow properties, boiling point/distillation curves, flash point, and cetane number (for diesel). Relevant values are presented in Table 3.1 alongside those of various hydrocarbons and oxygenates. Other important properties of fuels include lubricity, stability, corrosivity, cleanliness, and electrical conductivity, but these are typically governed by trace impurities rather than the bulk constituents.[13]

Table 3.1 | **Fuel-related properties of petroleum-derived fuels compared to various hydrocarbons and oxygenates.**

Fuel/Compound	Carbon range	Net heating value (MJ kg^{-1})	Net heating value (MJ L^{-1})	Density (g mL^{-1})	Freezing point (°C)	Boiling point (°C)	Flash point (°C)	Max aromatic content (vol%)	Cetane
gasoline	4-12	43.3	31.8	0.735	-	40-215	-45	35	-
jet (A-1)	8-16	42.9	34.1	0.808	< -47	140-300	>38	25	-
diesel (#2-D)	10-22	42.6	36.2	0.850	-17[a]	170-370	>52	35	> 40
ethanol	2	26.8	21.1	0.789	-114	78	13	-	8
1-butanol	4	33.2	26.9	0.810	-90	117	29	-	19
diethyl ether	4	33.7	24.1	0.713	-116	35	-45	-	150
n-octane	8	44.4	31.0	0.699	-57	126	13	-	64
1-octene	8	44.2	31.6	0.715	-102	123	10	-	41
p-xylene	8	40.8	35.2	0.861	13	138	27	-	-13
ethylbenzene	8	41.0	35.5	0.867	-95	136	18	-	8
1-octanol	8	37.7	31.2	0.827	-16	195	81	-	39
2-ethyl-1-hexanol	8	37.7	31.4	0.834	-70	182	73	-	26
2-ethylhexanal	8	36.9	31.6	0.854	-85	163	46	-	59
di-*n*-butyl ether	8	38.0	29.2	0.768	-95	142	25	-	90
1-decanol	10	38.7	32.2	0.830	7	230	108	-	50
1-dodecanol	12	39.5	32.8	0.830	24	250	120	-	64
di-*n*-hexyl ether	12	39.7	31.4	0.790	-43	226	77	-	117
di-*n*-octyl ether	16	40.6	32.6	0.806	-8	287	110	-	118

Fuel data compiled from various sources.[13-19] Jet A-1 is the most common civilian jet fuel used internationally. Other jet fuels such as Jet A (commonly used as U.S. civilian fuel) and JP-5 (U.S. Navy fuel) possess higher minimum freezing points (-40°C and -46°C, respectively). The listed diesel freezing point is its cold filter plugging point. Pure compound thermodynamic data collected from HSDB, ILO-ICSC, and Yaws.[20-22] Flash points are closed-cup. Heating values estimated by subtracting enthalpies of vaporization from enthalpies of combustion calculated using data from Yaws. Cetane from Yanowitz et al., Saldana et al., and Nel and de Klerk.[23-25]

Jet fuels such as kerosene or wide-cut fuels consist primarily of C_8–C_{16} hydrocarbons in the form of isoparaffins and naphthenes, along with up to 25% aromatics.[18] Branched paraffins have lower freezing points than do linear paraffins, which have poor cold flow properties and are thus less amenable for use as jet fuels (Jet A has a maximum freezing point of −40°C). The presence of

aromatic groups is beneficial for lubricity and volumetric energy content but leads to the formation of carbonaceous deposits following combustion in jet engines.[26] Naphthenes have moderate energy content combined with excellent combustion and flow properties. Flash point and boiling point are also important specifications of a jet fuel, although the values required can vary depending on the application. A fuel must have a flash point of at least 38°C to be classified as Jet A-1, although fuel used by the US Navy (JP-5) must have a flash point of at least 60°C to satisfy stricter safety requirements. The distillation curve generally spans the range 140–300°C, although this range may be narrowed further depending on the application. From an energetic standpoint, aviation fuels have a higher volumetric energy density (net heating value = 34.1 MJ L^{-1}) than does gasoline (31.8 MJ L^{-1}). In general, jet fuel specifications are stricter than those of gasoline or diesel, which are typically more regionally determined.

One major challenge in producing renewable jet fuel for commercial applications is the extensive testing mandated by ASTM International (an international standards organization). ASTM standard D7566 describes the specifications for synthetic hydrocarbon fuels approved for use in jet applications.[27] At present, the specifications cover isoparaffins derived from hydroprocessing of fermented sugars (SIP) as well as paraffinic kerosene (SPK) derived from Fischer–Tropsch synthesis (FT-SPK), hydroprocessing of fatty acids and fatty acid esters (HEFA-SPK), and alcohol dehydration and oligomerization (ATJ-SPK). These and similar fuels have been the subject of several technoeconomic analyses, life-cycle assessments, and technological status evaluations.[28-33] Initially, the ASTM standard for ATJ-SPK only considered isobutanol as a feedstock, in particular the biomass-derived isobutanol[27] produced by Gevo, a renewable chemicals and advanced biofuels company. In 2018, the standard was updated to also include ATJ-SPK chemicals derived from EtOH. According to the ASTM D4054 standard, the validation of a

synthetic jet fuel is an iterative process that consists of a series of tests on sequentially larger volumes of fuel.[34] Specification tests (up to 10 gallons) are followed by fit-for-purpose tests (10–100 gallons), component and rig tests (250–10,000 gallons), and finally engine tests (225,000 gallons). Certification therefore can only be accomplished for processes that are proven on scales far larger than those achievable in the lab, and the fuel must still conform to the specifications in ASTM D7566.[35] These tight requirements may require modification of the standards in coordination with ASTM. The validation process has been applied to an EtOH-derived jet fuel produced by LanzaTech, a company that produces the required EtOH through fermentation of waste. This process will be discussed in further detail in future sections.

Diesel is the heavier fraction of middle-distillates and consists predominantly of C_{10}–C_{22} lightly-branched paraffins and naphthenes. In the US, diesel also comprises up to 35% aromatics, with the percentage differing from region to region. Although aromatics have high volumetric energy densities and enhanced cold flow properties, their combustion in diesel engines is typically slow, and this is reflected in their low cetane numbers (CNs). The minimum CNs for diesel fuel in the US and Europe according to standards ASTM 975 and EN590 are 40 and 51, respectively.[16,36] High CNs are desirable and are easily obtained when using fuels rich in C_{10+} linear paraffins, though these compound have poor cold flow properties for low-temperature applications. Relative to linear paraffins, naphthenes have lower CNs but improved cold flow properties.

A comparison of experimental CNs for various isoparaffins (branched alkanes) suggests that modest values (>35) can still be obtained if, as a first approximation, at least 70% of the C atoms are in the main chain. This percentage is only a crude estimation because specific structural properties, such as chain position and length, also contribute to CN. There now exist quantitative structure–property relationships, often derived from artificial neural networks, which allow one to

predict fuel properties such as flash point and cetane from the molecular structures of hydrocarbons and oxygenates.[24,37-40] Additionally, a compound in a mixture will generally contribute to the overall CN in line with its mole fraction.[41] The minimum flash point for diesel in the US is 54°C, which is based on safety rather than engine performance considerations. The boiling point range of diesel (170–370°C) is generally wider than that for jet fuel but will again depend on region. Diesel is more energetically dense (36.2 M J L^{-1}) than is jet fuel or gasoline, but the order is reversed when considering energy per unit mass.

Although petroleum-derived fuels are essentially oxygen-free, oxygenates have been used as additives or in some cases as drop-in replacements. Prominent oxygenates include EtOH and methyl *tert*-butyl ether (MTBE) for light-duty applications as well as fatty-acid methyl esters, which constitute biodiesel.[42,43] Jet fuels containing oxygenates have not yet been developed, and a C:O ratio of >13:1 is reportedly required for any molecule used in a jet fuel blend.[43] Relative to hydrocarbons, oxygenates typically have lower energy densities, higher aqueous solubilities, higher corrosiveness, higher melting points, and lower volatilities. Moreover, aldehyde and ketone functional groups are particularly problematic because they often lead to gum formation.[44] At the light end of middle-distillate fuels, C_8 oxygenates have ~15% lower energy density on a mass basis relative to *n*-octane (as one might expect from the former being more oxidized) but are more similar on a volumetric basis. To reach the energy density of a middle-distillate fuel, a mono-oxygenate must have approximately 16 or more C atoms. Larger molecules (especially linear ones) also typically have higher CNs, an added benefit for diesel applications. However, linear alcohols of this size have poor cold-flow properties, with C_{12+} *n*-alcohols being solids at room temperature. Therefore, branched alcohols such as 2-butyl-1-octanol and ethers such as di-*n*-hexyl ether may be more suitable oxygenates for fuel applications. Although branched alcohols have lower CNs

than their linear counterparts, C_{8+} ethers of *n*-alcohols have desirable values (>100) well above the requirements of a diesel fuel[25]—this will be particularly important in motivating the work in Chapter 5. The combustion of oxygenates also produces lower particulate emissions relative to conventional fuels.[43] If ETD routes afford useful fuel oxygenates they might be blended directly without the need for additional catalytic steps to convert them to hydrocarbons.

In the following sections, the ETD routes shown in Figure 3.2 and their underlying chemistries will be described. This will be followed by a comparison of the routes and the research required to improve the viability of each strategy. First the most heavily studied strategy is discussed: EtOH dehydration followed by olefin oligomerization.

3.3 Ethanol dehydration to ethylene

The past century has seen growing interest in the conversion of EtOH to ethylene over heterogeneous catalysts,[45,46] a process that is topical from mechanistic, catalytic, and industrial perspectives.[47-49] Unimolecular EtOH dehydration to ethylene is an endothermic reaction ($\Delta H° = \Delta H_{25°C} = 45.3$ kJ mol^{-1}) and is traditionally carried out at temperatures between 200 and 500 ºC. This and all following thermodynamic calculations are performed using tabulated data unless specified otherwise.[22] Diethyl ether (DEE) is the main side-product in ethylene production below 300°C, formed from the exothermic bimolecular dehydration of EtOH ($\Delta H° = -12.2$ kJ $\text{mol}_{\text{EtOH}}^{-1}$). Although DEE is the thermodynamic product at room temperature ($\Delta G°_{\text{ethylene}} = 7.8$ kJ $\text{mol}_{\text{EtOH}}^{-1} > \Delta G°_{\text{DEE}} = -7.2$ kJ $\text{mol}_{\text{EtOH}}^{-1}$), ethylene becomes more favorable at higher temperatures (>~130°C) on account of entropy. DEE has been proposed as a diesel fuel additive largely due to its desirable compression–ignition properties, as reflected in its cetane number near 150.[50] However, concerns over its use as a fuel include its health impacts, propensity to oxidize to explosive peroxides, low energy density, low boiling point, and low flash point. 1,1-

Diethoxyethane has similarly been proposed as a diesel additive, but also suffers from a low flash point and energy density.[51] In general, alcohol dehydration at lower temperatures often affords ethers, while higher temperatures lead to sequential reactions affording aromatics and paraffins.

There is continued debate as to whether ethylene is produced directly from EtOH, indirectly from the diethyl ether, or through both routes simultaneously. Nonetheless, the direct route is typically assumed to be dominant and can occur through three competitive elimination reaction mechanisms, namely E1, E2, and $E1_{cB}$ (Figure 3.3). The E1 reactions is a unimolecular elimination that involve protonation of the alcohol, a rate-limiting C-O cleavage to generate H_2O and $C_2H_5^+$, and β-H^+ elimination to yield ethylene. E2 elimination occurs through simultaneous cleavage of the C-O bond (abstraction of OH^- by an acid) and β-H^+ cleavage (abstraction by a base). Lastly, in the $E1_{cB}$ reaction, β-H^+ abstraction occurs first, with the resulting carbanion intermediate undergoing C-O cleavage. Originally detailed in 1968, the E2 mechanism is most commonly accepted for the dehydration of aliphatic alcohols over Al_2O_3.[52] More recent DFT calculations with the model Lewis acid Al_8O_{12} support this conclusion in the case of EtOH, for which the E1 transition state is less energetically accessible than the E2 transition state.[53] Notably, the latter has some carbenium character, and the activation barriers for more highly substituted alcohols are consequently lower. However, the E1 mechanism involves an alkoxy intermediate with strong carbenium character, leading to a higher energy barrier for the first step. The transition state structures and relative energetics calculated using Al_8O_{12} are generally valid for other Lewis acidic materials,[54,55] while those with more Brønsted acidic character, such as zeolites, are better able to stabilize transition states with strong carbenium character. In the presence of these Brønsted acids both E1 and E2 pathways are viable,[56-59] with the E_{1cB} pathway only being possible in the

presence of strongly basic materials.[60,61] Dehydration is often in competition with dehydrogenation with these basic materials.

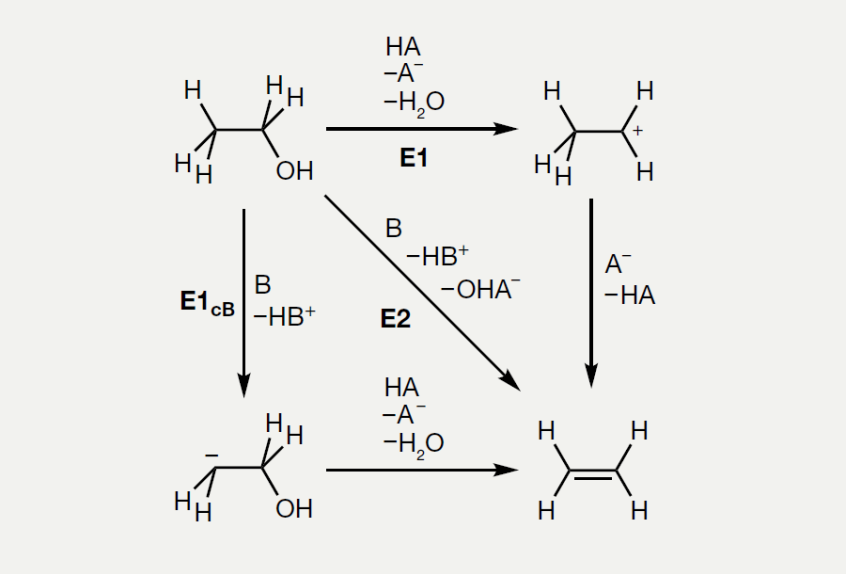

Figure 3.3 | **The possible elimination mechanisms of EtOH dehydration.** The E1 elimination mechanism involves protonation by a generic acid HA, C-O cleavage to generate a carbenium ion, and β-H^+ elimination. In the bimolecular E2 elimination, β-H^+ abstraction and C-O cleavage occur simultaneously over acid-base pairs in a concerted manner. The unimolecular conjugate base $E1_cB$ elimination first features β-H^+ abstraction to afford a carbanion, which undergoes C-O cleavage to afford ethylene.

EtOH dehydration has been extensively studied over solid acids including pure and modified Al_2O_3, molecular sieves, and heteropoly acids.[46,52,62-73] Typical catalysts and conditions used in EtOH dehydration are outlined in Table S3.1. The first catalysts used for commercial purposes were supported phosphoric acid materials that suffer from deactivation through coking.[48] Al_2O_3 undergoes deactivation more slowly and its modified derivatives in particular have been studied extensively.[47] Today, Al_2O_3-based catalysts such as Al_2O_3–MgO/SiO_2 (the SynDol catalyst) are among the most common dehydration catalysts for industrial ethylene production from EtOH, typically utilized at temperatures up to 500ºC. Heteropoly acids, particularly those dispersed on high-surface-area supports, have also gained attention owing to their high acidities. For example, $H_3[PW_{12}O_{40}]$ on SiO_2 affords >98% ethylene yield at temperatures between 170–

190ºC, while nearly 100% ethylene yields have been achieved using $H_4[W_{12}SiO_{40}]$ on the porous silicate MCM-41.[74,75] As with the phosphoric acids, these catalysts are prone to coking and can only be oxidatively regenerated at low temperatures when doped with metals capable of promoting combustion.[76]

Dehydration of aqueous EtOH has also been studied. EtOH is commonly produced in fermentation broths at concentrations typically in the range 5–12 wt%. Intensive purification is required to obtain pure EtOH streams from fermentation,[77] particularly if purities above 95 wt% (the H_2O–EtOH azeotrope) are required. Pure EtOH is most commonly obtained using molecular sieves to dry an ~92% EtOH solution obtained through distillation.[78] In 1989 the BioEtOH-to-Ethylene (B.E.T.E.) process was developed to dehydrate fermentation broths over CF_3SO_3H supported on the SiO_2-rich surface of the zeolite H-ZSM-5.[79] This high-yielding method proved useful for a range of aqueous EtOH concentrations (2–19v/v%) with a catalyst stable up to 200°C at atmospheric pressure. Kinetic studies for the dehydration of aqueous EtOH (0–20v/v%) over H-ZSM-5 have been performed at temperatures ranging from 140–200°C.[68] Even though the zeolite first undergoes deactivation due to coke formation, the presence of H_2O allows for a subsequent increase in activity and ethylene selectivity[68,80] attributed to the H_2O perhaps modifying the acid sites and suppressing further coking. Industrially, EtOH dehydration is most commonly performed using feeds with concentrations near the H_2O–EtOH azeotrope.[48,49] In 1981, Scientific Design Company, Inc. reported the development and use of the Syndol catalyst for the conversion of EtOH to ethylene.[64] They used an isothermal reactor, in which a 95v/v% EtOH feed was converted at 450°C to afford 98.9 mol% ethylene yield. The catalyst proved robust enough such that it lasted a year before regeneration was necessary. An economic analysis based on the production of 50,000 metric tons per year of polymer-grade ethylene indicated that using multi-stage adiabatic reactors

to recycle heat to drive the endothermic dehydration would be more efficient than isothermal reactors. Using two adiabatic reactors in series, a feed containing EtOH (25 wt% in steam, 450–500°C, 11.25 atm total inlet pressure) gave a 99.3% ethylene yield. With the same catalyst, Chematur Engineering AB took this a step further by using four tubular adiabatic reactors in series.[81] Here, the 95% EtOH feed is dehydrated at 99% conversion and 96.8% ethylene selectivity, with the product mixture being quenched, washed with caustic (NaOH), and dried (with molecular sieves) to obtain polymer-grade ethylene. Chematur produces 5,000–200,000 metric tons ethylene per year, and the Brazilian petrochemical company Braskem operates a plant on a comparable scale (200,000 metric tons per year), which in 2010 began converting sugarcane-derived EtOH to ethylene, most of which is for polymer synthesis.[82] For perspective, this capacity is approximately one-tenth that of a conventional ethane steam-cracking plant used for ethylene production.[47] Other noteworthy EtOH dehydration technologies include the Petron Scientech process,[83] the Atol technology,[84] and the Hummingbird technology,[85,86] which each operate on 20,000–400,000 metric tons per year scales and utilize proprietary catalysts. The commercialization of EtOH dehydration to ethylene by multiple companies suggests that this is not the limiting step in ETD technologies. Rather, it is the subsequent steps, including olefin oligomerization, that are typically more challenging.

3.4 Ethylene oligomerization through acid catalysis

Acid-catalyzed oligomerization of propene and butenes to produce gasoline emerged in the 1930s[87-89] and occurs predominantly through carbenium intermediates to afford a wide distribution of products. Ethylene first undergoes protonation to $C_2H_5^+$ by a Brønsted acid (Figure 3.4a), after which a C–C bond forms with another olefin. The slower rate of oligomerization for ethylene relative to C_{3+} olefins reflects the instability of primary carbenium ions relative to secondary and

tertiary carbeniums. Following nucleophilic attack of the π-bond on a carbenium, other reactions such as rapid hydride and methyl shifts are commonly observed on solid acids and afford complex quasi-equilibrated mixtures of isomers. The formation of isobutene through this mechanism is slow, however, as it involves the formation of a primary carbenium. Olefin cracking occurs via the reverse mechanism, which illustrated in the case of 3-ethylhex-3-ene in Figure 3.4b. Oligomers can therefore be produced directly using 'true' oligomerization or indirectly by cracking larger oligomers. Propene oligomerization over 1D zeolites (MOR, TON) and mesoporous acids (MCM-41, SiAl, HPW, HSiW) at 230°C has recently been shown to yield predominantly true oligomers a conversion as high as 10%.[90] As the conversion of an oligomerization reaction increases, there increasing rearrangement and cracking decreases the fraction of 'true' oligomerization products. However, when using 3D zeolites as catalysts (BEA, MFI, FAU), the observed oligomers are predominantly cracking products at all conversions. This has been rationalized in terms of cross-sectional fluctuations of the structures enabling the formation of heavy oligomers which cannot diffuse out through the narrow channels without first cracking. When catalyzed using a variety of solid acids, olefin isomerization is sufficiently rapid to produce equilibrated mixtures of skeletal and regioisomers over the range of 200–260°C even at low conversions (<5%), and the limitations on diffusion imposed by the framework likely affect the observed product distributions.

Carbenium chemistry also gives rise to cyclic species, which form especially at high temperatures by intramolecular attack of a carbenium centre on a π-bond (Figure 3.4c).[91,92] The requisite olefin bearing a carbenium must come from hydride abstraction from an alkene, which on purely acidic catalysts such as H-ZSM-5 must occur through intermolecular transfers because these materials do not process H_2.[93,94] A linear olefinic carbenium of sufficient size (C_{5+}) can then cyclize to give a naphthene cation, which can deliver H^+ to the catalyst and thus convert to a neutral

naphthene. Subsequent hydrogen transfer reactions lead to further unsaturation until aromatic species are formed (Figure 3.4c), the concomitant liberation of H_2 only being enabled by metals such as Ga and Zn.[93-95] Dehydrogenation on ZSM-5 materials is thought to be limited by the reacquisition of H atoms lost during C–H cleavage, not the C–H cleavage step itself. The predominant role of transition metal dopants is therefore to remove H atoms/ions from the surface by catalyzing their combination to produce H_2. Aromatic species produced through cyclization can also undergo alkylation (Figure 3.4d) as well as cracking to release olefin substituents; an understanding of this chemistry will be important in the later discussion of the alternative hydrocarbon pool mechanism.[96-99]

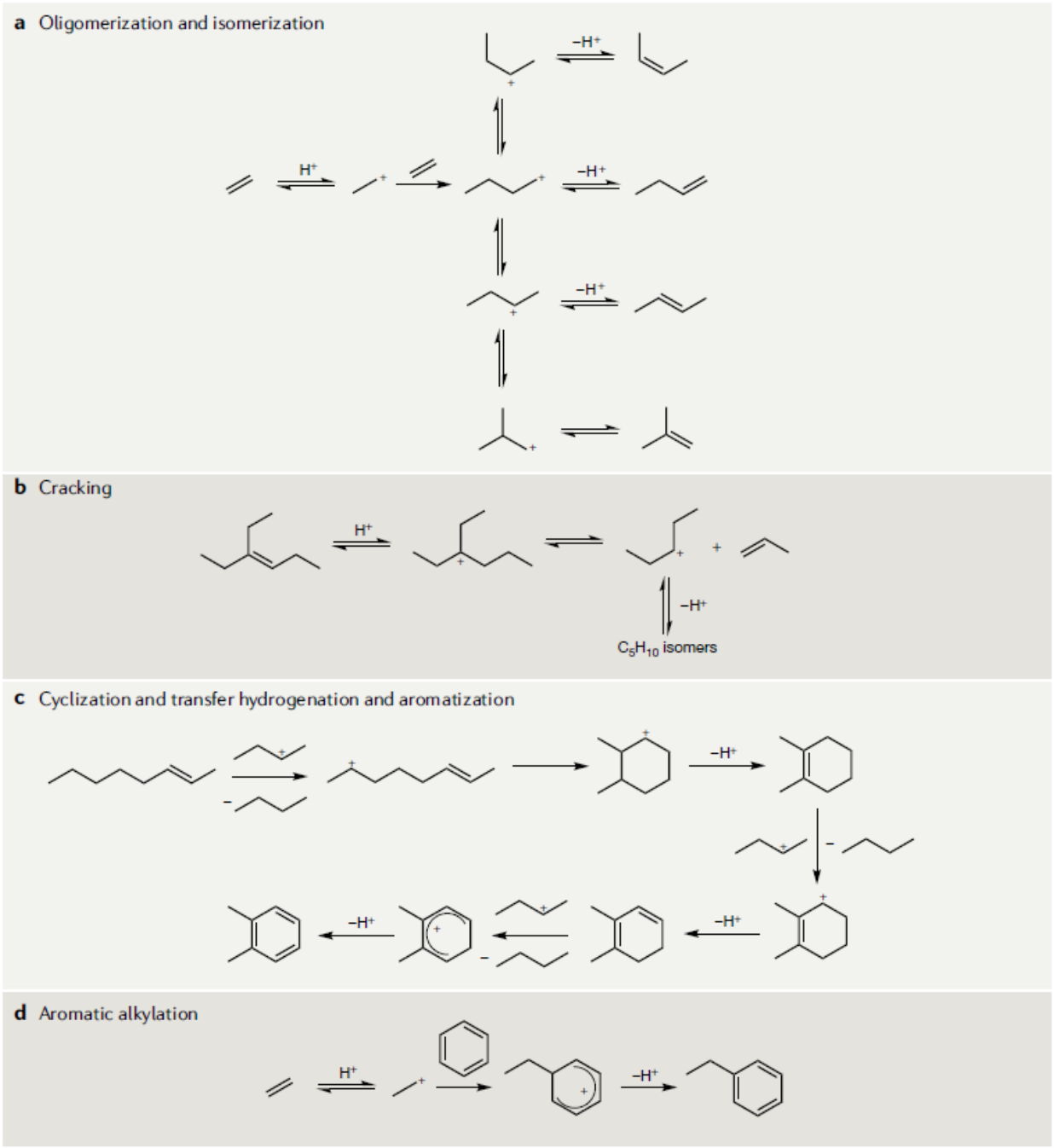

Figure 3.4 | **Carbenium chemistries involved in olefin conversion over solid acids. a** | Olefin oligomerization and isomerization is illustrated in the simple case of acid-catalyzed reactions between two ethylene molecules. **b** | Cracking of an olefin to smaller fragments is depicted here in the case of 3-ethylhex-3-ene, which can dissociate into propene and C_5H_{10} isomers. **c** | An olefin can undergo cyclization and transfer dehydrogenations to afford an aromatic product. This is exemplified in the conversion of 2-octene to *o*-xylene. **d** | Ethylene can be protonated to afford $C_2H_5^+$, which can participate in electrophilic aromatic substitution to give ethylbenzene.

Oligomerization and aromatization reactions are compared from a thermodynamic standpoint in Figure 3.5. Ethylene conversion on a 10 mole basis is considered for the following scenarios: oligomerization to light olefins (2-butene), oligomerization to heavy olefins (2-octene), aromatization with dehydrogenation to liberate H_2 alongside a mixture of aromatics (*o*-xylene) and olefins (2-butene), and aromatization accompanied by transfer hydrogenation to produce a mixture of aromatics (*o*-xylene) and paraffins (*n*-butane). The changes in Gibbs free energy for these four reactions (per mole ethylene) vary with temperature (Figure S3.1), and oligomerization is exothermic but has a negative entropy change that substantially contributes to overall Gibbs free energy changes. The formation of light olefins is thus more thermodynamically favorable than that that of heavy olefins at temperatures above 200°C. Further, under higher pressures the equilibrium product distribution shifts in favor of heavy olefins and one can kinetically promote oligomerization over cracking by encouraging intermolecular reactions. Aromatization is not substantially more thermodynamically favorable than is oligomerization. However, when the H_2 released in aromatization is used in the hydrogenation of other olefins, aromatization becomes thermodynamically preferred because the hydrogenation of olefins is highly exothermic (for example, $\Delta H° = -115.0$ kJ $\text{mol}_{\textit{trans}\text{-2-butene}}^{-1}$). Thermochemical data suggest that, in the absence of kinetic or steric restrictions, the moderately high temperatures (300–400°C) commonly used in acid-catalyzed ethylene oligomerization should afford mixtures of aromatics and light paraffins. Operating at lower temperatures and elevated pressures may enable the production of longer olefins if cyclization and transfer hydrogenation are sufficiently slow.

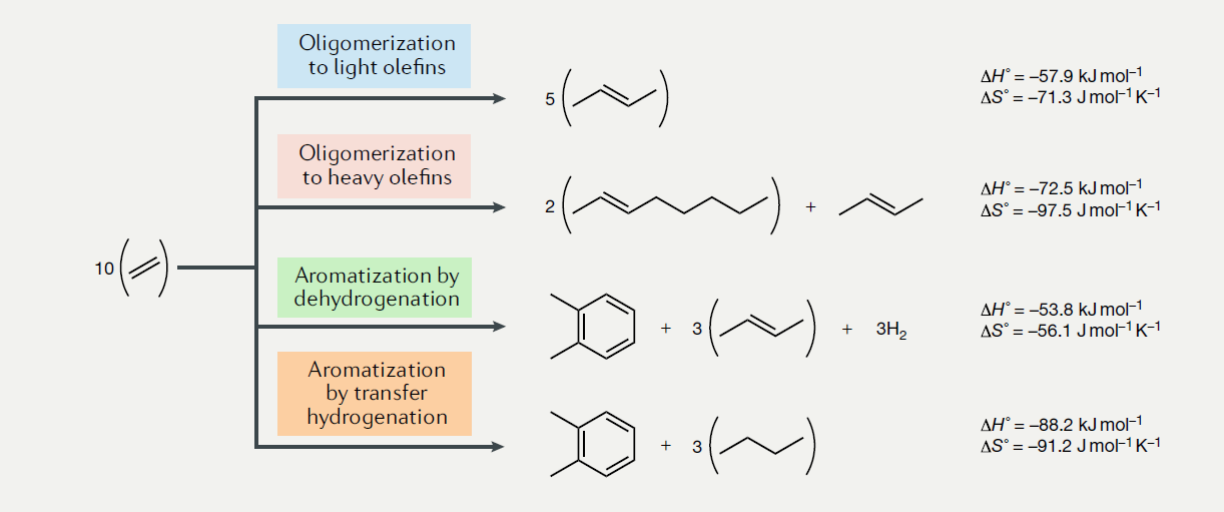

Figure 3.5 | **Thermodynamics of olefin oligomerization and aromatization.** The thermodynamics of four conversions of ethylene to heavier olefins are presented, as are the associated standard enthalpy and entropy changes per mole of ethylene.

Both EtOH dehydration and ethylene oligomerization are catalyzed by solid acids, thus the two reactions are more commonly performed in a single reactor than in series. EtOH dehydration is slower than ethylene oligomerization such that the reactor is typically held at temperatures above 300°C to promote the latter. The primary products of ethylene oligomerization are linear butenes that oligomerize more rapidly than does ethylene because their protonation can form secondary rather than primary carbenium ions.[56,100] In addition to oligomerization, butenes and C_{5+} olefins at these elevated temperatures undergo rapid side reactions including cracking, hydrogen transfer, and aromatization, with $C_{3–8}$ aliphatic paraffins and $C_{6–12}$ aromatics being the products.[101] The product distribution is reminiscent of a much more studied technology — the methanol-to-gasoline (MTG) process developed by Mobil in the 1970s as a means to convert natural gas to gasoline. Initiated in response to the 1973 oil crisis,[102,103] this process received considerable industrial attention, and a 14,500 barrels per day capacity plant was commercialized in New Zealand in 1985, though the MTG section of the plant was later shut down as oil prices declined (the methanol synthesis remained active).[104,105] The dehydration of methanol does not directly afford an olefin,

thus a number of mechanisms have been considered to describe the MTG process.[106] The most commonly accepted of these — the hydrocarbon pool mechanism (Figure 3.6) — has been adapted to also describe the EtOH conversion in an alternative mechanism to the sequential dehydration and oligomerization described above.[101,102]

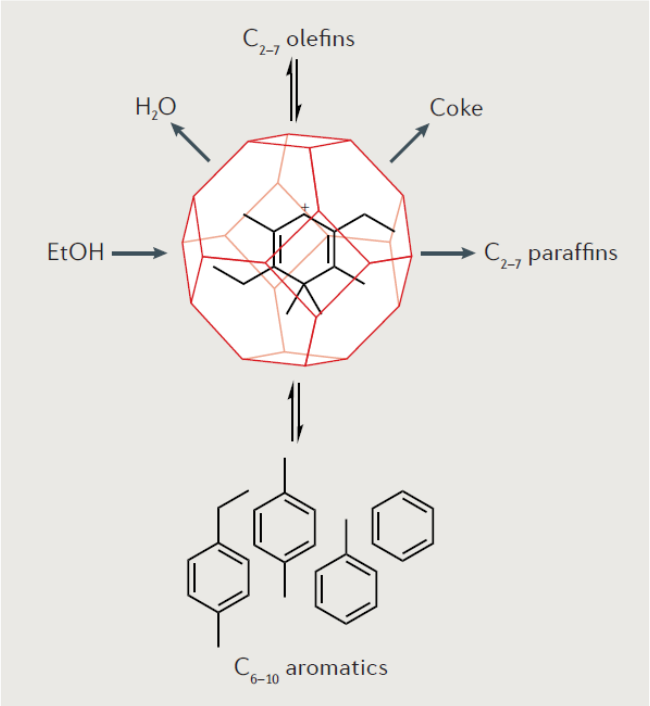

Figure 3.6 | **The hydrocarbon pool mechanism for EtOH transformation.** EtOH enters the acidic environment of zeolite pores, where it reacts directly with confined species rather than dehydrating directly to ethylene. Paraffins, olefins, and small aromatics that can diffuse out of the pores are observed in the product slate, whereas species that cannot escape are converted to coke.

The key feature of the hydrocarbon pool mechanism is the participation of confined cationic aromatic species as cocatalysts.[107-110] Alcohols and olefins directly alkylate these species, which either continue to grow and ultimately clog catalyst pores or fragment into olefins, paraffins, and aromatics small enough to diffuse out. Evidence of confined species has been obtained through analysis of the material trapped in catalyst pores after reaction with either methanol or EtOH.[111-113] Further, direct characterization of the compounds confined in catalyst pores has come from nuclear magnetic resonance (NMR) spectroscopy, which confirms the presence of cationic

aromatic species.[110,114,115] A recent report on EtOH conversion with ion-exchanged ZSM-5 catalysts using isotopically-labeled feeds suggests that EtOH dehydration is not essential for the production of heavier species — evidence that a hydrocarbon pool mechanism is more likely than sequential dehydration and oligomerization.[116] Although the dominant mechanisms by which EtOH is converted to heavier species is still debated, most studies accept ethylene as a key intermediate.[117-122] In reality, a combination of the two mechanisms — the dual-cycle concept[105,123] — is likely, and both mechanisms can explain the EtOH product distributions.

3.5 Combined dehydration and oligomerization of EtOH over solid acids

The conversion of EtOH over H-ZSM-5 to give liquid products has been extensively studied, and the effects that changing reaction parameters have on the product distribution are well-documented (Table S3.2).[101,117,122,124-127] The activity of H-ZSM-5 is strongly dependent on the Si:Al ratio, and when this exceeds 40:1 the material has lower catalytic activity. This is in part because the number of strong Brønsted acidic sites per unit cell decreases below 2 at ratios >40:1.[128] At Si:Al ratios >100:1, the number of sites per cell decreases below 1, and even lower activities are observed.[124,125,129] Zeolites with pores larger than H-ZSM-5, such as H-Y and H-β, undergo rapid coking and deactivation.[120] Coking is also rapid (but less so) over H-ZSM-5, such that only the dehydration product ethylene is observed after a few hours of continuous operation under most conditions. Following deactivation, one can recover catalytic activity by oxidizing the coke through high-temperature calcination. One way to slow down the deactivation process is the incorporation of metal ions into H-ZSM-5. The addition of Ga has been shown to both improve stability and liquid hydrocarbon yields (slightly).[130,131]

Regardless of the catalyst used, organic products that are liquids under ambient conditions are most selectively produced at temperatures in the range 300–400°C, below which small organics

are not converted and above which cracking and coking are extensive. Liquid yields up to ~50% can be achieved using H-ZSM-5 at atmospheric pressure and a few studies have noted that liquid yields approaching 80% can be achieved when using high pressures (20–50 bar).[129,132,133] The increased pressure does not have a large impact on oligomer size due to thermodynamic limitations, rapid cracking reactions, and pore geometry constraints. Regardless of the conditions utilized from the conversion of EtOH over H-ZSM-5, the liquid hydrocarbons produced are predominantly $C_{6–10}$ aromatics and $C_{5–8}$ paraffins. This limitation is largely imposed by the high-temperature (>300°C) requirement to activate ethylene, which in turn promotes aromatization and transfer hydrogenation. These aromatic and paraffin products are far too light to use as diesel fuel but are suitable for blending with gasoline and to some extent with jet fuel. However, the aromatic content (about 40–70C%) is too high for most fuel applications thus the mixture can only be used at lower blend levels unless the aromatics are partially removed.

One benefit of the this ETD route is that it is amenable to EtOH feeds with high H_2O contents, possibly reducing separation costs when using fermentation-derived feeds. The presence of H_2O attenuates coking and slows the ensuing reversible deactivation, but at high temperatures it also leads to irreversible deactivation through dealumination.[119,126] This irreversible deactivation can be avoided by operating below 450°C with H_2O contents below 50wt%. Using feeds with more H_2O can leads to lower yields of aromatics and other liquid products, although this can be compensated for by increasing residence times.[118,124,125,134]

With the parameter space well mapped out, it is clear that this ETD process is limited to producing mixtures of relatively light hydrocarbons, of which aromatics represent a considerable fraction. It does not appear possible to adjust the temperature, pressure, or catalyst to overcome this. Vertimass, LLC has demonstrated the process on a scale of ~2 $kg_{EtOH}\ day^{-1}$ (Figure 3.7a)[135]

by using V- or Ga-exchanged ZSM-5 to fully convert aqueous EtOH (50–60wt% H_2O, 350°C, 4 bar) to liquid hydrocarbons that are separated from H_2O and light gases (burned for process heat) in a decanter. Liquid yields ranging from ~70–85% can be achieved with combined yields of benzene, toluene, ethylbenzene and xylenes (BTEX) falling in the range ~50–90%. The product mixture is too rich in aromatic content for direct fuel applications, thus this stream is distilled to give three fractions: C_5 paraffins for gasoline, BTEX for chemicals, and C_{6+} paraffins and aromatics for gasoline or limited jet blending (a C_{6+} mixture with up to ~25% BTEX can be directly used in jet engines). Based on the liquid yield and this maximum tolerated BTEX content, the yield for EtOH conversion to drop-in distillate fuels is roughly 25%, though this percentage increases if blending at low levels. This low yield is not necessarily an economic problem because the individual BTEX products are more valuable as chemicals than they are as components in fuels. Byogy Renewables, Inc. has also examined two-stage conversion from EtOH → ethylene → oligomers, which is expected to afford similar product distributions when under acid catalysis.[136] The nature of this catalyst is unknown, however, thus it is possible that oligomerization is promoted by chemistries other than acid catalysis and therefore leads to different product distribution, which will be discussed in further detail later. Byogy has notably received support from multiple airlines as well as the US Department of Energy.[137-139]

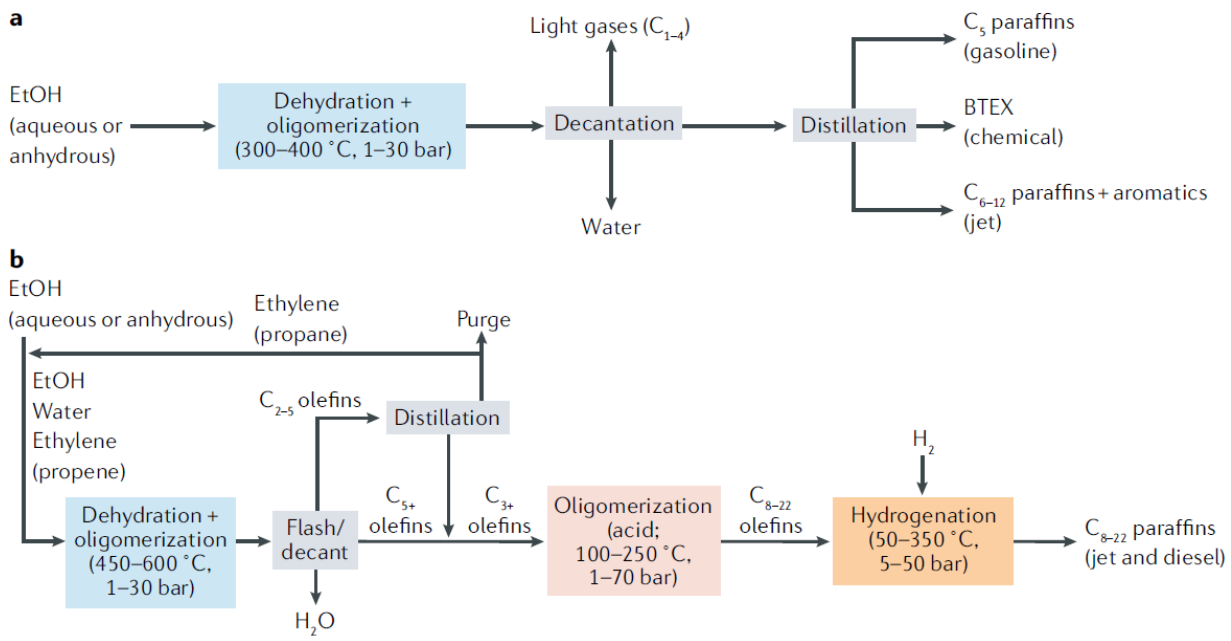

Figure 3.7 | **Block flow diagrams for acid-catalyzed conversion of EtOH through ethylene oligomerization. a** | The one-stage dehydration of EtOH and oligomerization of the resulting ethylene affords paraffins and aromatics, including benzene, toluene, ethylbenzene and xylenes (BTEX). EtOH is fed into a reactor containing a solid acid such as H-ZSM-5 to give products that are separated into light gases, H_2O, and liquid hydrocarbons (C_{5+}). The liquid hydrocarbons are further separated into C_5 paraffins for gasoline blending, $C_{6–12}$ for jet blending, and BTEX for the chemical industry. This design is based on the Vertimass process.[135] **b** | The two-stage acid-catalyzed oligomerization of EtOH, followed by hydrogenation, gives distillate-range paraffins. EtOH is first converted to C_{3+} olefins using solid acids at high temperatures. These olefins are then oligomerized at lower temperatures to distillate-range olefins, which can be hydrogenated to afford paraffins for use in jet or diesel applications.

3.6 Addressing ethylene activation challenges through two-stage operation

Olefin oligomerization is best carried out at lower temperatures (<300°C) to produce longer chain olefins while avoiding side-reactions such as aromatization, transfer hydrogenation and cracking. As mentioned above, a solid acid at low temperatures is insufficient to accelerate oligomerization of ethylene, but oligomerization of C_{3+} olefins does proceed because more highly substituted carbenium intermediates can be formed.[56,100] As a result, while ethylene conversion typically requires temperatures above 300°C, C_{3+} *n*-olefins can be converted effectively at 100–250°C, and isobutene conversion can be realized below 100°C. This order of reactivity means that

EtOH can be converted to distillate fuels through a two-step process whereby EtOH is first converted to $C_{3–4}$ olefins at high temperatures and then oligomerized to heavy olefins at low temperatures (Figure 3.7b). The first and second stages resemble the methanol-to-olefins (MTO) and Mobil olefin to gasoline and distillate (MOGD) processes, respectively.[103] The MTO process was notably brought to the commercial scale in 2010 by the Dalian Institute of Chemical Physics with the commissioning of a plant with a capacity of 600 kton of polyethylene and polypropylene per year, followed by the commissioning of several additional MTO plants.[140]

The conversion of EtOH to light olefins is typically performed using short contact times to limit further reactions of the olefinic products. To promote cracking of heavier olefins, the process is conducted at high temperatures (>450°C). Under these conditions, the dehydration of EtOH to ethylene is nearly quantitative even after short contact times, enabling the dehydration and ethylene conversion reactions to be treated as series reactions. The primary products of ethylene oligomerization are butenes, which react much more rapidly than ethylene and are therefore difficult to produce selectively (yields typically do not exceed 15%).[141,142] Propene is most likely formed either through the cracking of a C_{5+} olefin or fragmentation of a zeolite-confined species according to the hydrocarbon pool mechanism.[105,108,109,114,143] Thermodynamic calculations on a simple oligomerization model suggest that the maximum propene yield from ethylene is 42% (achievable at 600°C), although the model used does not take transfer hydrogenation and aromatization into account.[144] Experimentally, the highest propene yield from EtOH that has been achieved is ~30%.[142] The maximum C_{3-4} olefin yield from EtOH is therefore around 15% + 30% = 45%, with the propene:butene ratio being between 2:1 and 3:, and the major product being ethylene (~40% yield). As one might expect, decreasing the residence time favors lighter products such as ethylene, while increasing the reaction depth favors the formation of light paraffins and

C_{5+} species, many of which are aromatic. Since all C_{3+} products appear to be derived from ethylene, the limitations of the system can be more easily understood by considering the selectivity of transforming ethylene to C_{3-4} olefins as a function of conversion. At conversions of 10–15%, $C_{3–4}$ olefin selectivities as high as ~80% can be achieved,[145] while at a conversion of ~75% the selectivity is only ~50%. Aromatics, propane and, to a lesser extent, higher paraffins, are the major products under these conditions, regardless of whether aqueous or dry EtOH feeds are used.[126,141] These results suggest that the EtOH-to-olefins step should be performed at one of the two extremes of conversion. At one extreme, EtOH is fully converted to C_{3+} species, yielding large amounts of paraffinic and aromatic side products. Overall, this process is ~50% selective for C_{3-4} olefins. At the other extreme, ethylene is the major product and must be separated from the C_{3+} species after the reaction and recycled back into the reactor. The net yield of C_{3-4} olefins here is ~80%. This will ultimately lead to higher distillate yields but has much higher separation costs, especially if ethylene is to be fully separated from propene.

Oligomerization of C_{3-4} olefins over solid acids to produce gasoline-range iso-olefins was one of the first commercial catalytic processes in the petroleum industry. First utilized in 1935, the process has been extensively studied,[87,89,146] and zeolites are the most common catalyst used today.[147] For 1-butene oligomerization over H-ZSM-5, an optimal C_{8+} selectivity (86%) is obtainable at 200°C, 1 bar and <10% conversion.[148] The selectivity decreases with increasing temperature because cracking becomes more prevalent, such that it is important to use catalysts that are sufficiently active to enable low temperature operation. In the 80-162°C temperature range, several zeolites can convert 2-butene to C_{8+} products with >90% selectivity at 60–95% conversion.[149] C_{8+} selectivities above 98% can be achieved in some cases, with H-ZSM-57 having a particularly high selectivity for the dimers (86% at 89% conversion and 80°C). On the other

hand, when the more common H-ZSM-5 catalyst is used 94% C_{8+} selectivity is possible at 72% conversion, but this requires a temperature of 162°C. Relative to H-ZSM-5, the acidic resin Amberlyst 70 (polystyrene-co-divinylbenzene sulfonic acid) is more reactive, enabling higher conversions (99 vs 90%) at lower temperatures (170 vs 250°C), such that cracking is less prominent and higher C_{8+} selectivity (95 vs 89%) is possible.[150] Operation at higher 1-butene pressures (17 vs 1 bar) also allows for higher conversions to be obtained at lower temperatures. For example, another study shows that further increasing the pressure to 62.7 bar at 150°C affords supercritical butene, which undergoes oligomerization over the synthetic zeolite H-ferrierite, whose rate of deactivation is slowed under these conditions.[151] Overall, the general philosophy behind oligomerizing light olefins to afford products in the distillate range is to achieve high olefin conversions at temperatures below 200°C. Such a situation can arise if olefins are fed at elevated pressures over solid acids to minimize cracking. These studies clearly show that butene oligomerization is not a limiting step in this process because dimers through to pentamers are readily formed and all lie in the distillate range.

In contrast to butene dimers, propene dimers are not heavy enough to be used substantially in distillate fuels. Propene dimerizes in high yields over zeolite catalysts,[152] and supercritical propene (~70 bar, 180-250°C) undergoes dimer- and trimerization over H-ZSM-22, although dimers typically comprise a large fraction of the product (>30 wt%).[153,154] Diesel-range hydrocarbons have also been produced over modified ZSM-5 at selectivities of 60–75% (200°C, 40 bar), with catalyst modification enabling higher stabilities and activities, the latter likely due to the higher Brønsted acid site densities and lower crystallite sizes.[155] Studies on solid phosphoric acid and heteropoly acids, on the other hand, have demonstrated higher selectivities to $C_{9–12}$ olefins,[156-159] with solid phosphoric acid converting propene (200°C, 40 bar) to mostly nonene

(59.6%) and dodecene (19.1%) at 98% conversion.[159] If all olefins were equally reactive towards oligomerization, the resulting statistical product distribution would reflect a maximum C_{9-12} selectivity of ~45% based on the Schulz–Flory distribution, which will be discussed further later in the context of metal-catalyzed olefin oligomerization. The high C_{9+} selectivities may therefore be rationalized in part by propene oligomers being more reactive than propene, as might be expected given that the oligomers may feature tertiary C atoms that can readily form carbenium ions en route to heavier oligomers. Therefore, the selective oligomerization of C_{3-4} mixtures into the distillate range requires a careful choice of catalyst informed by the precise composition of the feed — a goal that appears to be feasible. It is important to note that the product olefins cannot be directly used in distillate fuels and must first be hydrogenated to the corresponding paraffins. While such hydrogenations are commonly performed with high selectivity on the commercial scale, external H_2 sources would be required.[160-165]

Paraffins produced from these ETD routes will have different fuel qualities depending on their level of branching. Branching is mechanistically favored over solid acids because substituted internal carbeniums form more readily than do terminal carbeniums, enabling a higher rate of C–C bond formation in the former case. Although branching of a hydrocarbon improves its cold-flow properties for both jet and diesel applications, it is detrimental to combustion in diesel engines as reflected in lower cetane numbers. In 1-butene oligomerization over H-ferrierite, branching increases with conversion and most dimers have two methyl branches.[151] This is approximately the most branched a molecule of this size can be while still exhibiting suitable diesel combustion; dimethylhexanes have cetane numbers in the range 30–40.[24] Generally, the extent of branching in the oligomer products increases with the geometric surface area of the catalyst framework's largest pore opening since smaller pores cannot accommodate substantial branching.[146] This correlation

can be seen in 1-butene oligomerization (160-240°C, 62 bar) over H-ZSM-23, H-ZSM-5, and H-ZSM-12 which possess pore opening areas of approximately 18, 23, and 26 $Å^2$, respectively, and produce C_{12+} fractions with cetane numbers of 41, 36, and 28, respectively.[166] The diesel fraction produced from H-ZSM-23 was notably obtained at >70% selectivity.[167] This catalyst is one of several one-dimensional, narrow pore solid acids with 10-membered rings known to produce oligomers with minimal branching. Trimerization of propene at 200°C, 68 bar over these catalysts (H-ZSM-22, H-ZSM-23, H-ZSM-48, SAPO-11) at 30% conversion produces dimers and trimers which are predominantly mono- and di-branched.[149] By contrast, mesoporous materials which do not possess substantial geometric constraints produce relatively low-cetane distillate. 1-Butene oligomerization over solid phosphoric acid (160-240°C, 62 bar) produces a C_{12+} fraction with a cetane number below 14,[166] while oligomerization over MCM-41 (160°C, 50 bar) produces a diesel fraction which, after hydrogenation, possesses a cetane of ~25 according to NMR.[168] Cetane numbers have also been evaluated for oligomerization products from mixed-olefin feeds, most notably those from the MOGD process and the similar "conversions of olefins to distillate" (COD) process developed by Mossgas (now a part of PetroSA). The latter was developed as a means to convert light Fischer–Tropsch-derived olefins into heavier products.[169,170] COD was studied at the pilot plant scale using amorphous SiO_2-Al_2O_3, solid phosphoric acid or H-ZSM-5 (100–700 g) as catalysts.[171-173] H-ZSM-5 mainly produces species with 2–5 methyl branches, and after hydrogenation the mixture has a cetane number of ~50 — higher than the cetane of ~30 achieved with the other catalysts. The MOGD process also utilizes H-ZSM-5 and has been tuned to produce a distillate cut at 82% yield (along with 15% gasoline and 3% light gases) with a cetane of 50, freezing point of −60°C, and boiling point of ~200–350°C.[174] The commercial scale-up of the

COD and MOGD processes is a promising sign for large-scale oligomerization of EtOH-derived light olefins.[173]

Specific applications of the two-stage process for EtOH as well as ethylene conversion have been described by IFP and ARCO (now owned by Tesoro), respectively.[175,176] The IFP process uses faujasite (325°C, 5 bar) to convert EtOH to a mixture rich in C_{2-3} hydrocarbons (49 wt%) with minimal C_{7+} species (6%). The majority of C_{4-6} species (83%) are olefins, though 34% of the overall mixture consists of paraffins and naphthenes. The C_{2-3} species are separated and recycled to the first reactor with a small purge stream (6%). The H_2O is removed while the C_{4+} products are sent to a separate reactor that includes H-ZSM-5 (250°C, 50 bar). Without accounting for carbon lost in the purge, the patent claims that the system can produce a 22wt% yield of gasoline-range products and a 63wt% yield of distillate-range products. The ARCO process operates with an ethylene feed at 88% conversion in the first stage (~360°C) to give mostly C_{5+} species (76%), only 50% of which are C_{8-12}. About 25% of the ethylene converted in this step is lost to C_{1-7} paraffins and aromatics. The second stage is not described in detail. LanzaTech's ETD technology also involves two oligomerization stages, with the first one likely being tuned to produce C_{4-6} olefins.[177] It is unknown whether both stages involve acid catalysis. Thus far, LanzaTech has produced over 4,500 gallons of distillate fuel with this process and has received support from the US Department of Energy (DOE) to build a facility with a capacity of 3 million gallons of fuel per year.[178,179] Construction of several gas-to-EtOH plants with capacities over 30 million gallons per year is also planned, underway, or nearly complete with their partners in China (Shougang), Belgium (ArcelorMittal), India (Indian Oil Company) and the United States (Aemetis).[180-183] Working closely with Virgin Atlantic, LanzaTech jet fuel has recently been successfully used in a commercial flight across the Atlantic Ocean.[184,185]

The performance of two-stage acid-catalyzed oligomerization is strongly dependent on the operation of the first stage. Running the first stage at high ethylene conversions will lead to the formation of side-products such as light paraffins and aromatics, thereby lowering distillate yields. However, it is expensive to run at low conversions because more ethylene will have to be recycled, necessitating high distillation capital/operating costs and larger reactors. A technoeconomic analysis would be necessary to determine how sensitive profitability is to conversion, and the ever-changing market prices of gasoline, diesel and jet fuel also play a large role. Overall, the maximum C yield of distillate fuels in this two-stage process is ~65–70%, because in each of the two steps 15–25% of the C atoms are converted into light gases and gasoline-range byproducts.

In general, processes relying on the acid-catalyzed oligomerization of ethylene (either in one or two stages) are limited because the high temperatures required to convert ethylene also accelerate side reactions. This temperature requirement can be alleviated by using transition metal catalysts, which have long been used in selective olefin oligomerization and polymerization reactions. Indeed, transition metals remain essential for the production of high density and linear low density polyethylene, two of the most commonly used plastics in the world.[186]

3.7 Low-temperature olefin oligomerization by transition metal catalysis

The finding by Ziegler, in 1954, that combinations of transition metal compounds such as $TiCl_4$ and alkylaluminium compounds polymerize ethylene into linear polyethylene, formed the basis for a technology that is used to produce polyethylene and higher linear α-olefins from ethylene.[187-189] The technology is nowadays referred to as Ziegler–Natta catalysis, and the mechanism was first described by Cossee in the early 1960s (Figure 3.8).[190,191] The active initiator forms when the electrophilic group 4 metal undergoes alkylation — either by an alkylaluminium such as $AlEt_3$ or methylaluminoxane (MAO), or even with ethylene itself in some cases.[192,193] The

group 4 alkyl then binds ethylene substrate, which undergoes 1,2-insertion into the M–Et bond to give a coordinatively unsaturated M–^{n}Bu fragment. Another ethylene can then coordinate and insert to continue the oligomerization or the chain can terminate, most commonly by β-hydride elimination onto the vacant coordination site, to give a linear α-olefin product. This reactivity is commonly referred to as the Cossee–Arlman mechanism and the product chain lengths depend on the relative rates of propagation and termination, which are typically independent of chain length. The oligomer distribution can therefore be described by a statistical Schulz–Flory product distribution, and catalysts that strictly operate through Cossee–Arlman oligomerization are therefore relatively non-selective to products of a specific length.[194]

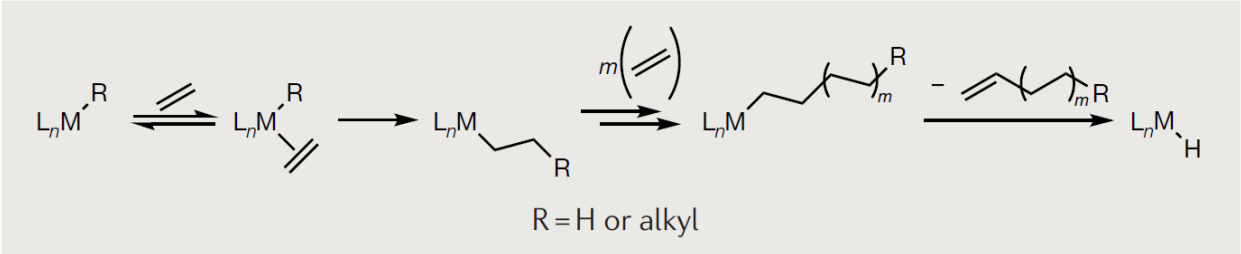

Figure 3.8 | **The generalized Cossee–Arlman mechanism for ethylene oligomerization.** Oligomerization begins with the formation of L_nMR from $AlEt_3$ or ethylene. The electrophilic, coordinatively unsaturated L_nMR, which can take the form of a solution species or an immobilized reactive site, readily coordinates ethylene, which then inserts into the M–R bond to afford a longer chain and regenerate the vacant coordination site. Continued coordination–insertion leads to longer alkyl chains until termination occurs, typically through β-hydride elimination.

The Schulz–Flory distribution is described by the chain growth probability α, the probability that a growing oligomer chain will propagate (experience an additional M–R insertion) rather than terminate. For a given α, the mole fraction of an oligomer comprising n monomer units (x_n) is computed using Equation 3.1. It follows that the carbon selectivity of forming an oligomer of length n relative to heavier oligomers ($n > 1$) can be calculated according to Equation 3.2 (derivation presented in the Supporting Information, Section 3.15).

Equation 3.1 $$x_n = (1-\alpha)\alpha^{n-1}$$

Equation 3.2 $$S_{C,n} = \frac{n(1-\alpha)^2\alpha^{n-2}}{(2-\alpha)}$$

One can thus plot $S_{C,n}$ versus n for a given α, and as one would expect, the selectivity peaks at greater lengths when α is larger (Figure 3.9a). Another way to visualize this is by considering the product distribution versus α (Figure 3.9b); when this value is 0.72 the single-pass selectivity to distillate-range products ($C_{8\text{-}22}$) reaches a maximum at 62%. The selectivity of the overall process may be improved by operating at lower α values (such as 0.5) and recycling C_{4-6} olefins back into the reactor. However, this may still afford a distribution that is unfavorably weighted toward lighter olefins.

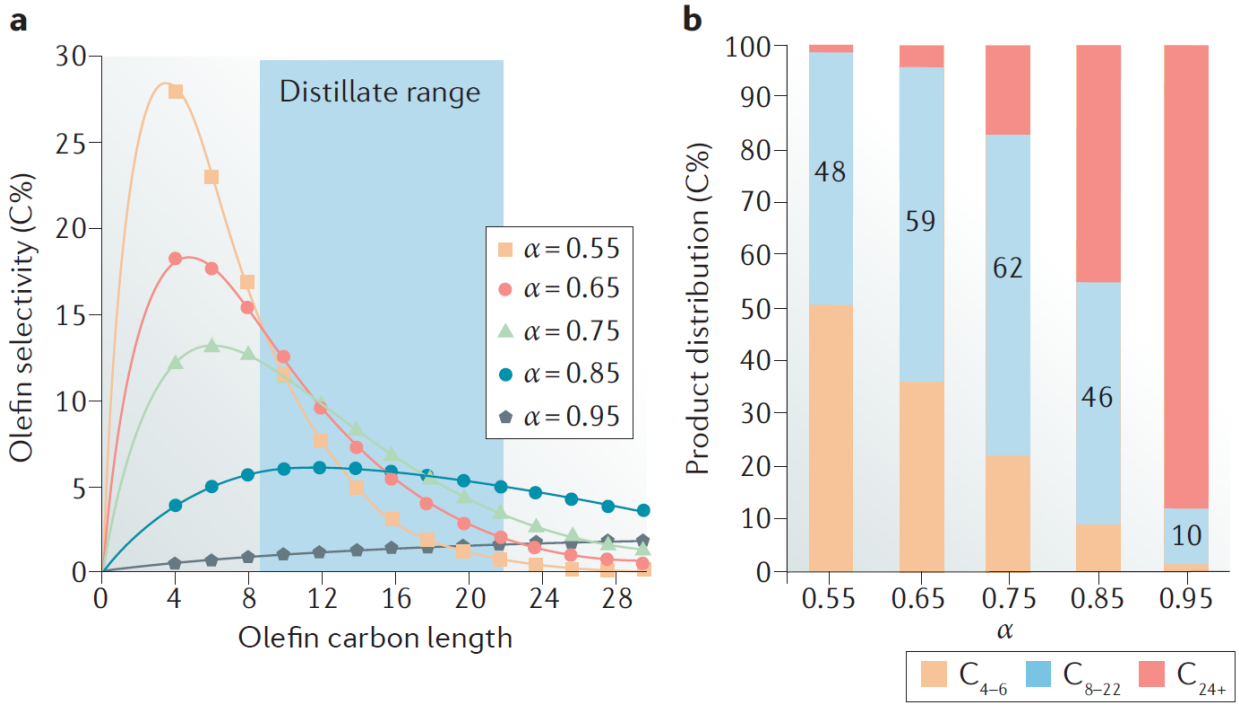

Figure 3.9 | **Computed Schulz–Flory distribution of olefins from ethylene oligomerization. a** | Olefin product selectivities depend on the chain growth probability α. **b** | One can group the olefins into light (C_{4-6}), middle-distillate (C_{8-22}), and heavy (C_{24+}) products.

This reaction often involves homogeneous catalysts, cocatalysts (such as $AlEt_3$) and/or solvents that require separation from the product mixture, after which the products reflect α values in the range 0.5–0.8.[195] This statistical method of oligomerization remains at the heart of many higher olefin production processes. Ziegler–Natta catalysis is behind the INEOS, Chevron Phillips,

Idemitsu, BP, IFP, DuPont, and Linde/SABIC technologies, which use $AlEt_3$ with or without the addition of Zr- or Ti-based complexes.[196,197] These oligomerization processes are conducted in the 120–220°C temperature range and at pressures up to 300 bar. Schulz–Flory product distributions are obtained from each process except the INEOS process, which affords a Poisson distribution. The INEOS process is not strictly Ziegler–Natta polymerization because it involves low-temperature oligomerization (120–150°C) with stoichiometric alkylaluminium species in one stage, followed by olefin displacement in a separate high temperature (280–320°C) stage. The Chevron Phillips process also only uses alkylaluminium species but is conducted at higher temperatures (180–220°C) to allow oligomerization and elimination to proceed in a single reactor. Shell and UOP utilized Ni-based catalysts in the absence of alkylating agents to afford Schulz–Flory product distributions. Shell developed the Shell Higher Olefins Process (SHOP), wherein a metathesis/isomerization–disproportionation step converts olefins outside of the desired $C_{12\text{-}18}$ range to internal olefins within it. Since the development of this process, however, the market for shorter chain olefins (such as 1-hexene or 1-octene) has grown such that this step likely is not performed on the same scale today.[198] In each of these processes, the product α-olefin mixtures are distilled to afford pure streams. The products also include polymers — undesired species that may build up in oligomerization reactors — whose formation can be partially mitigated through the choice of the solvent. It is important to note that the α-olefins produced in these processes are predominantly linear, although certain catalyst and operating conditions can lead to branching.[199] This results either from migration of the growing alkyl chain R such that it is no longer coordinated through a terminal C atom or through insertion of a C_{3+} olefin at an internal C site.[200,201]

Fully heterogeneous catalysts without activating agents, especially those based on Ni, have been used for ethylene oligomerization.[202,203] Ni-based catalysts are commonly supported on

silicates or aluminosilicates (such as MCMs or zeolites) and are typically utilized at 100–150°C and 30–40 bar to produce olefin products in Schulz–Flory distributions (Figure S3.2). Debate remains concerning the oligomerization mechanism for such catalysts, but recent evidence for a Cossee–Arlman coordination–insertion mechanism has been found computationally for Ni-SSZ-24[204] and experimentally for Ni-β.[205] Isomerization to internal olefins is commonly observed with these materials and is thought to be catalyzed by Ni^{2+} as well as H^+ from the support.[205-207] The relative free energies of olefin isomers supports high internal olefin selectivities unless oligomerization is performed at low temperatures (below 100°C).[208,209] Although branching is commonly observed in the C_{6+} fraction[206,207,210-212], at temperatures near 120°C the hexenes produced are predominantly linear (>70%) while the C_{8+} olefins are predominantly branched (>70%). In these systems, branching is generally thought to be catalyzed by the acid sites of the support, though it is also possible that Ni catalyzes branched olefin formation when C_{3+} olefins are prevalent (as noted above for homogeneous catalysis). For example, ethylene oligomerization over Ni-exchanged zeolite Y at 100–120°C affords a diesel cut (>165°C) which, after hydrogenation, has a calculated cetane number of 46, consistent with a product with moderate branching.[213] These products still fit a Schulz–Flory distribution and most products fall below the diesel range. Shifting to higher temperatures (>150°C) enables acid catalysis to become more prevalent and eventually dominate, leading to substantial cracking, cyclization, and hydrogen transfer. However, operating near this temperature limit can be beneficial as ethylene oligomerization at 150°C over Ni-MCM-41/H-MCM-41 catalyst mixtures (mesoporous SiO_2 with and without Ni loading) has been used to afford non-Schulz–Flory product distributions.[214] After 1 h reaction time, the olefin product distribution is bimodal and centered on C_4 and C_8. After 15 h the distribution is centered both on C_4 (~15% C_{4-6}) and C_{12} (~85% C_{8-18}). Similar results were recently obtained in continuous

operation using Ni-AlSBA-15 and Amberlyst-15 in sequence,[215] with the former catalyst performing olefin oligomerization while the latter can also perform acid-catalyzed cracking to overcome single-pass Schulz–Flory limitations. Altogether, heterogeneous Ni catalysts are promising for ethylene oligomerization but have yet to be used in large-scale oligomerization processes. It is expected that these will be more suitable for jet fuel production due to their tendency to form branched species, although adapting the processes to include heterogeneous Co catalysts may enable higher selectivities to linear olefins.[216-218]

Cossee–Arlman mechanisms typically do not enable selective ethylene oligomerization to an olefin of a specific chain length. This can be performed, however, using a catalyst that operates through the metallacycle mechanism, a pathway in which the metal catalyst undergoes redox (Figure 3.10).[219] Here, a transition metal complex (generically denoted L_nM) coordinates two ethylene molecules which then oxidatively couple to form a five-membered metallacycle $L_nM(C_4H_8)$. The ring either opens to give 1-butene or continues to grow through the insertion of another ethylene molecule, after which ring-opening would afford 1-hexene (a further insertion and opening would instead produce 1-octene, and so on). The product distributions are largely dictated by the stability of the different metallacycles, with 1-octene being the largest olefin produced selectively thus far because metallacycles larger than $L_nM(C_8H_{16})$ do not readily form.[220,221]

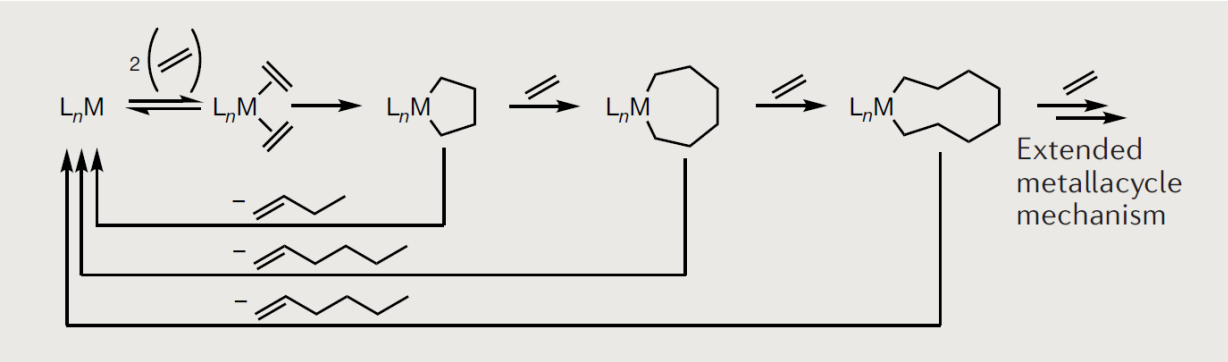

Figure 3.10 | **The generalized metallacycle mechanism for ethylene oligomerization.** A low-valent, coordinatively unsaturated metal site L_nM, which can take the form of a solution species or an immobilized reactive site, readily coordinates two ethylene molecules, whose reductive coupling gives a five-membered metallacycle. Further ethylene insertions afford larger metallacycles. This growth is terminated when elimination produces a linear terminal olefin. Propagation beyond a metallacyclononane is thought to proceed through an alternative extended metallacycle mechanism.

This oligomerization of ethylene to select products has been most thoroughly studied in the case of Cr-based homogeneous catalysts and MAO or $AlEt_3$ activators.[222] Sasol, BP, and Chevron Phillips took the original heterogeneous CrO_3/SiO_2 Phillips polymerization catalyst and developed modified Cr-based catalysts for the selective production of 1-hexene and 1-octene. Catalysts based on Ti, Zr, and Hf, as well as Ta, have also been investigated for metallacycle-mediated oligomerization, which in many cases can be nearly 100% selective for the desired olefin. These catalysts cannot make olefins larger than octenes, so in order to produce distillate fuels, a two-stage oligomerization process would be require in which these a second stage is used for full-range oligomerization. The following discussion covers how such a two-stage approach could be implemented.

3.8 Two-stage oligomerization of ethylene to distillate fuels using transition metal catalysis

Schulz–Flory limitations may be overcome by performing oligomerization in two stages: $C_{4\text{-}8}$ olefins are produced in one stage and oligomerization to middle-distillates in another (Figure S3.3). The block flow diagram is similar to the two-step process discussed above (Figure 3.7b)

and also requires unreacted ethylene to be recycled into the reactor. The second stage can be performed with either Cossee–Arlman or acid catalysis.

Sequential metallacycle and Cossee–Arlman catalysis can produce middle-distillate fuels with the 1-butene and/or 1-hexene formed in the first step then being exposed to MAO-activated [$(C_5H_5)_2ZrCl_2$] in the second step.[223,224] 1-Hexene can be fully converted to a mixture of dimers, trimers, and tetramers in a Schulz–Flory distribution with α ~0.3. Unlike in direct ethylene oligomerization, which affords predominantly linear species, each 1,2-insertion of 1-hexene introduces a branch. After hydrogenation, the products of 1-hexene oligomerization appear to be suitable for either jet or diesel applications, while the products of 1-butene oligomerization may be too heavily branched for diesel but would be excellent in jet fuel. The general use of metallocene catalysts to oligomerize $C_{2\text{-}8}$ olefins is summarized more thoroughly elsewhere.[225]

A rigorous analysis is necessary to evaluate the technoeconomics of metallacycle catalysis and to determine if there is a sufficient selectivity benefit to offset the high costs of recycling the activating agents and solvents. Distillate fuels are typically complex mixtures, and the benefits of producing well-defined mixtures of very few compounds are unclear and unlikely to be important. In addition, the metallacycle mechanisms afford linear terminal olefins that are ~2-3x more valuable than distillate fuels.[197] Thus, the conversion of 1-butene, 1-hexene, or 1-octene to fuels may not be economically attractive without government incentives. However, two-stage processes that avoid the Schulz–Flory product distribution remain potentially viable. Since all $C_{4\text{-}8}$ olefins can be dimerized into the distillate range, low-α Cossee–Arlman oligomerization can be employed as part of the two-stage process. Instead, IFP has proposed to use two sequential homogeneous Ziegler–Natta catalysts to convert ethylene to distillates.[226] However, separation costs are lowest when using fully heterogeneous catalysts, thus using a supported Ni catalyst in the first stage and

a solid acid in the second may be desirable. Such a process has recently been patented by Pacific Northwest National Lab (PNNL).[227] In the first stage, a Ni-loaded aluminosilicate (such as zeolite H-β or amorphous SiO_2-Al_2O_3) oligomerizes ethylene (85°C, 21.7 bar in N_2) at >95% conversion to products well-described by a Schulz–Flory distribution with α ~0.2. In the second stage, a similar catalyst without Ni present oligomerizes the olefins (200–350°C, 21.7 bar) to distillate-range products in yields above 70%. After hydrogenation of the products, one obtains almost entirely acyclic paraffins (>95%), most of which are branched.

The conversion of corn-derived EtOH to jet fuels through ethylene oligomerization pathways has been the subject of a recent technoeconomic analysis.[165] Assuming that a plant converts 2,000 dry metric tons of corn grain or corn stover feedstock per year to fuels, one can estimate the minimum prices at which fuels must be sold in the case of the first plant or the n^{th} plant (the situation in which the technology is mature). The process was modelled primarily using H-ZSM-5 for EtOH dehydration to ethylene, the two-step Ziegler process (INEOS) for oligomerization, a CoMo oxide for hydrotreating, and a Pt-containing zeolite for skeletal isomerization to yield branched hydrocarbons. After calculating the approximate distributions of fuel types produced, n^{th} plant minimum selling prices of $3.91 per gallon using corn grain and $5.37 per gallon from corn stover were determined. These prices are strongly tied to the feedstock price ($0.072/$lb_{corn\ grain}$ and $0.032/$lb_{corn\ stover}$), and determined from the total capital costs ($203 million for corn grain, $337 million for corn stover), of which $81-100 million is required for the ETD portion of the process. Product distributions were also examined assuming the use of other catalytic systems, including the two-stage sequential metallacycle/Cossee–Arlman process, and one-stage systems using a homogeneous MAO- or $AlEt_2Cl$-activated [Ni(α-diimine)Br_2] catalyst, Ni/SiO_2-Al_2O_3, Ni-MCM-41 or H-ZSM-5. The two-step Ziegler process was found to give the

most economical product distribution with 5wt% light gases, 26wt% gasoline (C_{6-8}), 61wt% jet (C_{9-16}), and 8wt% diesel (C_{17+}). Ni-MCM-41 affords a similar product distribution but the two-step Ziegler process was selected for direct assessment because of its greater technological readiness. This study provides a strong framework for economic analysis, though more rigorous analyses will be required for proper comparison of catalytic systems. These analyses should include finer categorization of products into fuel classes (beyond using just the number of C atoms), data for heterogeneous Ni catalysts under more optimal conditions, cost differentiation between heterogeneous and homogeneous systems, and evaluation of costs associated with utilizing series reactors and light olefin recycles in place of just a single pass process. Other studies have more generally analyzed the economics of EtOH-to-jet processes based on sequential dehydration–oligomerization–hydrogenation for comparison with other biomass-to-jet routes.[30,32,33] Collectively, these studies indicate that more information on EtOH-to-jet routes is required for proper economic analyses. These routes will have to compete economically with processes including hydroprocessing of esters and fatty acids, hydrothermal liquefaction, pyrolysis, and gasification combined with Fischer–Tropsch synthesis.

All of the EtOH-to-distillate routes discussed above rely on two simple steps — EtOH dehydration and olefin oligomerization — after which hydrogenation affords saturated products. The selectivity limitations of the routes result from the low reactivity of ethylene towards acid catalysts and the statistical limitations of the Schulz–Flory distribution. This problem may be partially overcome by using multiple-stage configurations as well as recycle loops. Another potential solution is to utilize alternative C–C coupling chemistries that do not require ethylene as a reactant. These processes rely mainly on aldolization, a key part of Guerbet coupling chemistry.

3.9 Oligomerization of EtOH through Guerbet condensation

Guerbet condensation (or Guerbet coupling) dates back to the 1899 discovery of Marcel Guerbet that two 1-butanol molecules condense to form 2-ethyl-1-hexanol heating with NaOR.[228] In recent years this has gained more attention as a means to convert EtOH to 1-butanol.[229,230] This reaction proceeds through the dehydrogenation of two alcohols to aldehydes, followed by aldolization to a β-hydroxyaldehyde, dehydration to a conjugated alkenal, and full hydrogenation to a saturated alcohol (Figure 3.11a). In this way, two EtOH molecules give 1-butanol, with further condensation affording both linear and branched C_{6+} alcohols. Linear alcohols can only be produced when the nucleophile originates from EtOH; nucleophiles derived from other alcohols lead to branching at the α position. In the context of EtOH-to-distillate conversion, this chemistry can be used either to directly produce distillate-range alcohols or to produce $C_{4–8}$ alcohols that can be selectively dehydrated and oligomerized into the distillate range. These routes will be discussed in further detail after a general discussion on Guerbet coupling.

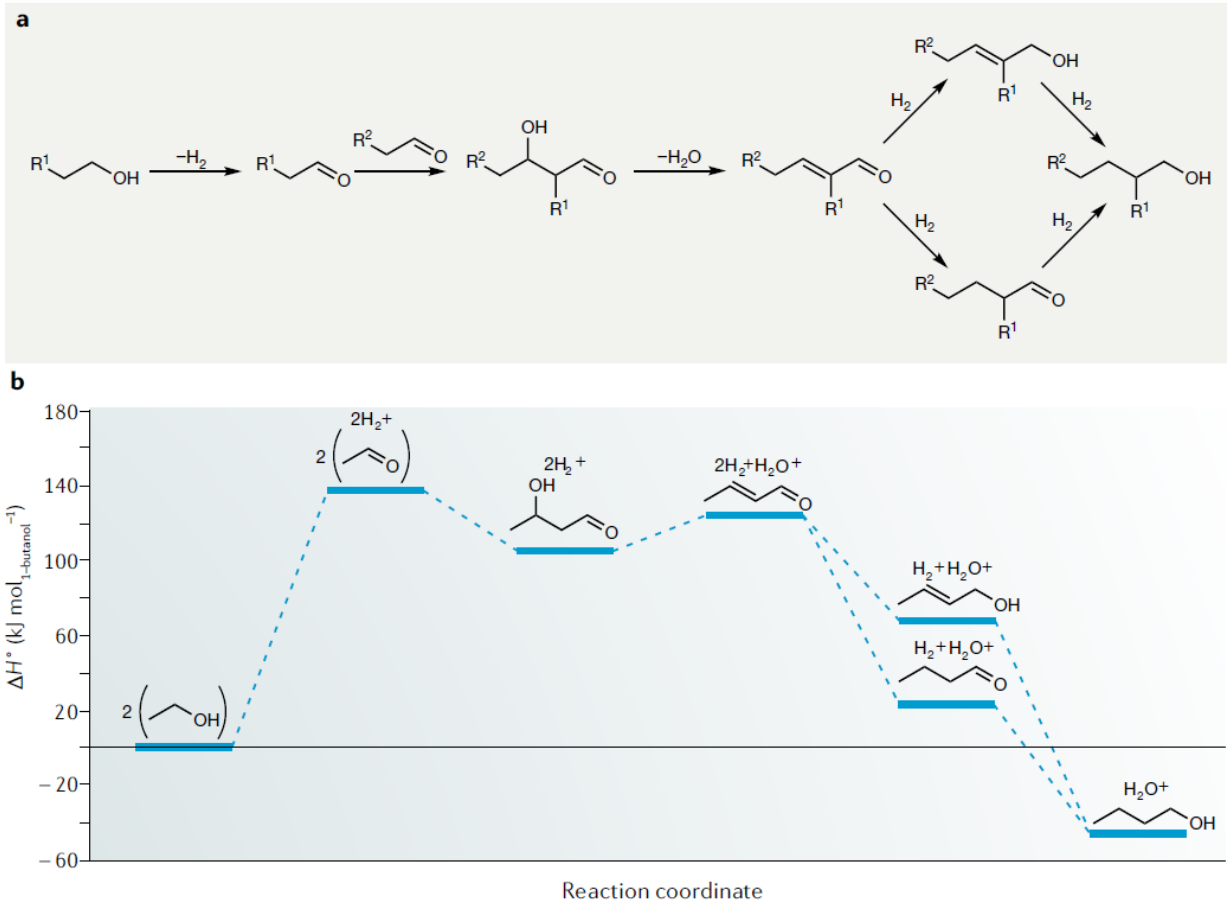

Figure 3.11 | **Guerbet condensation of primary alcohols affords an alcohol product. a |** The classical Guerbet pathway involves dehydrogenation of primary alcohols to afford aldehydes. Two aldehydes can condense to afford a β-hydroxyaldehyde, the dehydration of which affords a conjugated alkenal. The C=C and C=O bonds are then hydrogenated to give a saturated alcohol product. **b |** The enthalpy changes associated with the steps of the Guerbet conversion of EtOH to 1-butanol. The overall reaction is exothermic as well as exergonic at all temperatures. While hydrogen transfers are explicitly depicted here to involve H_2, it should be noted that several prominent catalysts for this reaction do not appreciably interact with H_2 and therefore rely upon alternate hydrogen transfer mechanisms.

The enthalpy changes involved in the Guerbet coupling of EtOH are first examined as shown in Figure 3.11b. Dehydrogenation of a primary alcohol is highly endothermic ($\Delta H° = 68.5$ kJ mol_{EtOH}^{-1} and 69.4 kJ $mol_{1\text{-butanol}}^{-1}$, respectively) and only becomes thermodynamically favorable ($\Delta G < 0$) above 320°C. Heterogeneous Guerbet condensation catalysts often possess some degree of acidity such that dehydration (a less endothermic reaction) often competes with dehydrogenation. Dehydration is thermodynamically favored over dehydrogenation (lower ΔG) at

all temperatures, thus control over catalyst acidity is important. Coupling of EtOH is typically performed in the range of 250–400°C to promote condensation without excessive dehydration. The free energy changes for acetaldehyde aldolization to 3-hydroxybutanal were calculated here using density functional theory (B3LYP/6-311+G(2d,p))[231] due to a lack of tabulated data for the aldol adduct. The reaction is exothermic ($\Delta H° = -31.6$ kJ $mol_{3\text{-hydroxybutanal}}^{-1}$) with a large entropic decrease ($\Delta S° = -163$ J mol^{-1} K^{-1}). The dehydration of this intermediate is slightly endothermic ($\Delta H° = 19$ kJ mol^{-1}) but is entropically desirable ($\Delta S° = 157$ J mol^{-1} K^{-1}), offsetting the entropic penalty of the aldolization. As a result, the condensation of acetaldehyde to crotonaldehyde is thermodynamically favorable ($\Delta G° = -10.7$ kJ $mol_{\text{crotonaldehyde}}^{-1}$) and is largely insensitive to temperature ($\Delta S° = -6.6$ J mol^{-1} K^{-1}). Efficient aldol condensation of acetaldehyde to crotonaldehyde can therefore be realized at temperatures below 100°C. Combined with dehydrogenation, the conversion of EtOH to crotonaldehyde (along with H_2 gas) is favorable above 275°C. The full hydrogenation of crotonaldehyde to 1-butanol is highly exothermic ($\Delta H° = -171$ kJ mol^{-1}), which allows for Guerbet condensation as a whole to be favorable at all realistic reaction temperatures ($\Delta G \sim -40$ kJ $mol_{1\text{-butanol}}^{-1}$). The equilibrium conversion therefore approaches 100% at atmospheric pressure over this whole range and is above 99% up to 10 bar (in the gas phase). Overall, Guerbet condensation is not thermodynamically limited, and the steps involving H_2 evolution or incorporation are associated with the largest energy changes.

Guerbet coupling over both homogeneous and heterogeneous catalysts has been discussed in detail in several recent reviews.[229,230,232-234] Homogeneous systems have not been extensively commercialized for this reaction (in contrast to olefin oligomerization), and the high costs typically associated with such systems direct the focus of this discussion toward heterogeneous catalysis. Common catalysts include MgO, mixed-metal oxides derived from double-layered hydroxides (for

example, Mg_xAlO_y), hydroxyapatite (HAP, $Ca_5(PO_4)_3(OH)$), basic zeolites (for example, ion-exchanged and impregnated zeolite X), and transition metals supported on Lewis-acidic metal oxides (for example, Ni/γ-Al_2O_3). Whether these catalysts strictly obey the Guerbet condensation mechanism discussed above has been heavily debated. Key challenges to the mechanism relate to the explicit involvement of aldehydes in C–C coupling and the role of H_2 in hydrogen transfers.

Evidence exists for a route in which condensation occurs directly between two alcohols without aldehyde intermediates. This was first proposed to describe EtOH condensation over Rb-LiX, in part because the rate of C_{4+} alcohol formation decreases on cofeeding crotonaldehyde, an intermediate in the formal Guerbet mechanism.[235] When using Mg_xAlO_y, a plot of 1-butanol production versus contact time is sigmoidal (Figure 3.12a), which suggests that 1-butanol forms both as a secondary product through an acetaldehyde intermediate and as a primary product through direct EtOH coupling.[236] A similar inflection observed using HAP suggests that the majority of 1-butanol is formed through the direct condensation route on this catalyst (Figure 3.12b).[237] The ratio [1-butanol]:[acetaldehyde] observed in the temperature range of 350–440°C is higher than is thermodynamically allowed through an acetaldehyde-mediated route in which the aldol condensation product is hydrogenated with H_2.[238] Key evidence in support of an aldolization mechanism is the first-order dependence of the condensation rate on [acetaldehyde] and slightly negative order (0.4 to −0.1) with respect to EtOH pressure.[239-241] The former suggests that enolate formation is the rate-limiting step and the latter indicates competition between EtOH and acetaldehyde adsorption.

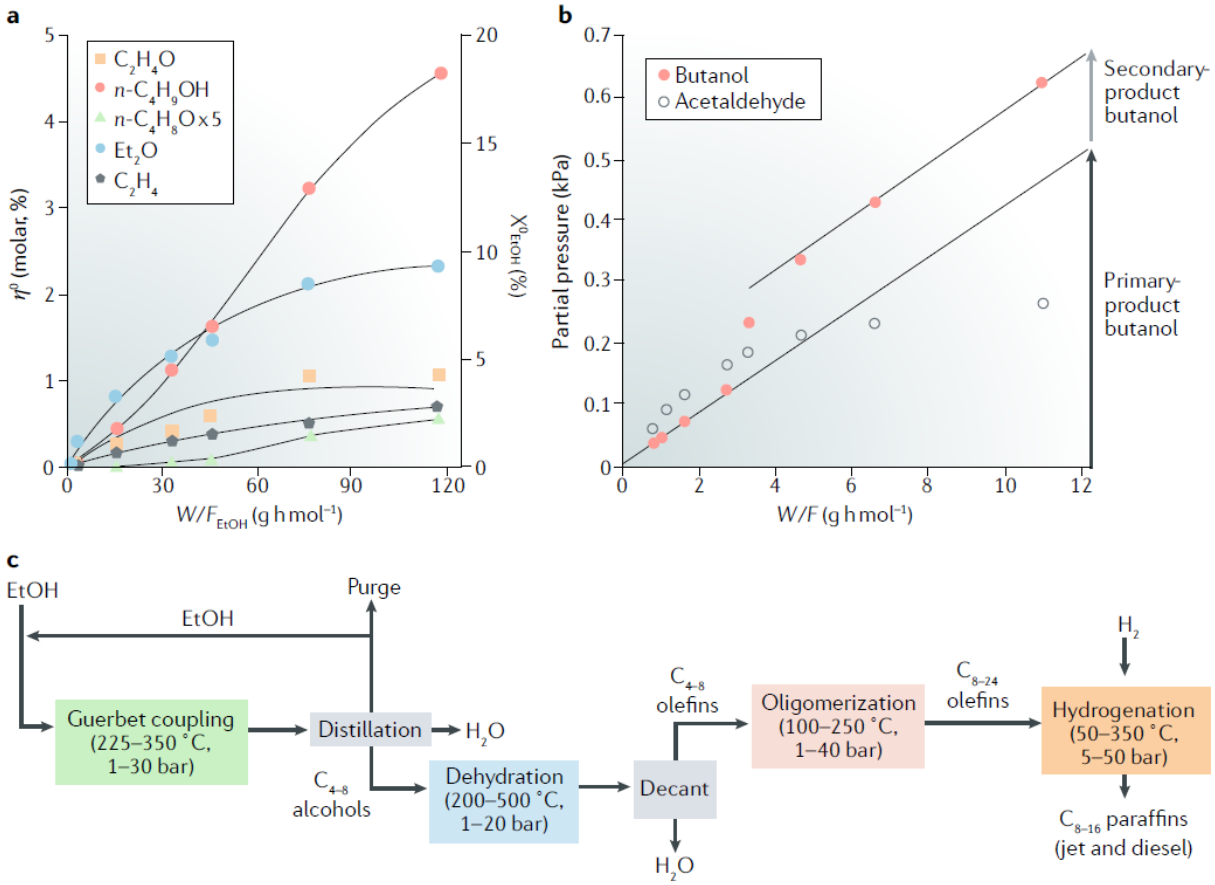

Figure 3.12 | **Contact time plots and block flow diagram for the Guerbet coupling of EtOH.** The contact time plots describe the growth of product concentrations over time spent over the catalyst. The curves indicate that both direct and indirect EtOH condensation mechanisms are operative. **a** | The conversion of EtOH (9% in N_2) over Mg_xAlO_y at 200°C and 1.0 bar.[236] **b** | The conversion of EtOH (7.6% in Ar) over hydroxyapatite at 300°C and 1.0 bar.[237] **c** | A block flow diagram for the Guerbet coupling of EtOH followed by dehydration and oligomerization. EtOH is first converted to higher alcohols at below full conversion, with EtOH being removed and recycled. H_2O cannot be present in this recycle stream, though it may be present at some level in the C_{4+} alcohol product stream. The product alcohols are then dehydrated to give olefins, which are oligomerized over a solid acid (or Cossee–Arlman catalyst). The oligomers are then hydrogenated to afford C_{8+} paraffins. a,b from Ref 1 adapted with permission from Refs 216 and 237, Elsevier.

The possibility that an aldehyde may not be formally involved in alcohol condensation casts doubt over the involvement of H_2 in the reaction. Neither HAP nor Mg_xAlO_y are capable of recombining H atoms to form gas phase H_2, such that alcohol dehydrogenation is commonly thought to occur by transfer hydrogenation to unsaturated condensation products such as crotonaldehyde.[236,239,241-243] Transfer hydrogenation may occur directly between species through a

Meerwein–Ponndorf–Verley (MPV) mechanism or through bound H atoms in a surface-mediated mechanism. Recent evidence suggests that C=O hydrogenation occurs largely through the MPV mechanism while C=C hydrogenation makes use of surface H atoms.[239] Transfer hydrogenation is also typically rapid under Guerbet coupling conditions and is not rate-limiting.[240,244] If hydrogenation and dehydrogenation do indeed occur through transfer hydrogenation mechanisms, then aldolization may be a thermodynamically plausible mechanism. While the rate of dehydrogenation is rapid relative to condensation on these catalysts, the first-order dependence of the condensation rate on acetaldehyde pressure suggests that increasing the extent of EtOH dehydrogenation — which depends on the ability of the catalyst to interact with H_2 — is still beneficial to the reaction rate. The ability of the catalyst to dissociate H_2 is readily increased by incorporating Group 10 or 11 transition metals such as Ni, Cu, or Pd. For example, EtOH conversion over Mg_5CeO_x (300°C) sees the rate of D_2 incorporation into EtOH increase by a factor of 20 when the catalyst includes 7wt% Cu.[245] This leads to an 80x increase in the EtOH conversion rate, though acetaldehyde was by far the dominant product rather than C_{4+} species. Separately, $NiMg_4AlO_y$ is almost 100x more active than Mg_4AlO_y (18.7% versus 0.2% conversion at fixed weight-hourly space velocity) for EtOH condensation at 250°C.[246] Furthermore, alcohol selectivities improved when using catalysts featuring a transition metal. The key discrepancy between these studies regarding the selectivity to condensation may be pressure: Cu/Mg_5CeO_x was studied at atmospheric pressure while $NiMg_4AlO_y$ was examined at 30 bar, at which the equilibrium aldehyde:alcohol ratio would be lower. High pressures are commonly utilized in Guerbet coupling when transition metal catalysts are used, although it is unclear why high pressure is needed since the analogous data at atmospheric pressure are typically not reported. The implications of high-pressure operation are complex, because H_2 partial pressure influences H_2 +

aldehyde ↔ alcohol equilibria, surface coverages, and potentially fluid phases: gas, liquid, and supercritical fluid. Although the main role of the transition metal is thought to be to accelerate H exchange between the gas and surface (spillover), it is also important to recognize that the metal can itself catalyze transformations of alcohols and aldehydes. This is particularly true of Cu, Ag and Au, which are often present in EtOH dehydrogenation catalysts[247-250] and can catalyze aldolization reactions.[251] Whether these metals directly catalyze aldolization to a significant extent during EtOH condensation is uncertain and likely depends on the system.

The side-reactions commonly observed for the Guerbet condensation include unimolecular dehydration (to a mono-ene), bimolecular dehydration (to an ether), Lebedev condensation (to a diene), esterification, ketone–aldehyde isomerization, decarbonylation, and complex oligomerization/cyclization reactions to form aromatics and coke. These side reactions become more important with increasing temperature. Olefins and ethers are the main side-products for catalysts such as MgO, Mg_xAlO_y, and HAP, which do not possess reducible transition metals.[61,252] Of these catalysts, HAP is the most selective for alcohols at elevated conversions, showing 86% selectivity to C_{4+} alcohols (55% to 1-butanol) at 52% conversion (275°C).[253] MgO is only about 33% selective to 1-butanol at 56% conversion (450°C), while Mg_3AlO_y is 50% selective at 44% conversion (300°C).[254,255] Lower temperatures lead to higher alcohol selectivities, but the low reaction rates at these temperatures make high conversions (>30%) difficult to achieve. Dehydration occurs to a lesser extent when using catalysts featuring Group 10 or 11 transition metals, in part because their higher activities in condensation reactions enable efficient catalysis at lower temperatures. Instead, catalysts with Group X metals tend to catalyze C–C cleavage reactions such as decarbonylation, while Group XI metals promote esterification.[248,251,256-258] Ketones and secondary alcohols also result from conversion of the β-hydroxyaldehyde product

prior to its dehydration. The catalysts most commonly examined in the literature include Ni- or Cu-promoted Al_2O_3 or Mg_xAlO_y, and these are typically used at conversions below 30% or are nonselective to alcohols (<50% selective at around 50% conversion).[246,258-260] In contrast, patented Pd-based catalysts can mediate high conversion while maintaining high selectivities. Thus, Pd/Mg_xAlO_y shows 73% selectivity at 67% conversion (250°C) and Pd/ZrO_2 shows 86% selectivity at 78% conversion (360°C).[261,262] As described above, there are two main ways by which Guerbet coupling can be used to produce distillate fuels: condensation to C_{4-8} alcohols followed by dehydration and olefin oligomerization or direct oligomerization into the distillate range. The former (Figure 3.12c) has been examined as a means to convert syngas to distillate fuels as an alternative to the Fischer–Tropsch process.[31,263] These processes first convert syngas to EtOH-rich alcohol streams either through heterogeneous catalysis (for example, over MoS_2) or by fermentation. Guerbet coupling is then performed near 50% conversion followed by separation into three streams: EtOH, H_2O, and C_{4+} alcohols. The EtOH is recycled into the reactor, and it is important that this recycle stream does not contain H_2O, because this is known to substantially slow condensation reactions.[233,264] One effect of water is the unfavorable reconstruction of base sites, such as the conversion of strong Lewis basic O^{2-} sites to weaker Brønsted OH^-.[259,265,266] Further, the presence of water enables hydrolysis reactions, affording acids that poison base sites and may also chelate metals in liquid-phase conversions.[233,267,268] The butanol-rich C_{4+} alcohols stream is sequentially dehydrated to olefins, oligomerized with either a Ziegler–Natta or solid acid catalyst, and then hydrogenated. In principle, the final products of these processes consist of both jet- and diesel-range isoparaffins.

In order to produce alcohol mixtures heavy enough for direct use in distillate fuels, high EtOH conversions are required. Assuming that Guerbet coupling follows step-growth

oligomerization kinetics, a minimum conversion of 86.5% is required to produce a mixture of alcohols of average carbon number 10 or higher. This has not been achieved with heterogeneous catalysts, however. This may be in part because the majority of studies either focus on understanding mechanistic aspects of the Guerbet reaction or on selectively producing 1-butanol. Both such studies require operation at below 20% conversion, because higher conversions lead to lower 1-butanol selectivities as more and more C_{6+} alcohols are formed. The alcohol distributions obtained at elevated conversions are therefore largely unknown. As mentioned above, Guerbet condensation introduces alkyl branching at the α position when the nucleophile originates from a C_{3+} alcohol. For example, mixtures containing both EtOH and 1-butanol afford both 1-hexanol and 2-ethyl-1-butanol. 1-Hexanol forms when the nucleophile in the Guerbet coupling is EtOH, while 2-ethyl-1-butanol results when the nucleophile is 1-butanol. The degree to which α-substitution affects alcohol condensation rates is not well understood. The selectivities towards either branched or linear alcohols can be influenced by the structure of the aldehyde or alcohol as well as the nature and basicity of active sites on a catalyst. When solid bases deprotonate a carbonyl compound, an enolate results.[269] Alkyl substitution at the α-C will decrease the stability of the carbanion resonance form but will increase the stability of the oxyanion resonance form. EtOH condensation studies rarely address the notion of branching in the products in part because the results of experiments at high conversions (necessary to observe sufficient amounts of C_{6+} alcohols) have not been reported. Recently, however, the formation of higher alcohols over Ca- and Sr-HAP has been addressed.[239] These 'cascade' reactions afford C_{6+} alcohol products, with the distributions being consistent with a modified step-growth model wherein the rate of forming each alcohol is nearly entirely dependent on the concentration of its constituent reactants because differences between C_2 and C_{3+} linear enolates are for the most part kinetically irrelevant.

Nonetheless, 2-ethyl-1-butanol was produced at slightly higher levels than 1-hexanol and other catalysts have different propensities to form branched products. In the batch condensed-phase condensation of EtOH over Ni/Al_2O_3, 1-hexanol and 2-ethyl-1-butanol are formed in a ratio of up to 4:1.[270] In the cross-condensation of acetaldehyde and heptanal over Mg_3AlO_y, the ratio of linear to branched C_9 products varied between 0.8 and 1.5.[271] In aldol condensations, enolates of α-alkylaldehydes are too sterically hindered to serve as nucleophiles, while the α-alkylaldehydes are also too bulky to serve as electrophiles. This has been observed in the cross-condensation of butanal and 2-methylpropanal over $Pd/Na/SiO_2$.[272] The tendency of a catalyst to form linear versus branched alcohols is therefore important to converting EtOH to C_{8+} alcohols in high yields. If branching is favored, 2-ethyl-1-butanol and 2-ethyl-1-hexanol (from 1-butanol self-condensation) will be the main $C_{6–8}$ alcohol products and not appreciably react further. Thus, these condensation reactions are limited to producing alcohols just below the distillate range. Another challenge associated with reaching high conversions is that the condensation reaction produces H_2O, which can participate in the reverse reaction. Overcoming this necessitates high catalyst loadings to compensate for the decreasing reaction rates. The development of H_2O-tolerant catalysts is therefore an important research area.

An alternative to direct oligomerization of EtOH into distillates is to separate condensation into two steps: one which produces C_{4+} alcohols (mainly 1-butanol) and a second which condenses these C_{4+} alcohols to produce C_{8+} species. This approach can be challenging in that branched alcohols may form, and these exhibit limited reactivity. Eastman has patented a two-stage process in which two three-stage reactors were used to convert EtOH to 2-ethyl-1-hexanol (though not for fuel applications).[273] The intention of a direct oligomerization route is to use the alcohols directly in fuel blending. This would allow the process to remain hydrogen-neutral, which can be an

economically important factor in biomass-to-distillate processes as mentioned prior.[163] The lowest-boiling C_{8+} alcohol from Guerbet coupling is 2-ethyl-1-hexanol, the product of 1-butanol self-condensation. 2-Ethyl-1-hexanol has a suitable boiling point (185°C), freezing point (−70°C), density (0.83 g mL^{-1}), and flash point (72°C) to serve as a distillate fuel, though the cetane (~26) is somewhat low (Table 3.1). The 1-hexanol self-condensation product 2-butyl-1-octanol has a better cetane (~46). The net heating values of C_{8-12} alcohols fall in the range ~32–33 MJ L^{-1}, such that these species have lower volumetric energy densities than Jet A and diesel (34 and 36 MJ L^{-1}, respectively; Table 3.1). Although the C_{8-12} alcohols are not far off from Jet A in terms of heating values, blending them with jet fuels is difficult because these must theoretically have a minimum C:O ratio of 13.[43] In the event that these alcohols are deemed unsuitable for blending, they may instead be dehydrated and hydrogenated to give paraffins.

In general, the main challenge with using Guerbet coupling to produce distillate-range molecules is reaching high conversions while maintaining high selectivities for alcohol products. Several of the reasons behind this are associated with the presence of alcohols rather than with condensation itself. Alcohol dehydrogenation requires higher temperatures than does aldol condensation, such that side reactions are pervasive. Many of these side reactions also directly involve the alcohols themselves, with dehydration to olefins being problematic. Additionally, the alcohols in the feed compete with aldehydes for adsorption at catalytic sites, slowing down aldehyde conversions. These selectivity problems suggest that it may be beneficial to separate the Guerbet condensation steps into multiple stages, enabling condensation to be facilitated effectively at lower temperatures where side reactions are less prevalent. This is the focus of a separate ETD route discussed in the next section in which higher aldehydes are the target product.

3.10 Higher aldehydes from acetaldehyde condensation

One of the challenges inherent to heterogeneous Guerbet coupling is that EtOH dehydrogenation requires temperatures above 200°C — conditions where dehydration and decarbonylation also occur. Aldol condensation of linear aldehydes can occur at temperatures below 150°C. Thus, it is possible to separate dehydrogenation and aldol condensation into sequential stages to obtain higher selectivities for condensation products. EtOH dehydrogenation is most commonly performed over Group 11 transition-metal-containing catalysts under aerobic or anaerobic conditions,[247-250,274] affording up to 97% yield at temperatures between 200 and 300°C. The acetaldehyde can then be separately oligomerized, but this reaction is commonly accompanied by rapid catalyst deactivation[275,276] because the reactions of C=C bonds in successive condensation products lead to the formation of aromatics and coke. The formation of these side-products can be avoided by hydrogenating the C=C bonds between condensations without hydrogenating C=O bonds. This selective hydrogenation is kinetically possible with transition metals and is also thermodynamically favored because, as discussed with crotonaldehyde hydrogenation, C=C hydrogenation is highly exothermic.[277,278] Therefore, aldol condensation under H_2 in the presence of a reduced transition metal can proceed efficiently without substantial formation of unsaturated aldehydes or termination to alcohols. These steps are well-described by aldehyde-containing steps of Guerbet condensation (Figure 3.11a).

The approach using H_2 and transition metals has recently been proposed as an alternative to Guerbet coupling for the conversion of EtOH to drop-in fuel replacements.[279] Acetaldehyde undergoes complete conversion over Amberlyst 15 and Pd/C in a batch reactor filled with 6% H_2 in Ar to give a 79% yield of 2-ethylbutanal and a 13% yield of 2-ethylhexanal. This approach makes use of a two-stage heating program, holding the reaction at 60°C for 1 h and then at 100°C for 3 h. The product aldehydes were considered for use in diesel fuel either directly, after

hydrogenation to alcohols, after hydrodeoxygenation to alkanes, or after reactions with EtOH to give diethyl acetals. The cetane values for the aldehydes and acetals are in the range appropriate for diesel fuels, but the boiling point of 2-ethylbutanal is only 117°C — below the lower limits for both jet and diesel fuel. The heavier product, 2-ethylhexanal, has a boiling point of 163°C and is thus better suited for distillate fuels. Nevertheless, it is desirable for these products to undergo further condensation to afford heavier products with energy densities closer to distillate fuels. The preferential formation of 2-ethylbutanal and 2-ethylhexanal suggests that butanal and hexanal are more likely than acetaldehyde to serve as nucleophiles, which may be related to the relative stabilities of the corresponding enols in the acid-catalyzed aldol condensation. No di-α-alkylaldehydes or γ-alkylaldehydes were observed in the products of the previous study, suggesting that these α-alkylaldehydes are only minimally active in condensation (although 8% of the converted acetaldehyde was not identified). This observation is likely a result of steric inhibition. A linear product is possible if an enolate rather than enol is the nucleophile, and using a solid base would thus mean that the condensation may not be limited to $C_{6\text{-}8}$ aldehyde products because linear species in this range can continue to condense. As mentioned prior with respect to Guerbet coupling, cross-condensation of acetaldehyde and heptanal over Mg_xAlO_y can produce linear products more selectively than branched ones.[271] Additionally, condensation of butyraldehyde/isobutyraldehyde mixtures over Pd-Na/SiO_2 show that α-alkylaldehydes, under base catalysis, are reactive as electrophiles (though less so than linear aldehydes).[272] It is also important to note that the fully hydrogenated product 2-ethyl-1-hexanol, even under 8 bar H_2 at 350°C, represents less than 1% of the product mixture. If Ni/Ce-Al_2O_3 is used instead, full butyraldehyde conversion affords 2-ethyl-1-hexanol in 66.9% yield without any unsaturated C_8

products (batch, 170°C, 40 bar H_2).[280] The choice of metal may therefore be critical to this technology.

The use of solid acids or bases in concert with metals active for hydrogenation has been only minimally investigated in the context of upgrading acetaldehyde. However, the approach could be a promising ETD technology, either by means of a single-stage or two-stage condensation scheme (Figure S3.4). Single-stage operation aims to oligomerize directly into the distillate range, but a large fraction of the product mixture will be 2-ethylbutanal unless the acetaldehyde enolate can act as a much more effective nucleophile than that generated from butyraldehyde. 2-Ethylbutanal is not likely sufficient for distillate blending at high levels due to its low boiling point and energy density. The C_{4-6} aldehydes can be converted with EtOH to produce a high cetane diethyl acetal, though dioxygenates such as these possess low energy densities.[279] The viability of single-stage operation rests on the formation of hexanal in preference to 2-ethylbutanal. Further, high conversions are necessary but difficult to achieve with solid base catalysts due to the build-up of H_2O. Performing the aldol condensation at lower conversions with large recycle ratios may be costly because of the need for continuous H_2O removal, though the requisite H_2O–acetaldehyde separation is expected to be less costly than H_2O–EtOH due to the low boiling point of acetaldehyde (21°C). If one can isolate a mixture of acetaldehyde and butyraldehyde from the higher aldehydes, this can be recycled such that the overall system produces mainly C_{6+} (ideally C_{8+}) aldehydes. To push the distribution toward larger aldehydes, this stream could be co-fed with acetaldehyde in a second reactor, producing a stream of C_{8+} aldehydes more suitable for distillate fuels. In principle, the H_2 liberated from anaerobic EtOH dehydrogenation can be used to hydrogenate the C=C groups during condensation. The resulting aldehydes will be rather reactive, and this is expected to be detrimental for fuel stability. This is particularly the case for jet

applications, though the products may still be suitable for use in diesel fuel.[44] As in the case of Guerbet alcohols, these aldehydes can also simply be converted to paraffins if the oxygenates are deemed detrimental to fuel quality. This could be performed with sequential hydrogenation–dehydration–hydrogenation or through decarbonylation, though the latter would lower the carbon efficiency of the process. In sum, the acetaldehyde route to distillates approach is largely theoretical at this point, and realizing it on a commercial scale will require a great deal of further research. The final ETD route described here involves the more well-established technology of acid-catalyzed olefin oligomerization, which is applied to the $C_{3\text{-}4}$ olefins formed from concerted EtOH dehydrogenation and condensation chemistries.

3.11 Oligomerization of propene and isobutene produced directly from EtOH condensation

Rather than dehydrating EtOH to ethylene or oligomerizing EtOH to 1-butanol and dehydrating it to butenes, EtOH can be converted directly to $C_{3\text{-}4}$ olefins —propene and isobutene — through condensation reactions that proceed via acetone as an intermediate (Figure 3.13). EtOH condensation to acetone proceeds over metal oxides, and these commonly contain ZnO and/or ZrO_2 and can also have Cu, which is included to facilitate dehydrogenation.[281-283] The condensation of acetaldehyde is most commonly proposed to occur through either aldolization or ketonization, both of which require a catalyst with basic sites.[284,285] After aldolization, the coupled product is believed to undergo dehydrogenation to give a dicarbonyl that then decomposes to acetone and formic acid or to acetaldehyde and acetic acid.[284] Formic acid decomposes to CO or CO_2, while acetic acid ketonizes to acetone and CO_2. Alternatively, acetaldehyde can be directly oxidized to acetic acid via a surface-bound acetate intermediate.[285] Ketonization then produces acetone and CO_2. For most catalysts, it is still debated whether acetaldehyde reacts through aldolization or oxidation. The former route is supported by infrared spectra consistent with the

presence of a dicarbonyl species on Fe_2O_3-CaO, though no such species could be observed on ZrO_2.[284,286] The aldol condensation product crotonaldehyde has also been observed at low levels when using either ZnO or ZrO_2, though it disappears upon addition of H_2O.[286-288] The presence of H_2O encourages the formation of ethyl acetate, acetic acid, and acetone at 325°C,[286] but instead lowers ethyl acetate and acetic acid yields while promoting acetone formation at 400°C. These observations are more consistent with a ketonization mechanism. Both mechanisms are distinct from the aldol condensation mechanisms discussed in prior ETD technologies. The two mechanisms here involve carboxylic acid intermediates, the formation of which is promoted either through lattice O atoms or H_2O. In this way, acetone can then be hydrogenated and dehydrated to give propene or converted to isobutene via mesityl oxide as an intermediate.[289] Encouraging acetone hydrogenation favors the formation of propene. For example, the catalyst Sc/In_2O_3, wherein the role of Sc is mainly to stabilize In_2O_3, produces acetone in the presence of H_2 and isobutene in its absence.[290] Isobutene formation also notably requires Lewis acid–base pairs of balanced strengths, a notion gathered from comparing product distributions obtained from several $Zn_xZr_yO_z$ catalysts with different Zn/Zr ratios (~10 being optimal).[289,291,292]

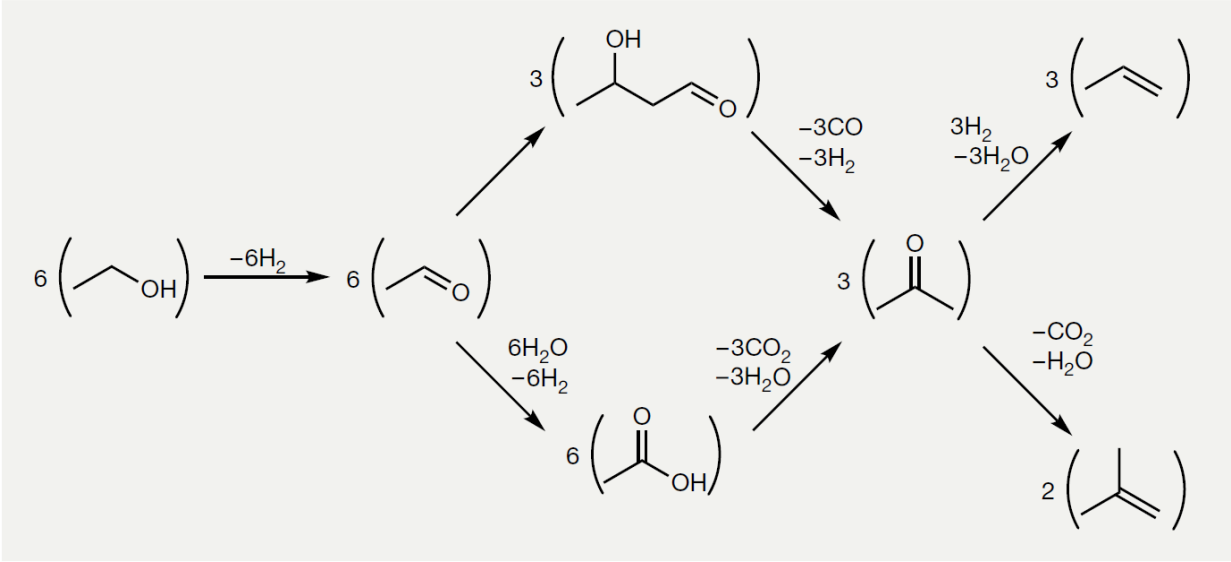

Figure 3.13 | **The direct conversion of EtOH to olefins through an acetone intermediate.** EtOH is first dehydrogenated to acetaldehyde, which may then be converted to acetone either through an aldol condensate or an acetate intermediate (represented here as HOAc for clarity; HOAc could take the form of a surface acetate or free HOAc). Acetone reacts further to give either propene or isobutene. The stoichiometries are written for balance, though interconversion of CO, CO_2, H_2O, H_2, and CH_4 may occur depending on the catalytic system.

As with Guerbet coupling, dehydrogenation of EtOH to acetaldehyde is the most endothermic step in the present $C_{3\text{-}4}$ olefin approach to fuels (Figure 3.13). Acetaldehyde conversion to acetone (through the acetate route with CO_2 production) is highly exothermic ($\Delta H°$ = −37 kJ $mol_{acetone}^{-1}$) and entropically favorable ($\Delta S°$ = 53 J K^{-1} $mol_{acetone}^{-1}$) such that the process is thermodynamically spontaneous at all practical temperatures ($\Delta G°$ = −52 kJ $mol_{acetone}^{-1}$). The conversion of acetone to isobutene or propene is less favorable ($\Delta G°$ = −16 and −13 kJ $mol_{acetone}^{-1}$, respectively) because the reactions are less exothermic ($\Delta H°$ = −5.5 and −3.8 kJ $mol_{acetone}^{-1}$, respectively). Transforming acetone to isobutene is the limiting reaction step in the overall EtOH conversion to isobutene.[289] Both conversions of EtOH to isobutene and propene are exergonic above 40°C and can be easily driven to full conversion at the temperatures commonly used (>450°C). It is also worth noting that a theoretical process for the conversion of EtOH to isobutene

without CO_x byproducts is highly exergonic at all temperatures ($\Delta G° = -63$ kJ $mol_{isobutene}^{-1}$, $\Delta S° = 106$ J K^{-1} $mol_{isobutene}^{-1}$).

Regardless of the mechanism of acetaldehyde condensation, one CO_x molecule must be liberated en route to forming acetone and another en route to isobutene. The theoretical maximum propene yield through this process is therefore 75%, while that of isobutene is only 67%. Large carbon losses are the main drawbacks of the present technologies because CO_x has essentially no value. Although the previously discussed ETD routes also give rise to low molecular weight side-products, these can usually be recycled, easily converted to chemicals or fuels by other means, or directly used in lighter fuel blends such as gasoline. One benefit of these routes briefly mentioned in the mechanistic discussion is the beneficial role of H_2O (for example, in assisting carboxylate formation), which may reduce purification costs associated with using aqueous bioEtOH. Thus, Sc/In_2O_3 operates on a mixture of 30vol% EtOH, 8.5vol% H_2O, and 30vol% H_2 with N_2 balance at 550°C to produce 82% of the theoretical propene yield (82% × 75% = 61% overall yield).[290] This feed could be supplied by aqueous bioEtOH containing 90wt% EtOH — well below the azeotrope. Although Sc/In_2O_3 loses some activity during operation, it is largely recoverable by reoxidation. $Zn_1Zr_{10}O_x$ was used with a mixture of EtOH, H_2O, and N_2 (H_2O:C ratio = 5:1) at 450°C to afford isobutene in 83% theoretical yield (55% overall).[291] This feed corresponds to a dilute bioEtOH stream of 11wt% EtOH — approximately the concentration present in fermentation broths. To remove impurities, some level of EtOH purification will still be required, and the requisite purification should be examined to understand the potential lowering of distillation costs. H_2 is also evolved in the process and could potentially be reused downstream to hydrogenate the olefin oligomers to paraffins, thereby decreasing and possibly eliminating the need for external H_2.

Dimerization of an isobutene feed affords products in the distillate range and can be performed at temperatures as low as 40°C because protonation of isobutene readily forms a tertiary carbenium that can react with a neutral olefin.[293,294] Both isobutene dimerization and trimerization have been well studied because they are competing side-reactions in the synthesis of methyl *tert*-butyl ether from methanol and isobutene.[56,295-297] Efficient trimer- and tetramerization of isobutene occurs over H-β at 70°C, 15 bar with minimal, reversible catalyst deactivation observed over 70 h.[298] The oligomer distribution is approximately 10% dimer (C_8), 60% trimer (C_{12}) and 30% tetramer (C_{16}) at 100% conversion. Hydrogenation of the mixture would therefore produce highly branched $C_{8\text{-}16}$ paraffins that would likely be ideal for jet fuel blending at high levels (the low expected cetane would not make this a viable route for diesel). The block flow diagram for the propene and isobutene routes is presented in Figure S3.5. Notably, the isobutene route to jet fuel is under investigation by researchers at PNNL, who have analyzed the full process starting with fermentation of syngas to give EtOH.[164] Although the carbon yield of isobutene from EtOH is only 59% (with a 67% mechanistic maximum), oligomerization is 95% selective, and hydrogenation is essentially 100% selective. The profitability of these acetone-mediated routes will be dependent on potentially reducing costs with lesser bioEtOH purification while maintaining 100% selectivity after the initial EtOH conversion step.

While this ETD route has not thus far received substantial commercial attention, the isobutene oligomerization step is central to Gevo's alcohol-to-jet (ATJ) technology, which first produces isobutanol rather than EtOH from sugar fermentation.[299] Isobutanol is then dehydrated to isobutene (presumably using γ-Al_2O_3) and oligomerized to a mixture of branched olefins (presumably using Amberlyst 35) which are subsequently hydrogenated to produce a jet blendstock described as "synthesized paraffinic kerosene" (SPK). This fuel predominantly

comprises isomers of dodecane and hexadecane with extensive methyl branching (for example, 2,2,4,6,6-pentamethylheptane), with the US Navy jet fuel JP-5 being a much more complex mixture.[27] While Gevo does not use EtOH as the feedstock, the extensive validation of Gevo's fuels for jet applications is noteworthy. Thus far, the fuels have been tested directly as aviation fuel, received ASTM validation (D7566-18), were approved by the US Federal Aviation Administration, and have been successfully used in a series of commercial flights by Virgin Airlines in Australia.[300-302]

3.12 Comparison of ETD routes

The many routes for producing distillate fuels from EtOH described here are summarized in Figure 3.2 and Table S3.4. The chemistries involved in these routes include dehydration, acid-catalyzed oligomerization, metal-catalyzed oligomerization, dehydrogenation/hydrogenation, aldol condensation, esterification, and ketonization. The types of molecules produced include olefins, paraffins, aromatics, alcohols, ketones, and aldehydes. While the most easily understandable combinations of key chemistries have already been described, there is certainly room for further innovation. One example would be the direct high-temperature conversion of EtOH over HAP to gasoline or jet fuel. This process would be similar to the acid-catalyzed simultaneous dehydration/oligomerization process but with the addition of more complex chemistries such as those involved in the Guerbet coupling.[303,304]

A direct comparison of ETD routes can be found in Table S3.4. The technologies that have been demonstrated beyond the laboratory bench scale (>5 kg day^{-1}) rely on acid-catalyzed olefin oligomerization.[135,178] The simultaneous dehydration and oligomerization process is the simplest because fermentation broths may not require full purification, only a single reactor is required, and the products can be easily separated due to large differences in their volatilities and solubilities.

However, this process is incapable of producing distillate-range fuels in high yields, with most products being smaller than C_{10}. Moreover, aromatics dominate the liquid product distribution (~75%), limiting the blending of these products into fuels, which typically cannot have aromatic contents above 30%. This process may thus be more useful as a means of making both BTEX and gasoline, with only the heavy products being useful for jet fuels to enhance cold-flow properties. A similar approach is the sequential dehydration of EtOH to ethylene followed by acid-catalyzed oligomerization, from which similar results are expected because high temperatures (>300°C) are still required to activate ethylene — the reason behind the selectivity limitations of the simultaneous route. For these technologies, key areas of research are largely related to implementation — multiple-stage oligomerization is required to limit the production of aromatics and short-chain olefins. Rigorous technoeconomic analyses should be performed to identify the most promising multi-stage configurations, allowing us to identify the olefins that need to be recycled, their recycle ratios, and the optimal conversion at which the first reactor should operate.

Metal-catalyzed olefin oligomerization may be a practical route, particularly with heterogeneous catalysts such as Ni supported on an aluminosilicate. Such processes have not yet been commercialized and often afford branched products, a problem that may be addressed by using more selective Co catalysts. Commercial ethylene oligomerization systems involve homogeneous catalysts, cocatalysts, and/or solvents, all of which necessitate additional separations. Highly-selective homogeneous catalysts operating through a metallacycle mechanism are more suited toward producing targeted linear olefins for sale as commodity chemicals rather than distillate fuels. Implementing Cossee–Arlman catalysis to convert ethylene is likely more viable, though the resulting Schulz–Flory distribution of products limits single-pass distillate selectivities to ~63%. This motivates the use of multiple-stage configurations in which ethylene is

first converted to C_{4-8} oligomers in one stage which can be lengthened into distillates in a second stage. Economic analyses will be important in determining optimal configurations, with the following parameters likely to be instrumental: the α value associated with the first oligomerization step, the use of transition metals versus solid acids in the next stage, and the use of separation/recycle loops. In terms of catalysts, the simultaneous use of supported Ni and solid acids is potentially useful because it affords a more ideal carbon distribution. Implementation of such systems requires a better understanding of the impact of catalyst and reaction parameters as well as demonstration at larger scales.

Guerbet condensation routes are mainly limited by low single-pass conversions and the requirement of a pure EtOH feed. These processes may also require recycling, which can be costly. The effects of using high pressures in these reactions need to be better understood, especially when working with transition-metal-containing catalysts for hydrogenations. The ability to separate condensation and hydrogenation/dehydrogenation reactions also potentially allows for more control over selectivity for alcohols. Because both branched and linear alcohols can form, a fundamental understanding of the factors (including measurable properties of the catalyst) leading to one or the other is required. If Guerbet coupling is simply used as a way to produce C_{4+} olefins (after alcohol dehydration) for acid-catalyzed oligomerization, the economics of such a step must be compared with the acid-catalyzed and metal-catalyzed routes for producing C_{3+} olefin mixtures. To produce distillate-range alcohols (either in one or two stages), the condensation of C_{6+} alcohols, particularly α-alkyl-1-alcohols, requires further study. Linear alcohols are more reactive than these branched products, and if the latter react too slowly then their formations must be suppressed.

Aldol condensation when combined with C=C hydrogenation may be a viable route to fuels if large amounts of C_{8+} aldehydes can be produced. Base catalysis appears to be promising since

it is less prone than acid catalysis to producing branched alcohols. The limitations of this route to distillate-range alcohols are similar to those of Guerbet coupling, though the lower-temperature operation allows for more control over selectivity, and the absence of alcohols may increase condensation rates by freeing up catalytic sites. Parametric studies with solid bases can probe the present limitations of these systems, while fundamental examinations of the condensation can aid in the design of new catalysts and the identification of limitations associated with producing distillate-range aldehydes in this manner. The applicability of the resultant aldehydes in fuels must be more thoroughly examined. If such aldehydes are inherently unstable or cannot otherwise be used, decarbonylation or hydrogenation–dehydration–hydrogenation may be used to produce highly linear alkanes.

Direct isobutene formation from EtOH has been demonstrated near its theoretical limit, while the subsequent oligomerization can be used to produce jet-fuel-range olefins at selectivities approaching 100%. The key concern here is the theoretical yield limit of the EtOH-to-isobutene step, in which minimally one-third of the carbon is lost as CO_x. A potential benefit of the technology is its high H_2O tolerance, which may enables lower levels of bioEtOH purification. Some level of purification is still likely required, however, since impurities in the bioEtOH may detrimentally impact catalytic performance. Determining whether purification can be substantially reduced to offset carbon losses will be crucial in maximizing the profitability of such a route. If this is can be done, further catalyst optimization to achieve theoretical yields is desirable. Although the isobutene route may be useful, the propene route has high CO_x losses and is unlikely to be more economical than simple two-stage acid catalysis.

Altogether, it is difficult to be certain which of the above routes will ultimately be successful commercially. Jet fuel production has been proven on large scales through the

sequential EtOH dehydration and two-stage ethylene oligomerization over transition metal and solid acid catalysts. The production of diesel fuels from EtOH has not yet been commercially realized, though improvements in transition-metal-catalyzed oligomerization may change this. Further research into aldol condensation routes (Guerbet coupling and sequential dehydrogenation and condensation) will be required to evaluate their viabilities because the majority of the known limitations of these systems are related to catalyst development and a general lack of mechanistic understanding. Whether inherent limitations to the chemistry exist remain unclear. In principle, these routes may be used to produce compounds suitable for either jet or diesel, though further processing may be required if the aldehydes and alcohols cannot be directly blended with conventional fuels to appreciable extents. The acetone-mediated routes are necessarily accompanied by carbon losses, which will be difficult to offset even by the potential cost reductions associated with using lower purity EtOH. The acetone routes, based on the expected oligomerization products of propene and isobutene, also appear to afford products more suitable for jet fuels. An additional aspect that must be considered is the H_2 requirement, as some of these routes require H_2 (for example, to give the final paraffins) and some do not.

3.13 Conclusions and outlook

As demand for middle-distillate fuels continues to increase, sustainable approaches for their production will become increasingly important. The use of EtOH as a platform molecule for this purpose has received growing attention in recent years, notably with the ASTM approval of an EtOH-derived jet fuel and its successful use for a commercial flight in 2018. This success motivates research into the oligomerization chemistries that afford this fuel and also opens the door for the development other ETD processes. Understanding how to steer olefin oligomerization towards linear products is a classic challenge in heterogeneous catalysis that directly translates to

fuel quality — overly branched products are often formed and these are desirable for jet fuel but unsuitable for high-cetane diesel fuel. Aldolization may be used as an alternative EtOH oligomerization route to heavier products. This reaction has attracted recent attention as a key aspect in the Guerbet coupling of EtOH to 1-butanol, but the potential to extend the oligomerization remained generally unknown. Understanding the chemistries that can be utilized in the conversion of EtOH to longer-chain hydrocarbons and oxygenates will be critical to rationally guiding research efforts. This technical understanding must also be supplemented with technoeconomic analyses, which will be crucial in evaluating which technologies will ultimately be the most promising in producing diesel and jet fuels.

3.14 References

1 Eagan, N. M., Kumbhalkar, M. D., Buchanan, J. S., Dumesic, J. A. & Huber, G. W. Chemistries and processes for the conversion of ethanol into middle-distillate fuels. *Nature Reviews Chemistry* **3**, 223-249, (2019).

2 Balat, M. & Balat, H. Recent trends in global production and utilization of bio-ethanol fuel. *Appl. Energ.* **86**, 2273-2282, (2009).

3 Annual energy outlook 2019. (U.S. Energy Information Administration, 2019).

4 Warner, E., Schwab, A. & Bacovsky, D. 2016 survey of non-starch ethanol and renewable hydrocarbon biofuels producers. *National Renewable Energy Laboratory* (2017).

5 Silveira, M. H. L., Morais, A. R. C., da Costa Lopes, A. M., Olekszyszen, D. N., Bogel-Łukasik, R., Andreaus, J. & Pereira Ramos, L. Current pretreatment technologies for the development of cellulosic ethanol and biorefineries. *ChemSusChem* **8**, 3366-3390, (2015).

6 Lynd, L. R., Liang, X., Biddy, M. J., Allee, A., Cai, H., Foust, T., Himmel, M. E., Laser, M. S., Wang, M. & Wyman, C. E. Cellulosic ethanol: status and innovation. *Curr. Opin. Biotechnol.* **45**, 202-211, (2017).

7 Wyman, C. E., Cai, C. M. & Kumar, R. in *Encyclopedia of Sustainability Science and Technology* (ed Robert A. Meyers) 1-27 (Springer New York, 2017).

8 Barros, S. Brazil biofuels annual report 2018. *U. S. Department of Agriculture*

9 Hsieh, W.-D., Chen, R.-H., Wu, T.-L. & Lin, T.-H. Engine performance and pollutant emission of an SI engine using ethanol–gasoline blended fuels. *Atmos. Environ.* **36**, 403-410, (2002).

10 Agarwal, A. K. Biofuels (alcohols and biodiesel) applications as fuels for internal combustion engines. *Prog. Energy Combust. Sci.* **33**, 233-271, (2007).

11 Hansen, A. C., Zhang, Q. & Lyne, P. W. Ethanol–diesel fuel blends—a review. *Bioresour. Technol.* **96**, 277-285, (2005).

12 Shahir, S., Masjuki, H., Kalam, M., Imran, A., Fattah, I. R. & Sanjid, A. Feasibility of diesel–biodiesel–ethanol/bioethanol blend as existing CI engine fuel: an assessment of properties, material compatibility, safety and combustion. *Renew. Sust. Energ. Rev.* **32**, 379-395, (2014).

13 Bacha, J., Freel, J., Gibbs, A., Gibbs, L., Hemighaus, G., Hoekman, K., Horn, J., Ingham, M., Jossens, L., Kohler, D., Lesnini, D., McGeehan, J., Nikanjam, M., Olsen, E., Organ, R., Scott, B., Sztenderowicz, M., Tiedemann, A., Walker, C., Lind, J., Jones, J., Scott, D. & Mills, J. Diesel fuels technical review. *Chevron Corporation* (2007).

14 U.S. Environmental Protection Agency. 40 CFR 1065 Subpart H. *Engine fluids, test fuels, analytical gases and other calibration standards.* (2017).

15 ASTM International. ASTM D1655-17. *Standard specification for aviation turbine fuels.* (2017).
16 ASTM International. ASTM D975-17. *Standard specification for diesel fuel oils.* (2017).
17 Lapuerta, M., Garcia-Contreras, R., Campos-Fernández, J. & Dorado, M. P. Stability, lubricity, viscosity, and cold-flow properties of alcohol− diesel blends. *Energ. Fuel.* **24**, 4497-4502, (2010).
18 Hemighaus, G., Boval, T., Bacha, J., Barnes, F., Franklin, M., Gibbs, L., Hogue, N., Jones, J., Lesnini, D., Lind, J. & Morris, J. Aviation fuels technical review. *Chevron Products Company*, (2006).
19 UK Defence Standardization. Defence Standard 91-091. *Turbine fuel, aviation kerosine type, Jet A-1.* (2016).
20 Hazardous Substrances Data Bank. *U.S. National Library of Medicine*
21 International Chemical Safety Cards. *International Labour Organization*
22 Yaws, C. L. *Chemical properties handbook*. (McGraw-Hill, 1999).
23 Yanowitz, J., Ratcliff, M., McCormick, R., Taylor, J. & Murphy, M. Compendium of experimental cetane numbers. *National Renewable Energy Laboratory* (2017).
24 Saldana, D. A., Starck, L., Mougin, P., Rousseau, B., Pidol, L., Jeuland, N. & Creton, B. Flash point and cetane number predictions for fuel compounds using quantitative structure property relationship (QSPR) methods. *Energ. Fuel.* **25**, 3900-3908, (2011).
25 Nel, R. J. & de Klerk, A. Dehydration of C_5− C_{12} linear 1-alcohols over η-alumina to fuel ethers. *Ind. Eng. Chem. Res.* **48**, 5230-5238, (2009).
26 ASTM International. *ASTM Standard D7566-17a.* (2017).
27 Luning Prak, D. J., Jones, M. H., Trulove, P., McDaniel, A. M., Dickerson, T. & Cowart, J. S. Physical and chemical analysis of alcohol-to-jet (ATJ) fuel and development of surrogate fuel mixtures. *Energ. Fuel.* **29**, 3760-3769, (2015).
28 Mawhood, R., Gazis, E., de Jong, S., Hoefnagels, R. & Slade, R. Production pathways for renewable jet fuel: a review of commercialization status and future prospects. *Biofuel. Bioprod. Bior.* **10**, 462-484, (2016).
29 Wang, W.-C., Tao, L., Markham, J., Zhang, Y., Tan, E., Batan, L., Warner, E. & Biddy, M. Review of biojet fuel conversion technologies. *National Renewable Energy Laboratory* (2016).
30 De Jong, S., Hoefnagels, R., Faaij, A., Slade, R., Mawhood, R. & Junginger, M. The feasibility of short-term production strategies for renewable jet fuels–a comprehensive techno-economic comparison. *Biofuel. Bioprod. Bior.* **9**, 778-800, (2015).
31 Atsonios, K., Kougioumtzis, M.-A., Panopoulos, K. D. & Kakaras, E. Alternative thermochemical routes for aviation biofuels via alcohols synthesis: process modeling, techno-economic assessment and comparison. *Appl. Energ.* **138**, 346-366, (2015).
32 Diederichs, G. W., Mandegari, M. A., Farzad, S. & Görgens, J. F. Techno-economic comparison of biojet fuel production from lignocellulose, vegetable oil and sugar cane juice. *Bioresour. Technol.* **216**, 331-339, (2016).
33 Alves, C. M., Valk, M., de Jong, S., Bonomi, A., van der Wielen, L. A. M. & Mussatto, S. I. Techno-economic assessment of biorefinery technologies for aviation biofuels supply chains in Brazil. *Biofuel. Bioprod. Bior.* **11**, 67-91, (2017).
34 ASTM International. ASTM D4054-16. *Standard practice for qualification and approval of new aviation turbine fuels and fuel additives.* (2016).
35 Dorrington, G. in *Biofuels for Aviation* (ed Christopher J. Chuck) Ch. 3, 35-44 (Academic Press, 2016).
36 European Standards Organization. EN590 *Standard specification on the quality of European diesel fuel.* (2009).
37 Santana, R. C., Do, P. T., Santikunaporn, M., Alvarez, W. E., Taylor, J. D., Sughrue, E. L. & Resasco, D. E. Evaluation of different reaction strategies for the improvement of cetane number in diesel fuels. *Fuel* **85**, 643-656, (2006).
38 Katritzky, A. R., Kuanar, M., Slavov, S., Hall, C. D., Karelson, M., Kahn, I. & Dobchev, D. A. Quantitative correlation of physical and chemical properties with chemical structure: utility for prediction. *Chem. Rev.* **110**, 5714-5789, (2010).
39 Dahmen, M. & Marquardt, W. A novel group contribution method for the prediction of the derived cetane number of oxygenated hydrocarbons. *Energ. Fuel.* **29**, 5781-5801, (2015).
40 Kubic Jr, W. L., Jenkins, R. W., Moore, C. M., Semelsberger, T. A. & Sutton, A. D. Artificial neural network based group contribution method for estimating cetane and octane numbers of hydrocarbons and oxygenated organic compounds. *Ind. Eng. Chem. Res.* **56**, 12236-12245, (2017).

41 Ghosh, P. & Jaffe, S. B. Detailed composition-based model for predicting the cetane number of diesel fuels. *Ind. Eng. Chem. Res.* **45**, 346-351, (2006).

42 Karas, L. & Piel, W. Ethers. *Kirk-Othmer Encyclopedia of Chemical Technology*, (2004).

43 Jenkins, R. W., Moore, C. M., Semelsberger, T. A., Chuck, C. J., Gordon, J. C. & Sutton, A. D. The effect of functional groups in bio-derived fuel candidates. *ChemSusChem* **9**, 922-931, (2016).

44 de Klerk, A. Fischer–Tropsch refining: technology selection to match molecules. *Green Chem.* **10**, 1249-1279, (2008).

45 Engelder, C. J. Studies in contact catalysis. *J. Phys. Chem.* **21**, 676-704, (1916).

46 Adkins, H. & Perkins, P. P. Dehydration of alcohols over alumina. *J. Am. Chem. Soc.* **47**, 1163-1167, (1925).

47 Fan, D., Dai, D.-J. & Wu, H.-S. Ethylene formation by catalytic dehydration of ethanol with industrial considerations. *Materials* **6**, 101-115, (2013).

48 Zhang, M. H. & Yu, Y. Z. Dehydration of ethanol to ethylene. *Ind. Eng. Chem. Res.* **52**, 9505-9514, (2013).

49 Mohsenzadeh, A., Zamani, A. & Taherzadeh, M. J. Bioethylene production from ethanol: a review and techno-economical evaluation. *ChemBioEng Rev.*, (2017).

50 Bailey, B., Eberhardt, J., Goguen, S. & Erwin, J. Diethyl ether (DEE) as a renewable diesel fuel. *SAE technical paper* (1997).

51 Frusteri, F., Spadaro, L., Beatrice, C. & Guido, C. Oxygenated additives production for diesel engine emission improvement. *Chem. Eng. J.* **134**, 239-245, (2007).

52 Knözinger, H. Dehydration of alcohols on aluminum oxide. *Angewandte Chemie International Edition in English* **7**, 791-805, (1968).

53 Roy, S., Mpourmpakis, G., Hong, D. Y., Vlachos, D. G., Bhan, A. & Gorte, R. J. Mechanistic study of alcohol dehydration on gamma-Al_2O_3. *ACS Catal.* **2**, 1846-1853, (2012).

54 Kostestkyy, P., Yu, J., Gorte, R. J. & Mpourmpakis, G. Structure–activity relationships on metal-oxides: alcohol dehydration. *Catal. Sci. Technol.* **4**, 3861-3869, (2014).

55 Kostetskyy, P. & Mpourmpakis, G. Structure-activity relationships in the production of olefins from alcohols and ethers: a first-principles theoretical study. *Catal. Sci. Technol.* **5**, 4547-4555, (2015).

56 Aronson, M., Gorte, R. & Farneth, W. E. The influence of oxonium ion and carbenium ion stabilities on the alcohol/H-ZSM-5 interaction. *J. Catal.* **98**, 434-443, (1986).

57 Janik, M. J., Macht, J., Iglesia, E. & Neurock, M. Correlating acid properties and catalytic function: a first-principles analysis of alcohol dehydration pathways on polyoxometalates. *J. Phys. Chem. C* **113**, 1872-1885, (2009).

58 Chiang, H. & Bhan, A. Catalytic consequences of hydroxyl group location on the rate and mechanism of parallel dehydration reactions of ethanol over acidic zeolites. *J. Catal.* **271**, 251-261, (2010).

59 Kim, S., Robichaud, D. J., Beckham, G. T., Paton, R. S. & Nimlos, M. R. Ethanol dehydration in HZSM-5 studied by density functional theory: Evidence for a concerted peocess. *J. Phys. Chem. A* **119**, 3604-3614, (2015).

60 Gervasini, A., Fenyvesi, J. & Auroux, A. Study of the acidic character of modified metal oxide surfaces using the test of isopropanol decomposition. *Catal. Lett.* **43**, 219-228, (1997).

61 Di Cosimo, J., Dıez, V., Xu, M., Iglesia, E. & Apesteguıa, C. Structure and surface and catalytic properties of Mg-Al basic oxides. *J. Catal.* **178**, 499-510, (1998).

62 Pines, H. & Haag, W. O. Alumina: catalyst and support. I. Alumina, its intrinsic acidity and catalytic activity. *J. Am. Chem. Soc.* **82**, 2471-2483, (1960).

63 Chen, G., Li, S., Jiao, F. & Yuan, Q. Catalytic dehydration of bioethanol to ethylene over TiO_2/γ-Al_2O_3 catalysts in microchannel reactors. *Catal. Today* **125**, 111-119, (2007).

64 Kochar, N. K., Merims, R. & Padia, A. S. Ethylene from ethanol. *Chem. Eng. Prog.* **77**, 66-70, (1981).

65 El-Katatny, E. A., Halawy, S. A., Mohamed, M. A. & Zaki, M. I. Recovery of ethene-selective FeO_x/Al_2O_3 ethanol dehydration catalyst from industrial chemical wastes. *Appl. Catal. A-Gen.* **199**, 83-92, (2000).

66 Tsao, U. & Zasloff, H. B. Production of ethylene from ethanol. US patent 4,134,926 (1979).

67 Le Van Mao, R., Nguyen, T. M. & McLaughlin, G. P. The bioethanol-to-ethylene (B.E.T.E.) process. *Appl. Catal.* **48**, 265-277, (1989).

68 Phillips, C. B. & Datta, R. Production of ethylene from hydrous ethanol on H-ZSM-5 under mild conditions. *Ind. Eng. Chem. Res.* **36**, 4466-4475, (1997).

69 Ramesh, K., Jie, C., Han, Y. F. & Borgna, A. Synthesis, characterization, and catalytic activity of phosphorus modified H-ZSM-5 catalysts in selective ethanol dehydration. *Ind. Eng. Chem. Res.* **49**, 4080-4090, (2010).

70 Takahara, I., Saito, M., Inaba, M. & Murata, K. Dehydration of ethanol into ethylene over solid acid catalysts. *Catal. Lett.* **105**, 249-252, (2005).

71 Zhang, X., Wang, R. J., Yang, X. X. & Zhang, F. B. Comparison of four catalysts in the catalytic dehydration of ethanol to ethylene. *Micropor. Mesopor. Mater.* **116**, 210-215, (2008).

72 Varisli, D., Dogu, T. & Dogu, G. Ethylene and diethyl-ether production by dehydration reaction of ethanol over different heteropolyacid catalysts. *Chem. Eng. Sci.* **62**, 5349-5352, (2007).

73 Saito, Y. & Niiyama, H. Reaction mechanism of ethanol dehydration on/in heteropoly compounds: analysis of transient behavior based on pseudo-liquid catalysis model. *J. Catal.* **106**, 329-336, (1987).

74 Varisli, D., Dogu, T. & Dogu, G. Silicotungstic acid impregnated MCM-41-like mesoporous solid acid catalysts for dehydration of ethanol. *Ind. Eng. Chem. Res.* **47**, 4071-4076, (2008).

75 Micek-Ilnicka, A., Bielańska, E., Lityńska-Dobrzyńska, L. & Bielański, A. Carbon nanotubes, silica and titania supported heteropolyacid $H_3PW_{12}O_{40}$ as the catalyst for ethanol conversion. *Appl. Catal. A-Gen.* **421**, 91-98, (2012).

76 Kozhevnikov, I. Sustainable heterogeneous acid catalysis by heteropoly acids. *J. Mol. Catal. A: Chem.* **262**, 86-92, (2007).

77 Huang, H.-J., Ramaswamy, S., Tschirner, U. & Ramarao, B. A review of separation technologies in current and future biorefineries. *Sep. Purif. Technol.* **62**, 1-21, (2008).

78 Vane, L. M. Separation technologies for the recovery and dehydration of alcohols from fermentation broths. *Biofuel. Bioprod. Bior.* **2**, 553-588, (2008).

79 Le Van Mao, R. & Nguyen, T. M. Superacidic catalysts for low temperature conversion of aqueous ethanol to ethylene. US 4,847,223 (1989).

80 Nguyen, T. M. & Le Van Mao, R. Conversion of ethanol in aqueous-solution over ZSM-5 zeolites-Study of the reaction network. *Appl. Catal.* **58**, 119-129, (1990).

81 *Bio ethylene/ethene*, <https://chematur.se/process-areas/bio-chemicals/bio-ethylene-ethene> (2018).

82 *Braskem ethanol-to-ethylene plant, brazil*, <http://www.chemicals-technology.com/projects/braskem-ethanol/> (2018).

83 *Petron Scientich Inc. background*, <http://www.petronscientech.com/index.php?option=com_content&view=article&id=1&Itemid=115&lang=en> (2018).

84 Ondrey, G. The launch of a new bioethylene-production process. *Chemical Engineering* **121**, 11-12, (2014).

85 *Technip completes acquisition of Hummingbird technology from BP Chemicals Limited*, <http://www.technip.com/en/press/technip-completes-acquisition-hummingbird%C2%AE-technology-bp-chemicals-limited> (2016).

86 Lane, J. *New path to ethylene via ethanol: The Digest's 2017 Multi-Slide Guide to Technip's Hummingbird tech*, <http://www.biofuelsdigest.com/bdigest/2017/01/03/new-path-to-ethylene-via-ethanol-the-digests-2017-multi-slide-guide-to-technips-hummingbird-tech/> (2017).

87 Ipatieff, V., Corson, B. & Egloff, G. Polymerization, a new source of gasoline. *Ind. Eng. Chem.* **27**, 1077-1081, (1935).

88 Ipatieff, V. N. & Schaad, R. E. Heptenes and heptanes from propylene and butylenes. *Ind. Eng. Chem.* **37**, 362-364, (1945).

89 Pines, H. *The chemistry of catalytic hydrocarbon conversions*. (Elsevier, 2012).

90 Sarazen, M. L., Doskocil, E. & Iglesia, E. Effects of void environment and acid strength on alkene oligomerization selectivity. *ACS Catal.* **6**, 7059-7070, (2016).

91 Quann, R. J., Green, L. A., Tabak, S. A. & Krambeck, F. J. Chemistry of olefin oligomerization over ZSM-5 catalyst. *Ind. Eng. Chem. Res.* **27**, 565-570, (1988).

92 Lukyanov, D. B., Gnep, N. S. & Guisnet, M. R. Kinetic modeling of ethene and propene aromatization over HZSM-5 and GaHZSM-5. *Ind. Eng. Chem. Res.* **33**, (1994).

93 Guisnet, M., Gnep, N. & Alario, F. Aromatization of short chain alkanes on zeolite catalysts. *Appl. Catal. A-Gen.* **89**, 1-30, (1992).

94 Biscardi, J. A. & Iglesia, E. Structure and function of metal cations in light alkane reactions catalyzed by modified H-ZSM5. *Catal. Today* **31**, 207-231, (1996).

95 Choudhary, V. R., Panjala, D. & Banerjee, S. Aromatization of propene and n-butene over H-galloaluminosilicate (ZSM-5 type) zeolite. *Appl. Catal. A-Gen.* **231**, 243-251, (2002).

96 Anderson, J., Mole, T. & Christov, V. Mechanism of some conversions over ZSM-5 catalyst. *J. Catal.* **61**, 477-484, (1980).

97 Smirniotis, P. G. & Ruckenstein, E. Alkylation of benzene or toluene with MeOH or C_2H_4 over ZSM-5 or beta zeolite: effect of the zeolite pore openings and of the hydrocarbons involved on the mechanism of alkylation. *Ind. Eng. Chem. Res.* **34**, 1517-1528, (1995).

98 Degnan Jr, T. F., Smith, C. M. & Venkat, C. R. Alkylation of aromatics with ethylene and propylene: recent developments in commercial processes. *Appl. Catal. A-Gen.* **221**, 283-294, (2001).

99 Hansen, N., Brüggemann, T., Bell, A. T. & Keil, F. J. Theoretical investigation of benzene alkylation with ethene over H-ZSM-5. *J. Phys. Chem. C* **112**, 15402-15411, (2008).

100 Svelle, S., Kolboe, S. & Swang, O. Theoretical investigation of the dimerization of linear alkenes catalyzed by acidic zeolites. *J. Phys. Chem. B* **108**, 2953-2962, (2004).

101 Derouane, E. G., Nagy, J. B., Dejaifve, P., van Hooff, J. H., Spekman, B. P., Védrine, J. C. & Naccache, C. Elucidation of the mechanism of conversion of methanol and ethanol to hydrocarbons on a new type of synthetic zeolite. *J. Catal.* **53**, 40-55, (1978).

102 Chang, C. D. & Silvestri, A. J. The conversion of methanol and other O-compounds to hydrocarbons over zeolite catalysts. *J. Catal.* **47**, 249-259, (1977).

103 Tabak, S. & Yurchak, S. Conversion of methanol over ZSM-5 to fuels and chemicals. *Catal. Today* **6**, 307-327, (1990).

104 Yurchak, S. in *Stud. Surf. Sci. Catal.* Vol. 36 251-272 (Elsevier, 1988).

105 Teketel, S., Erichsen, M. W., Bleken, F. L., Svelle, S., Lillerud, K. P. & Olsbye, U. Shape selectivity in zeolite catalysis. The methanol to hydrocarbons (MTH) reaction. *Catalysis* **26**, 179-217, (2014).

106 Stöcker, M. Methanol-to-hydrocarbons: catalytic materials and their behavior. *Micropor. Mesopor. Mater.* **29**, 3-48, (1999).

107 Mole, T., Whiteside, J. A. & Seddon, D. Aromatic co-catalysis of methanol conversion over zeolite catalysts. *J. Catal.* **82**, 261-266, (1983).

108 Mole, T., Bett, G. & Seddon, D. Conversion of methanol to hydrocarbons over ZSM-5 zeolite: an examination of the role of aromatic hydrocarbons using ^{13}carbon-and deuterium-labeled feeds. *J. Catal.* **84**, 435-445, (1983).

109 Dahl, I. M. & Kolboe, S. On the reaction mechanism for propene formation in the MTO reaction over SAPO-34. *Catal. Lett.* **20**, 329-336, (1993).

110 Haw, J. F., Nicholas, J. B., Song, W., Deng, F., Wang, Z., Xu, T. & Heneghan, C. S. Roles for cyclopentenyl cations in the synthesis of hydrocarbons from methanol on zeolite catalyst HZSM-5. *J. Am. Chem. Soc.* **122**, 4763-4775, (2000).

111 Arstad, B. & Kolboe, S. The reactivity of molecules trapped within the SAPO-34 cavities in the methanol-to-hydrocarbons reaction. *J. Am. Chem. Soc.* **123**, 8137-8138, (2001).

112 Bjørgen, M., Olsbye, U., Petersen, D. & Kolboe, S. The methanol-to-hydrocarbons reaction: insight into the reaction mechanism from [^{12}C] benzene and [^{13}C] methanol coreactions over zeolite H-beta. *J. Catal.* **221**, 1-10, (2004).

113 Johansson, R., Hruby, S. L., Rass-Hansen, J. & Christensen, C. H. The hydrocarbon pool in ethanol-to-gasoline over HZSM-5 catalysts. *Catal. Lett.* **127**, 1, (2009).

114 Goguen, P. W., Xu, T., Barich, D. H., Skloss, T. W., Song, W., Wang, Z., Nicholas, J. B. & Haw, J. F. Pulse-quench catalytic reactor studies reveal a carbon-pool mechanism in methanol-to-gasoline chemistry on zeolite HZSM-5. *J. Am. Chem. Soc.* **120**, 2650-2651, (1998).

115 Xu, T. & White, J. L. Catalyst pretreatment in an oxygenate to olefins reaction system. US 6,734,330 B1 (2004).

116 Narula, C. K., Li, Z., Casbeer, E. M., Geiger, R. A., Moses-Debusk, M., Keller, M., Buchanan, M. V. & Davison, B. H. Heterobimetallic zeolite, InV-ZSM-5, enables efficient conversion of biomass derived ethanol to renewable hydrocarbons. *Sci. Rep.-UK* **5**, (2015).

117 Talukdar, A. K., Bhattacharyya, K. G. & Sivasanker, S. HZSM-5 catalysed conversion of aqueous ethanol to hydrocarbons. *Appl. Catal. A-Gen.* **148**, 357-371, (1997).

118 Gayubo, A. G., Tarrío, A. M., Aguayo, A. T., Olazar, M. & Bilbao, J. Kinetic modelling of the transformation of aqueous ethanol into hydrocarbons on a HZSM-5 zeolite. *Ind. Eng. Chem. Res.* **40**, 3467-3474, (2001).

119 Aguayo, A. T., Gayubo, A. G., Atutxa, A., Olazar, M. & Bilbao, J. Catalyst deactivation by coke in the transformation of aqueous ethanol into hydrocarbons. Kinetic modeling and acidity deterioration of the catalyst. *Ind. Eng. Chem. Res.* **41**, 4216-4224, (2002).

120 Madeira, F. F., Gnep, N., Magnoux, P., Maury, S. & Cadran, N. Ethanol transformation over HFAU, HBEA and HMFI zeolites presenting similar Brønsted acidity. *Appl. Catal. A-Gen.* **367**, 39-46, (2009).

121 Sun, J. & Wang, Y. Recent advances in catalytic conversion of ethanol to chemicals. *ACS Catal.* **4**, 1078-1090, (2014).

122 Galadima, A. & Muraza, O. Zeolite catalysts in upgrading of bioethanol to fuels range hydrocarbons: a review. *J. Ind. Eng. Chem.* **31**, 1-14, (2015).

123 Erichsen, M. W., Svelle, S. & Olsbye, U. The influence of catalyst acid strength on the methanol to hydrocarbons (MTH) reaction. *Catal. Today* **215**, 216-223, (2013).

124 Costa, E., Uguina, A., Aguado, J. & Hernandez, P. J. Ethanol to gasoline process: effect of variables, mechanism, and kinetics. *Ind. Eng. Chem. Proc. DD* **24**, 239-244, (1985).

125 Schulz, J. & Bandermann, F. Conversion of ethanol over zeolite H-ZSM-5. *Chem. Eng. Technol.* **17**, 179-186, (1994).

126 Aguayo, A. T., Gayubo, A. G., Tarrío, A. M., Atutxa, A. & Bilbao, J. Study of operating variables in the transformation of aqueous ethanol into hydrocarbons on an HZSM-5 zeolite. *J. Chem. Technol. Biot.* **77**, 211-216, (2002).

127 Viswanadham, N., Saxena, S. K., Kumar, J., Sreenivasulu, P. & Nandan, D. Catalytic performance of nano crystalline H-ZSM-5 in ethanol to gasoline (ETG) reaction. *Fuel* **95**, 298-304, (2012).

128 Chaudhuri, S. N., Halik, C. & Lercher, J. A. Reactions of ethanol over HZSM-5. *J. Mol. Catal.* **62**, 289-295, (1990).

129 Ferreira Madeira, F., Ben Tayeb, K., Pinard, L., Vezin, H., Maury, S. & Cadran, N. Ethanol transformation into hydrocarbons on ZSM-5 zeolites: influence of Si/Al ratio on catalytic performances and deactivation rate. Study of the radical species role. *Appl. Catal. A-Gen.* **443**, 171-180, (2012).

130 Saha, S. K. & Sivasanker, S. Influence of Zn- and Ga-doping on the conversion of ethanol to hydrocarbons over ZSM-5. *Catal. Lett.* **15**, 413-418, (1992).

131 Inaba, M., Murata, K., Saito, M. & Takahara, I. Ethanol conversion to aromatic hydrocarbons over several zeolite catalysts *React. Kinet. Catal. Lett.* **88**, 135-141, (2006).

132 Chang, C., Lang, W. & Smith, R. The conversion of methanol and other O-compounds to hydrocarbons over zeolite catalysts: II. Pressure effects. *J. Catal.* **56**, 169-173, (1979).

133 Ramasamy, K. K. & Wang, Y. Ethanol conversion to hydrocarbons on HZSM-5: Effect of reaction conditions and Si/Al ratio on the product distributions. *Catal. Today* **237**, 89-99, (2014).

134 Oudejans, J. C., Van Den Oosterkamp, P. F. & Van Bekkum, H. Conversion of ethanol over zeolite H-ZSM-5 in the presence of water. *Appl. Catal.* **3**, 109-115, (1982).

135 Hannon, J. One-step high-yield production of fungible gasoline, diesel, and jet fuel blend stocks from ethanol without added hydrogen. *Vertimass* (2017).

136 El-Halwagi, M. M., Hall, K. R. & Spriggs, H. D. Integrated biofuel processing system. US 8,802,905 B2 (2014).

137 Warwick, G. *Airlines and industry pursue biofuels that recycle trash and do no harm to the environment*, <http://atwonline.com/eco-aviation/waste-watch> (2015).

138 Lane, J. *DOE pushes renewable jet fuel towards commercial-scale with key grants to LanzaTech, Byogy, AVAPCO-led teams*, <http://www.biofuelsdigest.com/bdigest/2016/12/30/doe-pushes-renewable-jet-fuel-towards-commercial-scale-with-key-grants-to-lanzatech-byogy-avapco-led-teams/> (2016).

139 Nelson, K. *AVAPCO, BYOGY Renewables, and Petron Scientech announce partnership to demonstrate technologies in the ABBA integrated biorefinery project*, <http://www.prweb.com/releases/2017/10/prweb14773964.htm> (2017).

140 Tian, P., Wei, Y., Ye, M. & Liu, Z. Methanol to Olefins (MTO): from fundamentals to commercialization. *ACS Catal.* **5**, 1922-1938, (2015).

141 Takahashi, A., Xia, W., Nakamura, I., Shimada, H. & Fujitani, T. Effects of added phosphorus on conversion of ethanol to propylene over ZSM-5 catalysts. *Appl. Catal. A-Gen.* **423**, 162-167, (2012).

142 Li, X., Kant, A., He, Y., Thakkar, H. V., Atanga, M. A., Rezaei, F., Ludlow, D. K. & Rownaghi, A. A. Light olefins from renewable resources: selective catalytic dehydration of bioethanol to propylene over zeolite and transition metal oxide catalysts. *Catal. Today* **276**, 62-77, (2016).

143 Ingram, C. W. & Lancashire, R. J. On the formation of C_3 hydrocarbons during the conversion of ethanol using H-ZSM-5 catalyst. *Catal. Lett.* **31**, 395-403, (1995).

144 Lehmann, T. & Seidel-Morgenstern, A. Thermodynamic appraisal of the gas phase conversion of ethylene or ethanol to propylene. *Chem. Eng. J.* **242**, 422-432, (2014).

145 Lin, B., Zhang, Q. & Wang, Y. Catalytic conversion of ethylene to propylene and butenes over H-ZSM-5. *Ind. Eng. Chem. Res.* **48**, 10788-10795, (2009).

146 Nicholas, C. P. Applications of light olefin oligomerization to the production of fuels and chemicals. *Appl. Catal. A-Gen.* **543**, 82-97, (2017).

147 Tabak, S., Krambeck, F. & Garwood, W. Conversion of propylene and butylene over ZSM-5 catalyst. *AlChE J.* **32**, 1526-1531, (1986).

148 Coelho, A., Caeiro, G., Lemos, M., Lemos, F. & Ribeiro, F. R. 1-Butene oligomerization over ZSM-5 zeolite: part 1–effect of reaction conditions. *Fuel* **111**, 449-460, (2013).

149 Martens, J. A., Ravishankar, R., Mishin, I. E. & Jacobs, P. A. Tailored alkene oligomerization with H-ZSM-57 zeolite. *Angew. Chem. Int. Ed.* **39**, 4376-4379, (2000).

150 Bond, J. Q., Alonso, D. M., Wang, D., West, R. M. & Dumesic, J. A. Integrated catalytic conversion of γ-valerolactone to liquid alkenes for transportation fuels. *Science* **327**, 1110-1114, (2010).

151 Kim, Y. T., Chada, J. P., Xu, Z., Pagan-Torres, Y. J., Rosenfeld, D. C., Winniford, W. L., Schmidt, E. & Huber, G. W. Low-temperature oligomerization of 1-butene with H-ferrierite. *J. Catal.* **323**, 33-44, (2015).

152 Nicholas, C. P. in *Zeolites in Industrial Separation and Catalysis* 355-402 (Wiley-VCH Verlag GmbH & Co. KGaA, 2010).

153 Martens, L. R., Verduijn, J. & Mathys, G. The development of an environmental friendly catalytic system for the conversion of olefins. *Catal. Today* **36**, 451-460, (1997).

154 Martens, J. A., Verrelst, W. H., Mathys, G. M., Brown, S. H. & Jacobs, P. A. Tailored catalytic propene trimerization over acidic zeolites with tubular pores. *Angew. Chem. Int. Ed.* **44**, 5687-5690, (2005).

155 Corma, A., Martínez, C. & Doskocil, E. Designing MFI-based catalysts with improved catalyst life for $C_{=3}$ and $C_{=5}$ oligomerization to high-quality liquid fuels. *J. Catal.* **300**, 183-196, (2013).

156 Yinong, L. & Qinghua, D. Investigation of propene oligomerization catalyzed by phosphotungstic acid catalysts. *China Pet. Process. Pe.* **14**, 10-16, (2012).

157 Vaughan, J., Oconnor, C. & Fletcher, J. High-pressure oligomerization of propene over heteropoly acids. *J. Catal.* **147**, 441-454, (1994).

158 Zhirong, Z., Zaiku, X., Yongfu, C., Refeng, W. & Yaping, Y. Free phosphoric acid of diatomite-phosphate solid acid and its catalytic performance for propylene oligomerization. *React. Kinet. Catal. Lett.* **70**, 379-388, (2000).

159 Zhang, J., Yan, Y., Chu, Q. & Feng, J. Solid phosphoric acid catalyst for propene oligomerization: effect of silicon phosphate composition. *Fuel Process. Technol.* **135**, 2-5, (2015).

160 Rylander, P. in *The Catalytic Hydrogenation in Organic Syntheses* 31-63 (Academic Press, 1979).

161 Bartholomew, C. H. & Farrauto, R. J. *Fundamentals of industrial catalytic processes*. 411-473 (John Wiley & Sons, 2011).

162 Davis, R., Tao, L., Tan, E., Biddy, M., Beckham, G., Scarlata, C., Jacobson, J., Cafferty, K., Ross, J. & Lukas, J. Process design and economics for the conversion of lignocellulosic biomass to hydrocarbons: dilute-acid and enzymatic deconstruction of biomass to sugars and biological conversion of sugars to hydrocarbons. *National Renewable Energy Laboratory* (2013).

163 Davis, R. T., L.; Scarlata, C.; Tan, E.C.D.; Ross, J.; Lukas, J.; Sexton, D. Dilute-acid and enzymatic deconstruction of biomass to sugars and catalytic conversion of sugars to hydrocarbons. *National Renewable Energy Laboratory* (2015).

164 Dagle, V. L., Smith, C., Flake, M., Albrecht, K. O., Gray, M. J., Ramasamy, K. K. & Dagle, R. A. Integrated process for the catalytic conversion of biomass-derived syngas into transportation fuels. *Green Chem.* **18**, 1880-1891, (2016).

165 Tao, L., Markham, J. N., Haq, Z. & Biddy, M. J. Techno-economic analysis for upgrading the biomass-derived ethanol-to-jet blendstocks. *Green Chem.* **19**, 1082-1101, (2017).

166 Nicholas, C. P., Rathbun, W. E., Kruse, T. M. & Pham, H. A. Composition of oligomerate. US 9,644,159 B2 (2017).

167 Nicholas, C. P., Krupa, S. L., Bussche, K. M. V. & Kruse, T. M. Process for making diesel by oligomerization of gasoline. US 9,663,415 B2 (2017).

168 Catani, R., Mandreoli, M., Rossini, S. & Vaccari, A. Mesoporous catalysts for the synthesis of clean diesel fuels by oligomerisation of olefins. *Catal. Today* **75**, 125-131, (2002).

169 Knottenbelt, C. Mossgas "gas-to-liquid" diesel fuels—an environmentally friendly option. *Catal. Today* **71**, 437-445, (2002).

170 Du Toit, F. B. Process and apparatus for the production of diesel fuels by oligomerisation of olefinic feed streams. US 7,271,304 B2 (2007).

171 de Klerk, A. Distillate production by oligomerization of Fischer−Tropsch olefins over solid phosphoric acid. *Energ. Fuel.* **20**, 439-445, (2006).

172 de Klerk, A. Oligomerization of Fischer−Tropsch olefins to distillates over amorphous silica−alumina. *Energ. Fuel.* **20**, 1799-1805, (2006).

173 de Klerk, A. Properties of synthetic fuels from H-ZSM-5 oligomerization of Fischer–Tropsch type feed materials. *Energ. Fuel.* **21**, 3084-3089, (2007).

174 Avidan, A. Gasoline and distillate fuels from methanol. *Stud. Surf. Sci. Catal.* **36**, 307-323, (1988).

175 Guillon, E., Cadran, N., Touchais, N. & Bournay, L. Flexible process for transformation of ethanol into middle distillates. (2016).

176 Mazurek, H. Two stage process for catalytic conversion of olefins to higher hydrocarbons. 4,925,996 (1990).

177 Lane, J. *The Digest's 2017 Multi-Slide Guide to LanzaTech/PNNL Syngas-to-ATJ Fuels*, <http://www.biofuelsdigest.com/bdigest/2017/08/28/the-digests-2017-multi-slide-guide-to-the-lanzatechpnnl-route-to-fuels-from-biomass-syngasmarch/> (2017).

178 *LanzaTech awarded $4M from DOE for low carbon jet and diesel demonstration facility*, <http://www.lanzatech.com/lanzatech-awarded-4m-doe-low-carbon-jet-diesel-demonstration-facility/> (2016).

179 *Energy department announces six projects for pilot- and demonstration-scale manufacturing of biofuels, bioproducts, and biopower*, <https://www.energy.gov/eere/articles/energy-department-announces-six-projects-pilot-and-demonstration-scale-manufacturing> (2016).

180 *ArcelorMittal, LanzaTech and Primetals Technologies announce partnership to construct breakthrough €87m biofuel production facility* <http://corporate.arcelormittal.com/news-and-media/news/2015/july/13-07-2015> (2015).

181 *Aemetis acquires license from LanzaTech with California exclusive rights for advanced ethanol from biomass including forest and ag wastes*, <http://www.lanzatech.com/aemetis-acquires-license-lanzatech-california-exclusive-rights-advanced-ethanol-biomass-including-forest-ag-wastes/> (2016).

182 *IOC and LanzaTech ink Rs 350 crore pact to construct bio-ethanol facility at Panipat refinery*, <https://energy.economictimes.indiatimes.com/news/oil-and-gas/ioc-and-lanzatech-to-construct-worlds-first-refinery-off-gas-to-bioethanol-production-facility-at-iocs-panipat-refinery/59529506> (2017).

183 *Beijing iron maker to turn waste gas into biofuels*, <http://www.ecns.cn/business/2018/02-28/293914.shtml> (2018).

184 Burton, F. *Low carbon fuel achieves breakthrough*, <http://www.lanzatech.com/low-carbon-fuel-project-achieves-breakthrough-lanzatech-produces-jet-fuel-waste-gases-virgin-atlantic/> (2017).

185 *Virgin Atlantic and LanzaTech celebrate as revolutionary sustainable fuel project takes flight*, <http://www.lanzatech.com/virgin-atlantic-lanzatech-celebrate-revolutionary-sustainable-fuel-project-takes-flight/#_ftn1> (2018).

186 McDaniel, M. P. & DesLauriers, P. J. in *Kirk-Othmer Encyclopedia of Chemical Technology* (John Wiley & Sons, Inc., 2000).

187 Ziegler, K., Holzkamp, E., Breil, H. & Martin, H. Polymerisation von äthylen und anderen olefinen. *Angew. Chem.* **67**, 426-426, (1955).

188 Martin, H. & Ziegler, K. Production of dimers and low molecular polymerization products from ethylene. 2,943,125 (1960).

189 Cecchin, G., Morini, G. & Piemontesi, F. in *Kirk-Othmer Encyclopedia of Chemical Technology* (John Wiley & Sons, Inc., 2000).

190 Cossee, P. On the reaction mechanism of the ethylene polymerization with heterogeneous Ziegler-Natta catalysts. *Tetrahedron Lett.* **1**, 12-16, (1960).

191 Cossee, P. Ziegler-Natta catalysis I. Mechanism of polymerization of α-olefins with Ziegler-Natta catalysts. *J. Catal.* **3**, 80-88, (1964).

192 Peuckert, M. & Keim, W. A new nickel complex for the oligomerization of ethylene. *Organometallics* **2**, 594-597, (1983).

193 Jordan, R. F., Bajgur, C. S., Willett, R. & Scott, B. Ethylene polymerization by a cationic dicyclopentadienyl zirconium (IV) alkyl complex. *J. Am. Chem. Soc.* **108**, 7410-7411, (1986).

194 Britovsek, G. J. P., Malinowski, R., McGuinness, D. S., Nobbs, J. D., Tomov, A. K., Wadsley, A. W. & Young, C. T. Ethylene oligomerization beyond Schulz–Flory distributions. *ACS Catal.* **5**, 6922-6925, (2015).

195 Forestière, A., Olivier-Bourbigou, H. & Saussine, L. Oligomerization of monoolefins by homogeneous catalysts. *Oil Gas Sci. Technol.* **64**, 649-667, (2009).

196 Lappin, G. R., Nemec, L. H., Sauer, J. D. & Wagner, J. D. in *Kirk-Othmer Encyclopedia of Chemical Technology* (John Wiley & Sons, Inc., 2000).

197 Greiner, E. O. C., Blagoev, M. & Yamaguchi, Y. *Linear alpha-olefins*. (2013).

198 Keim, W. Oligomerization of ethylene to α-olefins: discovery and development of the Shell Higher Olefin Process (SHOP). *Angew. Chem. Int. Ed.* **52**, 12492-12496, (2013).

199 Skupińska, J. Oligomerization of α-olefins to higher oligomers. *Chem. Rev.* **91**, 613-648, (1991).

200 Svejda, S. A. & Brookhart, M. Ethylene oligomerization and propylene dimerization using cationic (α-diimine) nickel (II) catalysts. *Organometallics* **18**, 65-74, (1999).

201 Gates, D. P., Svejda, S. A., Oñate, E., Killian, C. M., Johnson, L. K., White, P. S. & Brookhart, M. Synthesis of branched polyethylene using (α-diimine) nickel (II) catalysts: influence of temperature, ethylene pressure, and ligand structure on polymer properties. *Macromolecules* **33**, 2320-2334, (2000).

202 Zhang, H., Li, X., Zhang, Y., Lin, S., Li, G., Chen, L., Fang, Y., Xin, H. & Li, X. Ethylene oligomerization over heterogeneous catalysts. *Energy Environ. Focus* **3**, 246-256, (2014).

203 Finiels, A., Fajula, F. & Hulea, V. Nickel-based solid catalysts for ethylene oligomerization–a review. *Catal. Sci. Technol.* **4**, 2412-2426, (2014).

204 Brogaard, R. Y. & Olsbye, U. Ethene oligomerization in Ni-containing zeolites: theoretical discrimination of reaction mechanisms. *ACS Catal.* **6**, 1205-1214, (2016).

205 Joshi, R., Zhang, G., Miller, J. T. & Gounder, R. Evidence for the coordination-insertion mechanism of ethene dimerization at nickel cations exchanged onto beta molecular sieves. *ACS Catal.* **8**, 11407-11422, (2018).

206 Andrei, R. D., Popa, M. I., Fajula, F. & Hulea, V. Heterogeneous oligomerization of ethylene over highly active and stable Ni-AlSBA-15 mesoporous catalysts. *J. Catal.* **323**, 76-84, (2015).

207 Toch, K., Thybaut, J., Arribas, M., Martínez, A. & Marin, G. Steering linear 1-alkene, propene or gasoline yields in ethene oligomerization via the interplay between nickel and acid sites. *Chem. Eng. Sci.* **173**, 49-59, (2017).

208 Lallemand, M., Finiels, A., Fajula, F. & Hulea, V. Catalytic oligomerization of ethylene over Ni-containing dealuminated Y zeolites. *Appl. Catal. A-Gen.* **301**, 196-201, (2006).

209 Lallemand, M., Rusu, O. A., Dumitriu, E., Finiels, A., Fajula, F. & Hulea, V. NiMCM-36 and NiMCM-22 catalysts for the ethylene oligomerization: Effect of zeolite texture and nickel cations/acid sites ratio. *Appl. Catal. A-Gen.* **338**, 37-43, (2008).

210 Martínez, A., Arribas, M. A., Concepción, P. & Moussa, S. New bifunctional Ni–H-Beta catalysts for the heterogeneous oligomerization of ethylene. *Appl. Catal. A-Gen.* **467**, 509-518, (2013).

211 Moussa, S., Arribas, M. A., Concepción, P. & Martínez, A. Heterogeneous oligomerization of ethylene to liquids on bifunctional Ni-based catalysts: the influence of support properties on nickel speciation and catalytic performance. *Catal. Today* **277**, 78-88, (2016).

212 Hwang, A., Kim, S., Kwak, G., Kim, S. K., Park, H.-G., Kang, S. C., Jun, K.-W. & Kim, Y. T. Low temperature oligomerization of ethylene over Ni/Al-KIT catalysts. *Catal. Lett.* **147**, 1303-1314, (2017).

213 Heveling, J., van der Beek, A. & de Pender, M. Oligomerization of ethene over nickel-exchanged zeolite Y into a diesel-range product. *Appl. Catal.* **42**, 325-336, (1988).

214 Lacarriere, A., Robin, J., Świerczyński, D., Finiels, A., Fajula, F., Luck, F. & Hulea, V. Distillate-range products from non-oil-based sources by catalytic cascade reactions. *ChemSusChem* **5**, 1787-1792, (2012).

215 Babu, B. H., Lee, M., Hwang, D. W., Kim, Y. & Chae, H.-J. An integrated process for production of jet-fuel range olefins from ethylene using Ni-AlSBA-15 and Amberlyst-35 catalysts. *Appl. Catal. A-Gen.* **530**, 48-55, (2017).

216 Schultz, R. G. Olefin dimerization over cobalt-oxide-on-carbon catalysts: III. Oligomerization of ethylene. *J. Catal.* **7**, 286-290, (1967).

217 Xu, Z., Zhao, D., Chada, J. P., Rosenfeld, D. C., Rogers, J. L., Hermans, I. & Huber, G. W. Olefin conversion on nitrogen-doped carbon-supported cobalt catalyst: effect of feedstock. *J. Catal.* **354**, 213-222, (2017).

218 Xu, Z., Chada, J. P., Xu, L., Zhao, D., Rosenfeld, D. C., Rogers, J. L., Hermans, I., Mavrikakis, M. & Huber, G. W. Ethylene Dimerization and Oligomerization to 1-Butene and Higher Olefins with Chromium-Promoted Cobalt on Carbon Catalyst. *ACS Catal.* **8**, 2488-2497, (2018).

219 Emrich, R., Heinemann, O., Jolly, P. W., Krüger, C. & Verhovnik, G. P. J. The role of metallacycles in the chromium-catalyzed trimerization of ethylene. *Organometallics* **16**, 1511-1513, (1997).

220 Overett, M. J., Blann, K., Bollmann, A., Dixon, J. T., Haasbroek, D., Killian, E., Maumela, H., McGuinness, D. S. & Morgan, D. H. Mechanistic investigations of the ethylene tetramerisation reaction. *J. Am. Chem. Soc.* **127**, 10723-10730, (2005).

221 McGuinness, D. S. Olefin oligomerization via metallacycles: dimerization, trimerization, tetramerization, and beyond. *Chem. Rev* **111**, 2321-2341, (2011).

222 Dixon, J. T., Green, M. J., Hess, F. M. & Morgan, D. H. Advances in selective ethylene trimerisation–a critical overview. *J. Organomet. Chem.* **689**, 3641-3668, (2004).

223 Wright, M. E., Harvey, B. G. & Quintana, R. L. Highly Efficient Zirconium-Catalyzed Batch Conversion of 1-Butene: A New Route to Jet Fuels. *Energ. Fuel.* **22**, 3299-3302, (2008).

224 Harvey, B. G. & Meylemans, H. A. 1-Hexene: a renewable C6 platform for full-performance jet and diesel fuels. *Green Chem.* **16**, 770-776, (2014).

225 Janiak, C. Metallocene and related catalysts for olefin, alkyne and silane dimerization and oligomerization. *Coord. Chem. Rev.* **250**, 66-94, (2006).

226 Berard, S., Harry, S., Touchais, N., Magna, L., Olivier-Bourbigou, H., Popelin, C., Proriol, D. & Saussine, L. Process for the production of a fuel base from an ethylene feedstock implementing at least one oligomerization stage in the presence of a homogeneous catalytic system. US 8,957,270 B2 (2015).

227 Lilga, M. A., Hallen, R. T., Albrecht, K. O., Cooper, A. R., Frye, J. G. & Ramasamy, K. K. Systems and processes for conversion of ethylene feedstocks to hydrocarbon fuels. US patent 9,932,531 B2 (2018).

228 Guerbet, M. Action des alcools ethylique, isobutylique, isoamylique sur leurs derives sodes. *CR Hebd. Acad. Sci.* **128**, 1002-1004, (1899).

229 Aitchison, H., Wingad, R. L. & Wass, D. F. Homogeneous ethanol to butanol catalysis—Guerbet renewed. *ACS Catal.* **6**, 7125-7132, (2016).

230 Galadima, A. & Muraza, O. Catalytic upgrading of bioethanol to fuel grade biobutanol: a review. *Ind. Eng. Chem. Res.* **54**, 7181-7194, (2015).

231 Gaussian 09 v. Revision A.02 (Gaussian, Inc., Wallingford, CT, 2016).

232 Kozlowski, J. T. & Davis, R. J. Heterogeneous catalysts for the Guerbet coupling of alcohols. *ACS Catal.* **3**, 1588-1600, (2013).

233 Gabriëls, D., Hernández, W. Y., Sels, B., Van Der Voort, P. & Verberckmoes, A. Review of catalytic systems and thermodynamics for the Guerbet condensation reaction and challenges for biomass valorization. *Catal. Sci. Technol.* **5**, 3876-3902, (2015).

234 Wu, X., Fang, G., Tong, Y., Jiang, D., Liang, Z., Leng, W., Liu, L., Tu, P., Wang, H. & Ni, J. Catalytic upgrading of ethanol to n-butanol: progress in catalyst development. *ChemSusChem* **11**, 71-85, (2018).

235 Yang, C. & Meng, Z. Bimolecular condensation of ethanol to 1-butanol catalyzed by alkali cation zeolites. *J. Catal.* **142**, 37-44, (1993).

236 Di Cosimo, J., Apesteguía, C., Ginés, M. & Iglesia, E. Structural requirements and reaction pathways in condensation reactions of alcohols on Mg_yAlO_x catalysts. *J. Catal.* **190**, 261-275, (2000).

237 Scalbert, J., Thibault-Starzyk, F., Jacquot, R., Morvan, D. & Meunier, F. Ethanol condensation to butanol at high temperatures over a basic heterogeneous catalyst: How relevant is acetaldehyde self-aldolization? *J. Catal.* **311**, 28-32, (2014).

238 Meunier, F. C., Scalbert, J. & Thibault-Starzyk, F. Unraveling the mechanism of catalytic reactions through combined kinetic and thermodynamic analyses: application to the condensation of ethanol. *CR Chim.* **18**, 345-350, (2015).

239 Moteki, T. & Flaherty, D. W. Mechanistic insight to C–C bond formation and predictive models for cascade reactions among alcohols on Ca-and Sr-hydroxyapatites. *ACS Catal.* **6**, 4170-4183, (2016).

240 Ogo, S., Onda, A., Iwasa, Y., Hara, K., Fukuoka, A. & Yanagisawa, K. 1-Butanol synthesis from ethanol over strontium phosphate hydroxyapatite catalysts with various Sr/P ratios. *J. Catal.* **296**, 24-30, (2012).

241 Ho, C. R., Shylesh, S. & Bell, A. T. Mechanism and kinetics of ethanol coupling to butanol over hydroxyapatite. *ACS Catal.* **6**, 939-948, (2016).

242 Tsuchida, T., Kubo, J., Yoshioka, T., Sakuma, S., Takeguchi, T. & Ueda, W. Reaction of ethanol over hydroxyapatite affected by Ca/P ratio of catalyst. *J. Catal.* **259**, 183-189, (2008).

243 Ogo, S., Onda, A. & Yanagisawa, K. Selective synthesis of 1-butanol from ethanol over strontium phosphate hydroxyapatite catalysts. *Appl. Catal. A-Gen.* **402**, 188-195, (2011).

244 Hanspal, S., Young, Z. D., Shou, H. & Davis, R. J. Multiproduct steady-state isotopic transient kinetic analysis of the ethanol coupling reaction over hydroxyapatite and magnesia. *ACS Catal.* **5**, 1737-1746, (2015).

245 Gines, M. J. & Iglesia, E. Bifunctional condensation reactions of alcohols on basic oxides modified by copper and potassium. *J. Catal.* **176**, 155-172, (1998).

246 Pang, J., Zheng, M., He, L., Li, L., Pan, X., Wang, A., Wang, X. & Zhang, T. Upgrading ethanol to n-butanol over highly dispersed Ni–MgAlO catalysts. *J. Catal.* **344**, 184-193, (2016).

247 Tu, Y.-J. & Chen, Y.-W. Effects of alkali metal oxide additives on Cu/SiO_2 catalyst in the dehydrogenation of ethanol. *Ind. Eng. Chem. Res.* **40**, 5889-5893, (2001).

248 Ni, M., Leung, D. Y. & Leung, M. K. A review on reforming bio-ethanol for hydrogen production. *Int. J. Hydrogen Energy* **32**, 3238-3247, (2007).

249 Takei, T., Iguchi, N. & Haruta, M. Synthesis of acetoaldehyde, acetic acid, and others by the dehydrogenation and oxidation of ethanol. *Catal. Surv. Asia* **15**, 80-88, (2011).

250 Wang, C., Garbarino, G., Allard, L. F., Wilson, F., Busca, G. & Flytzani-Stephanopoulos, M. Low-temperature dehydrogenation of ethanol on atomically dispersed gold supported on $ZnZrO_x$. *ACS Catal.* **6**, 210-218, (2016).

251 Neurock, M., Tao, Z., Chemburkar, A., Hibbitts, D. D. & Iglesia, E. Theoretical insights into the sites and mechanisms for base catalyzed esterification and aldol condensation reactions over Cu. *Faraday Discuss.* **197**, 59-86, (2017).

252 Tsuchida, T., Sakuma, S., Takeguchi, T. & Ueda, W. Direct synthesis of n-butanol from ethanol over nonstoichiometric hydroxyapatite. *Ind. Eng. Chem. Res.* **45**, 8634-8642, (2006).

253 Moteki, T., Rowley, A. T. & Flaherty, D. W. Self-terminated cascade reactions that produce methylbenzaldehydes from ethanol. *ACS Catal.* **6**, 7278-7282, (2016).

254 Ndou, A. S., Plint, N. & Coville, N. J. Dimerisation of ethanol to butanol over solid-base catalysts. *Appl. Catal. A-Gen.* **251**, 337-345, (2003).

255 Ramasamy, K. K., Gray, M., Job, H., Santosa, D., Li, X. S., Devaraj, A., Karkamkar, A. & Wang, Y. Role of calcination temperature on the hydrotalcite derived $MgO–Al_2O_3$ in converting ethanol to butanol. *Top. Catal.* **59**, 46-54, (2016).

256 Ferrin, P., Simonetti, D., Kandoi, S., Kunkes, E., Dumesic, J. A., Nørskov, J. K. & Mavrikakis, M. Modeling ethanol decomposition on transition metals: a combined application of scaling and Brønsted− Evans− Polanyi relations. *J. Am. Chem. Soc.* **131**, 5809-5815, (2009).

257 Wang, J.-H., Lee, C. & Lin, M. Mechanism of ethanol reforming: theoretical foundations. *J. Phys. Chem. C* **113**, 6681-6688, (2009).

258 Sun, Z., Couto Vasconcelos, A. s., Bottari, G., Stuart, M. C., Bonura, G., Cannilla, C., Frusteri, F. & Barta, K. Efficient catalytic conversion of ethanol to 1-butanol via the Guerbet reaction over copper-and nickel-doped porous. *ACS Sustain. Chem. Eng.* **5**, 1738-1746, (2016).

259 Marcu, I.-C., Tichit, D., Fajula, F. & Tanchoux, N. Catalytic valorization of bioethanol over Cu-Mg-Al mixed oxide catalysts. *Catal. Today* **147**, 231-238, (2009).

260 Riittonen, T., Eränen, K., Mäki-Arvela, P., Shchukarev, A., Rautio, A.-R., Kordas, K., Kumar, N., Salmi, T. & Mikkola, J.-P. Continuous liquid-phase valorization of bio-ethanol towards bio-butanol over metal modified alumina. *Renew. Energ.* **74**, 369-378, (2015).

261 Zhang, C., Borlik, M. & Weiner, H. Coated hydrotalcite catalysts and processes for producing butanol. US 2014/0171693 A1 (2012).

262 Zhang, C., Balliet, K. & Johnston, V. J. Catalysts and processes for producing butanol. US 8,962,897 B2 (2015).

263 Tan, E. C., Snowden-Swan, L. J., Talmadge, M., Dutta, A., Jones, S., Ramasamy, K. K., Gray, M., Dagle, R., Padmaperuma, A. & Gerber, M. Comparative techno-economic analysis and process design for indirect liquefaction pathways to distillate-range fuels via biomass-derived oxygenated intermediates upgrading. *Biofuel. Bioprod. Bior.* **11**, 41-66, (2017).

264 Hanspal, S., Young, Z. D., Prillaman, J. T. & Davis, R. J. Influence of surface acid and base sites on the Guerbet coupling of ethanol to butanol over metal phosphate catalysts. *J. Catal.* **352**, 182-190, (2017).

265 Rao, K. K., Gravelle, M., Valente, J. S. & Figueras, F. Activation of Mg–Al hydrotalcite catalysts for aldol condensation reactions. *J. Catal.* **173**, 115-121, (1998).

266 Sels, B. F., De Vos, D. E. & Jacobs, P. A. Hydrotalcite-like anionic clays in catalytic organic reactions. *Cataly. Rev.* **43**, 443-488, (2001).

267 Gangadharan, A., Shen, M., Sooknoi, T., Resasco, D. E. & Mallinson, R. G. Condensation reactions of propanal over CexZr1− xO2 mixed oxide catalysts. *Appl. Catal. A-Gen.* **385**, 80-91, (2010).

268 Shen, W., Tompsett, G. A., Xing, R., Conner Jr, W. C. & Huber, G. W. Vapor phase butanal self-condensation over unsupported and supported alkaline earth metal oxides. *J. Catal.* **286**, 248-259, (2012).

269 Corma, A. & Iborra, S. Optimization of alkaline earth metal oxide and hydroxide catalysts for base-catalyzed reactions. *Adv. Catal.* **49**, 239-302, (2006).

270 Jordison, T. L., Lira, C. T. & Miller, D. J. Condensed-phase ethanol conversion to higher alcohols. *Ind. Eng. Chem. Res.* **54**, 10991-11000, (2015).

271 Tichit, D., Lutic, D., Coq, B., Durand, R. & Teissier, R. The aldol condensation of acetaldehyde and heptanal on hydrotalcite-type catalysts. *J. Catal.* **219**, 167-175, (2003).

272 Hamilton, C. A., Jackson, S. D. & Kelly, G. J. Solid base catalysts and combined solid base hydrogenation catalysts for the aldol condensation of branched and linear aldehydes. *Appl. Catal. A-Gen.* **263**, 63-70, (2004).

273 Norman, D. W., Billodeaux, D. R. & Page, M. D. Dual catalyst system for the self-condensation of alcohols. (2014).

274 Hagemeyer, H. J. in *Kirk-Othmer Encyclopedia of Chemical Technology* (2014).

275 Rekoske, J. E. & Barteau, M. A. Kinetics, selectivity, and deactivation in the aldol condensation of acetaldehyde on anatase titanium dioxide. *Ind. Eng. Chem. Res.* **50**, 41-51, (2010).

276 Young, Z. D., Hanspal, S. & Davis, R. J. Aldol condensation of acetaldehyde over titania, hydroxyapatite, and magnesia. *ACS Catal.* **6**, 3193-3202, (2016).

277 Vannice, M. A. & Sen, B. Metal-support effects on the intramolecular selectivity of crotonaldehyde hydrogenation over platinum. *J. Catal.* **115**, 65-78, (1989).

278 Claus, P. Selective hydrogenation of α,β-unsaturated aldehydes and other C=O and C=C bonds containing compounds. *Top. Catal.* **5**, 51-62, (1998).

279 Moore, C. M., Staples, O., Jenkins, R. W., Brooks, T. J., Semelsberger, T. A. & Sutton, A. D. Acetaldehyde as an ethanol derived bio-building block: an alternative to Guerbet chemistry. *Green Chem.* **19**, 169-174, (2017).

280 Liang, N., Zhang, X., An, H., Zhao, X. & Wang, Y. Direct synthesis of 2-ethylhexanol via n-butanal aldol condensation–hydrogenation reaction integration over a Ni/Ce-Al_2O_3 bifunctional catalyst. *Green Chem.* **17**, 2959-2972, (2015).

281 Nakajima, T., Nameta, H., Mishima, S., Matsuzaki, I. & Tanabe, K. A highly active and highly selective oxide catalyst for the conversion of ethanol to acetone in the presence of water vapour. *J. Mater. Chem.* **4**, 853-858, (1994).

282 Bussi, J., Parodi, S., Irigaray, B. & Kieffer, R. Catalytic transformation of ethanol into acetone using copper–pyrochlore catalysts. *Appl. Catal. A-Gen.* **172**, 117-129, (1998).

283 Nishiguchi, T., Matsumoto, T., Kanai, H., Utani, K., Matsumura, Y., Shen, W.-J. & Imamura, S. Catalytic steam reforming of ethanol to produce hydrogen and acetone. *Appl. Catal. A-Gen.* **279**, 273-277, (2005).

284 Murthy, R. S., Patnaik, P., Sidheswaran, P. & Jayamani, M. Conversion of ethanol to acetone over promoted iron oxide catalysis. *J. Catal.* **109**, 298-302, (1988).

285 Nakajima, T., Tanabe, K., Yamaguchi, T., Matsuzaki, I. & Mishima, S. Conversion of ethanol to acetone over zinc oxide-calcium oxide catalyst: optimization of catalyst preparation and reaction conditions and deduction of reaction mechanism. *Appl. Catal.* **52**, 237-248, (1989).

286 Rahman, M. M., Davidson, S. D., Sun, J. & Wang, Y. Effect of water on ethanol conversion over ZnO. *Top. Catal.* **59**, 37-45, (2016).

287 Rodrigues, C. P., Zonetti, P. C., Silva, C. G., Gaspar, A. B. & Appel, L. G. Chemicals from ethanol—The acetone one-pot synthesis. *Appl. Catal. A-Gen.* **458**, 111-118, (2013).

288 Orozco, L. M., Renz, M. & Corma, A. Carbon–carbon bond formation and hydrogen production in the ketonization of aldehydes. *ChemSusChem* **9**, 2430-2442, (2016).

289 Sun, J., Baylon, R. A., Liu, C., Mei, D., Martin, K. J., Venkitasubramanian, P. & Wang, Y. Key roles of Lewis acid–base pairs on $Zn_xZr_yO_z$ in direct ethanol/acetone to isobutene conversion. *J. Am. Chem. Soc.* **138**, 507-517, (2015).

290 Iwamoto, M., Mizuno, S. & Tanaka, M. Direct and selective production of propene from bio-ethanol on Sc-loaded In_2O_3 catalysts. *Chem. Eur. J.* **19**, 7214-7220, (2013).

291 Sun, J., Zhu, K., Gao, F., Wang, C., Liu, J., Peden, C. H. & Wang, Y. Direct conversion of bio-ethanol to isobutene on nanosized $Zn_xZr_yO_z$ mixed oxides with balanced acid–base sites. *J. Am. Chem. Soc.* **133**, 11096-11099, (2011).

292 Liu, C., Sun, J., Smith, C. & Wang, Y. A study of $Zn_xZr_yO_z$ mixed oxides for direct conversion of ethanol to isobutene. *Appl. Catal. A-Gen.* **467**, 91-97, (2013).

293 Saus, A. & Schmidl, E. Benzyl sulfonic acid siloxane as a catalyst: Oligomerization of isobutene. *J. Catal.* **94**, 187-194, (1985).

294 Hauge, K., Bergene, E., Chen, D., Fredriksen, G. R. & Holmen, A. Oligomerization of isobutene over solid acid catalysts. *Catal. Today* **100**, 463-466, (2005).

295 Rehfinger, A. & Hoffmann, U. Formation of di-isobutene, main by-product of methyl tertiary butyl ethyl ether synthesis catalyzed by ion exchange resin. *Chem. Eng. Technol.* **13**, 150-156, (1990).

296 Izquierdo, J., Vila, M., Tejero, J., Cunill, F. & Iborra, M. Kinetic study of isobutene dimerization catalyzed by a macroporous sulphonic acid resin. *Appl. Catal. A-Gen.* **106**, 155-165, (1993).

297 Alcántara, R., Alcántara, E., Canoira, L., Franco, M. a. J., Herrera, M. & Navarro, A. Trimerization of isobutene over Amberlyst-15 catalyst. *React. Funct. Polym.* **45**, 19-27, (2000).

298 Yoon, J. W., Chang, J.-S., Lee, H.-D., Kim, T.-J. & Jhung, S. H. Trimerization of isobutene over a zeolite beta catalyst. *J. Catal.* **245**, 253-256, (2007).

299 Peters, M. W. & Taylor, J. D. Renewable jet fuel blendstock from isobutanol. US 8,975,461 B2 (2015).

300 ASTM International. ASTM D7566-18. *Standard specification for aviation turbine fuel containing synthesized hydrocarbons.* (2018).

301 Bomgardner, M. M. Gevo isobutyl alcohol power army copter. *Chem. Eng. News* **92**, 11, (2014).

302 *Virgin Australia leads effort to use Gevo renewable jet fuel at the Brisbane airport in Queensland, Australia*, <https://www.marketwatch.com/press-release/virgin-australia-leads-effort-to-use-gevo-renewable-jet-fuel-at-the-brisbane-airport-in-queensland-australia-2018-09-12> (2018).

303 Tsuchida, T., Yoshioka, T., Sakuma, S., Takeguchi, T. & Ueda, W. Synthesis of biogasoline from ethanol over hydroxyapatite catalyst. *Ind. Eng. Chem. Res.* **47**, 1443-1452, (2008).

304 Lovón-Quintana, J. J., Rodriguez-Guerrero, J. K. & Valença, P. G. Carbonate hydroxyapatite as a catalyst for ethanol conversion to hydrocarbon fuels. *Appl. Catal. A-Gen.*, (2017).

305 Kojima, M., Aida, T. & Asami, Y. Catalyst for production of ethylene from ethanol. US 4,302,357 A (1981).

306 Sheng, Q., Guo, S., Ling, K. & Zhao, L. Catalytic dehydration of ethanol to ethylene over alkali-treated HZSM-5 zeolites. *J. Brazil Chem. Soc.* **25**, 1365-1371, (2014).

307 Riittonen, T., Toukoniitty, E., Madnani, D. K., Leino, A.-R., Kordas, K., Szabo, M., Sapi, A., Arve, K., Wärnå, J. & Mikkola, J.-P. One-pot liquid-phase catalytic conversion of ethanol to 1-butanol over aluminium oxide—the effect of the active metal on the selectivity. *Catalysts* **2**, 68-84, (2012).

308 Antolín, R. A., Yagüe, J. L. S., Canós, A. C., Domine, M. E., Barrero, F. V. & Vidal, F. A. L. D. G. Method for obtaining higher alcohols. US 9,475,741 B2 (2016).

3.15 Supplemental Information

Table S3.1 | **Overview of the most-studied heterogeneous catalysts for ethanol dehydration.**

Catalyst	Feed Concentration	Temperature (°C)	Conversion (%)	Selectivity (C%)	Ref.
10 wt% TiO_2/γ-Al_2O_3	12-100 wt% in water	360-500	95.0-100	96-99.3	63
Al_2O_3-MgO/SiO_2 (Syndol)	95 vol%	335-450	97.3-100	94.5-98.9	64
10 wt% FeO_x/Al_2O_3	2 vol% in N_2	250	60.0	88.5	65
0.5 wt% $MgHPO_4/Al_2O_3$	-	370	96.0	94.0	305
H-ZSM-5 (steamed)	10 wt% in water	275	99.7	99.7	80
NaOH treated H-ZSM-5	20 vol% in water with N_2	265	99.7	99.6	306
P modified H-ZSM-5	10 wt% in water	350	100	98	69
2 wt% TFA/H-ZSM-5	10 wt% in water	205	98.2	99.0	79
Ni-substituted SAPO-34	70 vol% in N_2	350	93.9	98.3	71
$H_4SiW_{12}O_{40}$/MCM-41	48 vol% in He	275	99.0	99.9	74

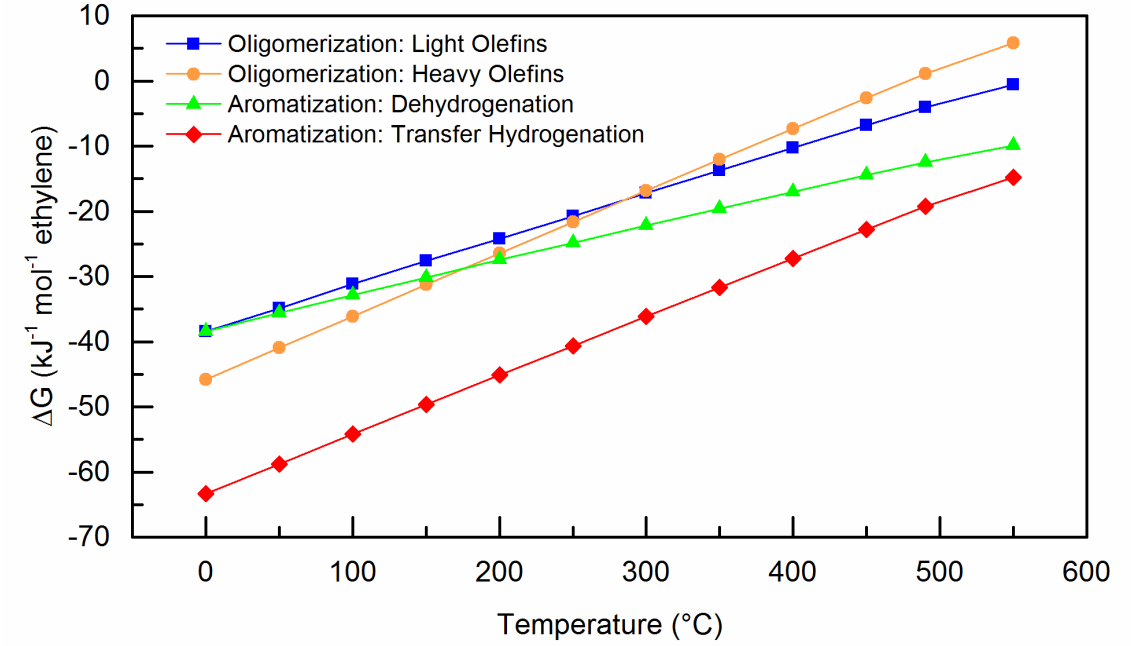

Figure S3.1 | **Thermodynamics of ethylene oligomerization versus aromatization as a function of temperature.** They include light olefin formation, heavy olefin formation, aromatization with liberated H_2, and aromatization with transfer hydrogenation (i.e. saturation of olefins with hydrogen removed in aromatization). These scenarios are detailed in Figure 3.5.

Table S3.2 | **Summary of the influence of parameters in ethanol conversion over H-ZSM-5.** Entries 1-4 show the effect of temperature. 4-7 show the effect of water content. 7-8 show the effect of space velocity with an aqueous feed. 9-12 show the effect of Si:Al ratio at elevated pressure. Entry 13 shows a data point at a particularly high pressure where liquid yields are high.

Entry	Si:Al Ratio	Pressure (MPa)	Feed Water Content (wt%)	Temp. (°C)	LHSV[a] (hr^{-1})	Liquid (C_{5+}) Hydrocarbon Yield	Aromatic Fraction of Liquid Hydrocarbons (%)	Ethylene Yield	Ref.
1	44	0.1	0	250	0.98	0.0	-	98.8	101
2	44	0.1	0	300	0.98	26.6	9.8	46.0	101
3	44	0.1	0	350	0.98	51.2	55.6	2.2	101
4	44	0.1	0	400	0.98	47.3	70.4	3.3	101
5	85	0.1	4	400	1.0	50.5	60.6	11.1	124
6	85	0.1	15	400	1.0	12.5	51.2	36.8	124
7	85	0.1	30	400	1.0	15.3	54.2	40.0	124
8	85	0.1	30	400	0.25	49.3	77.1	3.3	124
9	16	3.0	0	350	5.3	63.3	59.7	0.0	129
10	40	3.0	0	350	5.3	56.8	63.5	0.0	129
11	140	3.0	0	350	5.3	49.1	38.7	17.0	129
12	500	3.0	0	350	5.3	7.2	23.0	65.3	129
13	80[b]	5.0	0	370	1.2	73.2	45.1	1.8	132
14	25	0.1	0	350	3.0[c]	58.1	65.4	32.2	125
15	25	0.1	0	400	3.0[c]	56.3	65.6	30.0	125
16	25	0.1	0	450	3.0[c]	45.9	67.8	42.1	125
17	25	0.1	0	500	3.0[c]	41.5	71.5	48.8	125
18	25	0.1	0	550	3.0[c]	36.9	75.1	55.9	125

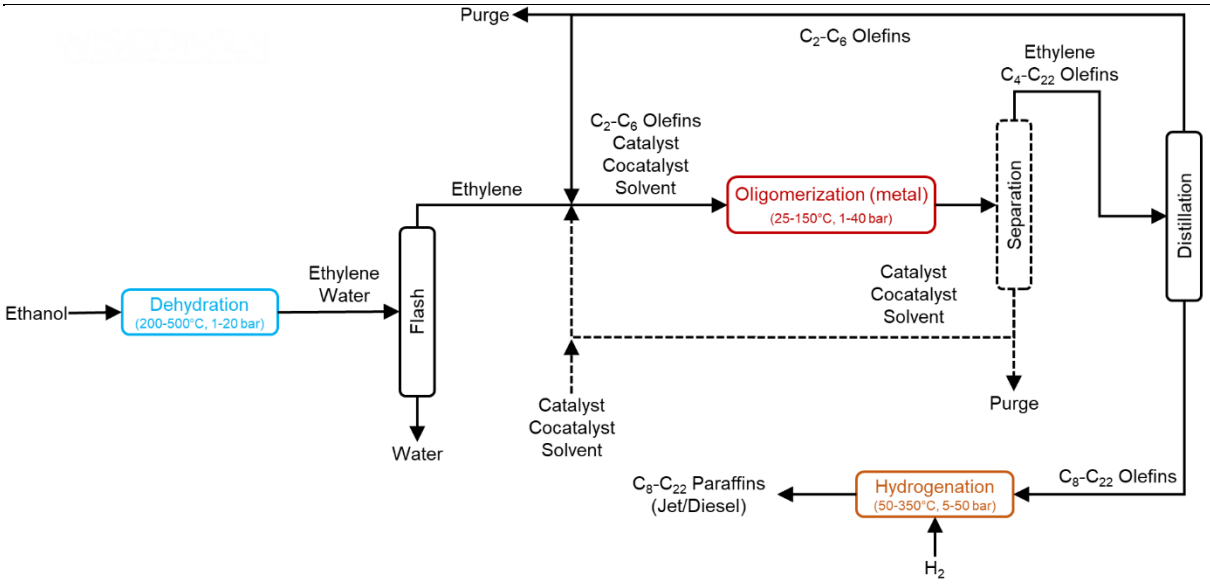

Figure S3.2 | **Block flow diagram for ethanol dehydration followed by metal-catalyzed oligomerization via Cossee-Arlman catalysis.** Dotted lines represent streams which are present in some configurations, particularly homogeneous systems, which require continuous addition of catalyst, cocatalyst (e.g. TEA), or solvents. These components must be separated after the reactor and recycled or removed. Distillate-range olefins are separated from C_2-C_6 olefins, which are recycled to the oligomerization reactor.

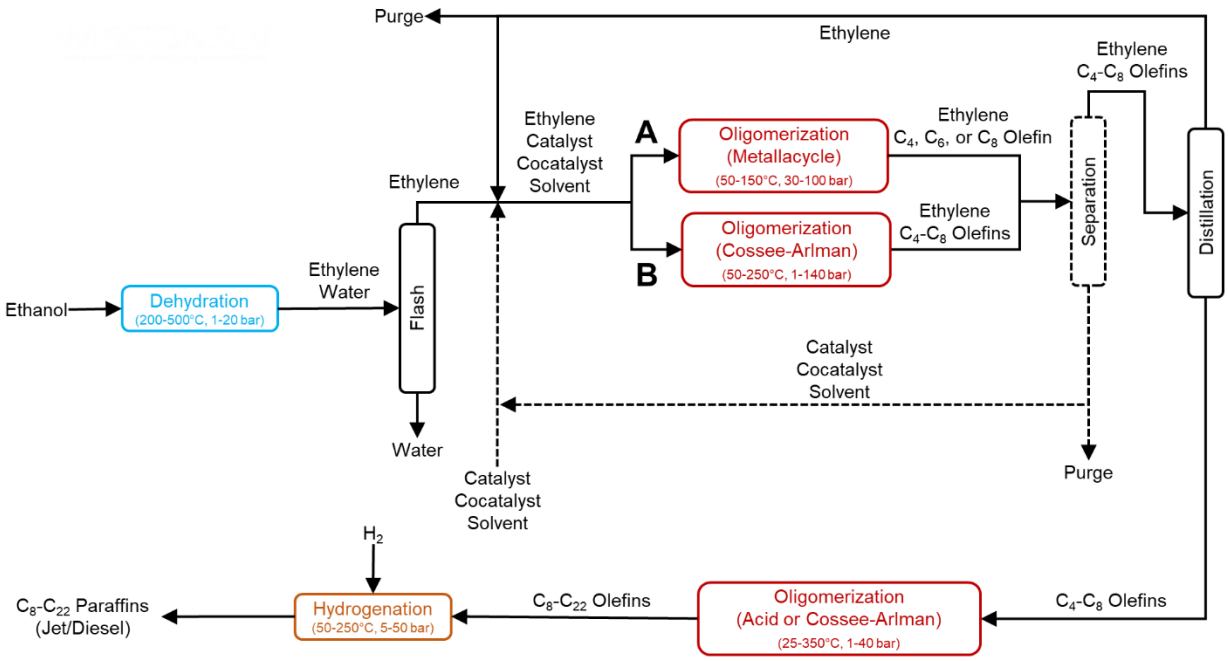

Figure S3.3 | **Block flow diagram for dehydration followed by two-stage metal-catalyzed oligomerization.** Pathway A utilizes metallacycle catalysis in the first stage while pathway B utilizes Cossee-Arlman catalysis in the first stage. These may require the addition of solvents, homogeneous catalysts, and cocatalysts, which would have to be separated from the product mixture prior to further use. The resulting olefin stream which is rich in C_4-C_8 olefins are then be distilled to remove ethylene for recycle. The C_4-C_8 products are then converted either via acid or Cossee-Arlman catalysis to distillate-range olefins. If homogeneous catalysts are involved, additional streams and separation processes may be required. The olefins are then hydrogenated for use as jet or diesel paraffins.

Table S3.3 | **Heterogeneous catalysts commonly used for the Guerbet coupling of ethanol.**

Catalyst	Batch/ Flow	Temp. (°C)	Pressure (bar)	Conv. (%)	1-butanol Selectivity (C%)	C_{4+} Alcohol Selectivity (C%)	C_{4+} Alcohol Yield (C%)	Ref.
Ca-HAP	Flow	275	1.0	52.0	55.0	86.0	44.7	[253]
MgO	Flow	450	1.0	56.1	32.8	-	>18.4	[254]
Mg_3AlO_y	Flow	300	1.0	43.7	49.6	-	>21.7	[255]
Ni/Al_2O_3	Batch	250	70	26	82	-	>21.3	[307]
Ni/Al_2O_3	Flow	240	70	25	58	-	>14.5	[260]
Mg_4AlO_y	Flow	250	30	0.2	57.1	59.1	0.1	[246]
$NiMg_4AlO_y$	Flow	250	30	18.7	55.3	86.1	16.1	[246]
Pd/Mg_xAlO_y	Flow	250	34	67.0	67.0	86.0	57.6	[261]
Pd/Mg_4AlO_y	Batch	200	30	12.1	95.8	-	>11.6	[308]
$Cu_{0.3}Ni_{0.3}Mg_{2.4}AlO_y$	Batch	310	~80	47.6	45.6	58.6	27.9	[258]
Pd/ZrO_2	Flow	360	34	78	51	73	56	[262]

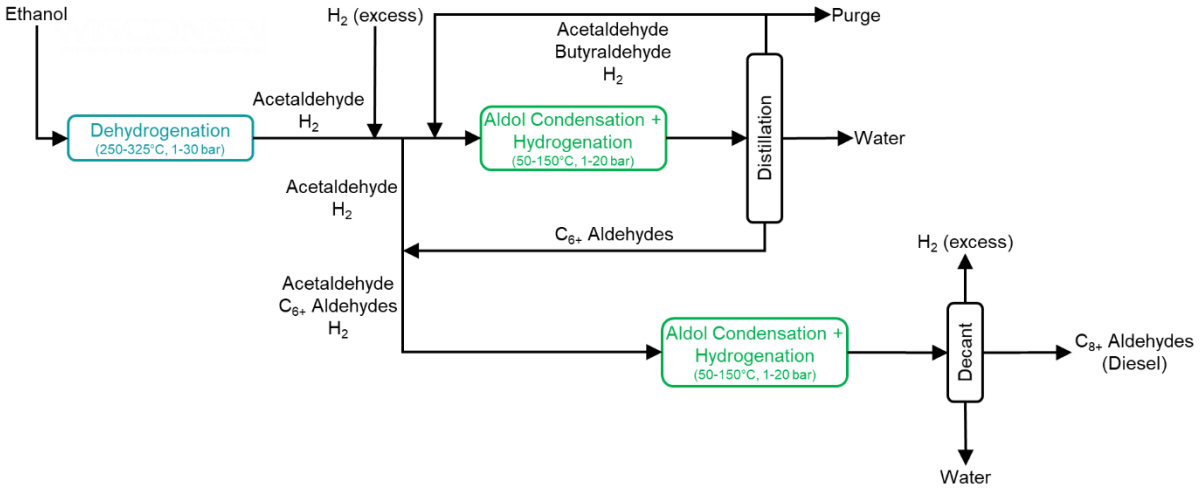

Figure S3.4 | **Distillate-range aldehydes through acetaldehyde aldol condensation with C=C hydrogenation in two stages.** Ethanol is first dehydrogenated to acetaldehyde under anaerobic conditions. This is then oligomerized via a solid base in the presence of a transition metal under a hydrogen environment in order to hydrogenate C=C double bonds immediately after production. Acetaldehyde, butyraldehyde, and hydrogen are separated from the product mixture and recycled. The C_{6+} aldehydes are then cofeed with a stream of acetaldehyde to produce C_{8+} aldehydes which may be useful in diesel blending.

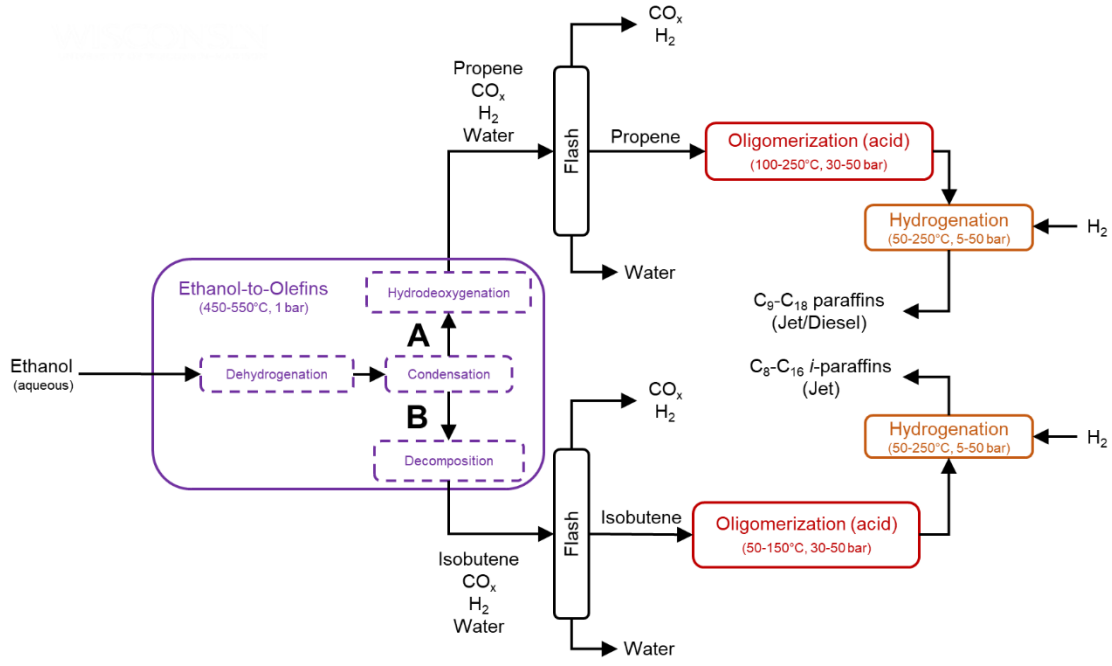

Figure S3.5 | **Block diagram for aqueous ethanol condensation and decomposition to propene and isobutene followed by acid-catalyzed oligomerization.** Aqueous feeds can be used in both cases. External H_2 is required for the propene route. After oligomerization, the olefins are hydrogenated to iso-paraffins.

Table S3.4 | **Comparison of ethanol to distillate routes.** Technologies with * for distillate yield have too many uncertainties to appropriately estimate yields. Technologies are described based upon the individual chemistries involved; each abbreviation is described as follows. A slash (/) indicates the chemistries occur in a single step, while a dash (-) indicates that they occur in series, potentially with separations and recycles in between. D=dehydration, A=acid-catalyzed oligomerization, H=hydrogenation, M=transition metal-catalyzed oligomerization, G=Guerbet coupling, AL=aldol condensation mediated by C=C hydrogenation, I=ethanol-to-isobutene.

Technology (Chemistries, Figure #)	Estimated Distillate Yield (C%)	Main Side Products	Key Benefits	Key Limitations
One-stage dehydration and oligomerization (D/A, Figure 3.7a)	25	BTEX, gasoline	-Aqueous feed possible -Single step -Hydrogen neutral -Possibly valuable side-products -Process at demonstration scale	-Side-reactions at high temperatures -Predominantly branched products
Two-stage acid-catalyzed oligomerization (D/A-A-H, Figure 3.7b)	70	Gasoline, BTEX	-Aqueous feed possible -Dynamic operation -Gasoline side-products -Technologies proven at commercial scales	-Side-reactions at high temperatures. -Possible challenge with propene trimerization requirement. -Predominantly branched products
Metal-catalyzed ethylene oligomerization (D-M-H, Figure S3.2)	60	Light (C_4-C_6) olefins	-Aqueous feed possible -Highly selective to olefins -Proven at commercial scale -Selective to linear olefins	-Constraints from statistical distributions. -Catalyst/solvent separations in commercialized systems -Metal vs. solid acid cost
Two-stage metal-catalyzed ethylene oligomerization (D-M-M-H, Figure S3.3)	>95	Heavy (>C_{22}) olefins	-Aqueous feed possible -Highly selective to olefins -Oligomerization proven at commercial scale -Selective to linear olefins	-Catalyst/solvent separations in commercialized systems -Metal vs. solid acid cost
Sequential metal- and acid-catalyzed ethylene oligomerization (D-M-A-H, Figure S3.3)	>95	Heavy (>C_{22}) olefins	-Aqueous feed possible -Highly selective to olefins -Solid acid lower cost than metal -Oligomerization proven at commercial scale -Selective to linear olefins	-Catalyst/solvent separations in commercialized systems -Branching favored in second stage
Guerbet coupling followed by dehydration and olefin oligomerization (G-D-A-H, Figure 3.12c)	*	Diethyl ether, ethylene, ethyl acetate	No theoretical limits on high selectivities	-Few studies with high Guerbet selectivities at high conversions -Low water tolerance of Guerbet catalysts

Two-stage Guerbet coupling to distillate alcohols (G-G)	*	Diethyl ether, ethylene, ethyl acetate	-Hydrogen-neutral -Alcohols may improve engine performance	-Guerbet challenges (above) -Difficult branching control; statistical limitations. -Alcohol blending needs testing
Two-stage aldol condensation of acetaldehyde with C=C hydrogenation (D'-AL-AL,Figure S3.4)	*	Light (C_4-C_6) aldehydes, possibly CO_x	-Hydrogen-neutral -Removes high-temperature challenges of Guerbet coupling	-Aldehyde stability in engines concerning -Branching limits size Minimal relevant studies
Direct ethanol-to-isobutene followed by olefin oligomerization (I-A-H, Figure S3.5)	65	CO_x	-Aqueous feed possible -Isobutene oligomerization rapid for high-quality jet fuel; fuel validated by ASTM. -Oligomerization proven at commercial scale	-CO_x loss during isobutene formation.

Schulz-Flory Selectivity Derivation

Initial moles: N^i
Chain growth probability: α
Oligomer #: n
Moles C per mole monomer: γ
Mole fraction of product of oligomer n: $x_n = (1-\alpha)\alpha^{n-1}$
Final C moles: $N_C = N_C^i = \gamma N^i$
Final moles: $N = N^i(1-\alpha)$
Final C moles oligomer n: $N_{C,n} = \gamma n x_n N = \gamma n N^i (1-\alpha)^2 \alpha^{n-1}$
Final C moles product: $N_{C,P} = N_C - N_{C,1} = \alpha\gamma N^i (2-\alpha)$
Carbon selectivity to oligomer n: $S_{C,n} = \frac{N_{C,n}}{N_{C,P}} = \frac{\boldsymbol{n(1-\alpha)^2\alpha^{n-2}}}{\boldsymbol{(2-\alpha)}}$

Chapter 4. Ethanol Condensation at Elevated Pressure over Copper on AlMgO and AlCaO Porous Mixed-Oxide Supports

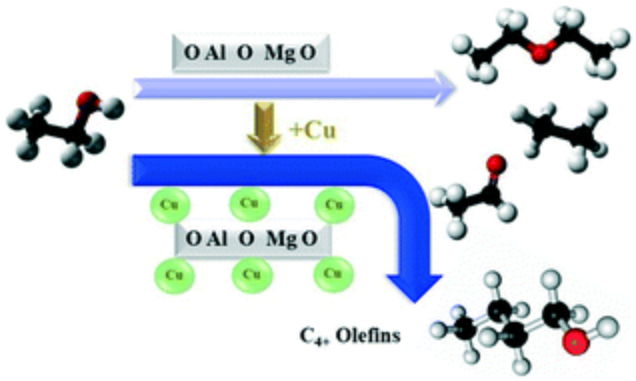

Figure 4.1 | **Conversion of ethanol to higher alcohols and byproducts over Cu-doped AlMgO and AlCaO oxides.**[1] Chapter adapted from Ref 1.

4.2 Introduction

Mixed Mg-Al oxides have received considerable attention for the Guerbet condensation of ethanol.[2-5] These Mg-Al mixed oxides are conventionally prepared via decomposition of hydrotalcites which are synthesized via coprecipitation of Mg and Al precursors (*e.g.* nitrates) at high pH. In previous work by our collaborators, an emulsion-mediated synthesis method was used to produce these materials with additional porosity, where the formation of a sol-gel transition in an emulsion acts as a soft template with a nonpolar phase dispersed in an aqueous phase.[6-8] Inorganic precursors organize around the droplets of the nonpolar phase, which then chemically gel the sol. The removal of droplets upon drying and calcination creates a unique pore structure. Increasing the surface area of a material increases the potential number of available catalytically active sites and promotes the dispersion of added metals.[9-13] Furthermore, the presence of amphipathic molecules and apolar molecules in the synthesis can alter the strength of the sites in the catalyst due to interactions between the templates and the surface of the metal oxides.[14,15] In this way, the efficiency of the material can be increased by modifying its structural and chemical

properties, the composition, and organization of the surface atoms, as shown previously.[6,14,16,17] The activity of alumina and AlMgO for ethanol (EtOH) dehydration and 2-propanol conversion, respectively, strongly depends on the pore structure produced with this method.[8,15] Efficient EtOH dehydrogenation catalysts have also been produced via the addition of Cu to porous alumina catalysts.[16,18,19] The improved dehydrogenation activity upon addition of Cu or Ni can be leveraged to improve EtOH condensation on mixed Mg-Al oxides which are otherwise believed to rely upon intermolecular hydrogen transfers.[20-22]

In this chapter, AlMgO and AlCaO oxides synthesized via emulsion-mediated synthesis with and without the addition of Cu are evaluated for the condensation of EtOH at elevated hydrogen pressures. Previous studies by our collaborators examining EtOH conversion over Cu-promoted alumina did not show extensive C-C coupling, which is typically slow for alumina compared to Mg-Al oxides.[5] The substitution of magnesium by calcium was intended to change the basicity and acidity of the material and thus influence catalytic performance.[17] Here high hydrogen pressures (32 bar) were utilized to promote the saturation of Guerbet intermediates and increase the selectivity of aldol condensation products.

4.3 Experimental Methods

4.3.1 Catalyst preparation

The synthesis of the porous oxides involved the use of aluminum tri-*sec*-butoxide (Al(O-*s*-But)$_3$) and magnesium nitrate or calcium nitrate. The assembly of the emulsified system occurred by the simultaneous utilization of n-dodecane, Pluronic P123 (block copolymer, 20 EO : 70 PO : 20 EO, Mw. of 5826 g/mol) and EtOH as solvent, where Pluronic P123 and n-dodecane were the organic pore structure directing agents (PSDA).[8,14]

The dispersion of the *n*-dodecane in EtOH occurred at room temperature. The final mole composition of the sol was: 0.01 Pluronic: 1 ($Al(O\text{-}s\text{-}But)_3$): 1 $Mg(NO_3)_2$ or $Ca(NO_3)_2$: 15 EtOH. A 29 wt.% solution of ammonium hydroxide was added dropwise under stirring to produce the sol-gel transition (pH 10). The reference samples were prepared in the same procedure, though without addition of PSDA. The as-synthesized samples were calcined at 700°C for 6 h under air flow to produce mixed oxides. For synthesis of Cu-doped catalysts, the mixed oxides were then dispersed in Milli-Q water, and tetraamminecopper(II) sulfate monohydrate [$Cu(NH_3)_4SO_4 \cdot H_2O$, Sigma-Aldrich] was added to the suspension under continuous mixing at room temperature. The pH was adjusted to 9 through dropwise addition of dilute 2 mol L^{-1} nitric acid (Sigma-Aldrich). The mixture was aged for 20 h while being stirred at room temperature, and the solid material was then filtered and washed with deionized water. The sample was dried overnight at 110°C in air. The dried catalyst was pretreated in a flow-through cell at a temperature of 500°C (with a heating rate of 1°C min^{-1}) under a helium flow (30 mL min^{-1}) for 3 h, followed by air flow, switched to He for 20 min, reduced under hydrogen flow, and finally passivated at room temperature with 1% O_2 in He. AlMgO and AlCaO catalysts were prepared with and without an emulsion, with the former denoted by "-P" to imply the added porosity. All catalysts were examined for catalytic activity with and without the addition of Cu.

4.3.2 Catalyst characterization

Nitrogen adsorption-desorption isotherms were recorded at -195°C and P/P_0 ranging between 0.001 and 0.998, using a Micromeritics ASAP 2020 instrument. Samples were degassed prior to analysis at 200°C for 6 h under a vacuum of 10 μPa. The specific surface area was calculated according to the BET equation[39] and the pore size distribution was determined using the BJH equation.

The thermal behavior of the AlMgO and AlCaO samples, calcined and exposed to atmospheric environment, was investigated by thermogravimetric analysis, performed from room temperature up to 900°C under air flow (50 mL min^{-1}), by using a SDT600 TA Instruments at a heating rate of 10°C min^{-1}.

Scanning Transmission Electron Microscopy (STEM) was performed using a FEI Titan STEM instrument with a Cs probe aberration corrector operated at 200 kV with a spatial resolution of < 0.1 nm. A high-angle annular dark-field (HAADF) mode with a HAADF detector angle ranging from 54 to 270 mrad, a probe convergence angle of 24.5 mrad, and a probe current of approximately 25 pA was used to record the images. Catalyst samples were suspended in EtOH and then dropped on a holey carbon Au TEM grid. Samples were plasma cleaned before being loaded into the microscope. Particle sizes were calculated based on a minimum of 800 particles for each sample.

The Cu loading of catalysts were determined with Inductively Coupled Plasma Absorption Emission Spectroscopy (ICP-AES) using a PerkinElmer Plasma 400 ICP Emission Spectrometer. Typically, 20 mg catalyst samples were digested with a mixture of 3 mL of nitric acid (Fischer, 65%) and 7 mL of hydrochloric acid (Fischer, 37%) in a Teflon beaker at 120°C. The digested mixture was cooled to room temperature, diluted in water, filtered, and analyzed. Cu standards for ICP analyses were prepared from a concentrated Cu ICP standard (Fluka, 1000 ± 2 mg/L).

The number of Cu surface sites was determined using reactive N_2O chemisorption.[40] Prior to the measurement, catalysts were reduced *in situ* at 500°C (with a heating rate of 1°C min^{-1}) under a H_2 flow for 2 h. After reduction, the samples were cooled to 90°C, and the cell was evacuated to 10^{-5} Torr. N_2O was then introduced and reacted with surface metallic Cu to produce

N_2 gas and chemisorbed O. The stoichiometry for the adsorption of O on the Cu surface was assumed to be 1/2 based on Equation 4.1 where Cu_s denotes as Cu surface sites.

Equation 4.1 $$2Cu_s + N_2O \rightarrow (Cu_s)_2O + N_2$$

The amount of O adsorbed on the surface was quantified by monitoring the N_2 pressure using a gas handling system and a volumetric system employing Baratron capacitance manometers for precision pressure measurement (5×10^{-5} Torr) after condensation of N_2O in a cold trap using liquid nitrogen.

Acidities and basicities of the samples were determined by temperature programmed desorption of ammonia (NH_3-TPD) and carbon dioxide (CO_2-TPD), respectively, using a Micromeritics AutoChem II 2920 apparatus. Samples were pretreated in H_2 (30 mL min^{-1}) at 500°C (1°C min^{-1}) and held for 2 h to remove adsorbed species and to reduce the Cu for consistency with catalytic experiments. Prior to NH_3-TPD, samples were then cooled to 150°C in He (50 mL min^{-1}) prior to NH_3 adsorption. A stream containing 1 vol.% NH_3 in He (50 mL min^{-1}) was introduced for 30 min until adsorption equilibrium was achieved. Physisorbed NH_3 was then purged at 150°C under a flow of He for 60 min. Chemisorbed NH_3 was then desorbed in a 50 mL min^{-1} flow of He heating from 150 to 500°C at a rate of 10°C min^{-1} with the NH_3 evolution monitored by an online mass spectrometer (Cirrus 2, MKS Instruments), which was integrated to determine the number of acid sites and deconvoluted to determine acid strengths. CO_2-TPD was performed in the same manner but with the uptake conducted at 50°C in a stream of 50 vol.% CO_2 in He (30 mL min^{-1}) for 1 h followed by 1 h of He flow to remove weakly adsorbed CO_2. The temperature was then increased to 500°C at a rate of 10°C min^{-1} in He (30 mL min^{-1}) with CO_2 evolution monitored by an online mass spectrometer.

The surface acid sites of Cu samples were further analyzed by Fourier transform infrared spectroscopy (FTIR) using a Shimadzu Prestige 21 spectrophotometer with pyridine as the probe molecule. The spectral resolution was 4 cm^{-1}, and 40 scans were accumulated. For each sample, 15 mg of catalyst were pressed into 13 mm diameter pellets without dilution. All catalysts were reduced under 25 mL min^{-1} 4% H_2/N_2 at 1 ºC min^{-1} to 500°C with a 2 h hold. After cooling to 100°C, N_2 was flowed for 1 h to remove physisorbed H_2. After cooling to room temperature, N_2 was flowed through a pyridine bubbler and over the catalyst for 5 min, followed by a switch to N_2 without pyridine. The catalysts were heated at 1°C min^{-1} to 150°C and held for 1 h to remove physisorbed pyridine. Samples were then cooled to room temperature prior to data collection. Spectra were recorded at room temperature with background subtraction based on a previously-recorded spectrum of the dehydrated sample. The relative contributions of Lewis and Brønsted acid sites after adsorption and partial desorption of pyridine were obtained by integration of the bands at 1440 cm^{-1} (Lewis sites) and 1540 cm^{-1} (Brønsted sites). The relative concentration Brønsted/Lewis acid sites was determined by means of the Beer-Lambert Law for an Emeis molar extinction factor of 1.67 cm/mol for band at 1540 cm^{-1} and 2.22 cm/mol for band at 1450 cm^{-1}.

4.3.3 Catalytic activity

EtOH coupling reactions were performed in fixed-bed stainless-steel tubular flow reactors (40 cm long, 0.46 cm inner diameter) heated with a tube furnace (Lindberg Blue M Mini-Mite) with a 30 cm heated region. Reactors were packed with 225-675 mg of catalyst at the center of the heated region with quartz beads and quartz wool on either side. An aluminum block was utilized between the furnace coils and reactor to maintain a 30 cm isothermal region. Temperature was measured via a thermocouple positioned alongside the reactor with the tip at the center of the bed. Prior to reaction, all samples were pretreated in H_2 (100 mL min^{-1}) at 500°C (1°C min^{-1}, 2 h) with

the flow rate controlled via a mass-flow controller (SLA 5850, Brooks Instruments). During reaction, neat EtOH (Decon's Pure Ethanol, 200 proof) was fed at flow rates between 10 and 30 μL min^{-1} via a syringe pump (Teledyne Isco 500D) into a stream of 30-90 standard mL min^{-1} of H_2 flowing downward through a preheated region prior to the reactor. All reactions were performed at 325°C. Below the furnace products were fed through a 300 mL condenser kept at 0°C via an ice bath. Species which did not fully condense then passed through a back-pressure regulator set at 32 bar to an online GC (Shimadzu GC-2014) equipped with both a flame-ionization detector (FID) and a thermal conductivity detector (TCD). The gas was analyzed every 4-12 h directly prior to liquid collection. The condenser contents were collected directly into 1,4-dioxane to fully solubilize all components and minimize flashing of volatile components. Samples were then further diluted in a 1,4-dioxane solution containing a *n*-decane tracer (1.5 wt.%) and analyzed via GC FID (Shimadzu GC-2010). Product identification was validated using GC MS for selected samples. Quantification was performed using response factors developed from external calibration curves. Compounds for which standards could not be easily obtained were quantified using their effective carbon numbers according to Scanlon and Willis,[41] though all major components were quantified using standards. Reactions were performed for 32-80 h. Carbon balances (carbon detected in the product minus the carbon fed into the reactor) for reported data were between 95 and 105%. Tabulated values are averages based on time points which demonstrate carbon balances in this regime, typically three points. Yields, conversion, and selectivities are defined on a carbon basis (referred to as C%). Conversion is calculated as the sum of yields rather than directly from the change in EtOH flow rate in order to minimize amplification of minute analytical errors. This includes an approximate yield to species detected via GC that were not identifiable.

4.4 Results and discussion

4.4.1 Structural characteristics of the catalysts

Textural properties of the mesopores were determined by nitrogen physisorption measurements with BJH pore size distribution curves obtained from the desorption branches of the isotherms (Figure 4.2). The emulsion method proved to be effective for the creation of materials with greater porosity (AlMgO-P and AlCaO-P) compared to the reference materials (AlMgO and AlCaO) as shown in Table 4.1. The hysteresis between the adsorption and desorption curves is typically evidence of the existence of mesopores as shown in AlMgO-P and AlCaO-P. However, the absence of a plateau in the P/P_0 region near 1 is characteristic of the type II isotherms often observed for solids in which macropores are present as well. According to the IUPAC classification, the shallow slopes of the isotherms for the samples together with the non-parallel behavior of the adsorption/desorption curves indicate a H3 hysteresis cycle.

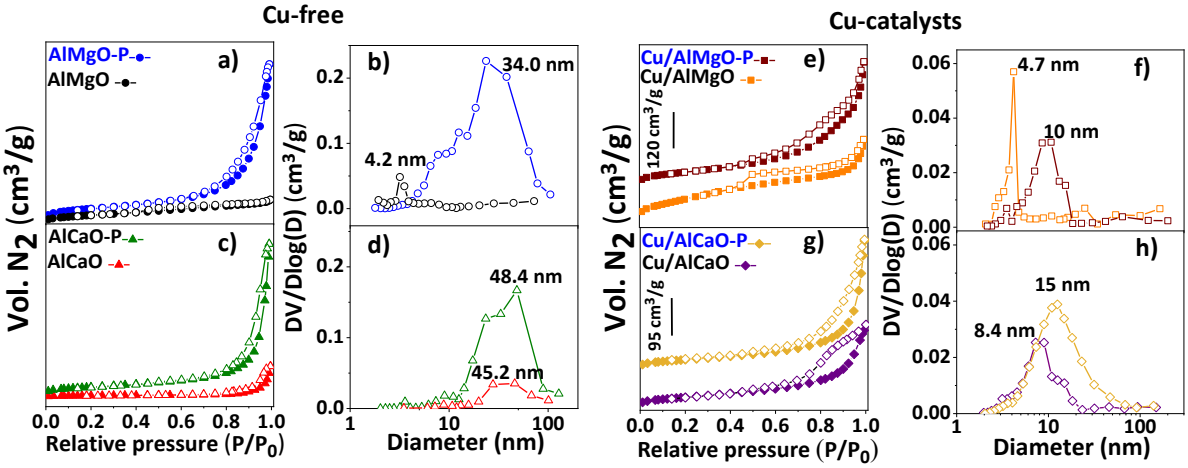

Figure 4.2 | **Nitrogen physisorption of AlMgO and AlCaO catalysts before (a-d) and after the addition of Cu (e-h).** Nitrogen adsorption-desorption isotherms present in (a, c, e, g). BJH pore size distributions in (b, d, f, h).

Table 4.1 | **Measured surface and bulk material properties of mixed oxide catalysts.**

Sample	BET area (m^2/g)	Cu loading[a] (%)	Cu particle size[b] (nm)	Cu^0 sites[c] (μmol/g)	Total NH_3[d] (μmol/g)	Total CO_2 [e] (μmol/g)
Cu/AlMgO	106	8.0	3.7	67	92.9	115
Cu/AlMgO-P	171	8.0	2.1	91	106	78.6
Cu/AlCaO	102	9.0	2.6	118	10.1	52.4
Cu/AlCaO-P	120	9.6	3.1	140	12.5	49.7
AlMgO	191	-		-	76.9	192
AlMgO-P	315	-		-	85.6	238
AlCaO	133	-		-	-*	43.8
AlCaO-P	202	-		-	4.0	46.9

a. Cu loading determined by ICP; b. Cu particle sizes obtained from STEM; c. Metallic copper sites quantified by N_2O chemisorption; d. Acid sites quantified from NH_3-TPD profiles; e. Base sites quantified with CO_2-TPD profiles; *Without significant acidity.

Physisorption measurements were additionally performed on catalysts with copper. The shape of the hysteresis does not change significantly, however the pore diameter greatly decreases. The addition of copper likely blocks certain pores of the material which also leads to lower BET surface areas. The pore distribution also shows a well-defined porous structure for the porous catalyst with diameters of 10 and 15 nm for Cu/AlMgO-P and Cu/AlCaO-P, respectively, according to Figure 4.2b and d. The emulsion method also increased BET surface area relative to the reference catalysts.

Cu particles were examined by STEM. Figure 4.3 shows representative transmission electron micrographs and the corresponding particle size distributions for Cu catalysts after reduction and passivation. Cu/AlMgO-P exhibits a lower average Cu particle size and more narrow distribution than the reference material, possibly indicating a more homogeneous surface for the porous support. The average size of the Cu particles decreased from 3.7 to 2.1 nm when using the porous support. This behavior was not observed for the Ca samples, however, as the emulsion-mediated method resulted in a slight increase in Cu particle size from 2.6 to 3.1 nm without a large effect on the sharpness of the distribution.

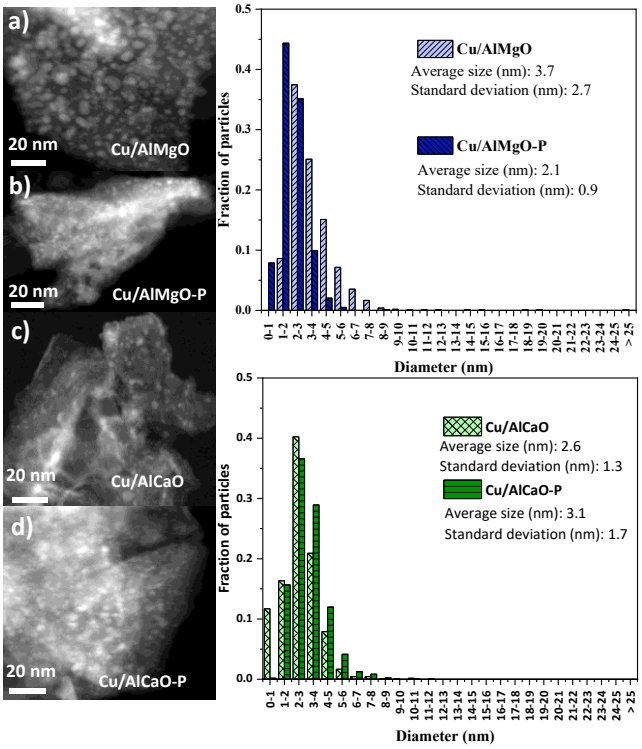

Figure 4.3 | **Transmission electron microscopy images and particle size distributions.**

Cu site densities were additionally quantified using reactive N_2O chemisorption (Table 4.1), which increased for both AlMgO and AlCaO when an emulsion-mediated synthesis was used. The AlCaO catalysts generally possessed higher Cu site densities, which is in part due to their higher Cu loadings.

The acid and base properties of the catalysts were examined via NH_3-TPD and CO_2-TPD, respectively, with the smoothed profiles shown in Figure S4.1. Peak deconvolution with Gaussian profiles was performed to separate the CO_2-TPD profiles into weak, medium and strong sites and the NH_3-TPD profiles into weak and strong sites based on the methods used by Di Cosimo *et al.* with Mg_yAlO_x catalysts.[5] These deconvolutions are not strongly quantiative in nature, however, and therefore will not be discussed in detail. The emulsion method was found to increase both the acid and base site densities for AlMgO possibly as a simple consequence of an increase in surface area. AlCaO catalysts were found to possess reduced acidity and basicity compared to AlMgO

with less than 25% of the base sites of AlMgO catalysts and less than 6% of the acid sites, which were too low for quantification with AlCaO. The lower basicity of AlCaO can be attributed to surface carbonates, which remain present even after 500°C calcination as shown by thermogravimetric analyses (Figure S4.2). After calcination and exposure to atmosphere, AlCaO-P continues to lose appreciable weight above 600°C while minimal weight loss occurs for AlMgO-P above 500°C. Cu addition greatly decreases the number of base sites available on AlMgO catalysts, while AlCaO catalysts experience a more minor increase.

The distributions of Brønsted *versus* Lewis acid sites on the Cu catalysts were determined via pyridine FTIR analyses in the range of 1350-1650 cm^{-1} (Figure 4.4). The absence of a band near 1540 cm^{-1} indicative of pyridinium cations (PyH^{+}) reflects the lack of Brønsted acid sites (B), while a band centered at 1450 cm^{-1} - corresponding to pyridine chemisorbed on Lewis acid sites (L) - was clearly observed. The ratio of Brønsted sites to total acid sites (T) was found to be close to zero for all catalysts, indicating that only Lewis acidity is present. A physisorbed pyridine band is observed for AlCaO catalysts, which is a result of the overall low acidity of these catalysts as supported by NH_3-TPD measurements. These results are in agreement with those of Lercher[23] and Prescott *et al.*[24] who observed only Lewis acidity on Al_2O_3-MgO catalysts.

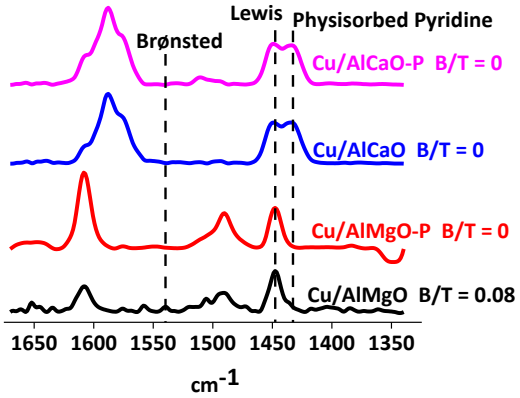

Figure 4.4 | **IR spectra of adsorbed pyridine on Cu catalysts.**

4.4.2 Catalytic performance in high-pressure Guerbet coupling of ethanol

As noted prior, the main purpose of adding Cu to the AlMgO and AlCaO supports is to promote EtOH dehydrogenation to acetaldehyde (AcAl), accelerating aldol condensation rates through the increase in AcAl pressure. The Cu allows for such H-transfers to be mediated by H_2, which the catalysts cannot activate in its absence. This may also allow for control over alcohol-aldehyde equilibria which strongly depends on the reaction pressure and the partial pressure of H_2 in the reactor feed. In previous studies using similar catalysts, elevated pressures are always used though the impacts of doing so on this dehydrogenation behavior have not yet been clarified.[21,25,26]

The effect of varying system pressure on ethanol coupling over Cu/AlMgO in a H_2 atmosphere (12 mol% ethanol) was examined between 1 and 31 bar total pressure at 325°C (Figure 4.5). At atmospheric pressure the catalyst produced predominantly AcAl at 17.9% conversion with a selectivity of 56C%, while the desired coupling products (C_{4+} alcohols and aldehydes) were produced with only 22.1% selectivity. Increasing the pressure to 10 bar doubled the selectivity to desired products (to 43.1%) while the AcAl selectivity was halved (to 26.7%) and the conversion was increased slightly (to 21.1%). Further increasing the pressure to 24 and then 31 bar had a negligible impact on conversion (to 19.5 and 19.7%, respectively) while the desired product selectivity increased (to 44.5 and 49.2%, respectively) and the selectivity to AcAl decreased (to 14.9 and 12.8%, respectively). The fairly constant conversion observed over the entire pressure range is due to the simultaneous decrease in the yield of AcAl (10.1 to 2.5%) and increase in the yield of all other products (7.9 to 17.2%). The former is likely related to ethanol dehydrogenation equilibrium, as will be discussed in further detail, while the latter is likely related to the increased catalyst surface coverages of reactants at elevated pressures.

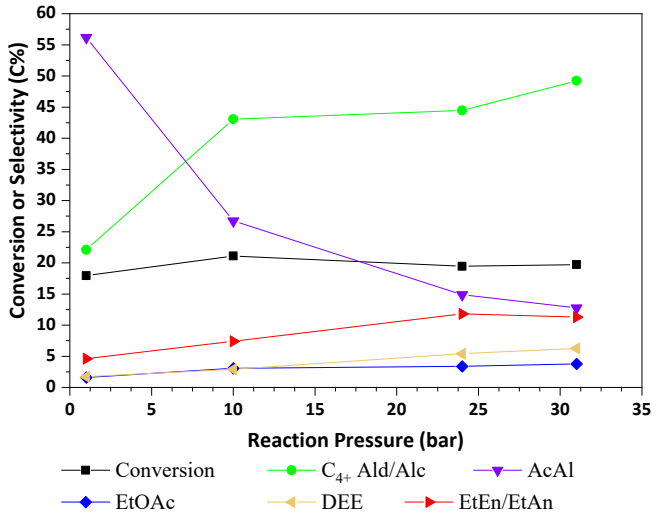

Figure 4.5 | **Ethanol conversion over Cu/AlMgO at total pressures of 1, 10, 24, and 31 bar.** Conditions: 325°C, 225 mg catalyst, 10 μL min^{-1} ethanol, 30 mL min^{-1} H_2. C_{4+} Ald/Alc= C_{4+} aldehydes and alcohols (desired products), AcAl=acetaldehyde, EtOAc=ethyl acetate, DEE=diethyl ether, EtEn/EtAn=ethylene and ethane.

EtOH-AcAl equilibrium can be modeled using tabulated thermodynamic data[27] to provide further insight into the effects of changing the reaction pressure (Table S4.1). With a 12 mol% EtOH/H_2 feed at 325°C, the equilibrium molar ratio of AcAl to EtOH decreases (1.22, 0.11, 0.06, 0.04) as the system pressure increases (1, 20, 24, 31 bar). At atmospheric pressure, the experimental ratio is far below equilibrium (0.12 versus 1.22), though the equilibrium ratio is approached at higher pressures (0.03 versus 0.04 at 31 bar). While the mole fraction of AcAl therefore decreases as pressure increases, the partial pressure of AcAl still increases since the total pressure of the system does as well. The equilibrium pressure of AcAl therefore increases over this range (6.4, 13.4, 14.5, 14.7 kPa), which asymptotically approaches ~15 kPa upon further increases in pressure. Reaction rates which depend on AcAl partial pressures, such as aldolization, are therefore expected to improve with increases in the reaction pressure, especially between 1 and 15 bar. Catalyst surface coverages are also expected to follow an asymptotic trend as full saturation is approached, however, thus the effect of pressure is too complex to establish a clear causal link

between AcAl pressure and condensation rates. The equilibrium pressure of AcAl can be further increased by operating with an inert gas co-feed. Operating at 31 bar with Ar instead of H_2 increases the equilibrium AcAl pressure by over an order of magnitude from 14.7 to 151.7 kPa while the ratio of AcAl:EtOH increases from 0.04 to 0.72. Experimentally, operating with an Ar feed produced an AcAl:EtOH ratio of 0.07, far below equilibrium. This was accompanied by a large increase in conversion from 19.7 to 32.5 %. The main product was ethyl acetate (34.6 % selectivity), which is produced at much lower levels with a H_2 atmosphere (0.7 versus 11.2 % yield). Simultaneously, the yield of desired products decreased by about 40% (9.7 to 5.7 %). This high esterification selectivity has also been noted previously in batch reactions of Cu-doped AlMgxOy in air.[22] High H_2 pressures therefore inhibit esterification, which is known to be catalyzed by Cu sites via the Tischenko reaction.[28,29] Whether this is caused by alteration of the Cu oxidation state or competitive adsorption between alcohols and aldehydes with H_2 is uncertain. Altogether, these results provide a general understanding of how the gaseous environment can be manipulated to promote Guerbet coupling when using catalysts capable of mediating EtOH dehydrogenation through H_2. Increasing pressure promotes condensation while favorably decreasing the AcAl selectivity. These effects are strongest up to ~15 bar, above which increasing pressure has a minimal impact, in qualitative agreement with thermodynamic calculations. Such calculations are expected to be particularly useful in guiding the use of catalysts, which are more active for dehydrogenation than the Cu/AlMgO-P used here, since the activity was not sufficient to achieve equilibrium under most conditions.

Based on these findings, the catalysts synthesized in this study were compared in a H_2 environment at 32 bar total pressure. The major products observed and generalized recation pathways for EtOH are summarized in Figure 4.6. Stable performance was observed for all

catalysts between 10 and 30 h time-on-stream (TOS). Conversions and selectivities for Cu-doped catalysts are reported in Figure 4.7. Cu/AlMgO and Cu/AlMgO-P showed similar activities with conversions of 19.7 and 23.3 %, respectively. These catalysts were more active than their Ca counterparts with conversions of 8.7 and 8.4 % for Cu/AlCaO for Cu/AlCaO-P, respectively. At these conditions, Cu/AlMgO and Cu/AlMgO-P were also more selective to desired condensation products (54.8 and 48.8 %, respectively) than Cu/AlCaO and Cu/AlCaO-P (21.8 and 23.5 %, respectively). The Ca catalysts were more selective to AcAl at these conditions, though the AcAl yield was similar for all catalysts. As noted earlier, AcAl is produced at nearly equilibrium levels on these catalysts, thus it may be more informative to compare product selectivities with the omission of AcAl. In this case, Mg catalysts remain more selective to C_{4+} aldehydes and alcohols than the Ca catalysts with adjusted selectivities of 62.5% and 54.0 % for Cu/AlMgO and Cu/AlMgO-P, respectively, *versus* 35.7 % and 38.5 % for Cu/AlCaO and Cu/AlCaO-P, respectively. These comparisons are notably made at different conversions, though it is unlikely that Ca catalysts will show improved adjusted selectivities upon increasing conversion.

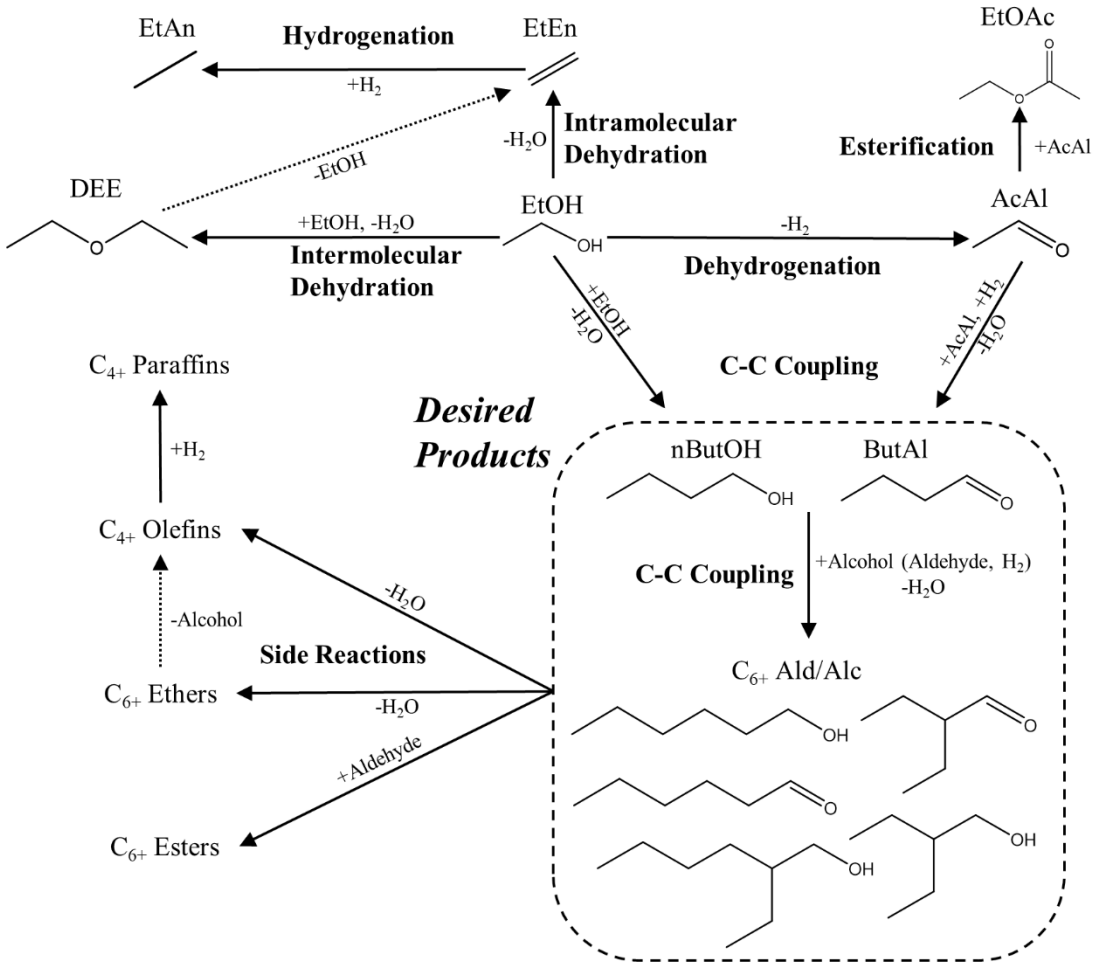

Figure 4.6 | **Major products and generalized reaction pathways involved in the high-pressure conversion of ethanol over mixed-metal oxides doped with transition metals.** Ethanol coupling may occur directly or through an aldehyde intermediate. Side-reactions include intramolecular dehydration to olefins, intermolecular dehydration to ethers, and esterification to esters. Paraffins can also be formed from olefin hydrogenation.

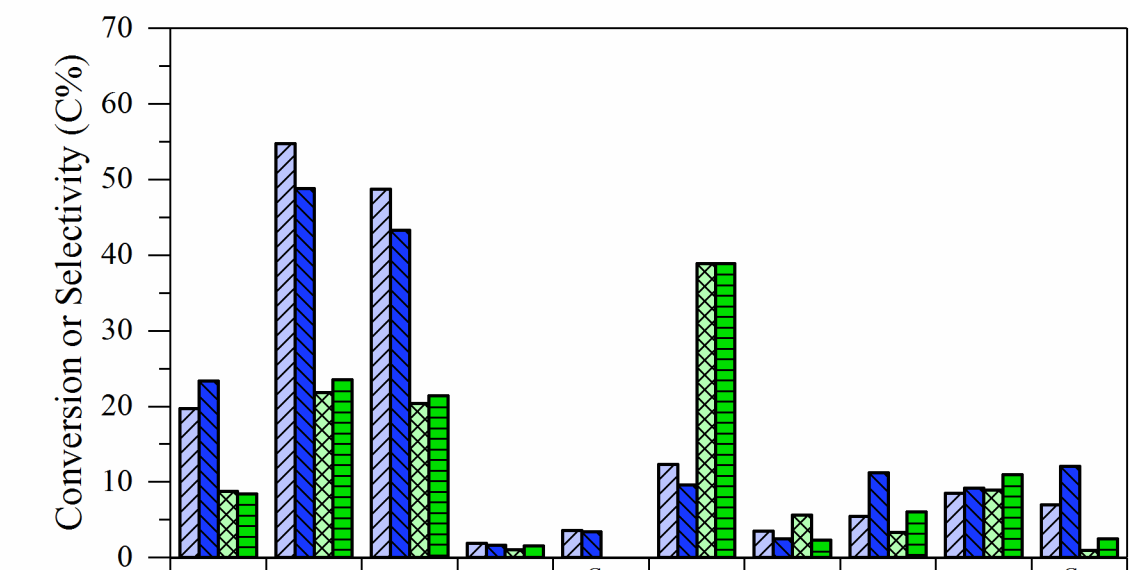

	Conv.	Desired	nButOH	ButAl	C_{6+} Ald/Alc	AcAl	EtOAc	DEE	EtEn/An	C_{4+} AlkEn/An
Cu/AlMgO	19.7	54.8	48.7	1.9	3.6	12.4	3.5	5.5	8.5	7.0
Cu/AlMgO-P	23.3	48.8	43.3	1.6	3.4	9.6	2.5	11.2	9.1	12.1
Cu/AlCaO	8.7	21.8	20.4	1.1	0.0	38.9	5.6	3.4	8.9	0.9
Cu/AlCaO-P	8.4	23.5	21.4	1.5	0.0	38.9	2.3	6.0	11.0	2.5

Figure 4.7 | **Conversion and selectivities to major species in ethanol conversion over Cu-doped catalysts**. Conditions: 325°C, 225 mg catalyst, 10 μL min^{-1} ethanol, 30 mL min^{-1} H_2, 32 bar total pressure. nButOH=n-butanol, ButAl=butyraldehyde, Ald/Alc=aldehydes and alcohols, AcAl=acetaldehyde, EtOAc=ethyl acetate, DEE=diethyl ether, EtEn/An=ethylene and ethane, AlkEn/An=alkenes and alkanes.

In the absence of Cu, lower activities were observed with AlMgO and AlMgO-P achieving only 7.1 and 11.1 % conversion, respectively and AlCaO and AlCaO-P demonstrating essentially no activity with ~0.2 % conversion (Figure S4.3). The particularly low activities of the Cu-free Ca catalysts are consistent with their low numbers of acid and base sites compared to the Mg catalysts, as measured by TPD. Upon Cu addition, the AcAl yield increased by 10-15 times for the Mg catalysts and 70-75 times for the Ca catalysts, consistent with the observation by Gines *et al.* that EtOH dehydrogenation rate over K-Mg_5CeO_x at atmospheric pressure increased by nearly two orders of magnitude upon addition of 7 wt% Cu, allowing for equilibration to occur at longer contact times.[20] The desired product yield also increased by 2-5 times for the Mg catalysts and 14-30 times for the Ca catalysts upon Cu addition. These increases may be due to either (1) the

increase in AcAl pressures resulting from Cu-catalyzed EtOH dehydrogenation, (2) the addition of sites which enable H-transfer between the support and the gas-phase, or (3) the addition of Cu sites capable of catalyzing condensation reactions independently from the support. The first would be true if aldolization is a key condensation pathway. The second has notably been proposed by Gines *et al.* to explain the improved condensation rates with Cu addition to K-Mg_5CeO_x at atmospheric pressure with an inert co-feed gas.[20] The third has been noted to occur over Cu, though it is typically observed alongside substantial esterification.[29] The role that Cu plays is dependent on the mechanism of alcohol condensation, which remains debated in the literature as discussed prior in Section 3.9. The two general mechanisms proposed for alcohol condensation on heterogeneous catalysts are the Guerbet coupling reaction (which formally involves aldolization with aldehyde intermediates) and direct alcohol condensation (wherein aldehydes do not serve as key intermediates). An aldehyde-mediated route must play some role for the Cu/AlMgO and Cu/AlCaO catalysts based on the butyraldehyde:*n*-butanol ratios observed. If only direct condensation mechanisms are present, butyraldehyde can only be produced via *n*-butanol dehydrogenation, thus the butyraldehyde:*n*-butanol ratio must be less than or equal to the equilibrium ratio (estimated to be 0.034 at these conditions). The calculated ratio is higher than this for all catalysts (between 0.037 and 0.071), however, thus an alternate condensation mechanism must be present to explain butyraldehyde formation. Additionally, the improved condensation yields measured upon Cu addition are more mechanistically consistent with promotion of an aldehyde-mediated route than a direct condensation route. The possibility that both direct and indirect condensation mechanisms are active cannot be discounted, however, especially for Cu/AlMgO catalysts. Given that AlCaO and AlCaO-P are essentially inactive before Cu addition, the indirect route is also most likely dominant for Cu/AlCaO catalysts.

Other than AcAl, the main side-products observed with Cu-doped catalysts were ethylene/ethane (8.5-11.0% selectivity), C_{4+} alkenes/alkanes (0.9-12.1%), diethyl ether (3.4-11.2%), and ethyl acetate (2.3-5.6%). In the absence of Cu, diethyl ether is the dominant side-product on Mg catalysts with ~50 % selectivity. The higher yield of diethyl ether *versus* ethylene has been commonly observed over $AlMg_xO_y$ catalysts.[5,30] Diethyl ether production on Mg catalysts is greatly inhibited upon Cu addition, thus dispersed Cu particles may cover sites which promote intramolecular dehydration. Another possibility is that new sites are formed upon Cu addition which promote dehydration of diethyl ether to ethylene, since the yield of ethylene/ethane increase upon Cu addition (with the latter forming via ethylene hydrogenation). Both possibilities are consistent with the simultaneous decrease in basicity (thought to catalyze bimolecular dehydration) and increase in acidity (thought to catalyze intramolecular dehydration) upon Cu addition to Mg catalysts, as measured by TPD.[5] Ethyl acetate is also absent on Cu-free catalysts, consistent with the aforementioned expectation that esterification is promoted via Cu sites as is known in the literature.[28,29]

Previous studies on EtOH to ethene, diethyl ether, AcAl and/or ethyl acetate pointed out that the support porosity played an important role to give the highest selectivity to the targeted product.[14,18,19] Therein the synthesis method was important because it influenced acidity/basicity, and the formed porosity influenced copper particle size and the oxidation state of copper, properties that were fine-tuned on a porous support. Application of the emulsion-mediated method altered the textural properties of the catalysts and improved the overall catalytic performance. However, these changes did not reflect improvement in the Guerbet reaction as occurred before, as it was mostly influenced by reaction pressure and the presence of copper. AlCaO catalysts were employed to increase basicity and decrease acidity relative to AlMgO in order to promote

condensation reactions while reducing EtOH dehydration. Though dehydration decreased, the *n*-butanol yield also decreased possibly because CaO is prone to carbonation in ambient air. These carbonates are highly stable and require high temperatures to decompose. For instance, Granados et al. found that amorphous carbonates formed on CaO due to air exposure could not be removed until above 700°C are often required to remove adsorbed CO_2 and moisture to produce an active catalyst.[31] These catalysts were therefore determined to be generally inferior to their Mg counterparts.

To achieve higher conversions, EtOH coupling over Cu/AlMgO-P was examined as a function of WHSV with a single catalyst bed (675 mg) as shown in Figure 4.8. Initially a WHSV of 2.10 h^{-1} was used for a direct comparison with the previous studies using lower catalyst loadings (225 mg) in order to test for transport limitations. The higher catalyst loading lead to a negligible increase in conversion (22.9 to 23.3%) while the selectivity to *n*-butanol decreased (43.3 to 35.8%) and the diethyl ether selectivity increased (11.2 to 19.7%). These selectivity shifts are more likely to result from catalyst batch deviations than transport limitations. In addition to these experimental results, calculations provided in the supplemental information suggest that such limitations are not present. Decreasing the WHSV to 1.40 h^{-1} and then to 0.70 h^{-1} increased conversion to 26.1 and 32.8%, respectively. These increases are lower than expected assuming that EtOH conversion can be approximated using a power law rate expression with an EtOH order of two or lower. First, second, and even third order rate expressions would predict EtOH conversion to increase by 140%, 110% and 90%, respectively, when decreasing the WHSV from 2.10 to 0.70 h^{-1}, though the conversion increased by only 40%. This therefore suggests either severe irreversible deactivation or reversible inhibition by strongly adsorbing products. Irreversible deactivation is not responsible for these trends since returning to the original WHSV showed that the catalytic activity had not

appreciably changed over 75 h. These trends are more therefore more likely due to reversible blocking of sites by species produced during the reaction, limiting EtOH adsorption either via competitive adsorption or reversible site alteration. Previous researchers have shown that water inhibits EtOH coupling over decomposed $Cu_xMg_yAlO_z$ hydrotalcites in batch mode, presumably via the conversion of Lewis basic O^{2-} sites into weaker Brønsted OH^- sites.[25] Minimal deviations in product distribution were observed over this WHSV range, which suggests that all reactions were inhibited to similar extents. Heavier condensation products (*i.e.* C_{6+} alcohols and aldehydes) increased to a small extent over this range as condensation reactions between butanol and EtOH became more prevalent, though conversions remained too low for significant production of these species. The AcAl yield also remained fairly constant over this WHSV range, a reflection of the fact that it is likely produced at near equilibrium levels.

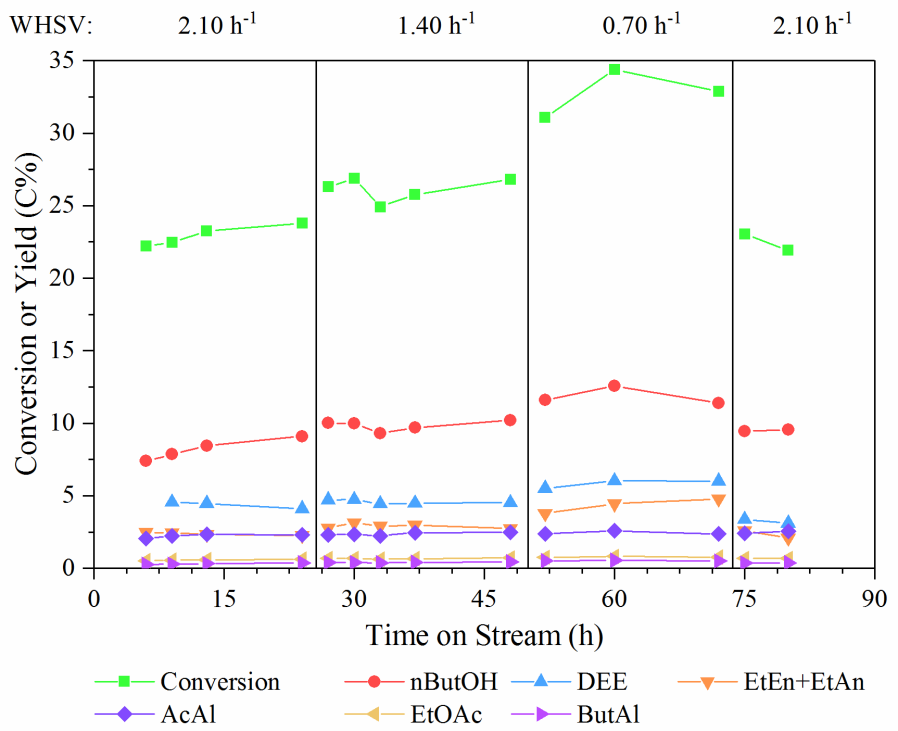

Figure 4.8 | **Conversions and yields in the conversion of ethanol over Cu/AlMgO-P at varying WHSV.** Conditions: 325°C, 675 mg catalyst, 10-30 μL min^{-1} ethanol, 30-90 mL min^{-1} H_2, 32 bar total pressure.

To examine the effect of water on the reaction, feeds containing water at levels between 0 and 11.3 wt.% were examined at a fixed WHSV of 2.10 h^{-1} (with respect to EtOH) as shown in Figure 4.9. An inhibiting effect was observed with 4.1 wt.% water in the feed, decreasing the conversion from 22.7 to 18.5%. This water content notably closely matches the amount produced with a neat EtOH feed at this WHSV. Further increasing the water content to 11.3 wt.% further decreased the conversion to 14.6%. Returning to the original conditions did not fully restore catalytic activity, thus irreversible deactivation may occur with high water contents (>4 wt.%) beyond those present in the WHSV experiments where the effects of water on catalytic activity were reversible. To more quantifiably assess the inhibiting role of water, a rate order for water was approximated to be -0.23 (Figure S4.4) from a log-log plot of the bed-averaged rate of ethanol conversion and water pressure. This does not rigorously account for the complex functional dependence of reaction rates on water as a function of conversion (which will be discussed in greater depth in Chapter 6), but does suggest that inhibition by water is not likely sufficiently strong to fully account for all inhibition observed with increasing conversion. Other species are therefore likely inhibiting EtOH conversion as well. Carboxylate species derived from AcAl or organic acids are also known to poison base sites.[32,33] While organic acids could not be detected in this study, they may be formed at low levels via ester hydrolysis.[34] The combination of water and strongly-binding species produced either from EtOH coupling or through side-reactions are therefore likely responsible for decreasing catalytic activity at elevated conversions, which can make EtOH coupling at high conversions difficult to obtain with these catalysts.

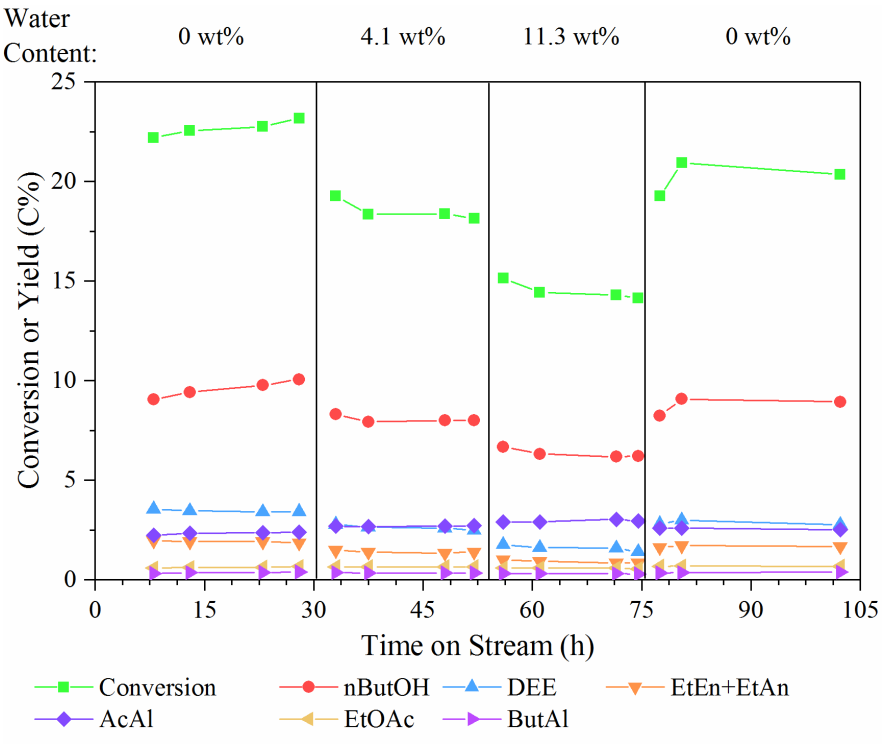

Figure 4.9 | **Ethanol conversion over Cu/AlMgO-P with varying amounts of water added to the ethanol feed**. Conditions: 325°C, 675 mg catalyst, 30-33 μL min^{-1} liquid feed (0-11.3 wt% water in ethanol), 86-90 mL min^{-1} H_2, 32 bar total pressure.

4.5 Conclusions

AlMgO and AlCaO mixed oxides derived from hydrotalcite have been shown to be effective supports for the preparation of well-dispersed Cu catalysts with various concentrations of metal, acid, and base sites, as demonstrated by the measurements of NH_3- and CO_2-TPD and infrared with pyridine as probe molecule. Application of the emulsion-mediated preparation method altered the textural properties of the catalysts and improved the exposure of Cu on the surface of the supports. The beneficial impact of operating at elevated H_2 pressures with Cu/AlMgO (increased yield and selectivity to desired products) has been shown experimentally and linked to the shifting EtOH dehydrogenation equilibrium, which leads to undesirable high AcAl selectivities at low pressures. At elevated pressures, Mg catalysts without Cu demonstrate moderate activity for EtOH conversion though Ca catalysts are essentially inactive. The addition

of Cu promoted dehydrogenation for all catalysts and thereby increased the activity for EtOH conversion. The selectivity to higher alcohols and aldehydes increased from 30.7 to 54.8% upon addition of Cu to AlMgO while the conversion increased from 7.1 to 19.7%. Diethyl ether formation was suppressed, shifting unfavorable dehydration toward olefin and paraffin production. The porosity had a small effect on the conversion of EtOH with the observed trends correlating more clearly with surface area changes. Increasing space time by three times increased EtOH conversion over Cu/AlMgO-P by a factor of only 1.4 times, which is attributed to inhibition by species produced in the reaction.

4.6 References

1 Petrolini[†,] D. D., Eagan[†,] N., Ball, M. R., Burt, S. P., Hermans, I., Huber, G. W., Dumesic, J. A. & Martins, L. Ethanol condensation at elevated pressure over copper on AlMgO and AlCaO porous mixed-oxide supports. *Catal. Sci. Technol.* **9**, 2032-2042, (2019).

2 Kozlowski, J. T. & Davis, R. J. Heterogeneous catalysts for the Guerbet coupling of alcohols. *ACS Catal.* **3**, 1588-1600, (2013).

3 Ordóñez, S., Díaz, E., León, M. & Faba, L. Hydrotalcite-derived mixed oxides as catalysts for different C–C bond formation reactions from bioorganic materials. *Catal. Today* **167**, 71-76, (2011).

4 Ramasamy, K. K., Gray, M., Job, H., Smith, C. & Wang, Y. Tunable catalytic properties of bi-functional mixed oxides in ethanol conversion to high value compounds. *Catal. Today* **269**, 82-87, (2016).

5 Di Cosimo, J., Dıez, V., Xu, M., Iglesia, E. & Apesteguıa, C. Structure and surface and catalytic properties of Mg-Al basic oxides. *J. Catal.* **178**, 499-510, (1998).

6 Martins, L., Rosa, M. A. A., Pulcinelli, S. H. & Santilli, C. V. Preparation of hierarchically structured porous aluminas by a dual soft template method. *Micropor. Mesopor. Mater.* **132**, 268-275, (2010).

7 Petrolini, D. D., Pulcinelli, S. H., Santilli, C. V. & Martins, L. Textured macro-and mesoporous alumina samples designed in the presence of different surfactant types. *J. Sol-Gel Sci. Technol.* **71**, 9-15, (2014).

8 Petrolini, D. D., Urquieta-González, E. A., Pulcinelli, S. H., Santilli, C. V. & Martins, L. Emulsion-mediated synthesis of hierarchical mesoporous-macroporous Al-Mg hydrotalcites. *Micropor. Mesopor. Mater.* **240**, 149-158, (2017).

9 Colombo, P. In praise of pores. *Science* **322**, 381-383, (2008).

10 Ohji, T. & Fukushima, M. Macro-porous ceramics: processing and properties. *Int. Mater. Rev.* **57**, 115-131, (2012).

11 Hammel, E., Ighodaro, O.-R. & Okoli, O. Processing and properties of advanced porous ceramics: An application based review. *Ceram. Int.* **40**, 15351-15370, (2014).

12 Fukushima, M., Yoshizawa, Y. i. & Ohji, T. Macroporous ceramics by gelation–freezing route using gelatin. *Adv. Eng. Mater.* **16**, 607-620, (2014).

13 Liu, B., Shioyama, H., Akita, T. & Xu, Q. Metal-organic framework as a template for porous carbon synthesis. *J. Am. Chem. Soc.* **130**, 5390-5391, (2008).

14 Petrolini, D. D., da Silva Neto, A. V., Urquieta-González, E. A., Pulcinelli, S. H., Santilli, C. V. & Martins, L. Catalytic performance of texturally improved Al–Mg mixed oxides derived from emulsion-synthesized hydrotalcites. *RSC Advances* **8**, 6039-6046, (2018).

15 Martins, L., Cardoso, D., Hammer, P., Garetto, T., Pulcinelli, S. H. & Santilli, C. V. Efficiency of ethanol conversion induced by controlled modification of pore structure and acidic properties of alumina catalysts. *Appl. Catal. A-Gen.* **398**, 59-65, (2011).

16 Cassinelli, W. H., Martins, L., Passos, A. R., Pulcinelli, S. H., Santilli, C. V., Rochet, A. & Briois, V. Multivariate curve resolution analysis applied to time-resolved synchrotron X-ray absorption spectroscopy monitoring of the activation of copper alumina catalyst. *Catal. Today* **229**, 114-122, (2014).

17 Passos, A. R., Martins, L., Pulcinelli, S. H., Santilli, C. V. & Briois, V. Correlation of Sol–Gel Alumina-Supported Cobalt Catalyst Processing to Cobalt Speciation, Ethanol Steam Reforming Activity, and Stability. *ChemCatChem* **9**, 3918-3929, (2017).

18 Cassinelli, W. H., Martins, L., Passos, A. R., Pulcinelli, S. H., Rochet, A., Briois, V. & Santilli, C. V. Correlation between structural and catalytic properties of copper supported on porous alumina for the ethanol dehydrogenation reaction. *ChemCatChem* **7**, 1668-1677, (2015).

19 Cassinelli, W. H., Martins, L., Magnani, M., Pulcinelli, S. H., Briois, V. & Santilli, C. V. Time-resolved XAS/MS/Raman monitoring of mutual copper self-reduction and ethanol dehydrogenation reactions. *RSC Advances* **6**, 20453-20457, (2016).

20 Gines, M. J. & Iglesia, E. Bifunctional condensation reactions of alcohols on basic oxides modified by copper and potassium. *J. Catal.* **176**, 155-172, (1998).

21 Pang, J., Zheng, M., He, L., Li, L., Pan, X., Wang, A., Wang, X. & Zhang, T. Upgrading ethanol to n-butanol over highly dispersed Ni–MgAlO catalysts. *J. Catal.* **344**, 184-193, (2016).

22 Sun, Z., Couto Vasconcelos, A. s., Bottari, G., Stuart, M. C., Bonura, G., Cannilla, C., Frusteri, F. & Barta, K. Efficient catalytic conversion of ethanol to 1-butanol via the Guerbet reaction over copper-and nickel-doped porous. *ACS Sustain. Chem. Eng.* **5**, 1738-1746, (2016).

23 Lercher, J. Acid-base properties of Al_2O_3/MgO oxides, II. Infrared study of adsorption of pyridine. *React. Kinet. Catal. Lett.* **20**, 409-413, (1982).

24 Prescott, H. A., Li, Z.-J., Kemnitz, E., Trunschke, A., Deutsch, J., Lieske, H. & Auroux, A. Application of calcined Mg–Al hydrotalcites for Michael additions: an investigation of catalytic activity and acid–base properties. *J. Catal.* **234**, 119-130, (2005).

25 Marcu, I.-C., Tichit, D., Fajula, F. & Tanchoux, N. Catalytic valorization of bioethanol over Cu-Mg-Al mixed oxide catalysts. *Catal. Today* **147**, 231-238, (2009).

26 Antolín, R. A., Yagüe, J. L. S., Canós, A. C., Domine, M. E., Barrero, F. V. & Vidal, F. A. L. D. G. Method for obtaining higher alcohols. US 9,475,741 B2 (2016).

27 Yaws, C. L. *Chemical properties handbook*. (McGraw-Hill, 1999).

28 Neurock, M., Tao, Z., Chemburkar, A., Hibbitts, D. D. & Iglesia, E. Theoretical insights into the sites and mechanisms for base catalyzed esterification and aldol condensation reactions over Cu. *Faraday Discuss.* **197**, 59-86, (2017).

29 Ro, I., Liu, Y., Ball, M. R., Jackson, D. H. K., Chada, J. P., Sener, C., Kuech, T. F., Madon, R. J., Huber, G. W. & Dumesic, J. A. Role of the Cu-ZrO2 Interfacial Sites for Conversion of Ethanol to Ethyl Acetate and Synthesis of Methanol from CO2 and H2. *ACS Catal.* **6**, 7040-7050, (2016).

30 Ramasamy, K. K., Gray, M., Job, H., Santosa, D., Li, X. S., Devaraj, A., Karkamkar, A. & Wang, Y. Role of calcination temperature on the hydrotalcite derived MgO–Al_2O_3 in converting ethanol to butanol. *Top. Catal.* **59**, 46-54, (2016).

31 Granados, M. L., Poves, M. Z., Alonso, D. M., Mariscal, R., Galisteo, F. C., Moreno-Tost, R., Santamaría, J. & Fierro, J. Biodiesel from sunflower oil by using activated calcium oxide. *Applied Catalysis B: Environmental* **73**, 317-326, (2007).

32 Carvalho, D. L., Borges, L. E., Appel, L. G., de la Piscina, P. R. & Homs, N. In situ infrared spectroscopic study of the reaction pathway of the direct synthesis of n-butanol from ethanol over MgAl mixed-oxide catalysts. *Catal. Today* **213**, 115-121, (2013).

33 Shen, W., Tompsett, G. A., Xing, R., Conner Jr, W. C. & Huber, G. W. Vapor phase butanal self-condensation over unsupported and supported alkaline earth metal oxides. *J. Catal.* **286**, 248-259, (2012).

34 Gabriëls, D., Hernández, W. Y., Sels, B., Van Der Voort, P. & Verberckmoes, A. Review of catalytic systems and thermodynamics for the Guerbet condensation reaction and challenges for biomass valorization. *Catal. Sci. Technol.* **5**, 3876-3902, (2015).

4.7 Supplemental Information

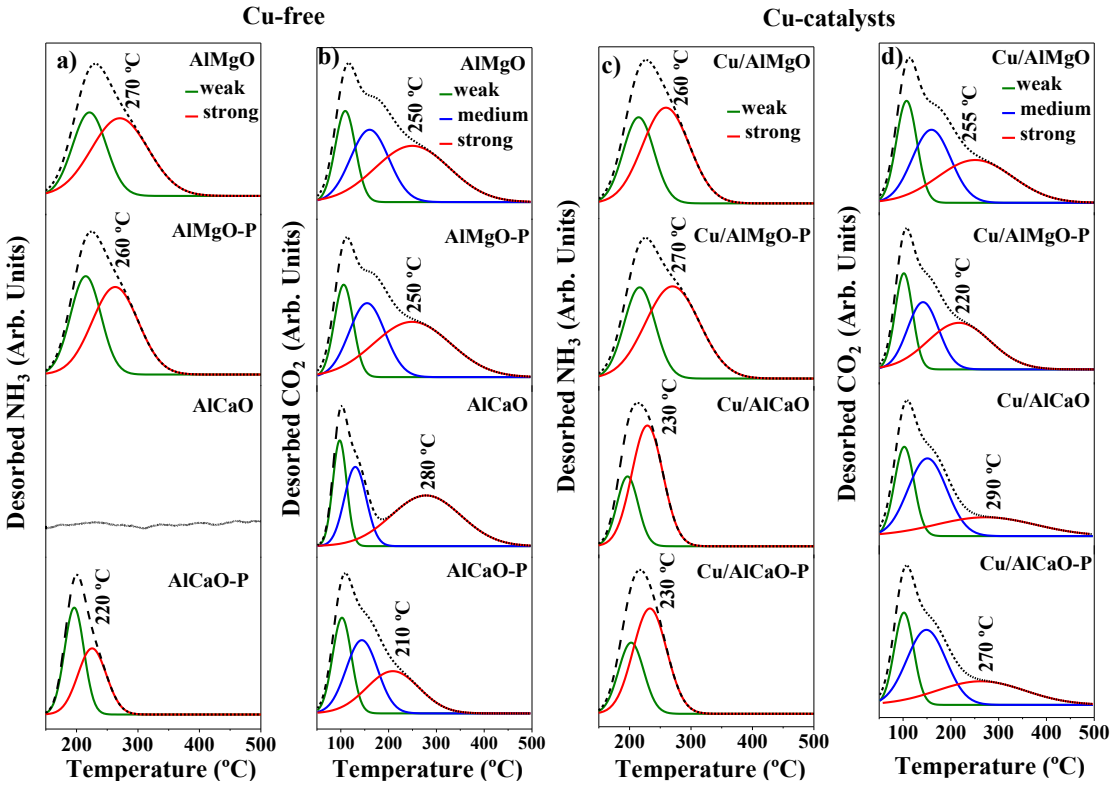

Figure S4.1 | **Deconvolutions of NH_3-TPD profiles and CO_2-TPD profiles of Cu-free and Cu-catalysts. a |** Cu-free NH_3-TPD. **b |** Cu-free CO_2-TPD. **c |** Cu-doped NH_3-TPD. **d |** Cu-doped CO_2-TPD.

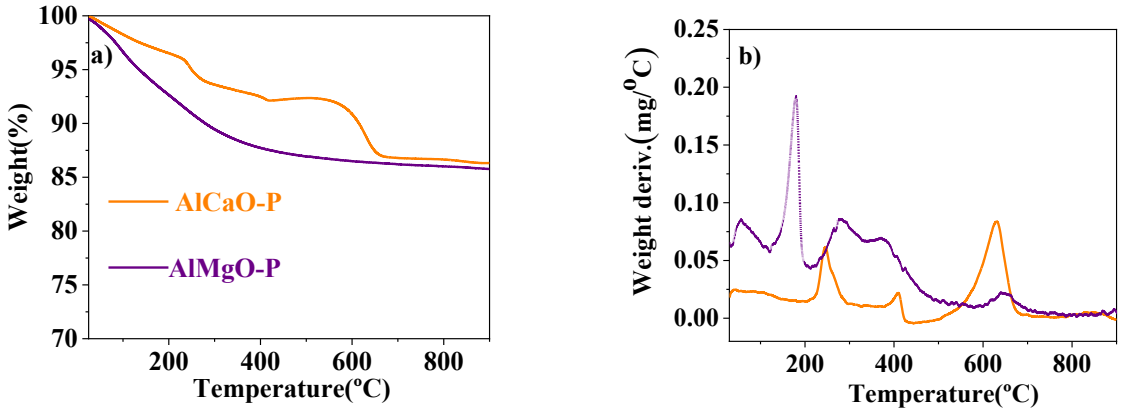

Figure S4.2 | **Thermogravimetric analysis of AlCaO-P and AlMgO-P catalysts. a |** Thermogravimetric curves. **b |** Weight derivatives. Materials were calcined and exposed to open air prior to analysis.

Table S4.1 | **Ethanol (EtOH) dehydrogenation to acetaldehyde (AcAl) equilibrium as a function of pressure compared to experiment.** y_{AcAl} is the molar concentration of AcAl in the gas. Temperature = 325°C, EtOH feed concentration = 12.3 vol%, balance H_2 or Ar.

Pressure (bar)	**1-H_2**	**10-H_2**	**24-H_2**	**31-H_2**	**31-Ar**
Equilibrium					
AcAl yield (C%)	55.0	11.1	4.9	3.9	42.0
P_{AcAl} (kPa)	6.40	13.43	14.49	14.67	151.7
y_{AcAl} (mol%)	6.3	1.3	0.6	0.5	4.9
AcAl:EtOH (mol/mol)	1.22	0.13	0.05	0.04	0.72
Experiment					
AcAl yield (C%)	10.1	5.6	2.9	2.5	4.4
P_{AcAl} (kPa)	1.2	6.9	8.4	9.7	17.0
y_{AcAl} (mol%)	1.2	0.7	0.4	0.3	0.5
AcAl:EtOH (mol/mol)	0.12	0.07	0.04	0.03	0.07

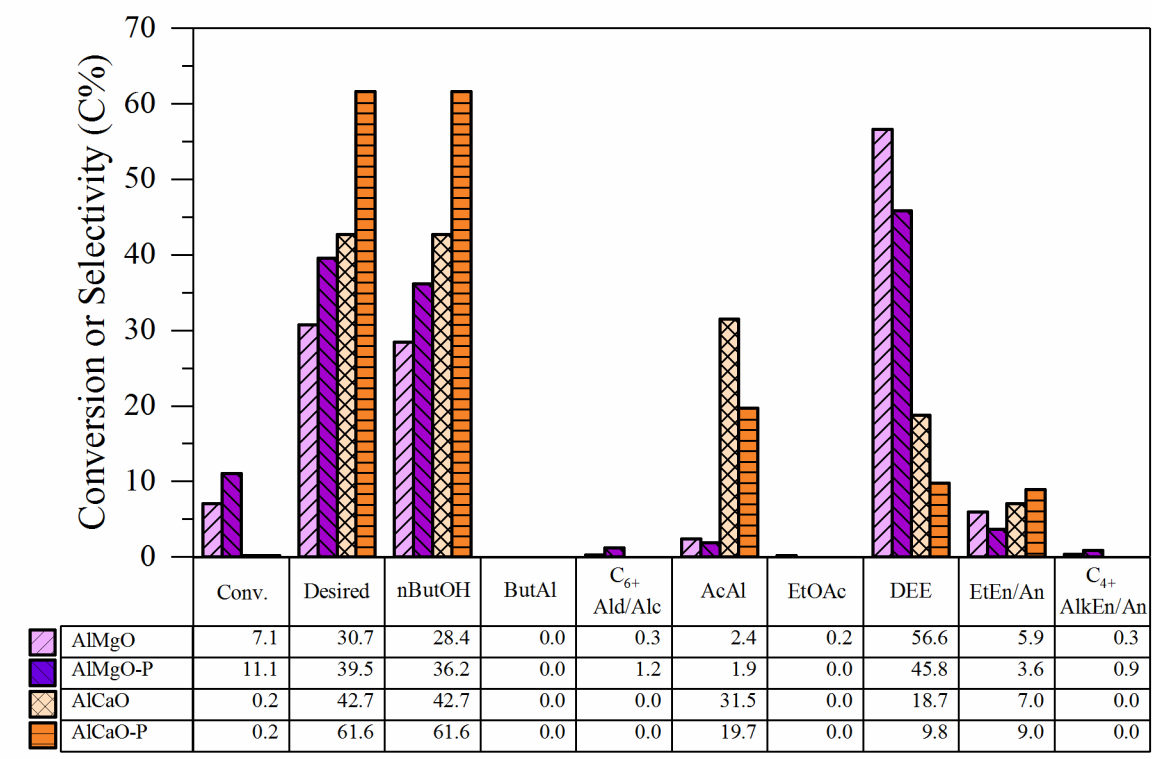

	Conv.	Desired	nButOH	ButAl	C_{6+} Ald/Alc	AcAl	EtOAc	DEE	EtEn/An	C_{4+} AlkEn/An
AlMgO	7.1	30.7	28.4	0.0	0.3	2.4	0.2	56.6	5.9	0.3
AlMgO-P	11.1	39.5	36.2	0.0	1.2	1.9	0.0	45.8	3.6	0.9
AlCaO	0.2	42.7	42.7	0.0	0.0	31.5	0.0	18.7	7.0	0.0
AlCaO-P	0.2	61.6	61.6	0.0	0.0	19.7	0.0	9.8	9.0	0.0

Figure S4.3 | **Conversion and selectivities to major species in ethanol conversion over Cu-free catalysts**. Conditions: 325°C, 225 mg catalyst, 10 µL min-1 ethanol, 30 mL min-1 H2, 32 bar total pressure. nButOH=n-butanol, ButAl=butyraldehyde, Ald/Alc=aldehydes and alcohols, AcAl=acetaldehyde, EtOAc=ethyl acetate, DEE=diethyl ether, EtEn/An=ethylene and ethane, AlkEn/An=alkenes and alkanes.

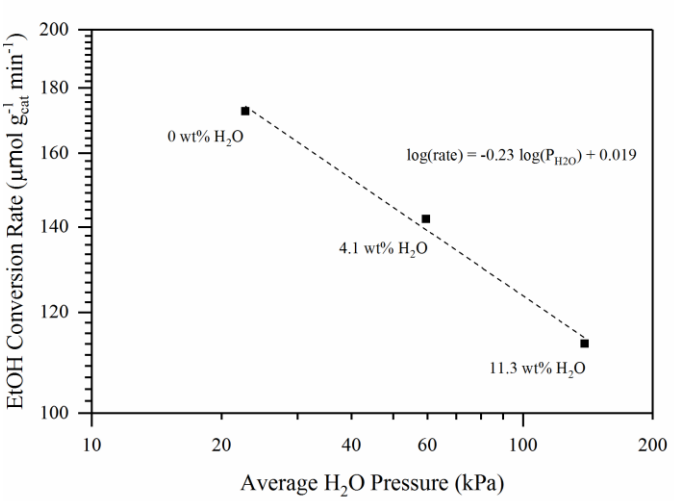

Figure S4.4 | **Ethanol conversion rate vs. the average partial pressure of water across the catalyst bed calculated based upon the observed products and assumed reaction stoichiometries.** The log-log plot provides a rate order for water of -0.23 with respect to ethanol conversion.

Transport Calculations:

The possibility that reaction rates were limited by heat or mass transport was examined through evaluation of several transport criteria which must be satisfied to ensure that this is not the case. These criteria have been notably applied and discussed by Shabaker et al. The criteria considered and their evaluations are shown below. Descriptions and approximations for each parameter are also provided. Ethanol condensation to 1-butanol and water was assumed to be the main reaction when one was required for estimation purposes, such as for the absolute heat of reaction. For parameters which were not measured, worst-case approximations were assumed (e.g. a high activation barrier, low particle thermal conductivity, high rate order). **In all cases, the tests were satisfied by multiple orders of magnitude.**

J.W. Shabaker, R.R. Davda, G.W. Huber, R.D. Cortright, J.A. Dumesic, Aqueous-phase reforming of methanol and ethylene glycol over alumina-supported platinum catalysts, J. Catal. 215 (2003) 344-352.

Table S4.2 | **Transport limitation calculations for EtOH conversion over Cu/AlMgO.**

Test	**Equation**	**Evaluation**
Interphase heat transport	$\frac{q\,\mathscr{R} r_p}{h\,T_B} < 0.15\frac{R\,T_B}{E}$	$3.98 * 10^{-5} \ll 7.46 * 10^{-3}$
Intraparticle heat transport	$\frac{q\,\mathscr{R} r_p^2}{\lambda\,T_S} < 0.75\frac{R\,T_S}{E}$	$3.83 * 10^{-5} \ll 3.73 * 10^{-2}$
Interphase mass transport	$\frac{\mathscr{R} r_p^2}{C_b k_c} < \frac{0.15}{n}$	$3.28 * 10^{-8} \ll 7.50 * 10^{-2}$
Intraparticle mass transport	$\frac{\mathscr{R} r_p^2}{C_s D_{eff}} < 0.3$	$3.33 * 10^{-4} \ll 3.00 * 10^{-1}$

Parameter	**Definition**	**Approximate Value**
q	Absolute heat of reaction	$21{,}517\ J\ mol^{-1}\ ethanol$
$\mathscr{R}$	Volumetric reaction rate	$8.86\ mol\ m^{-3}\ s^{-1}$
r_p	Catalyst particle radius	$1.25 * 10^{-4}\ m$
R	Gas constant	$8.314\ J\ mol^{-1}K^{-1}$
T_B	Bulk temperature	$598\ K$
T_S	Catalyst surface temperature	$598\ K$
h	Heat transfer coefficient	$1000\ W\ m^{-2}K^{-1}$
E	Activation barrier	$100{,}000\ J\ mol^{-1}K^{-1}$
λ	Thermal conductivity of catalyst particle	$0.13\ W\ m^{-1}\ K^{-1}$
C_b	Bulk concentration of ethanol	$79.1\ mol\ ethanol\ m^{-3}$
C_s	Ethanol surface concentration	$79.1\ mol\ ethanol\ m^{-3}$
k_c	Surface-bulk mass transfer coefficient	$5.34 * 10^{-2}\ m\ s^{-1}$
n	Rate order	2
D_{eff}	Effective diffusivity	$5.25 * 10^{-6}\ m^2\ s^{-1}$

Chapter 5. Catalytic Synthesis of Distillate-Range Ethers and Olefins from Ethanol through Guerbet Coupling and Etherification

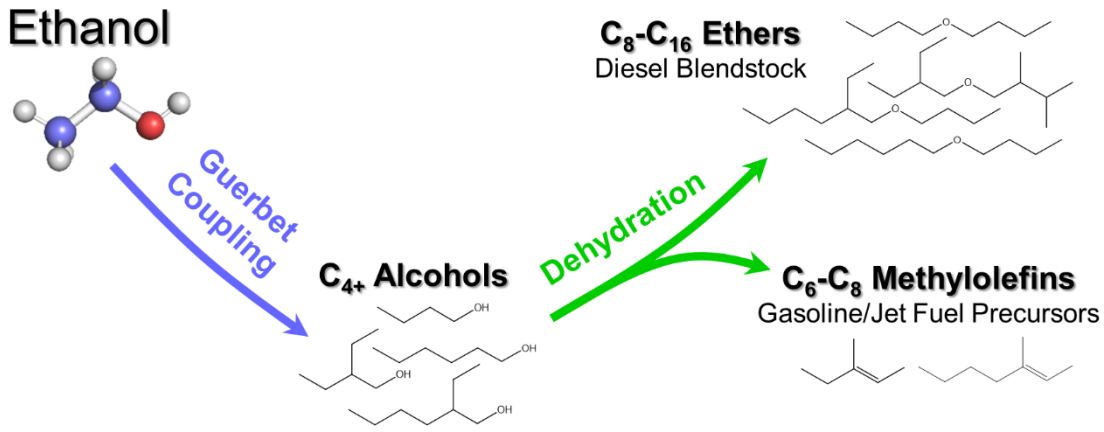

Figure 5.1 | **Catalytic conversion of ethanol to distillate-range ethers and olefins through sequential Guerbet coupling and dehydration.**[1] Chapter adapted from Ref 1.

5.2 Introduction

The Cu-doped mixed-oxide catalysts examined in the previous chapter showed clear selectivity and conversion challenges that make it difficult to use to oligomerization ethanol (EtOH) into the distillate range. As noted in Chapter 3, calcium hydroxyapatite (HAP) has also been proposed as a candidate for the efficient catalytic conversion of EtOH to higher alcohols.[2-7] While such catalytic systems generally appear to be less active, substantially higher selectivities above 80% are commonly observed. Such metrics often dominate the economic efficiencies of biomass valorization technologies,[8-10] thus HAP may be a more technologically promising system for EtOH oligomerization through Guerbet coupling. The potential of using these catalysts for distillate-range alcohol synthesis remains unclear, however, since Guerbet coupling is typically studied well below 50% conversion where C_4-C_6 alcohols are the major products. Higher conversions require low space velocities or high temperatures which promote dehydration to olefins, limiting alcohol selectivities.[11] It may therefore be challenging to use EtOH

oligomerization via Guerbet coupling to directly produce distillate-range alcohols. If selective coupling can only be performed at low conversions, additional catalytic steps may therefore be required to convert EtOH to distillate fuels through Guerbet coupling.

One potential method to valorize Guerbet coupling products is etherification. Ethers possess high CNs and can be produced selectively from the acid-catalyzed etherification of linear primary alcohols. As noted in Chapter 3, diethyl ether has been proposed as a diesel additive due to its CN of ~150, much higher than the 40 minimum required for #2 diesel fuel.[12,13] Its use is limited, however, by its low energy density (~34 MJ kg^{-1}) and high volatility (35°C boiling point). Boiling points and heating values more compatible with diesel can be achieved with heavier ethers such as di-*n*-butyl ether and di-*n*-hexyl ether while maintaining high CNs of 85 and 117, respectively (Table 3.1). Di-*n*-butyl ether may also decrease soot and particulate emissions, though the literature is inconsistent on this point.[14-16] Nel and de Klerk proposed the use of acid-catalyzed etherification to produce diesel-range ethers from the C_5-C_{12} *n*-alcohols produced at low levels (<12 C%) during low-temperature Fischer-Tropsch synthesis.[17,18] Tejero, Bringue, and coworkers examined these reactions in further detail with a variety of solid acids (e.g. Amberlyst™, Nafion™, H-BEA) to convert *n*-alcohols into ethers at selectivities above 90% at conversions above 50%.[19-24] Olefins are the main side-products in these reactions. Mixtures of *n*-alcohols have also been examined, with cross-etherification occurring to produce asymmetric ethers in compositions that directly reflect the alcohol feed composition.[25] Etherification of branched primary alcohols has not been extensively investigated, however. Rorrer et al. recently reported that branching at the α position can greatly decrease etherification selectivities with >99% selectivity to olefins observed for 2-methyl-1-pentanol conversion at conditions where 1-hexanol could be converted with >99% ether selectivity (WO_x-ZrO_2 catalyst, 120°C, 14 and 10%

conversion respectively).[25] It is therefore unclear how effectively the C_{4+} linear and branched alcohol mixtures produced from Guerbet coupling can be converted to ethers.

In this chapter, it will be shown that Guerbet coupling and bimolecular dehydration can be combined in two separate steps to produce distillate range ethers from EtOH at overall yields between 59 and 77%. The Guerbet coupling step is demonstrated for both EtOH and 1-butanol feeds using HAP at conversions between 10 and 90%, which inversely correlate with alcohol selectivities between 89 and 35%. Production of distillate-range alcohols from Guerbet coupling is therefore difficult to achieve selectively (e.g. above 40% conversion). Etherification reactions of single-component alcohol feeds, mixed-alcohol feeds representative of the products produced in Guerbet coupling, and a feed produced directly from Guerbet coupling are demonstrated over the acidic resin Amberlyst^{TM} 70 at conversions above 60%. Branched alcohols are found to be much more selective to olefins than ethers, though cross-etherification between alcohols occurs and improves the viability of converting mixtures containing branched alcohols. The olefins produced are predominantly mono-branched C_6 and C_8 olefins which can be partially hydrogenated for gasoline blending or combined with the C_{2+} olefins produced in Guerbet condensation and oligomerized to jet-range compounds with an approximate overall process selectivity of 15%. The overall scheme for the conversion of EtOH to diesel-range ethers and olefins for use as gasoline or jet-fuel precursors is represented in Figure 5.1. Altogether, this process can be used to convert EtOH to distillate-range ethers and paraffins at yields above 80%.

5.3 Experimental methods

5.3.1 Guerbet coupling methods

Guerbet coupling was performed in stainless-steel fixed-bed reactors (40 cm long, 0.95 cm outer diameter) packed with 6.0 g of calcium hydroxyapatite (HAP, Acros Organics) pelletized

and sieved to a particle size of 250-354 μm. Prior to reaction, HAP was calcined in 65 mL min^{-1} air at 500°C (2°C min^{-1}, 2 h hold). Alcohols were fed (10-50 μL min^{-1}) with a syringe pump (Teledyne ISCO) concurrently with H_2 gas (50-200 mL min^{-1}) at atmospheric pressure in the downflow configuration through a preheated evaporation region maintained at >200°C prior to entering the reactor. H_2 was chosen because its presence was noted in a previous study to decrease the rate of coke formation on HAP.[7] Otherwise it has been well-established that H_2 does not play any catalytic role in EtOH conversion over these catalysts.[5,7,26] The reactor was heated with a tube furnace (Lindberg Blue M Mini-Mite) with the temperature kept uniform via an aluminum block (30 cm long) positioned between the reactor and furnace coils. Prior to data collection with either EtOH or 1-butanol feeds, EtOH was initially converted at 400°C for ~28 h during which the catalyst was partially deactivated. This was performed to ensure that contact time and the alcohol feed could be varied at temperatures up to 375°C without altering the catalyst's intrinsic performance. Figure S5.1 shows that EtOH conversion and alcohol selectivity at 350°C, 1050 s kg_{HAP} mol_{EtOH}^{-1}, 8 kPa EtOH, 93 kPa H_2 could be replicated after various reaction condition changes (temperature, contact time, feed alcohol) with or without regeneration via calcination at the same conditions used in the initial pretreatment. Below the furnace, the products were kept heated at >150°C prior to passing through a removable 110 mL glass condenser (Ace Glass) submerged in an ice bath. Gases which did not condense were sent to a three-way valve positioned to flow either through a bubble-flow meter and then to vent or to an online gas GC (Shimadzu 2010) equipped with a flame ionization detector (FID) and a thermal conductivity detector (TCD). The FID line utilized a Rt-Q-BOND column (Restek), while the TCD line utilized a Hayesep D column (Supelco). Negligible permanent gases were detected via the TCD, thus this line was not used for quantification. Gas and liquid samples were collected simultaneously generally every 4-

10 hours. Gas samples were first injected into the GC via a six-way valve, after which the gas flow rate was measured via the bubble flow meter. The liquid flow was then stopped, the gas flow was redirected to vent rather than through the reactor, and the reactor was isolated. The ice bath was then lowered, and the condenser was removed and replaced with another. To reduce sampling error caused by transient vapor-liquid equilibria and low product volumes (e.g. <2 mL), 10-20 mL of 1-propanol was generally added to the condenser prior to collection. Flows were immediately resumed after sampling unless changing the temperature, which was first allowed to stabilize. When collecting products to be used in etherification, no solvent was utilized in the condenser, and longer sampling times were typically utilized (10-70 h) after steady-state was achieved. After collection, the sample mass was weighed, and the liquid was diluted with 1-propanol including a known amount of 1-pentanol as an internal standard. The products were then analyzed and quantified via GC-FID (Shimadzu 2014) equipped with a RTX-VMS column (Restek). Representative samples were additionally analyzed qualitatively via GC-MS-EI (Shimadzu QP2010S) equipped with a RTX-VMS column (Restek). Representative gas samples were also analyzed via GC-MS-EI after collection into a gas bag. Products were quantified with GC-FID via external standards when reference compounds could be obtained. When they could not, response factors were estimated via the effective carbon number method. For liquid samples, responses were scaled based on the internal standard response; an adjustment of typically less than 2%.

Yields were calculated on a carbon basis according to Equation 5.1 where $\dot{n}_{C,i}$ is the flow rate of carbon for species or species category i.

Equation 5.1 $$Yield_i = Y_i = \frac{\dot{n}_{C,i,out}}{\dot{n}_{C,in}}$$

At alcohol conversions below ~60%, conversion was calculated as the sum of all observed products according to Equation 5.2. This was performed since small changes in feed alcohol quantification can lead to large nonphysical fluctuations in the calculated conversion; carbon balances (carbon out divided by carbon in) ranged between 95 and 105 C%. The yield of unidentified GC-detected species was estimated by multiplying the unidentified GC area by the total yield of identified products divided by the total GC area of such products. At elevated conversions where carbon balances are lower (85-95%), conversion was calculated based on the disappearance of the feed alcohol (Equation 5.3Equation 5.2) since Equation 5.2 does not account for undetected heavy species which are more likely to be present at these conversions.

Equation 5.2 $$Conversion = X = \sum Y_i$$

Equation 5.3 $$Conversion = X = \frac{\dot{n}_{C,feed\ alcohol\ in} - \dot{n}_{C,feed\ alcohol\ out}}{\dot{n}_{C,feed\ alcohol\ in}}$$

Selectivities are calculated on a carbon basis from the yield and the relevant metric for conversion based on Equation 5.4. Conversions, yields, and selectivities are reported as averages of at least two time points after steady-state performance was achieved.

Equation 5.4 $$Selectivity_i = S_i = \frac{Y_i}{X}$$

5.3.2 Etherification methods

Etherification reactions were performed in a 45 mL Parr batch reactor with a 2.22 cm stir rod. Amberlyst™ 70 was crushed and sieved to <177 μm and dried at 110°C prior to reaction. In a typical reaction, 15g of feed were first added to the reactor along with 750 mg of Amberlyst™ 70. The reactor was then sealed and pressurized with argon to ~20 bar stirring at 750 rpm. The temperature was then heated to 150°C with a ramp time of ~10 minutes prior to a 24 h hold. This temperature was chosen to balance activity and selectivity, as increasing temperature decreases the ether selectivity while decreasing temperature decreases rates and therefore requires longer

residence times to obtain the same conversion.[19] After 24 h the reactor was immediately submerged in an ice bath and cooled to <15°C to minimize loss of volatile components. On several occasions the gases were collected and analyzed to ensure that this had been achieved. In the case of 1-butanol conversion, for example, less than 0.1% of the carbon fed was observed in the gas. After careful depressurization, the liquid products and catalyst were collected. The reactor and reactor head were then thoroughly rinsed (~75 mL total) with 1,4-dioxane to ensure full product collection. The resulting solution was then mixed and filtered through a 0.22 μm syringe filter. This solution was then further diluted in dioxane (20:1 by volume), and 1-pentanol was added as an internal standard prior to analysis. The analysis of these products was otherwise the same as in Guerbet coupling (i.e. GC methods). For these products, however, products were often grouped by retention time since isomer mixtures were commonly produced (i.e. olefin and ether isomers). The conversion of a specific species i (X_i) was calculated according to its disappearance according to Equation 5.3 since carbon balances were often below 95%, suggesting that undetectable species were being produced. Yields and selectivities were additionally calculated according to Equation 5.4, respectively. When multiple components were present in the feed, yields and selectivities were defined either with respect to the conversion of a single compound or with respect to all feed carbon.

5.3.3 Additional analytical techniques

Additional information on GC-detectable products was obtained by GC coupled to field ionization mass spectrometry (GC-FI-MS). A JEOL AccuToF GCv 4G instrument equipped with a RTX-VMS column (60 m, 0.32 mm ID) was used to determine the molecular weights of the products by time-of-flight mass spectrometry. The inlet was maintained at 240°C with a 10:1 split for the 1 μL injection. The GC oven was held at 40°C for 5 minutes, ramped to 100°C at 5°C/min,

ramped to 240°C at 20°C/min, and held at 240°C for 11 minutes. Helium was used as the carrier gas at a constant pressure of 60 kPa. The transfer line to the MS was maintained at 240°C.

A Bruker solariX XR Fourier-transform ion cyclotron resonance (FT-ICR) mass spectrometer with a 15 T actively shielded superconducting magnet was used to examine the heavier products. Instrument control, data acquisition and preliminary processing were performed on Bruker Daltonics ftmsControl and Bruker Compass DataAnalysis software. Each sample was ionized by both sodium ion doped electrospray ionization (ESI) and atmospheric pressure chemical ionization (APCI). Samples were diluted 100-fold by volume in LCMS grade isopropanol (for ESI) or hexane (for APCI) prior to analysis. Sodium formate dopant was added at 0.1 mM. The diluted samples were injected using the instrument-controlled syringe pump at a flow rate of 2-4 μL/h, and flow was adjusted for signal stability. Nitrogen was used for all drying and sheath gases. The data was processed by using the full-sine apodization method. Each mass spectrum is an average of at least 40 scans over a mass range of 50-3000 m/z. After acquisition, elemental formulas for each peak were assigned by PetroOrg software.[27]

The ether products of 2-ethyl-1-butanol conversion were characterized by quantitative ^{13}C, Dept 135, HSQC, and HMBC NMR. The ethers were first separated from lighter products via distillation and dissolved to 4.6 wt% in cyclohexane-d_{12}. The quantitative ^{13}C and DEPT 135 experiments were acquired on a Bruker Biospin (Billerica, MA) AVANCE III 500 MHz spectrometer fitted with a DCH (^{13}C-optimized) cryoprobe. The quantitative ^{13}C experiments were conducted using Bruker pulse sequence “zgig30” with an inter-scan relaxation delay of 15 s, a sweep width of 240 ppm, O1P at 110 ppm, TD of 59520 with an acquisition time of 1 s, and 512 scans. The DEPT 135 were conducted using Bruker pulse sequence “deptsp135” with an inter-scan relaxation delay of 2 s, a sweep width of 240 ppm, O1P at 110 ppm, TD of 59520 with an

acquisition time of 1 s, and 512 scans The HSQC and HMBC experiments were acquired on a Bruker Biospin (Billerica, MA) AVANCE 600 MHz spectrometer fitted with a cryogenically cooled 5 mm TXI gradient probe using Bruker pulse sequences "hsqcedetgpsisp2p3" and "hmbcetgpl3nd" with an inter-scan relaxation delay of 2 s, 2 scans, sweep widths of 220 ppm in F1 and 12 ppm in F2, O1P of 110 ppm in F1 and 5.5 ppm in F2, and TD of 3366 in F1 and 1000 in F2. The solvent peak was used as the internal reference for all spectra (δ_H/δ_C: Cyclohexane-d_{12} 1.38/26.43).

5.4 Results and Discussion

5.4.1 Guerbet coupling of ethanol and n-butanol

Guerbet coupling of EtOH and 1-butanol with HAP at 325°C, 101 kPa are compared in Table 5.1 at a contact time of 520 s kg_{cat} $mol_{alcohol}^{-1}$. The conversion of EtOH is twice that of 1-butanol (11.9 versus 5.2%), while the rate of EtOH condensation is three times that of 1-butanol (213 versus 66 μmol kg_{HAP}^{-1} s^{-1}). Previous studies focusing on EtOH conversion have suggested that condensation rates are largely unaffected by alcohol structure, though these conclusions were largely derived from EtOH-rich feeds.[5,7] The butanol feed used here may therefore lead to different conclusions because of large differences in surface coverages. EtOH is known to bind strongly to HAP such that it inhibits acetaldehyde (AcAl) binding and therefore slows condensation, thus the binding strength of 1-butanol relative to butyraldehyde may be of importance.[7,28] EtOH conversion is 89.3% selective to higher alcohols at these conditions while 1-butanol condensation is 62.1% selective. 1-Butanol is more selective to its aldehyde than EtOH is at 29.3 versus 4.1%, respectively. The aldehydes are intermediates to condensation, produced rapidly and reversibly via Meerwein-Ponndorf-Verley (MPV) H-transfer reactions.[2,28-30] The notion that aldehydes and

alcohols are likely in alcohol-aldehyde pseudo-equilibrium through these reactions will be discussed in further detail in Chapter 6.

Table 5.1 | **Product distribution from Guerbet coupling of ethanol and 1-butanol with HAP.** The letter "n" corresponds to the feed alcohol chain length (n=2 for EtOH and n=4 for 1-butanol). Conditions: 325°C, 520 s kg_{HAP} $mol_{alcohol}^{-1}$, 8 kPa alcohol, 93 kPa H_2.

Feed alcohol:	ethanol	1-butanol
Conversion (%)	11.9	5.2
Selectivity (C%)		
C_n Aldehydes	4.1	29.3
C_n Olefins	1.1	2.7
C_{2n} Ethers	0.0	1.6
C_{2n+} Alcohols	89.3	62.1
1-butanol	75.3	-
1-hexanol	2.1	-
2-ethyl-1-butanol	5.3	-
2-ethyl-1-hexanol	0.0	46.8
butenols	6.7	-
2-ethylhexenols	-	15.4
C_{2n} Aldehydes[a]	0.2	1.8
C_{2n} Olefins	2.1	1.4
C_{2n} alkenes	0.1	0.0
C_{2n} dienes	2.0	1.4
Other detectable species	3.0	2.9

The alcohols produced from EtOH at these conditions are 1-butanol, 2-ethyl-1-butanol, and 1-hexanol, as shown in Table 5.1. 1-Hexanol is produced from an EtOH-derived nucleophile and a butanol-derived electrophile, while 2-ethyl-1-butanol is produced from the same alcohols in the opposite roles. The branched alcohol is produced at higher yields, consistent with previous reports.[5,7] Branching is always introduced at the α-position when the nucleophile is derived from a C_{3+} primary alcohol (Figure 5.2). 2-Ethyl-1-hexanol and 1-octanol are additionally observed with increasing contact time. The only alcohol observed in 1-butanol condensation at this contact time is 2-ethyl-1-hexanol, though a C_{12} alcohol (based on GC-MS) is observed at higher conversions. While the specific structure could not be determined, the alcohol is likely 2,4-diethyl-1-octanol, the product of a butanol-derived nucleophile and an electrophile derived from 2-ethyl-1-hexanol.

The alcohol produced from these species in the opposite roles (2-butyl-2-ethyl-1-hexanol) is unlikely to form due to the steric hindrance involved in H^+-abstraction from 2-ethylhexanal and the subsequent bond-formation step. Higher aldehydes are also observed though typically at much lower levels than the alcohols.

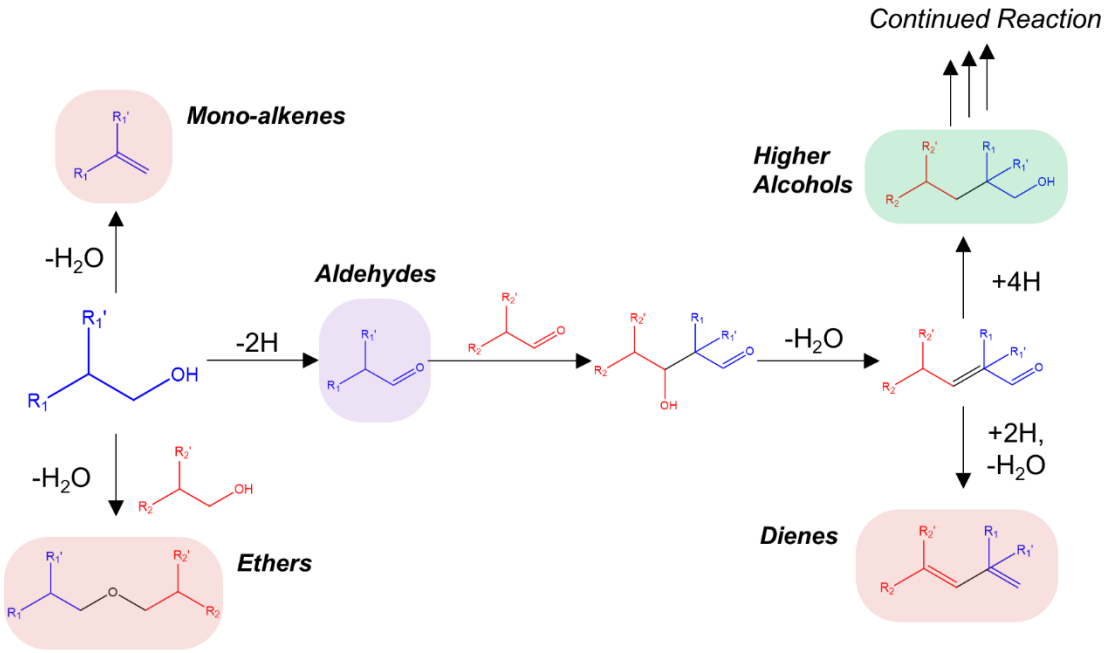

Figure 5.2 | **Alcohol coupling pathway along with key side-reactions.** An alcohol first dehydrogenates to an aldehyde via surface-mediated or MPV transfers. The aldehyde can then undergo aldolization with another aldehyde, shown here acting in a nucleophilic role. After dehydration to an alkenal, full hydrogenation produces an alcohol (Guerbet condensation) likely through an alkenol intermediate (not shown). Partial hydrogenation and dehydration instead leads to a diene (Lebedev condensation). Rather than dehydrogenation, the feed alcohol can undergo unimolecular dehydration to a mono-alkene or bimolecular dehydration to an ether.

The main side-products observed in alcohol coupling result from undesired dehydration reactions as pictured in Figure 5.2. These include mono-alkenes, dienes, and, to a lesser extent, ethers. Mono-enes are produced directly from alcohol dehydration. The main mono-enes observed in EtOH conversion are ethylene, 1-butene, 1-hexene, and 2-methylenepentane. These olefins are the least thermodynamically-favorable of their regioisomers, thus isomerization of the C=C bond under Guerbet coupling conditions is slow. Dienes are commonly thought to be produced via the

Lebedev mechanism, which proceeds via aldol condensation of two aldehydes followed by hydrogenation of the C=O bond and dehydration of the resulting alcohol.[5,31] This reaction closely mirrors Guerbet condensation, thus the dienes produced should be similar in structure to the alcohols. The main diene formed in EtOH conversion is 1,3-butadiene, while at higher contact times both 1,3-hexadiene and 3-methylene-1-pentene are observed. These are consistent with the Lebedev mechanism which only produces 1,3-dienes. A single diene is observed in 1-butanol conversion. Its structure is uncertain since the expected diene (3-methylene-1-heptene) does not have a published MS EI spectrum, though the closest match is the regioisomer 3-methyl-1,4-heptadiene. Aromatics such as ethylbenzene and xylenes are also observed at higher contact times in both EtOH and butanol conversion, though at selectivities well below 5%. This result from reactions involving dienes or unsaturated oxygenate intermediates. Moteki and Flaherty notably combined HAP and Cu-ZnO to convert EtOH to methylbenzaldehydes at selectivities above 30% via AcAl oligomerization and cyclization.[32] The ethers observed are predominantly symmetric ethers since production rates are low and only the feed alcohol is dominant at the conditions studied, though cross-etherification is possible.

Conversions and product distributions as a function of contact time are shown for EtOH and 1-butanol in Figure 5.3. EtOH and 1-butanol conversions increase from 11.9 to 30.6% and 5.2 to 17.1% over this contact time range, respectively. The selectivity to higher alcohols decreases from 89.3 to 85.3% with EtOH feeds while it increases from 62.1 to 75.7% with 1-butanol feeds. The increase in the latter case is due to the decreasing butyraldehyde selectivity, the yield of which is nearly constant over this range. While the AcAl yield is also nearly constant with an EtOH feed, the impact on selectivity is less prominent due to the lower AcAl yields observed. The reversible nature of dehydrogenation the involvement of aldehdyeas as coupling intermediates motivate the

comparison of conversions and selectivities with respect to consumption of both the reactant alcohol and its aldehyde. These metrics better reflect the tendency of the catalyst to promote desired alcohol coupling reactions *versus* undesired dehydration side reactions. As such, an "effective" conversion and an "effective" selectivity can be defined according to Equations Equation 5.5 and Equation 5.6.

Equation 5.5 $$Conversion_{Effective} = X_{Eff} = X_{C_n\ alcohol} - Y_{C_n\ aldehyde}$$

Equation 5.6 $$Selectivity_{i,Effective} = S_{i,Eff} = \frac{Y_i}{X_{Eff}}$$

Here "C_n aldehyde" represents the aldehyde with the same carbon number as the feed alcohol, i.e. AcAl for EtOH and butyraldehyde for 1-butanol. Over the contact time range discussed, the effective conversions of EtOH and 1-butanol according to these metrics therefore increase from 11.4 to 30.5% and from 3.7 to 15.1%, respectively. The effective alcohol selectivities decrease with conversion for both feeds, from 93.2 to 86.5% for EtOH and from 87.9 to 85.5% for 1-butanol. These are accompanied by increasing olefin selectivities.

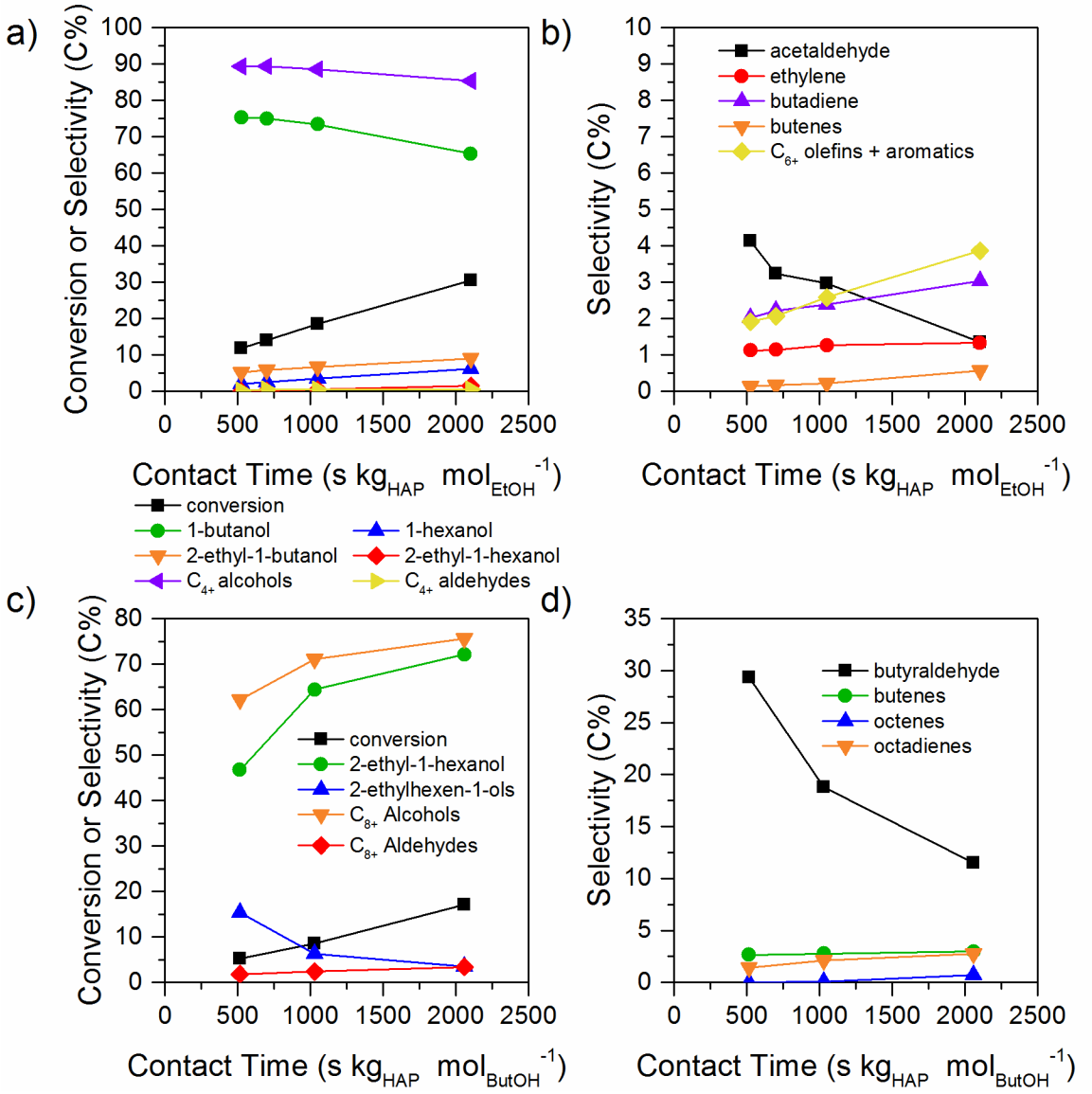

Figure 5.3 | **Guerbet coupling of (a,b) ethanol and (c,d) 1-butanol with HAP as a function of contact time at 325°C**. Gas composition: 8 kPa alcohol, 93 kPa H_2. Absolute (rather than "effective") conversions and selectivities are plotted.

EtOH and 1-butanol condensation were additionally examined at 350°C as shown in Figure 5.4 (data at 520 s kg_{HAP} $mol_{alcohol}^{-1}$ provided in Table S5.1). The absolute conversion of EtOH increases with contact time from 26.5 to 55.9% while 1-butanol conversion increases from 14.8 to 41.4%. The "effective" conversion of EtOH increases over this range from 25.2 to 55.0% while that of 1-butanol increases from 11.8 to 38.3%. These data indicate that all reaction rates decrease

with increasing contact time. Given that previous studies on HAP have shown EtOH condensation to be nearly zero order in EtOH pressure at similar conditions,[7,26,28] it is unlikely that these decreases are solely due to decreasing reactant concentrations. Water is known to inhibit EtOH conversion rates on HAP,[6] thus it is likely that byproduct water at least partially contributes to these declining rates. The rates of desired reactions leading to higher alcohols notably decrease more than those of undesirable dehydration reactions, which is reflected in decreasing alcohol selectivities. These trends were also observed at 325°C but are more apparent at 350°C. At this elevated temperature, effective alcohol selectivities decrease from 84.5 to 77.0% for EtOH conversion and from 81.3 to 73.8% for 1-butanol conversion across the contact time changes examined here. At fixed conversion, alcohol selectivities also decrease with the increase in temperature. At 31% EtOH conversion, a lower effective alcohol selectivity (83.0 versus 86.5%) and a higher olefin selectivity (8.4 versus 7.4%) are observed at 350 versus 325°C.

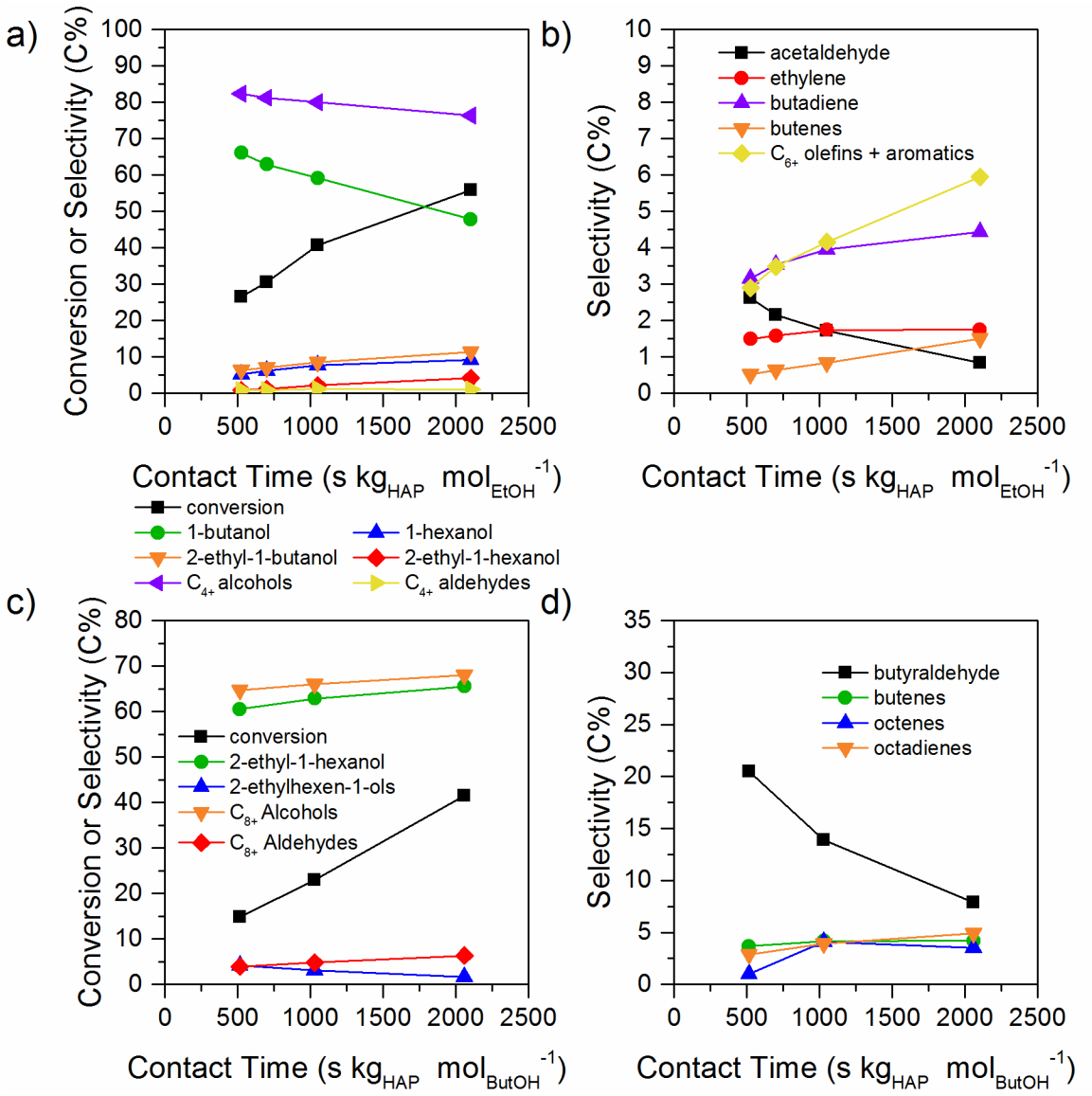

Figure 5.4 | **Guerbet coupling of (a,b) ethanol and (c,d) 1-butanol with HAP as a function of contact time at 350°C**. Gas composition: 8 kPa alcohol, 93 kPa H_2. Absolute (rather than "effective") conversions and selectivities are plotted.

In order to examine the high-conversion selectivity limits of Guerbet coupling, EtOH and 1-butanol conversion were additionally examined at 375°C with the highest contact time (2100 s kg$_{HAP}$ mol$_{alcohol}^{-1}$), as shown in Table 5.2. This leads to an EtOH conversion of 90% and a 1-butanol conversion of 74% with alcohol selectivities of 37% and 47%, respectively. Phase separation was observed in the liquid products with an organic phase comprising mostly C_{4+} species and an

aqueous phase containing mostly EtOH. Butanol preferentially partitions (>95%) into the organic phases of both butanol and EtOH products. In EtOH condensation, 36% of the EtOH is converted to unidentified species, approximately one-third of which is GC-detectable though broadly distributed across over 40 species. GC-MS-FI shows that these species are largely unsaturated C_{8+} species with one or no oxygens. FT-ICR-MS also confirms the presence of C_{12}-C_{26} species (mainly C_{12}-C_{20}) in the liquid product (Figure S5.2) which have predominantly zero or one oxygen atom per molecule. Deoxygenated species predominantly possess three double-bond equivalents (DBE) and are therefore most likely trienes. Oxygenates possess one, three, or four DBE and therefore are not saturated alcohols. These may be aldehydes, alkenols, alkenals, and alkylbenzenemethanols. As mentioned prior, Moteki and Flaherty showed that alkadienals and alkatrienals can be produced from AcAl oligomerization on HAP, the latter of which can be cyclized when the species is larger than C_8.[32] Of the products identified, only 65% are higher alcohols or aldehydes while 31% are olefins and aromatics. The butanol condensation products are largely detectable (95%) with 47% selectivity to alcohols, 18% selectivity to olefins and aromatics, 10% to 2-ethylhexanal, 5% to butyraldehyde, and 8% to unidentified detectable species. The higher carbon balance for 1-butanol is likely due to the lower conversion achieved.

Table 5.2 | **Product distribution from the Guerbet coupling of ethanol versus 1-butanol with HAP.** Conditions: 375°C, 2100 s kg_{HAP} $mol_{alcohol}^{-1}$, 8 kPa alcohol, 93 kPa H_2. Absolute (rather than "effective") conversions and selectivities are tabulated.

Feed Alcohol	ethanol	1-butanol
Conversion (%)	89.9	74.2
Selectivity (C%)		
C_n Aldehyde	0.5	4.8
C_n Olefins	1.6	5.7
C_{2n} Ether	0.3	0.6
C_{2n+} Alcohols	36.7	47.3
1-butanol	14.8	-
1-hexanol	3.8	-
2-ethyl-1-butanol	8.4	-
2-ethyl-1-hexanol	4.6	45.1
butenols	0.4	-
2-ethylhexenols	0.0	0.7
C_{2n+} Aldehydes	3.9	10.3
C_{2n+} Olefins+Aromatics	19.4	18.0
C_{2n} alkenes	2.1	10.0
C_{2n} dienes	4.4	8.0
Other GC-detected species	13.2	7.9
Undetected species	22.3	5.4

Figure 5.5 plots the effective alcohol selectivity and average alcohol carbon number as a function of conversion for both EtOH and 1-butanol feeds. This figure illustrates the major challenge with Guerbet coupling to the distillate range: the decreasing selectivity to higher alcohols observed with increasing conversion. EtOH condensation drops below a target 80% selectivity around 40-50% conversion, while butanol condensation drops below this threshold around 20-30% conversion. At these conditions, the average carbon number of the EtOH-derived alcohols is around 5 while that of the 1-butanol products is around 8. Distillate fuels are heavier, however, ranging from 8 to 22 carbon atoms per molecule. Heavier alcohol mixtures theoretically can be produced by operating at higher conversions. The simplest model which can be used to approximate the alcohol distribution as a function of conversion is step-growth. Previous studies have shown that this is generally true in the regimes they examined, up to about 50% conversion.[5,7]

Figure 5.5 shows the average carbon number of the alcohol product as a function of conversion according to step-growth kinetics (relationship derived in the supplemental information). Alcohol mixtures with average carbon numbers of at least 10 (to meet the average boiling point of jet fuel) can therefore be theoretically obtained from EtOH above 86.6% conversion or from 1-butanol above 42.4% conversion. Selective coupling therefore must be achieved at much higher conversions than achieved in the present study if direct distillate-range alcohol synthesis is to be achieved, especially with EtOH feedstocks. Additionally, the step-growth model overpredicts the average alcohol carbon number for EtOH coupling at conversions above 50% and for 1-butanol at nearly all conversions. This deviation is most likely because the dehydration selectivity increases with conversion and because condensation rates between branched alcohols are likely slower than between linear alcohols, a clear violation of step-growth kinetics. In lieu of further catalyst improvements, the key to utilizing this alcohol oligomerization chemistry for distillate fuel synthesis is therefore to valorize alcohol mixtures which can be produced selectivity at lower conversions, up to about 40% in this case. One such method is to perform bimolecular dehydration to convert these alcohols to heavy ethers.

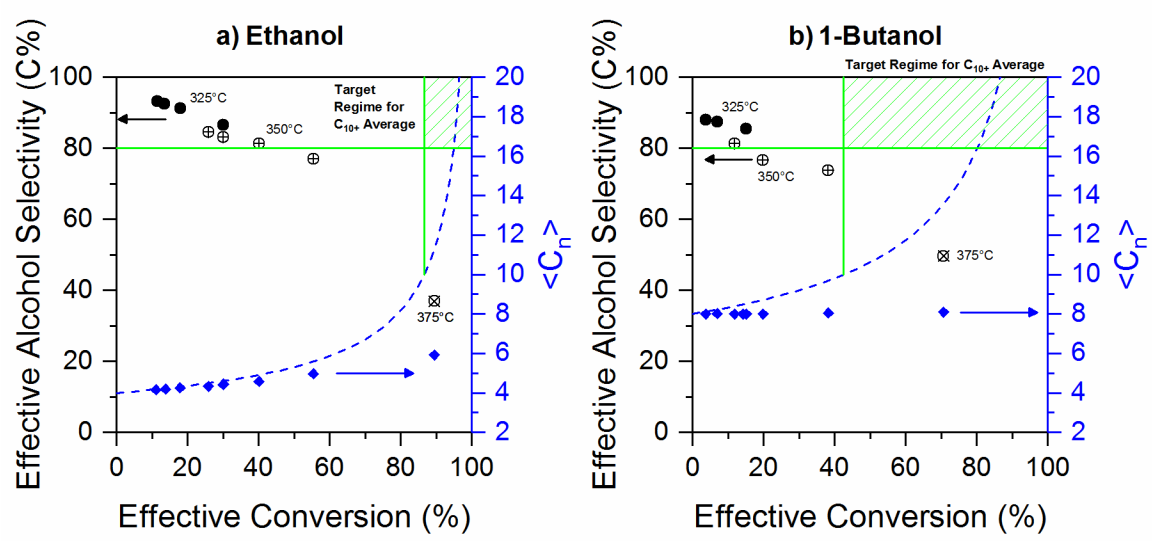

Figure 5.5 | **Higher alcohol selectivity (effective) and average alcohol carbon number (<C_n>) versus conversion (effective) for Guerbet coupling of (a) ethanol and (b) 1-butanol.** The target regimes represent conversions at which an alcohol product with an average carbon number of at least C_{10} is obtained with at least 80 C% selectivity. Selectivities shown as circles: ● collected at 325°C, ⊕ at 350°C, ⊗ at 375°C. Average alcohol carbon number shown in diamonds ◆. Predicted average carbon number based on step-growth oligomerization shown via dotted line. Data collected at contact times between 520 and 2100 s kg_{HAP} $mol_{alcohol}^{-1}$.

5.4.2 Etherification of n-alcohols and α-branched primary alcohols

Etherification was first performed using the four main alcohols observed in Guerbet condensation individually: 1-butanol, 1-hexanol, 2-ethyl-1-butanol, and 2-ethyl-1-hexanol as shown in Figure 5.6. All reactions were performed in the absence of a solvent to reduce separation costs in larger-scale implementation. Both *n*-alcohols are highly selective to ethers, 97.0% for 1-butanol and 96.9% for 1-hexanol. A single symmetric ether is the dominant product in both cases (di-*n*-butyl ether and di-*n*-hexyl ether), though trace amounts of asymmetric isomers are produced as well (<3% of total ethers). The only other products observed are olefins, which are produced from unimolecular dehydration of the parent alcohol or from decomposition of the ether into an olefin and an alcohol. Mixtures of olefins are produced via rapid C=C isomerization. The conversion of 1-hexanol is 38% higher than that of 1-butanol (78.7 vs. 59.1%), which is likely due

to the lower number of reactant moles in the 1-hexanol feed (by 28%) since fixed-mass feeds are used.

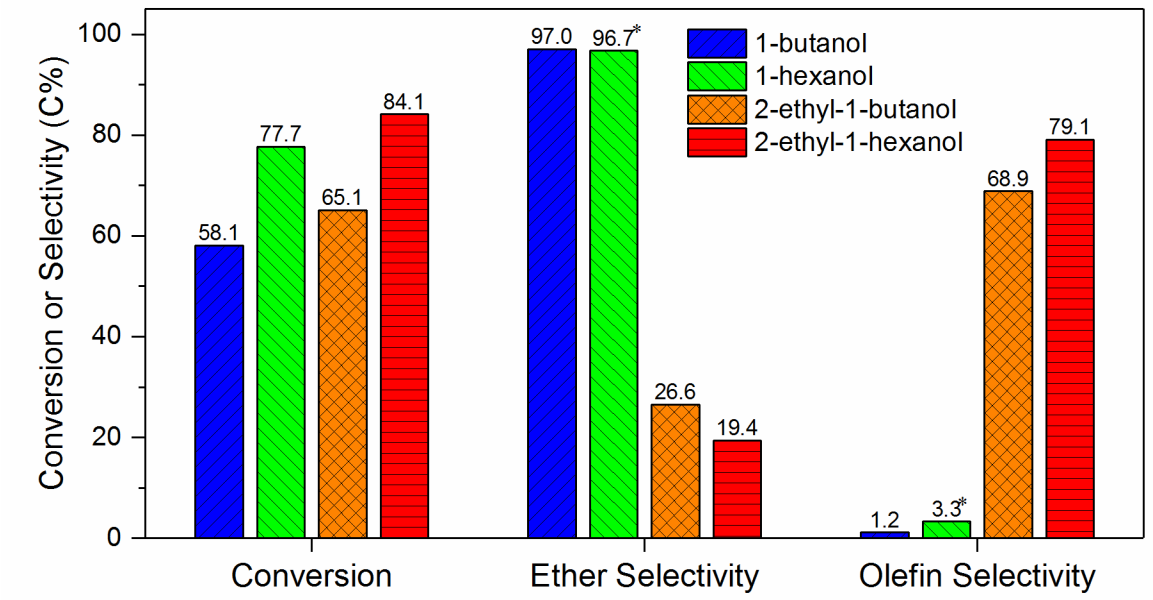

Figure 5.6 | **Conversions and selectivities in the dehydration of single-component alcohol feeds.** *1-hexanol product selectivities scaled down to 100% since carbon balance of 102.6% was observed. Conditions: 15 g alcohol, 0.75 g Amberlyst™ 70, 150°C, 24h.

Since etherification is only a slightly exothermic reaction (ΔH°=-18 kJ mol^{-1} for gas-phase 1-hexanol conversion) and is entropically disfavored (ΔS°=-35.7 J mol^{-1} K^{-1}), equilibrium limitations may be present at reaction conditions. Thermodynamic calculations were performed using Aspen Plus® with the UNIFAC property method to examine the equilibrium limits of etherification in the liquid phase. At 150°C the equilibrium ether yields are 92% from a 1-butanol feed and 96% from a 1-hexanol feed, thus the batch reactions performed here are below equilibrium conversion. This was further examined experimentally by extending the 1-hexanol reaction time for an additional 24h, which led to a minor ether yield increase from 75.4 to 78.5% alongside a minor olefin yield increase from 2.4 to 2.6%. Olefin formation is not equilibrium-limited at these conditions, thus the small difference with an additional 24h of reaction could be due to product-induced inhibition or deactivation. This was additionally verified by running a

reaction for 24h, adding fresh catalyst, and running for another 24h, which resulted in increases in both ether and olefin yields to 85.8% and 5.4%, respectively. This suggests that deactivation is present, though it does not rule out the possibility of inhibition by products. The inhibiting effect of water is noted later with respect to the conversion of feeds derived from EtOH coupling.

The etherification of 2-ethyl-1-butanol and 2-ethyl-1-hexanol, the major branched alcohols formed from the Guerbet conversion of EtOH, were also examined individually (Figure 5.6). These reactants are more selective to olefins than linear alcohols are. 2-Ethyl-1-butanol is 64.8% selective to 3-methylpentenes, and 2-ethyl-1-hexanol is 74.9% selective to 3-methylheptenes. The increased olefin selectivities are consistent with the recent findings of Rorrer et al. regarding the effects of alkyl branching on primary alcohol etherification over tungstated zirconia.[25] These authors suggested that this is because unimolecular dehydration barriers are lower for α-substituted alcohols than for linear primary alcohols while the barriers for etherification are similar. The olefins produced here are a mixture of isomers produced via C=C isomerization of the primary olefin product. This mixture is dominated by the most thermodynamically-favorable regioisomers and may be equilibrated. Trace amounts of skeletal isomers were also observed. In direct contrast to linear alcohol etherification, multiple high-boiling species were observed in the conversion of the branched alcohols (chromatograms compared in Figure S5.3). 2-Ethyl-1-butanol products were analyzed further via GC-MS-FI to determine the molecular weights of these compounds. The majority of these possess a molecular formula of $C_{12}H_{26}O$, consistent with their assignment as ethers. Trace amounts of $C_{12}H_{24}$ olefins are also observed. Since the temperature and catalyst used here are also suitable for olefin oligomerization, these C_{12} olefins are likely produced from the dimerization of methylpentenes.[33-35]

The ethers produced from 2-ethyl-1-butanol were separated from the feed alcohol and light olefins via distillation for analysis via NMR to gain further insight into their structure. Quantitative ^{13}C NMR shows a 5:1 ratio of C-C aliphatic to C-O aliphatic carbons, consistent with their ether assignments. As expected from GC-MS-FI, only trace amounts of C=C aliphatic carbons were detected. HSQC and HMBC were used to gain further insight into the structures of these ethers. 17 distinct C-O carbons were identified, accounting for 96% of the C-O carbon present. Correlations between these revealed the presence of 9 total ethers as summarized in Table S5.2. The other carbon atoms largely could not be identified due to extensive overlap between the different species present. All ethers possess at least one O-CH_2 carbon. The main ether (45%) possesses two identical O-CH_2 carbons. Full NMR identification of the four distinct carbons of this ether (Table S5.3) suggest that this a symmetric ether with two 2-ethyl-1-butyl fragments. The second-most dominant ether (17%) possesses an O-C, while the next two most common (8% and 10%) possess an O-CH and appear to be structurally similar. The other ethers observed possess an O-CH (6% for one, 5% for another), an O-CH_2 (4%), or possess an ether carbon which could not be determined with reasonable confidence (2%).

We hypothesize that the asymmetric olefins are produced via an indirect etherification mechanism which involves the reaction of an alcohol with an olefin, similar to the synthesis of methyl tert-butyl ether (MTBE) from methanol and isobutene.[36,37] After an olefin is produced from unimolecular dehydration of 2-ethyl-1-butanol, it undergoes rapid isomerization before reacting with an alcohol to form an ether. Ether isomers are therefore produced due to isomerization of the olefins prior to C-O bond formation. All ethers therefore should possess at least one O-CH_2 derived from the parent 2-ethyl-1-butanol, while the substitution of the other ether carbon depends on the alkene involved in the reaction. An O-C ether can be formed from the reaction of an alcohol with

the tertiary carbon of a 3-methylpentene, while O-CH ethers can be formed from reaction with the secondary carbons of the 3-methylpentene. The latter ether possesses four stereoisomers, though only the two pairs of enantiomers can be distinguished via NMR. This mechanism is therefore consistent with the four major ethers identified via NMR, which comprise 83% of all ethers observed. The origin of the remaining ethers is uncertain. This indirect etherification mechanism is notably severely equilibrium-limited. At 150°C the maximum di-*n*-hexyl ether yield thermodynamically achievable from this route was calculated to be only ~0.07% (achieved at ~50% 1-hexanol conversion). While this is not meant to quantitatively describe branched alcohol conversion, it strongly suggests that this mechanism cannot be used to selectively produce ethers.

The reaction pathways involved in the acid-catalyzed etherification of primary alcohols are summarized in Figure 5.7 using 2-ethyl-1-butanol as a representative alcohol. The direct mechanism involves reaction of two alcohol molecules to produce a single ether and occurs for both linear and branched alcohols. Olefins are produced by either a unimolecular dehydration of the alcohol or by the reversible decomposition of the ether. The C=C bonds in the olefins rapidly isomerize to produce mixtures dictated by thermodynamic equilibrium. A mixture of ethers can then be formed via the reaction of an alcohol with one of these olefins—this is termed here as indirect etherification. Since the dominant olefin is internal (3-methylpent-2-ene in this case), this is most likely to yield asymmetric ethers.

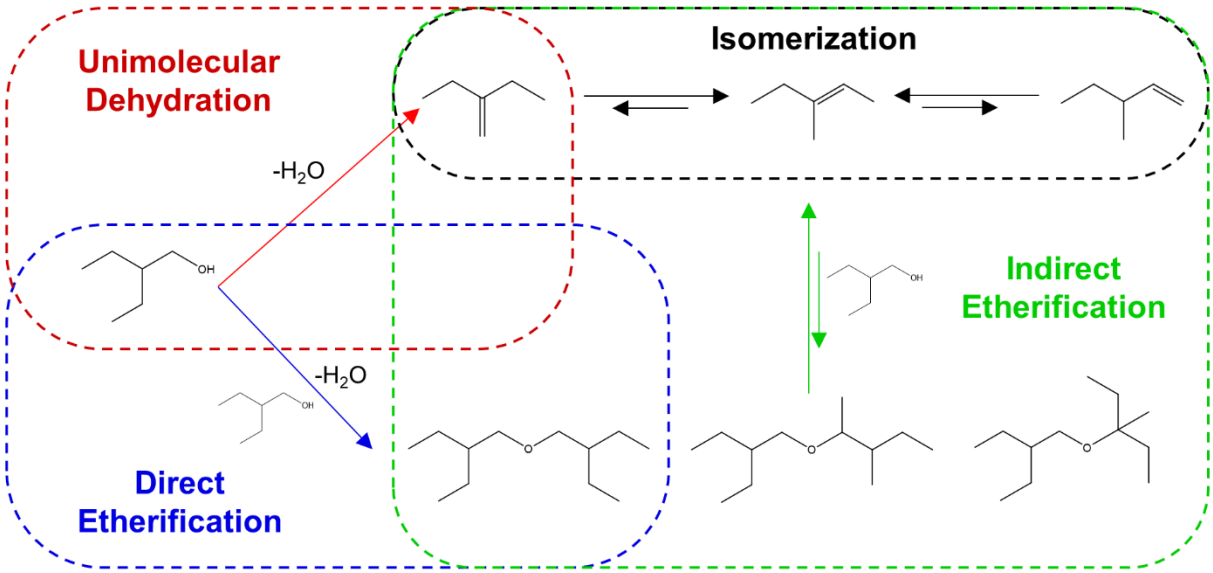

Figure 5.7 | **The pathways for acid-catalyzed dehydration of alcohols to mixtures of ethers and olefins using 2-ethyl-1-butanol as a representative branched alcohol.** The main reactions involved are direct etherification of two alcohols, unimolecular dehydration, olefin isomerization, and indirect etherification between an alcohol and olefin.

5.4.3 Etherification of model mixed-alcohol feeds

Etherification of mixed-alcohol feeds were examined to understand the conversion of Guerbet condensation products. Previous studies have shown that mixtures of *n*-alcohols undergo cross-etherification to produce mixed ethers.[25,38] Cross-etherification of linear and branched alcohols is not as well-understood, however, thus mixtures of 1-butanol and 2-ethyl-1-hexanol were examined first with molar ratios of 8:1, 2:1, 1:1, and 1:2 (Figure 5.8). These mixtures represent the alcohol distributions which would result from the Guerbet condensation of 1-butanol at conversions ranging from 20 to 80%. Feeds with higher 1-butanol contents show higher ether selectivities and lower olefin selectivities with strong correlations shown in Figure 5.9a. No species other than light olefins and ethers were observed, thus the 4-7% selectivity unaccounted for in these data indicates that either undetected products are formed or that the response factors assumed for the C_{12+} ethers are overestimated. The conversion of a 1:1 molar ratio of 1-butanol and 2-ethyl-

1-hexanol leads to an ether selectivity of 59% and an olefin selectivity of 33% at 66% feed conversion. The conversion of 1-butanol is 79% while that of 2-ethyl-1-hexanol is lower at 59%. The cross-etherification product 1-butoxy-2-ethylhexane was positively identified via GC-MS-EI, clearly showing that cross-etherification does occur between linear and branched alcohols. The selectivity to this C_{12} ether was also maximized with this equimolar feed as shown in Figure 5.9b. Guilera et al. similarly observed that the selectivity to ethyl octyl ether in the cross-etherification of EtOH and 1-octanol over Amberlyst^{TM} 70 was maximized with an equimolar feed.[38] This maximum would be consistent with a rate-limiting step either involving bond formation between the two alcohols (which may or may not be bound to the catalyst) or the decomposition of an equilibrated surface dimer to form an ether. The former is supported by Guilera et al., though Song et. al have provided evidence for the latter in the Brønsted acid catalyzed etherification of 1-octadecanol catalyzed over zeolite H-BEA.[39] The presence of mass transport limitations in the current study also cannot be ruled out despite the high stir rates (750 RPM) and low particle sizes used (<177 μm). Additionally, Guilera and coworkers previously found that the presence of water formed during dehydration can affect cross-etherification selectivities with Amberlyst^{TM} 70 due to a combination of site-blocking and resin swelling, the latter of which alters the accessibility of acid sites to alcohols.[40]

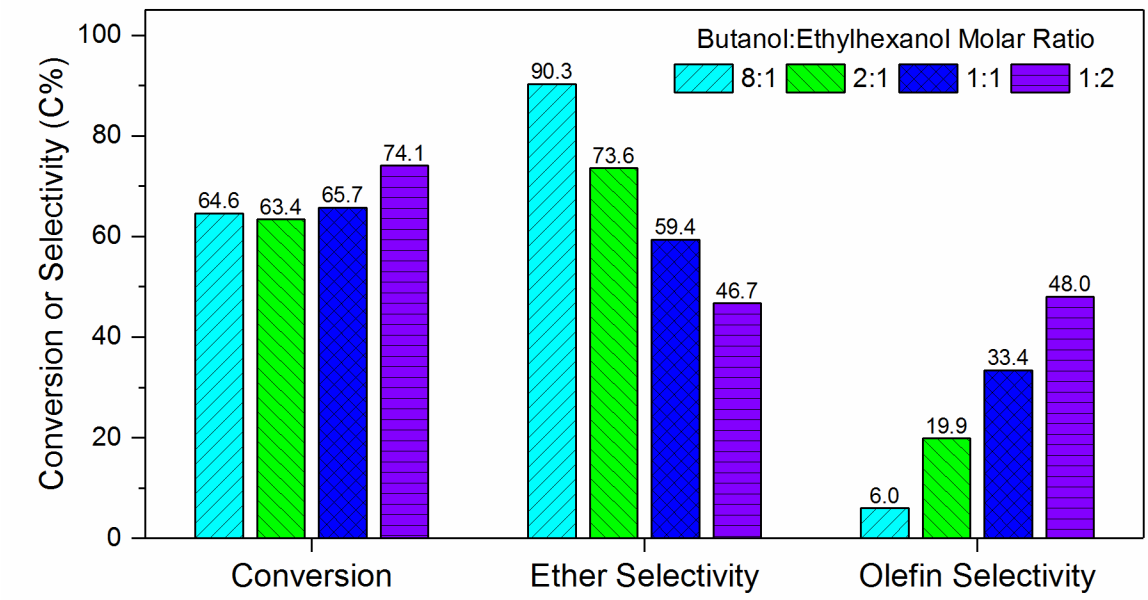

Figure 5.8 | **Conversions and selectivities in the dehydration of mixtures of 1-butanol and 2-ethyl-1-hexanol.** Conditions: 15 g alcohol mixture, 0.75 g Amberlyst^{TM} 70, 150°C, 24h.

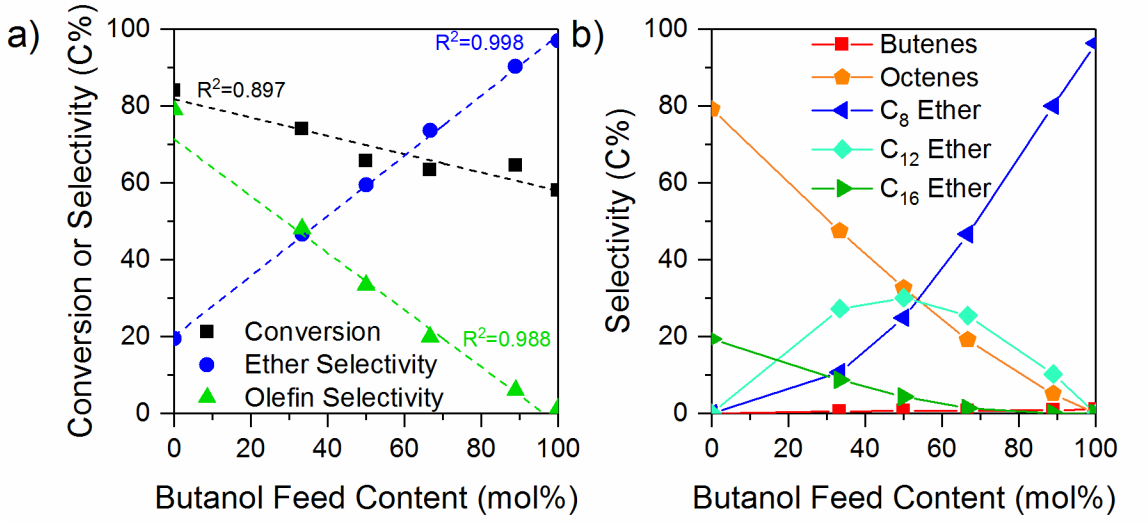

Figure 5.9 | **Conversion and selectivities in the etherification of 1-butanol and 2-ethyl-1-hexanol mixtures as a function of butanol feed content.** (a) Correlations between overall conversion, ether selectivity, and olefin selectivity. (b) Selectivities to specific olefins and ethers. Conditions: 15 g alcohol mixture, 0.75 g Amberlyst^{TM} 70, 150°C, 24h.

The specific selectivities of each alcohol in the conversion of an equimolar mixture of 1-butanol and 2-ethyl-1-hexanol are depicted in Figure 5.10. 1-Butanol is less selective to ethers in the presence of 2-ethyl-1-hexanol (87%) than when converted alone (97%). The opposite is

observed with 2-ethyl-1-hexanol, as it is 41% selective to ethers in the mixture while only 19% selective in the absence of 1-butanol. The dominant ether formed from 2-ethyl-1-hexanol is the cross-ether, while the dominant ether formed from 1-butanol is di-*n*-butyl ether. The improved ether selectivity for 2-ethyl-1-hexanol conversion can be explained either by an increased rate of etherification or a decreased rate of ether decomposition. Destabilizing steric interactions may play a large role in either case. Such interactions are expected to contribute more significantly to the formation and decomposition rates of di-(2-ethylhexyl) ether than to those of 1-butoxy-2-ethylhexane.

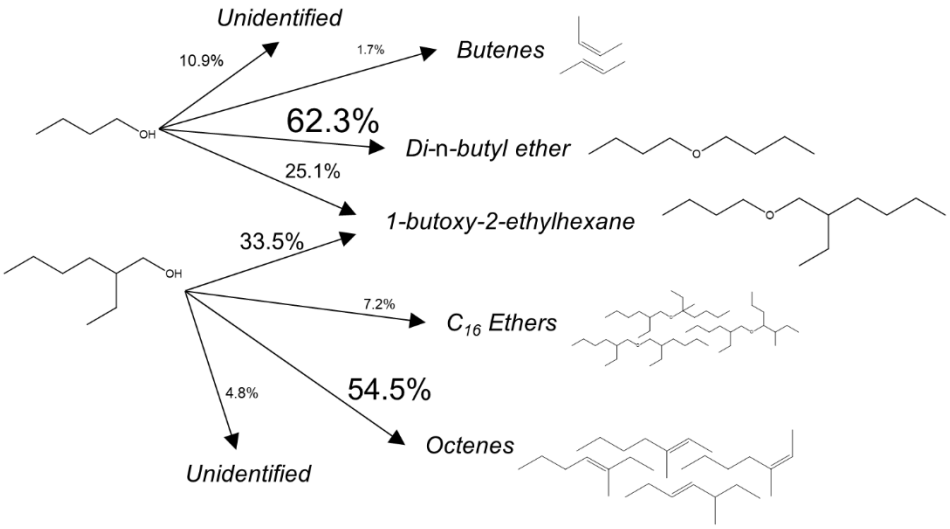

Figure 5.10 | **Specific selectivities of products from 1-butanol and 2-ethyl-1-hexanol from an equimolar etherification feed.** Conditions: 15 g alcohol mixture, 0.75 g Amberlyst^{TM} 70, 150°C, 24h.

Alcohol feeds comprising all four major alcohols were then examined to evaluate the conversion of products derived from EtOH condensation. EtOH was not included in these feeds since it would lead to the formation of diethyl ether and other light ethers less suitable for diesel fuel. EtOH therefore must be removed from Guerbet products prior to etherification. The alcohol distributions at different EtOH conversion were approximated using a simplified kinetic model which assumes that all condensation events occur with the same intrinsic kinetics, though α-alkyl

alcohols were assumed to be inactive as nucleophiles. While over 50 alcohols were modeled for completeness, the only alcohols used in the model feeds were 1-butanol, 1-hexanol, 2-ethyl-1-butanol, and 2-ethyl-1-hexanol. These make up over 99 mol% of the alcohols at 20% conversion and 82% at 80% conversion. Model feeds were prepared based on 20, 50, 67, and 80% conversion, resulting in linear:branched alcohol ratios of 12.5:1, 5.3:1, 3.2:1, and 2:1, respectively. In all cases, the dominant alcohol was 1-butanol (89.8-52.3 mol%); the full composition of each feed can be found in Table S5.4.

As shown in Figure 5.11, the mixtures react to 65.0-69.5% conversion under these reaction conditions with ether selectivities ranging from 65.0-81.8%. Cross-etherification was observed between the various alcohols with ethers positively identified based on molecular weight via GC-MS-FI (Figure S5.4). Approximately 15% of the products could not be identified regardless of the composition, which once again implies that either unobserved products are formed or that response factors are overestimated for many of the higher ethers. As in the etherification of butanol-ethylhexanol mixtures, ether and olefin selectivities are directly correlated with the linear:branched alcohol feed ratio, though ether selectivities are slightly lower than with the two-component feed. This implies that performing Guerbet condensation at higher conversions where the linear:branched alcohol ratio is lower will result in lower ether selectivities, though these ethers will be larger and therefore possess higher energy densities. The olefins are almost entirely 3-methylpentenes and 3-methylheptenes derived from the branched alcohols. These could be partially hydrogenated and utilized in gasoline or oligomerized with solid acids and hydrogenated to jet-range paraffins.

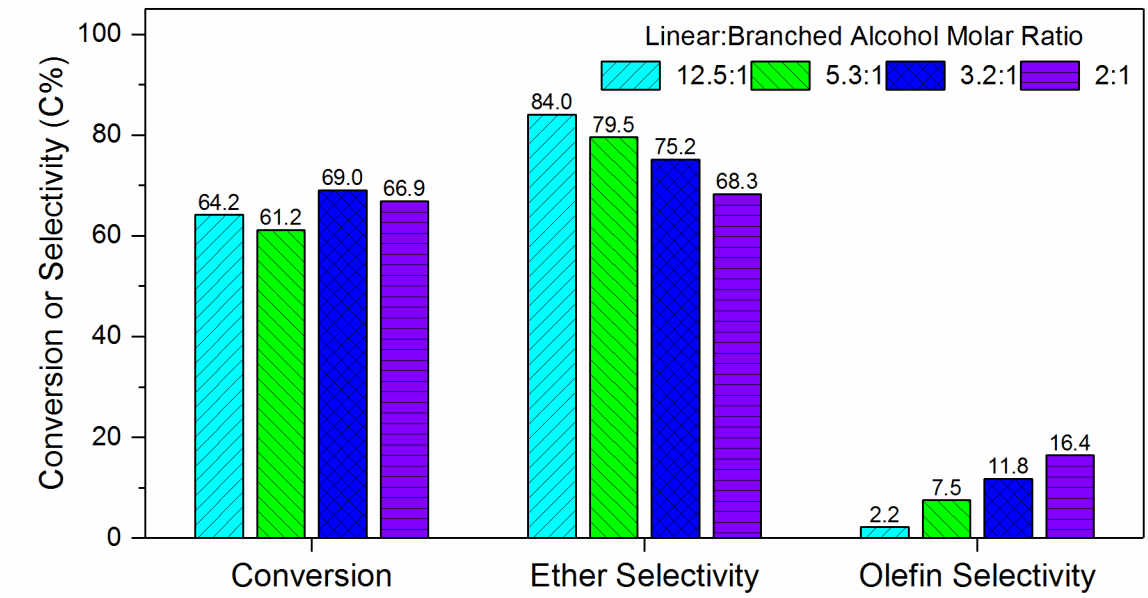

Figure 5.11 | **Conversions and selectivities in the dehydration of model alcohol mixtures representative of ethanol condensation products.** Conditions: 15 g alcohol mixture, 0.75 g Amberlyst^{TM} 70, 150°C, 24h.

5.4.4 Distillate-range fuel production from the combination of Guerbet coupling and etherification

After validation of the individual reaction stages, the two were combined in series to produce a mixture of distillate-range ethers from EtOH. EtOH condensation was first carried out at 42% conversion to produce C_{4+} alcohols at 82% selectivity. The product distribution remained steady for over 400h time-on-stream (Figure S5.5), the longest reported stability in the literature for heterogeneous Guerbet coupling to our knowledge. Water is known to inhibit etherification reactions[20,41,42] and therefore must be removed from the coupling products prior to reaction. Here the addition of 7.4 wt% water to a model mixture of 1-butanol and 2-ethyl-1-hexanol was found to decrease conversion from 66 to 12% (Figure S5.6), though drying with molecular sieves fully recovered the activity. Sieves were therefore used to reduce the water content of the EtOH-derived feed from 15 to less than 0.5 wt%. EtOH was then removed via distillation since etherification reactions involving EtOH would produce significant amounts of volatile C_4-C_6 ethers. The major components in the resulting feed were 1-butanol (51.8 wt%), 2-ethyl-1-butanol (13.6 wt%), 1-

hexanol (12.5 wt%), and 2-ethyl-1-hexanol (4.1 wt%) with the remainder comprising other alcohols (4.7 wt%) and species not detected via GC (13.2 wt%). 79.9 mol% of the alcohols in this feed are linear. Using correlations between the linear alcohol contents of model feeds and their etherification product distributions, an ether selectivity of 76.4% and an olefin selectivity of 9.8% were expected. In close agreement with these expectations, the feed was converted to ethers with 73.5% alcohol conversion, 71.6% ether selectivity, and 10.2% olefin selectivity. This demonstrates that combination of the two catalytic steps in series necessitates only conventional separation processes already common in alcohol purification (i.e. distillation and drying with molecular sieves) and that etherification selectivities can be reasonably predicted based on model reactions and the feed alcohol distribution.

A proposed block flow diagram of this technology is shown in Figure 5.12. Here the approximate carbon flows of key streams are displayed assuming that Guerbet condensation is performed at 50% conversion with 77% selectivity to alcohols. The product is then separated into four streams: water, EtOH, olefins, and C_{4+} alcohols with other heavy byproducts. The EtOH is recycled to the Guerbet reactor. The alcohols and heavy byproducts are fed to the etherification reactor. The selectivities of the etherification process are directly linked to the ratio of linear:branched alcohols in this feed, which in this case are 80 and 6% for ethers and olefins, respectively. The product stream is separated into four streams: olefins, ethers, water, and byproducts. As discussed previously, these olefins could be suitable for gasoline blending after partial hydrogenation.[43] Here, however, we envision combining this stream with the olefins produced during Guerbet coupling into a stream which can be oligomerized via acid or metal catalysis and then hydrogenated to jet-range paraffins. The composition of this stream on a carbon basis is approximately 12% C_2, 40% C_4, 40% C_6, and 8% C_8. Oligomerization is conservatively

estimated to be 80% selective to the distillate range since oligomerization of C_4-rich streams is selective to this range and the subsequent hydrogenation is well-established to be a highly selective process.[33,44,45] The process overall demonstrates a 62% yield of diesel-range ethers and a 14% yield of jet-range paraffins with an overall 76% distillate fuel yield from EtOH. To understand the sensitivity of this yield to the conversion at which the Guerbet reactor is operated, correlations can be drawn between EtOH conversion and alcohol selectivity, olefin selectivity, and the linear:branched alcohol ratio. These can be then be combined with correlations between the etherification feed composition and product selectivities to predict overall process yields as a function of Guerbet conversion. Increasing EtOH conversion from 10 to 60% shifts overall ether yields from 77 to 59% while olefin yields increase from 5 to 16% with total distillate yields of 82 to 75% as shown in Figure S5.8. Combined with the maximum theoretical EtOH yield achievable from glucose fermentation (67% carbon basis), this technology could be used to produce distillate fuel from sugars at yields of 50-55%. The byproducts of this process are light olefins, unsaturated C_{8+} hydrocarbons and oxygenates, and unidentified species. The unidentified species may also be useful in fuel blendstocks but are conservatively assumed here to have no value. While only conventional separation schemes are likely required in this process (e.g. distillation, adsorption with molecular sieves, liquid-liquid extraction), we have chosen not to specify them in the current diagram in accordance with a level 3 system analysis as described by Douglas in the hierarchical design of chemical processes.[46] These separations can be performed in a multitude of ways depending on how the process is designed. For instance, removal of water from EtOH condensation products may only require molecular sieves if condensation is performed at low conversions. Operation at higher conversions may require both distillation and molecular sieves. Operation at yet higher conversions would additionally allow for the production of a biphasic

product, thus water removal would only occur after C_{4+} organic products are removed via decantation. Such a phase separation could also be induced via the recycling of a heavy phase if this improves process economics. Since the Guerbet condensation conversion strongly impacts the final distribution of products, it is unclear which separation schemes will be the most economical without detailed technoeconomic analyses, a focus of our future work.

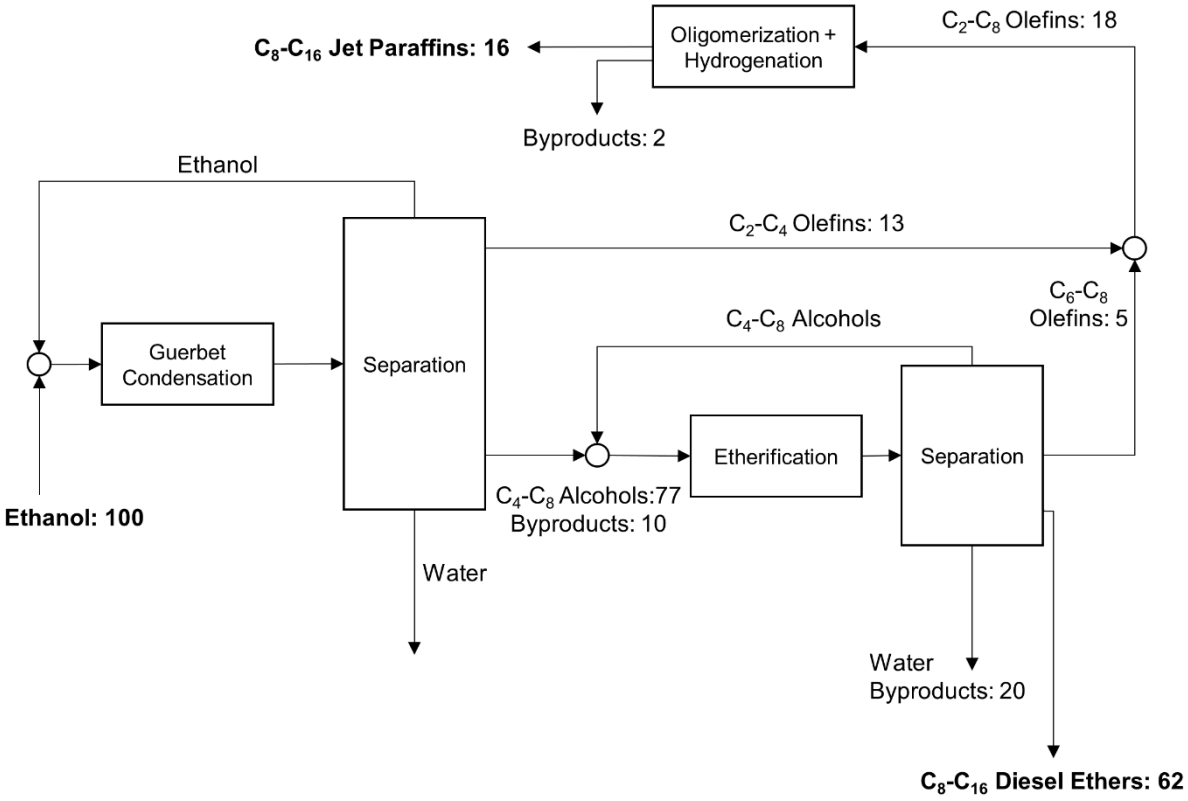

Figure 5.12 | **Block diagram for the conversion of ethanol to distillate-range ethers and paraffins through a combination of Guerbet condensation, etherification, olefin oligomerization, and hydrogenation.** The numbers depicted are carbon flows based on a process in which Guerbet coupling is performed at 50% conversion and etherification is performed at 65% conversion. Olefin oligomerization is assumed to be 80% selective to jet-range olefins, which can be fully hydrogenated to paraffins. The byproducts are comprised of aldehydes and unidentified species.

Compared to conventional EtOH-to-distillate technologies, this process possesses several benefits. The C_{8+} ethers have much higher cetane than the products from acid-catalyzed olefin

oligomerization. These ethers also have lower freezing points than linear paraffins of the same carbon number that can be produced through metal-catalyzed olefin oligomerization (followed by hydrogenation). The freezing points of dodecane and hexadecane, for example, are -10 and 18°C, respectively, while those of di-*n*-hexyl ether and di-*n*-octyl ether are -43 and -8°C, respectively. The proposed process additionally uses solely inexpensive heterogeneous catalysts and does not require added solvents. The catalyst utilized in Guerbet coupling also demonstrates high stability (>400h time-on-stream).

Several aspects of this technology warrant further investigation. Engine testing is required to understand the full potential of the ether product as a diesel blendstock. Due to the high concentration of 1-butanol in the etherification feeds used here, the dominant ether is di-*n*-butyl ether, which possesses a boiling point below the diesel range (142°C versus 170-300°C). The other ethers produced contain predominantly one or no alkyl branches, since cross-etherification with 1-butanol leads to most ethers possessing at least one *n*-butyl fragment. The impact of alkyl branching on the high CNs typically associated with dialkyl ethers is largely unknown, though dibranched isobutyl ether (C_8) and isoamyl ether (C_{10}) notably still possess high cetane with values of 60 and 96, respectively.[47] The potential soot-reducing benefits of these ether mixtures must also be determined. It should additionally be noted that C_{12+} ethers (especially C_{28}-C_{32}) may be useful as synthetic lubricants, as several related physical properties of such compounds have been found to be superior to those of more conventional poly-α-olefin synthetic lubricants.[48] If ethers heavier than this are produced at certain conditions (e.g. when high Guerbet condensation conversions are used), they may therefore be valuable for as a diesel fuel blend. From a process perspective, the cost and nature of the individual separations must also be assessed. Water is detrimental in both reactors and therefore must be almost completely removed. As noted prior, detailed

technoeconomic analyses are required to understanding how this should be performed. With respect to Guerbet condensation chemistry, the fundamental causes of the conversion-selectivity tradeoff must also be better understood to rationally design new catalytic systems with higher activities and selectivities. Control over product branching is also desirable since it strongly affects the overall ether and olefin yields of the process. With respect to the etherification process, the identification and minimization of byproducts must be performed since these products account for approximately half of the total byproduct yield. Further investigation into the effect of temperature on etherification rates and selectivities with mixed linear/branched primary alcohol mixtures is also warranted. The activation barrier for etherification of linear primary alcohols is commonly found to be lower than that of unimolecular dehydration to olefins, though branching can affect this trend.[19,25,39] The temperature used here (150°C) was chosen to approximately balance selectivity and activity though further optimization is possible. The stability of the etherification catalyst in continuous operation also requires further investigation. In previous studies, the Amberlyst™ 70 catalyst has been shown to steadily deactivate with approximately 15% activity loss over 50 h TOS in the etherification of EtOH-octanol mixtures, though this was shown to be fully reversable upon the removal of water.[40] If this deactivation is an issue for economics, alternative solid acids may be used for selective etherification. In the present system, water plays a key role in decreasing reaction rates for both catalytic steps, thus the development of water-tolerant catalysts is also important to improving process economics. This may reduce separation costs and allow for the use of hydrous EtOH as the process input, further reducing costs.

5.5 Conclusions

Synthesis of diesel-range ethers from biomass-derivable alcohols was accomplished using two catalytic conversion stages: Guerbet coupling and intermolecular dehydration. The former

stage was performed using ethanol and 1-butanol with a calcium hydroxyapatite catalyst which remained stable for over 400h time-on-stream. Both feeds maintain alcohol selectivities above 80% up to about 40% conversion, above which side-reactions such as unimolecular dehydration to mono-enes and Lebedev condensation to dienes become more prominent. While these side-reactions are less severe at lower temperatures, operation at elevated conversions inherently lowers alcohols selectivities. In the second process stage, intermolecular dehydration using the acidic resin Amberlyst^{TM} 70 was shown to selectively convert linear primary alcohols to ethers at around 60% conversion, consistent with previous reports. The α-alkyl alcohols commonly produced in Guerbet coupling (e.g. 2-ethyl-1-butanol and 2-ethyl-1-hexanol) are much more selective to olefins, however. These olefins undergo rapid C=C isomerization to produce distributions dominated by the most thermodynamically-favorable regioisomers (e.g. internal olefins). The ethers produced are also broadly-distributed, in direct contrast to linear alcohol etherification which predominantly produces a single symmetric ether. The overall ether selectivity is directly correlated with the ratio of linear to branched alcohols in the feed. Lastly, etherification was performed using alcohols produced from ethanol condensation after removal of water and ethanol. These alcohols were successfully converted to ethers at 74% conversion with 72% selectivity alongside olefins at 10% selectivity. In a process involving ethanol coupling at 50% conversion, etherification at ~65% conversion, and recycle loops with separations, C_8-C_{16} ethers can be theoretically produced at a 62% yield. The olefins produced in the two stages can also be theoretically oligomerized and hydrogenated with proven technologies to jet-range paraffins with an overall estimated yield of 14%. Using this approach we show that distillate yields above 80% may be produced from ethanol. This study presents a novel technology for the conversion of

biomass-derived alcohols such as ethanol and 1-butanol to distillate-range molecules that overcomes some of the inherent challenges associated with current alcohol-to-distillate processes.

5.6 References

1 Eagan, N. M., Moore, B. M., McClelland, D. J., Wittrig, A. M., Canales, E., Lanci, M. P. & Huber, G. W. Catalytic synthesis of distillate-range ethers and olefins from ethanol through Guerbet coupling and etherification. *Green Chem.* **21**, 3300-3318, (2019).

2 Ogo, S., Onda, A. & Yanagisawa, K. Selective synthesis of 1-butanol from ethanol over strontium phosphate hydroxyapatite catalysts. *Appl. Catal. A-Gen.* **402**, 188-195, (2011).

3 Scalbert, J., Thibault-Starzyk, F., Jacquot, R., Morvan, D. & Meunier, F. Ethanol condensation to butanol at high temperatures over a basic heterogeneous catalyst: How relevant is acetaldehyde self-aldolization? *J. Catal.* **311**, 28-32, (2014).

4 Meunier, F. C., Scalbert, J. & Thibault-Starzyk, F. Unraveling the mechanism of catalytic reactions through combined kinetic and thermodynamic analyses: application to the condensation of ethanol. *CR Chim.* **18**, 345-350, (2015).

5 Tsuchida, T., Kubo, J., Yoshioka, T., Sakuma, S., Takeguchi, T. & Ueda, W. Reaction of ethanol over hydroxyapatite affected by Ca/P ratio of catalyst. *J. Catal.* **259**, 183-189, (2008).

6 Hanspal, S., Young, Z. D., Prillaman, J. T. & Davis, R. J. Influence of surface acid and base sites on the Guerbet coupling of ethanol to butanol over metal phosphate catalysts. *J. Catal.* **352**, 182-190, (2017).

7 Moteki, T. & Flaherty, D. W. Mechanistic insight to C–C bond formation and predictive models for cascade reactions among alcohols on Ca-and Sr-hydroxyapatites. *ACS Catal.* **6**, 4170-4183, (2016).

8 Davis, R. T., L.; Scarlata, C.; Tan, E.C.D.; Ross, J.; Lukas, J.; Sexton, D. Dilute-acid and enzymatic deconstruction of biomass to sugars and catalytic conversion of sugars to hydrocarbons. *National Renewable Energy Laboratory* (2015).

9 Huang, K., Won, W., Barnett, K. J., Brentzel, Z. J., Alonso, D. M., Huber, G. W., Dumesic, J. A. & Maravelias, C. T. Improving economics of lignocellulosic biofuels: An integrated strategy for coproducing 1,5-pentanediol and ethanol. *Appl. Energ.* **213**, 585-594, (2018).

10 Braden, D. J., Henao, C. A., Heltzel, J., Maravelias, C. C. & Dumesic, J. A. Production of liquid hydrocarbon fuels by catalytic conversion of biomass-derived levulinic acid. *Green Chem.* **13**, 1755-1765, (2011).

11 Tsuchida, T., Sakuma, S., Takeguchi, T. & Ueda, W. Direct synthesis of n-butanol from ethanol over nonstoichiometric hydroxyapatite. *Ind. Eng. Chem. Res.* **45**, 8634-8642, (2006).

12 Bailey, B., Eberhardt, J., Goguen, S. & Erwin, J. Diethyl ether (DEE) as a renewable diesel fuel. *SAE technical paper* (1997).

13 ASTM International. ASTM D975-17. *Standard specification for diesel fuel oils.* (2017).

14 García, A., Monsalve-Serrano, J., Heuser, B., Jakob, M., Kremer, F. & Pischinger, S. Influence of fuel properties on fundamental spray characteristics and soot emissions using different tailor-made fuels from biomass. *Energy Convers. Manage.* **108**, 243-254, (2016).

15 Damyanov, A., Hofmann, P., Geringer, B., Schwaiger, N., Pichler, T. & Siebenhofer, M. Biogenous ethers: production and operation in a diesel engine. *Automotive and Engine Technology* **3**, 69-82, (2018).

16 Miyamoto, N., Ogawa, H., Nurun, N. M., Obata, K. & Arima, T. Smokeless, low NOx, high thermal efficiency, and low noise diesel combustion with oxygenated agents as main fuel. *SAE transactions*, 171-177, (1998).

17 Nel, R. J. & de Klerk, A. Dehydration of C_5– C_{12} linear 1-alcohols over η-alumina to fuel ethers. *Ind. Eng. Chem. Res.* **48**, 5230-5238, (2009).

18 Dry, M. in *Stud. Surf. Sci. Catal.* Vol. 152 196-257 (Elsevier, 2004).

19 Bringué, R., Iborra, M., Tejero, J., Izquierdo, J. F., Cunill, F., Fité, C. & Cruz, V. J. Thermally stable ion-exchange resins as catalysts for the liquid-phase dehydration of 1-pentanol to di-n-pentyl ether (DNPE). *J. Catal.* **244**, 33-42, (2006).

20 Bringué, R., Tejero, J., Iborra, M., Izquierdo, J., Fité, C. & Cunill, F. Water effect on the kinetics of 1-pentanol dehydration to di-n-pentyl ether (DNPE) on Amberlyst 70. *Top. Catal.* **45**, 181-186, (2007).

21 Medina, E., Bringué, R., Tejero, J., Iborra, M. & Fité, C. Conversion of 1-hexanol to di-n-hexyl ether on acidic catalysts. *Appl. Catal. A-Gen.* **374**, 41-47, (2010).

22 Bringué, R., Ramírez, E., Iborra, M., Tejero, J. & Cunill, F. Kinetics of 1-hexanol etherification on Amberlyst 70. *Chem. Eng. J.* **246**, 71-78, (2014).

23 Pérez, M., Bringué, R., Iborra, M., Tejero, J. & Cunill, F. Ion exchange resins as catalysts for the liquid-phase dehydration of 1-butanol to di-n-butyl ether. *Appl. Catal. A-Gen.* **482**, 38-48, (2014).

24 Tejero, J., Fité, C., Iborra, M., Izquierdo, J. F., Cunill, F. & Bringué, R. Liquid-phase dehydrocondensation of 1-pentanol to di-n-pentyl ether (DNPE) over medium and large pore acidic zeolites. *Micropor. Mesopor. Mater.* **117**, 650-660, (2009).

25 Rorrer, J., Pindi, S., Toste, F. D. & Bell, A. T. Effect of Alcohol Structure on the Kinetics of Etherification and Dehydration over Tungstated Zirconia. *ChemSusChem* **11**, 3104-3111, (2018).

26 Ogo, S., Onda, A., Iwasa, Y., Hara, K., Fukuoka, A. & Yanagisawa, K. 1-Butanol synthesis from ethanol over strontium phosphate hydroxyapatite catalysts with various Sr/P ratios. *J. Catal.* **296**, 24-30, (2012).

27 PetroOrg Software (Florida State University: Tallahassee, FL, 2014).

28 Ho, C. R., Shylesh, S. & Bell, A. T. Mechanism and kinetics of ethanol coupling to butanol over hydroxyapatite. *ACS Catal.* **6**, 939-948, (2016).

29 Hanspal, S., Young, Z. D., Shou, H. & Davis, R. J. Multiproduct steady-state isotopic transient kinetic analysis of the ethanol coupling reaction over hydroxyapatite and magnesia. *ACS Catal.* **5**, 1737-1746, (2015).

30 Young, Z. D. & Davis, R. J. Hydrogen transfer reactions relevant to Guerbet coupling of alcohols over hydroxyapatite and magnesium oxide catalysts. *Catal. Sci. Technol.* **8**, 1722-1729, (2018).

31 Angelici, C., Weckhuysen, B. M. & Bruijnincx, P. C. Chemocatalytic conversion of ethanol into butadiene and other bulk chemicals. *ChemSusChem* **6**, 1595-1614, (2013).

32 Moteki, T., Rowley, A. T. & Flaherty, D. W. Self-terminated cascade reactions that produce methylbenzaldehydes from ethanol. *ACS Catal.* **6**, 7278-7282, (2016).

33 Bond, J. Q., Alonso, D. M., Wang, D., West, R. M. & Dumesic, J. A. Integrated catalytic conversion of γ-valerolactone to liquid alkenes for transportation fuels. *Science* **327**, 1110-1114, (2010).

34 Alcántara, R., Alcántara, E., Canoira, L., Franco, M. a. J., Herrera, M. & Navarro, A. Trimerization of isobutene over Amberlyst-15 catalyst. *React. Funct. Polym.* **45**, 19-27, (2000).

35 Yoon, J. W., Chang, J.-S., Lee, H.-D., Kim, T.-J. & Jhung, S. H. Trimerization of isobutene over a zeolite beta catalyst. *J. Catal.* **245**, 253-256, (2007).

36 Karas, L. & Piel, W. Ethers. *Kirk-Othmer Encyclopedia of Chemical Technology*, (2004).

37 Tejero, J., Cunill, F., Izquierdo, J., Iborra, M., Fité, C. & Parra, D. Scope and limitations of mechanistic inferences from kinetic studies on acidic macroporous resins The MTBE liquid-phase synthesis case. *Appl. Catal. A-Gen.* **134**, 21-36, (1996).

38 Guilera, J., Bringué, R., Ramírez, E., Fité, C. & Tejero, J. Kinetic study of ethyl octyl ether formation from ethanol and 1-octanol on Amberlyst 70. *AlChE J.* **60**, 2918-2928, (2014).

39 Song, W., Liu, Y., Barath, E., Wang, L. L., Zhao, C., Mei, D. & Lercher, J. A. Dehydration of 1-octadecanol over H-BEA: a combined experimental and computational study. *ACS Catal.* **6**, 878-889, (2016).

40 Guilera, J., Ramírez, E., Fité, C., Iborra, M. & Tejero, J. Thermal stability and water effect on ion-exchange resins in ethyl octyl ether production at high temperature. *Appl. Catal. A-Gen.* **467**, 301-309, (2013).

41 Hoek, I., Nijhuis, T., Stankiewicz, A. & Moulijn, J. Kinetics of solid acid catalysed etherification of symmetrical primary alcohols: zeolite BEA catalysed etherification of 1-octanol. *Appl. Catal. A-Gen.* **266**, 109-116, (2004).

42 Rorrer, J., He, Y., Toste, F. D. & Bell, A. T. Mechanism and kinetics of 1-dodecanol etherification over tungstated zirconia. *J. Catal.* **354**, 13-23, (2017).

43 Gibbs, L., Anderson, B., Barnes, K., Engeler, G., Freel, J., Horn, J., Ingham, M., Kohler, D., Lesnini, D., MacArthur, R., Mortier, M., Peyla, D., Taniguchi, B., Tiedemann, A., Welstand, S., Bernhardt, D., Collini, K., Farr, A., Jones, J., Lind, J., Tom, C. & Benson, J. Motor gasolines technical review. *Chevron Products Company*, (2009).

44 Dagle, V. L., Smith, C., Flake, M., Albrecht, K. O., Gray, M. J., Ramasamy, K. K. & Dagle, R. A. Integrated process for the catalytic conversion of biomass-derived syngas into transportation fuels. *Green Chem.* **18**, 1880-1891, (2016).

45 Martens, J. A., Ravishankar, R., Mishin, I. E. & Jacobs, P. A. Tailored alkene oligomerization with H-ZSM-57 zeolite. *Angew. Chem. Int. Ed.* **39**, 4376-4379, (2000).

46 Douglas, J. A hierarchical decision procedure for process synthesis. *AlChE J.* **31**, 353-362, (1985).
47 Yanowitz, J., Ratcliff, M., McCormick, R., Taylor, J. & Murphy, M. Compendium of experimental cetane numbers. *National Renewable Energy Laboratory* (2017).
48 Jadhav, D., Grippo, A. M., Shylesh, S., Gokhale, A. A., Redshaw, J. & Bell, A. T. Production of Biomass-Based Automotive Lubricants by Reductive Etherification. *ChemSusChem* **10**, 2527-2533, (2017).

5.7 Supplemental information

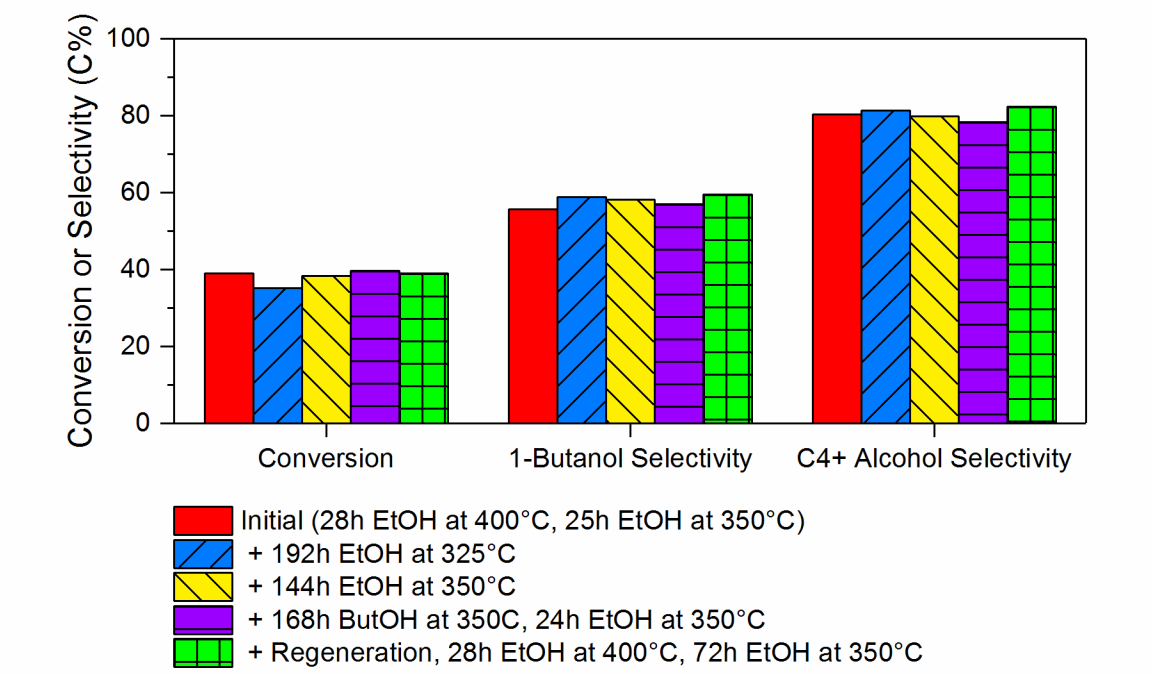

Figure S5.1 |**Replication of a base set of conditions after a series of parameter changes.** Base conditions: 350°C, 1050 s kg_{HAP} $mol_{ethanol}^{-1}$, 8 kPa ethanol, 93 kPa H_2.

Table S5.1. | **Product distribution from Guerbet coupling of ethanol and 1-butanol with HAP.** The letter "n" corresponds to the feed alcohol chain length (n=2 for ethanol and n=4 for 1-butanol). Conditions: 350°C, 520 s kg_{HAP} $mol_{alcohol}^{-1}$, 8 kPa alcohol, 93 kPa H_2.

Feed alcohol:	ethanol	1-butanol
Conversion (%)	26.5	14.8
Selectivity (C%)		
C_n Aldehydes	2.6	20.5
C_n Olefins	1.5	3.7
C_{2n} Ethers	0.5	1.3
C_{2n+} Alcohols	82.3	64.6
1-butanol	66.1	-
1-hexanol	5.3	-
2-ethyl-1-butanol	6.4	-
2-ethyl-1-hexanol	0.9	60.5
butenols	3.5	-
2-ethylhexenols	-	4.1
C_{2n} Aldehydes[a]	0.8	4.0
C_{2n} Olefins	3.7	3.9
C_{2n} alkenes	0.5	1.0
C_{2n} dienes	3.2	2.9
Other detectable species	8.6	2.0

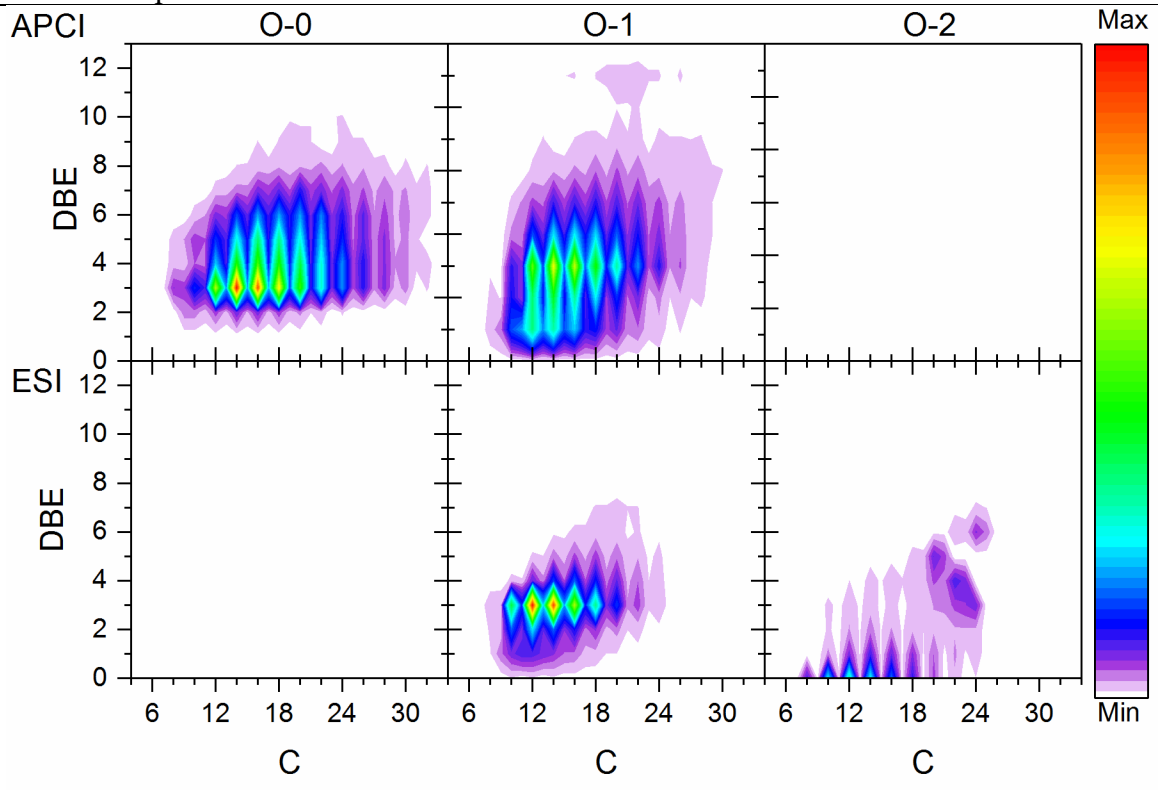

Figure S5.2 | **FT-ICR-MS compositional heat maps of products from ethanol coupling at 375°C using either APCI or Na-ESI ionization.**

Table S5.2 | **Assignment of C-O carbons in nine ethers identified via HSQC and HMBC experiments.** Hypothesized structures of main ethers presented based on proposed mechanism.

Ether #	Relative Abundance (C%)	O-C Multiplicities	$Q^{13}C$ Chemical Shift (ppm)	Hypothesized Structure
1	45.2	CH_2	73.93	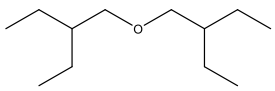
2	18.3	CH_2 C	62.63 76.01	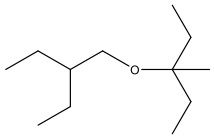
3	10.7	CH_2 CH	71.22 79.19	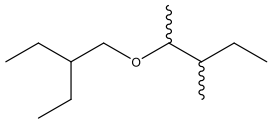
4	8.8	CH_2 CH	71.12 79.61	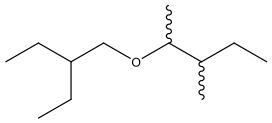
5	5.9	CH_2 CH	64.91 70.91	-
6	5.2	CH_2 CH	71.29 81.02	-
7	3.8	CH_2 CH_2	68.93 74.39	-
8	1.5	CH_2 CH_2	70.22 71.41	-
9	0.6	CH_2 CH	55.63 63.11	-

Table S5.3 | **Structure of symmetric ether of 2-ethyl-1-butanol determined by NMR (ether 1 from Table S5.2).**

Carbon	Structure	$Q^{13}C$ Chemical Shift (ppm)	Identification
A	CH_3	11.63	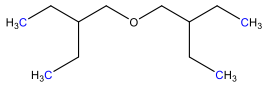
B	CH_2	24.49	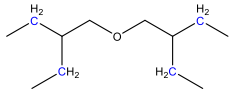
C	CH	42.59	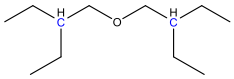
D	O-CH_2	73.93	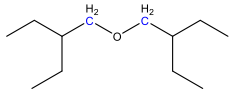

Table S5.4 | **Model-predicted compositions of four-component alcohol etherification feeds based on ethanol condensation.**

Guerbet Ethanol Conversion (%)	20	50	67	80
Linear:Branched Ratio	12.5	5.3	3.2	2.0
Composition (mol%)				
1-butanol	89.8	73.3	62.7	52.3
1-hexanol	4.7	10.8	13.5	14.9
2-ethyl-1-butanol	4.9	12.3	16.9	21.5
2-ethyl-1-hexanol	0.5	3.5	6.9	11.3

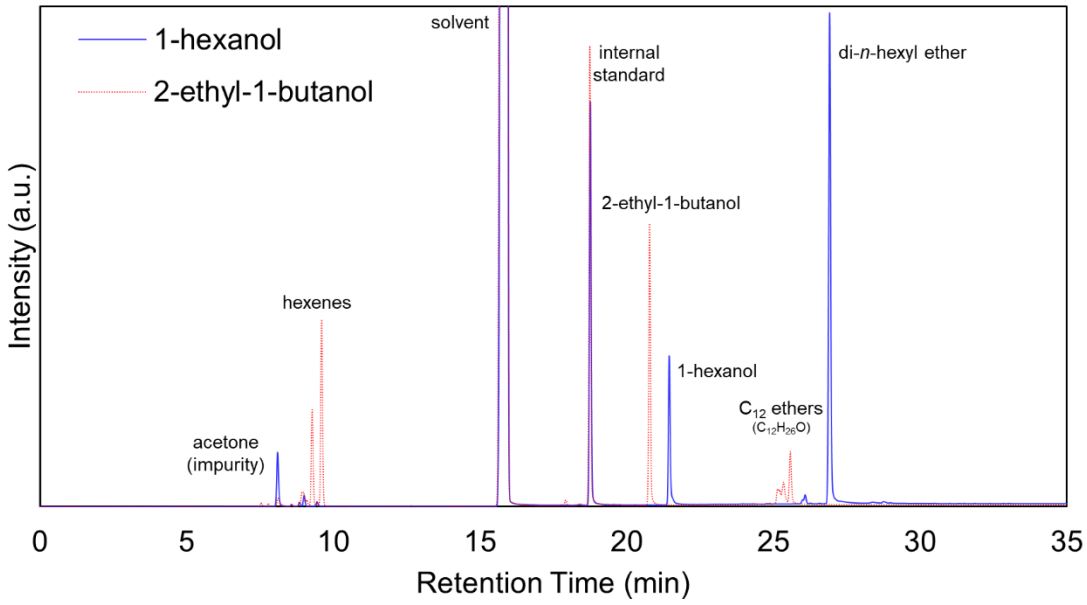

Figure S5.3 | **GC-FID chromatograms of etherification products from 1-hexanol and 2-ethyl-1-butanol feeds.** Conditions: 15 g alcohol, 0.75 g Amberlyst^{TM} 70, 150°C, 24h.

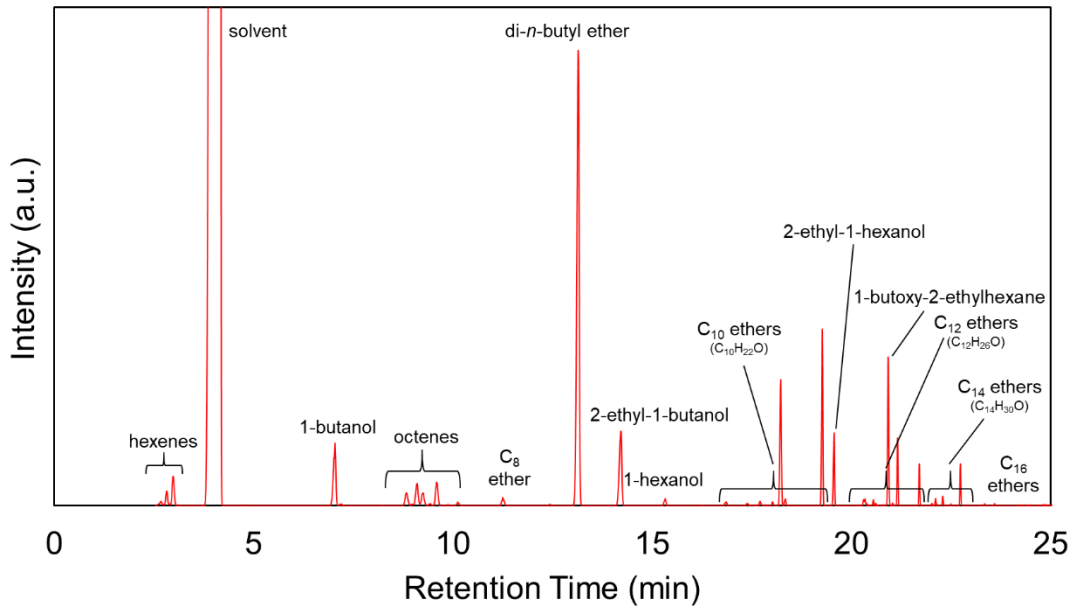

Figure S5.4 | **GC-MS-FI chromatograms of etherification production from mixed-alcohol feed based on ethanol condensation products at 80% conversion.** Conditions: 15 g alcohols, 0.75 g Amberlyst^{TM} 70, 150°C, 24h.

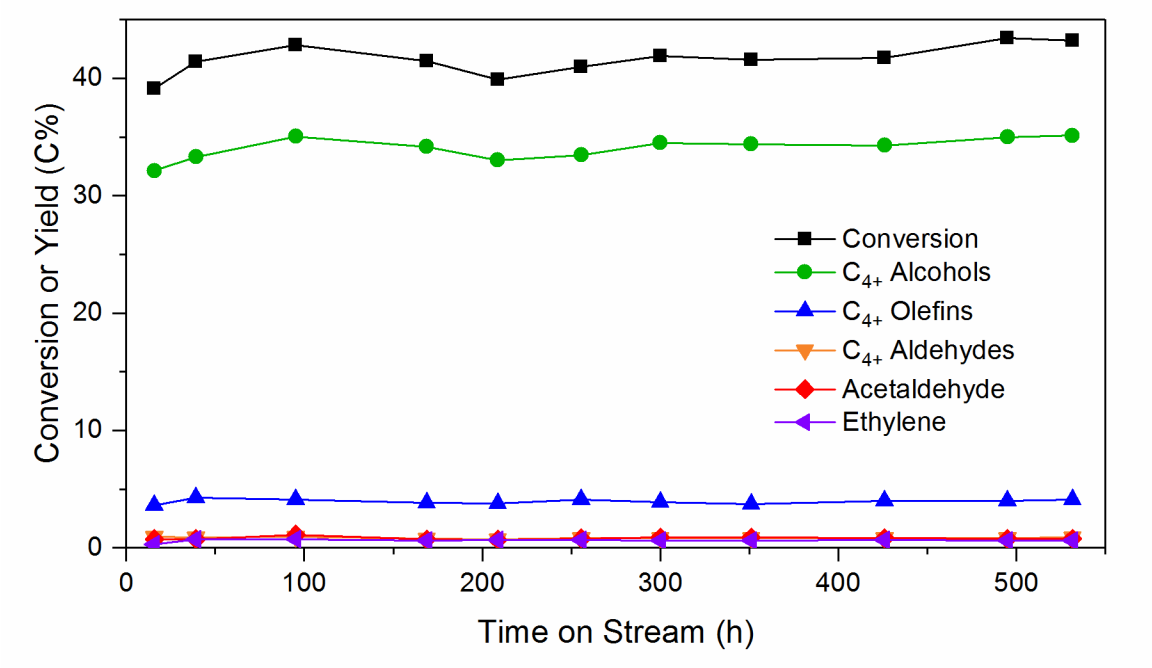

Figure S5.5 | **Guerbet conversion of ethanol versus time on stream at the conditions utilized to make an etherification feed.** Conditions: 350°C, 8 kPa ethanol, 93 kPa H_2, 1400 s kg_{HAP} mol_{EtOH}^{-1}, 6.0g HAP.

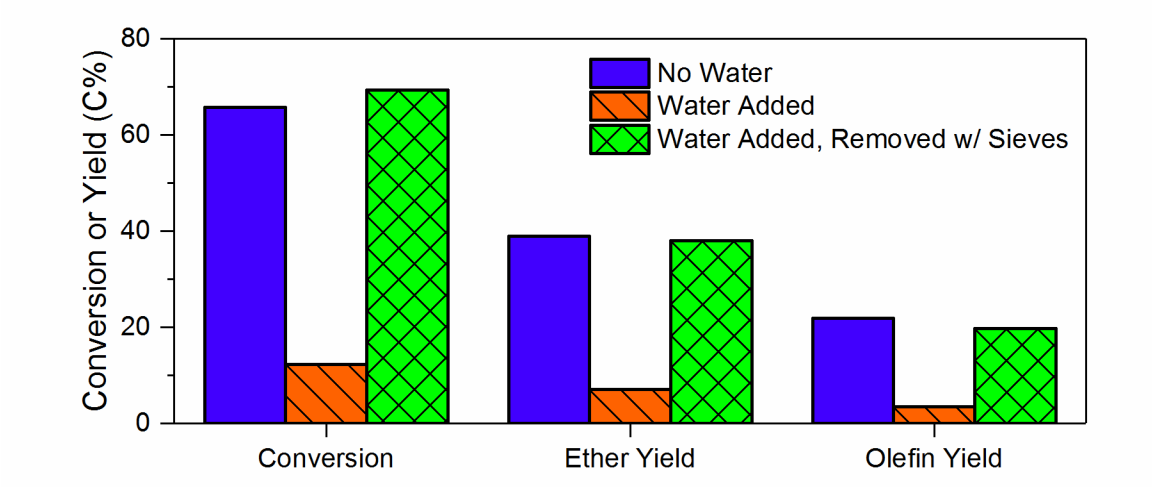

Figure S5.6 | **The effect of added water on the conversion of an equimolar mixture of 1-butanol and 2-ethyl-1-hexanol (15g).** 1.2g of water added, corresponding to 7.4 wt% overall. Feed containing water mixed with 3A molecular sieves (2:1 mass basis) overnight and filtered to remove water. Conditions: 0.75 g Amberlyst™ 70, 150°C, 24h.

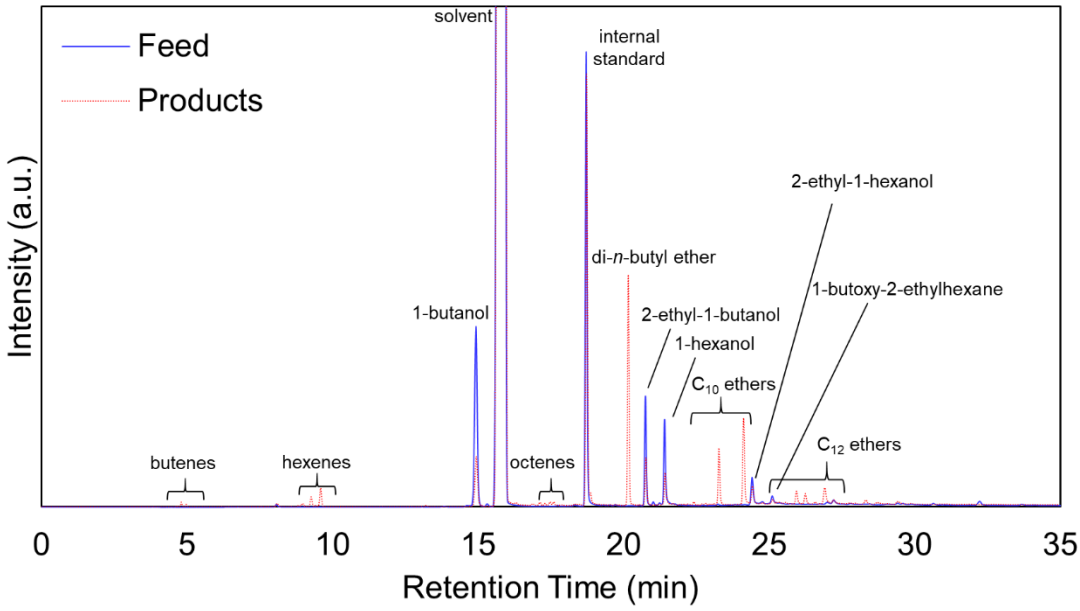

Figure S5.7 | **GC-FID chromatograms of the ethanol-derived etherification feed and products.** Conditions: 15 g alcohols, 0.75 g Amberlyst^{TM} 70, 150°C, 24h.

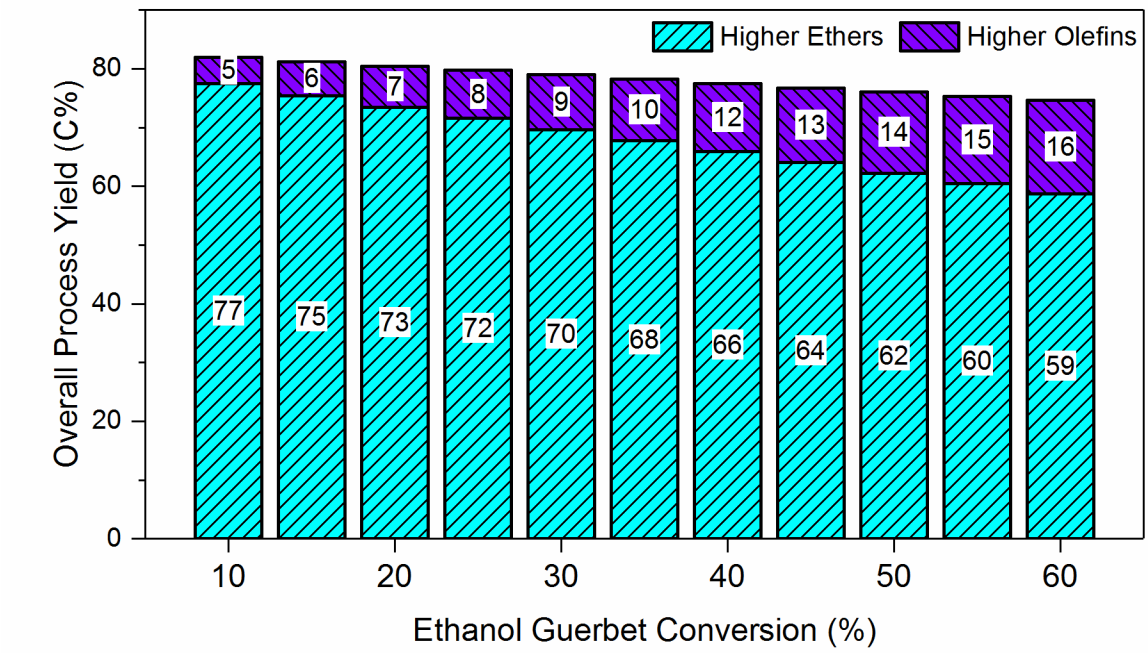

Figure S5.8 | **Overall process selectivities to diesel-range ethers or jet-range olefins as a function of ethanol conversion.** These are calculated based on correlations between ethanol conversion and Guerbet product distributions (alcohol selectivity, olefin selectivity, linear:branched alcohol ratio) and correlations between etherification product distributions and the linear:branched alcohol ratio of the feed alcohols.

Mass transport limitation calculations for ethanol coupling

The possibility that reaction rates were limited by heat or mass transport was examined through evaluation of several transport criteria which must be satisfied to ensure that this is not the case. These criteria have been notably applied and discussed by Shabaker et al. The criteria considered and their evaluations are shown below. Descriptions and approximations for each parameter are also provided. Ethanol condensation to 1-butanol and water was assumed to be the main reaction when one was required for estimation purposes, such as for the absolute heat of reaction. For parameters which were not measured, worst-case approximations were assumed (e.g. a high activation barrier, low particle thermal conductivity, high rate order). The calculations were performed based on ethanol conversion at 350°C with a contact time of 525 s kg_{HAP} mol^{-1} at which 26.5% conversion was achieved. **In all cases, the tests were satisfied by multiple orders of magnitude.**

J.W. Shabaker, R.R. Davda, G.W. Huber, R.D. Cortright, J.A. Dumesic, Aqueous-phase reforming of methanol and ethylene glycol over alumina-supported platinum catalysts, J. Catal. 215 (2003) 344-352.

Table S5.5 | **Transport limitation calculations for EtOH conversion over Cu/AlMgO.**

Test	Equation	Evaluation
Interphase heat transport	$\frac{q\,\mathscr{R} r_p}{h\,T_B} < 0.15\frac{R\,T_B}{E}$	$1.96 * 10^{-6} \ll 7.77 * 10^{-3}$
Intraparticle heat transport	$\frac{q\,\mathscr{R} r_p^2}{\lambda\,T_S} < 0.75\frac{R\,T_S}{E}$	$1.89 * 10^{-6} \ll 3.89 * 10^{-2}$
Interphase mass transport	$\frac{\mathscr{R} r_p^2}{C_b k_c} < \frac{0.15}{n}$	$2.35 * 10^{-9} \ll 7.50 * 10^{-2}$
Intraparticle mass transport	$\frac{\mathscr{R} r_p^2}{C_s D_{eff}} < 0.3$	$2.63 * 10^{-5} \ll 3.00 * 10^{-1}$

Parameter	Definition	Approximate Value
q	Absolute heat of reaction	$21{,}517\ J\ mol^{-1}\ ethanol$
$\mathscr{R}$	Rate per particle volume	$0.456\ mol\ m^{-3}\ s^{-1}$
r_p	Catalyst particle radius	$1.25 * 10^{-4}\ m$
R	Gas constant	$8.314\ J\ mol^{-1}K^{-1}$
T_B	Bulk temperature	$623.15\ K$
T_S	Catalyst surface temperature	$623.15\ K$
h	Heat transfer coefficient	$1000\ W\ m^{-2}K^{-1}$
E	Activation barrier	$100{,}000\ mol^{-1}K^{-1}$
λ	Thermal conductivity of catalyst particle	$0.13\ W\ m^{-1}\ K^{-1}$
C_b	Bulk concentration of ethanol	$1.51\ mol\ ethanol\ m^{-3}$
C_s	Ethanol surface concentration	$1.51\ mol\ ethanol\ m^{-3}$
k_c	Surface-bulk mass transfer coefficient	$2.0\ m\ s^{-1}$
n	Rate order	2
D_{eff}	Effective diffusivity	$1.79 * 10^{-4}\ m^2\ s^{-1}$

Chapter 6. Kinetic Modeling of Steady-State Alcohol Oligomerization over Calcium Hydroxyapatite

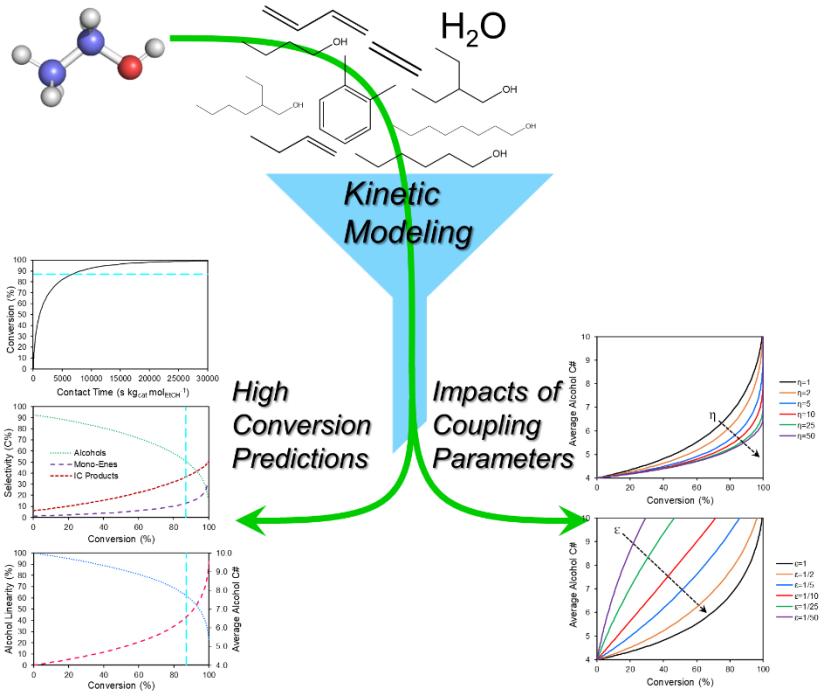

Figure 6.1 | **Kinetic modeling of ethanol coupling over hydroxyapatite.**

6.1 Introduction

In the previous chapter, the selective oligomerization of ethanol (EtOH) to C_{10+} distillate-range alcohols over calcium hydroxyapatite (HAP) was shown to be limited by the decreasing reaction rates and alcohol selectivities observed with increasing conversion. These phenomena were thought to be linked to inhibition by water as well as the slow rates of branched alcohol coupling. A more quantitative understanding of these effects is important in assessing the fundamental limitations behind using Guerbet coupling for EtOH oligomerization. Doing so requires bridging the gap between two key experimental regimes in catalysis: the regime where studies can most appropriately yield fundamental insights into the underlying catalysis and the regime where the chemistry can be most suitably applied in a technological setting. The former

often involves lower conversions (<20%), lower temperatures (to improve selectivities), and shorter reaction times where side-reactions and catalyst stability are not substantial concerns. The latter alternatively often involves higher conversions (>80%), higher temperatures (to improve rates), and longer reaction times where catalyst stability and separation costs can ultimately determine whether a process is viable. Oftentimes, major concerns in the latter regime are not apparent in the former or are not sufficiently prevalent to be considered significant.

In the present case, fundamental insights into EtOH coupling over HAP are informed by the studies of Bell,[1] Flaherty,[2] Davis,[3,4] Tsuchida,[5] Onda,[6] and Meunier.[7,8] While these inform how EtOH coupling mechanistically occurs (e.g. notions of hydrogen transfer and the roles of aldehydes), they do not generally address inhibition effects or side-reaction kinetics. High-conversions near 50% were studied by Moteki and Flaherty,[2] but at a moderately low temperature of 275°C which necessitated a very high contact time of 23,000 s kg_{cat} mol_{EtOH}^{-1}.[9] For perspective, the demonstration-scale methanol-to-olefins process mentioned in Chapter 3 operates at a contact time of only 20 s kg_{cat} $mol_{methanol}^{-1}$. Operating at higher temperatures where side reactions are prevalent is therefore likely necessary. In the absence of such complications, Moteki and Flaherty found that a step-growth oligomerization model can be used to directly connect EtOH conversion to the distribution of carbon chain lengths in the alcohols produced.[2] The chain length distribution still follows step-growth trends at higher temperatures (at least up to 20% conversion),[5] but it cannot be directly linked to conversion since EtOH is consumed via reactions other than coupling. At conversion above 50%, the substantial amounts of low-reactivity α-branched alcohols are also expected to slow coupling reactions and will likely cause deviations from step-growth predictions. Understanding how branching changes with conversion and how this may limit further coupling is therefore important in modeling elevated EtOH conversions. The impact of water on coupling

rates is also essential. Hanspal et al. showed that co-feeding 6 kPa water with 6 kPa EtOH fully inhibited EtOH coupling, though activity was mostly recovered when water was removed from the feed.[4] This 1:1 EtOH:water ratio reflects the amount of water produced at ~50% conversion, thus it is unclear to what extent water produced throughout oligomerization impacts reactivity. This also must be understood in order to utilize aqueous EtOH feeds, which may help to improve process economics by reducing separation costs associated with surpassing the EtOH-water azeotrope. These costs would be amplified by operating at low EtOH conversions where separation/recycle loops are necessary.

The purpose of this study is to use kinetic modeling to understand how phenomena observed in the low-conversion regime impact performance at elevated conversions where heavier alcohols can be produced. Specifically, this helps to understand how inhibition by water and the low coupling reactivity of branched alcohols impact the feasibility of performing direct EtOH oligomerization to C_{10+} distillate-range alcohols using HAP. These findings can then be extended to provide guidance for the development of new catalytic systems.

6.2 Experimental methods

6.2.1 Alcohol oligomerization methods

Alcohol oligomerization was performed in stainless-steel fixed-bed reactors (40 cm long, 0.95 cm outer diameter). Calcium hydroxyapatite (HAP, Acros Organics) was pelletized and sieved to a particle size of 350-600 μm and subsequently calcined in static air at 480°C for 2h after a 2°C min^{-1} ramp. The HAP was then diluted in 350-600 μm SiO_2 (Sigma Aldrich) and loaded into the reactor above inert layers of quartz wool and coarse SiO_2 (850-1750 μm). The temperature of the reactor was measured at the center of the bed using an internal thermocouple and was controlled using a tube furnace (Lindberg Blue M Mini-Mite) oriented vertically. Prior to reaction, the

catalyst was pretreated in flowing air (70 mL min^{-1}) at 500°C for 2h after a 2°C min^{-1} ramp. The reactor temperature was then set to 400°C. EtOH (and other liquid feeds) were fed via syringe pump (Teledyne ISCO 500D) downflow concurrently with argon into a preheated region (1/4" tubing packing with coarse SiO_2) kept above 200°C to ensure full evaporation of the feed alcohol prior to reaching the reactor. This feed was then fed into the reactor in the downflow configuration. Beneath the reactor, the products were directed to one of two 110 mL glass condensers kept cold in an ice bath. These condensers were typically filled with 15 mL 1-propanol prior to attachment to the system in order to minimize sample weight errors at low flow rates. Condensers were periodically removed and their contents sampled. The gas exiting the condensers was sent to a bubble flow meter for flow rate measurement or to an online gas chromatograph (GC) equipped with a flame-ionization detector (FID). Liquid products were further diluted in a 1-propanol solution containing 1-pentanol as an internal standard (~1 wt%) and analyzed via GC-FID. Retention times and response factors for each species were determined through external calibration curves when standards were available. When species could be confidently identified via GC with mass spectrometry (MS), their response factors were estimated using effective carbon number approximations.[10] For the first 27 h, EtOH was converted at 400°C with a contact time of 70 s kg_{cat} mol_{EtOH}^{-1} to reach a steady-state after an initial deactivation period. This ensures that subsequent data collection at 350°C would be free of deactivation when parameters were manipulated, as previously noted in Chapter 5. At each set of conditions discussed here, a minimum of 4 data points were collected over a 24h period to ensure that steady states were achieved. Reported data are averages over the latter three time points. Yields (Y_i) are reported on a carbon basis. The yield of unidentified species detected via GC was approximated based upon the unidentified GC area, the area of the identified products, and the yield of the identified products. Conversion (X) is reported

based on the sum of these yields (including unidentified species). Selectivity is defined on a carbon basis as yield divided by conversion.

6.3 Results and discussion

6.3.1 Ethanol oligomerization: observations with increasing contact time

The oligomerization of EtOH was first examined over a wide range of contact times (8.7-2102.0 s kg_{HAP} mol_{EtOH}^{-1}) at 350°C to illustrate how the alcohol distribution, by-product selectivities, and conversion change. Figure 6.2a shows conversion and yields to various products and product categories as a function of contact time. The conversion increases from 3.0% to 60.0% over this range, thus the rate of EtOH consumption must decrease with conversion by a greater extent than can be attributed to decreasing EtOH concentrations (see Figure S3.1 for details). As noted prior, this decrease is likely related to inhibition by products such as water. Figure 6.2b shows higher alcohols to be the major products across this range, increasing from 60% selectivity at 3.0% conversion to 82% at 11.5% conversion before decreasing to 70.2% at 60.0% conversion. The initial increase coincides with a decrease in acetaldehyde (AcAl) selectivity, the initial species formed from EtOH in the formal Guerbet coupling pathway.

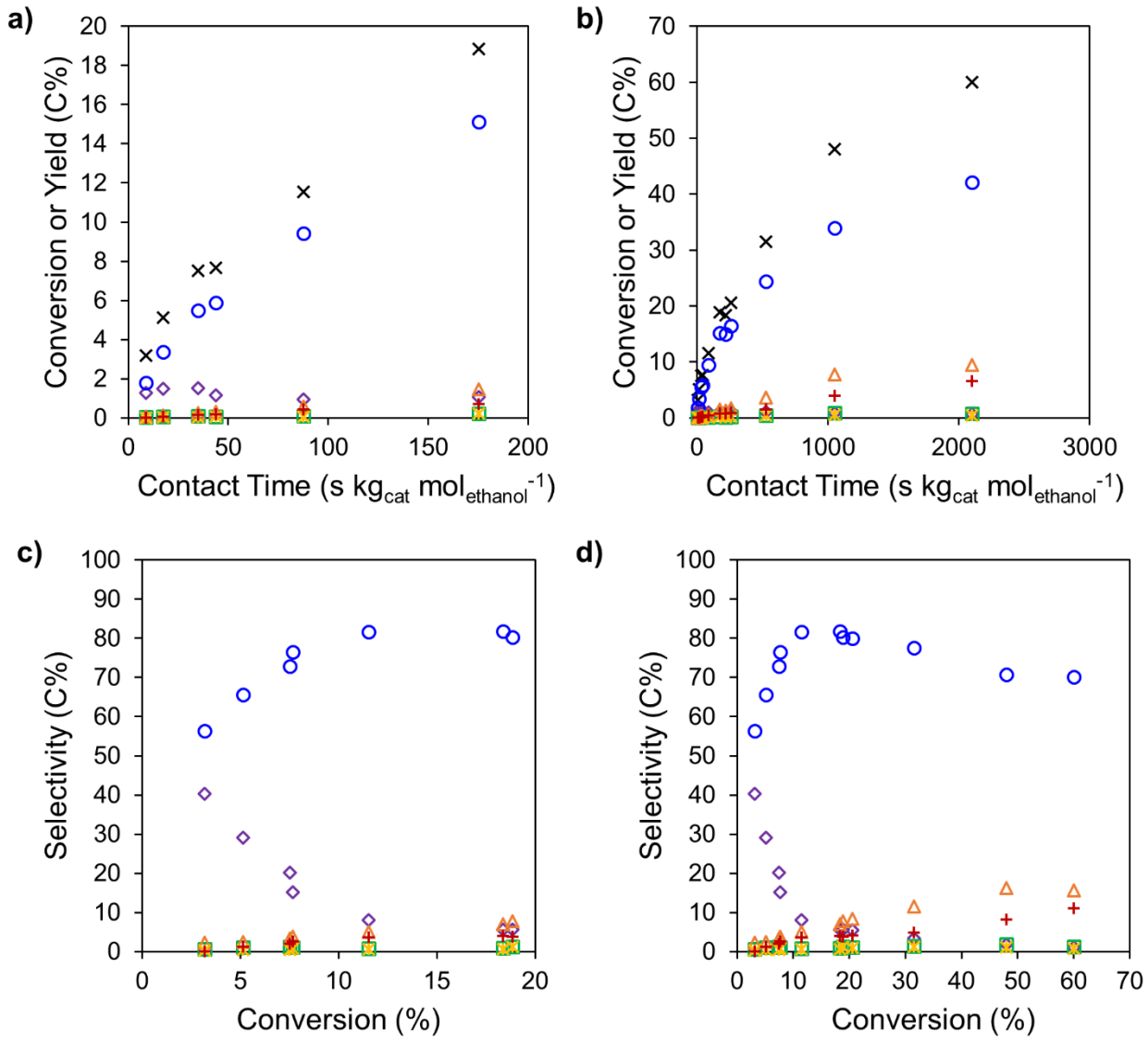

Figure 6.2 | **Ethanol oligomerization as a function of contact time. a,b |** Conversion and category yields *versus* contact time. **c,d |** Category selectivities *versus* conversion. (×) conversion, (◇) acetaldehyde, (○) higher alcohols, (□) higher aldehydes, (△) olefins, (✳) ethers, (+) other. Conditions: 350°C, 7.8 kPa ethanol, 93.5 kPa argon, 8.7-2102.0 s kg_{cat} $mol_{ethanol}^{-1}$.

The AcAl yield is fairly steady with a slow decline from 1.5 to 0.6% between 5 and 60% conversion, leading to a nearly constant EtOH:AcAl ratio of ~70. Ho et al. found that this nearly constant yield may result from the balanced kinetics of EtOH dehydrogenation and AcAl coupling above ~2% EtOH conversion at 330°C.[1] The destination of the abstracted H is unclear, however, since HAP cannot catalyze H-H recombination to a substantial extent[1,2,5,11], and no aldehydes are

initially present to act as H-acceptors through intermolecular Meerwein-Verley-Ponndorf (MPV) transfers. Such MPV transfers are generally thought to be responsible for the hydrogenation of coupling intermediates (e.g. crotonaldehyde), however.[1,3,11,12] Given that these reactions are known to be faster than coupling[13] and that they are not accompanied by large free energy changes ($\Delta G_{350°C} \sim$ -0.6 kJ mol^{-1} for EtOH + butyraldehyde → AcAl + 1-butanol), it is likely that these MPV reactions are equilibrated. Alcohols and their respective aldehydes are therefore likely in pseud-equilibria dictated by (1) the initial steady EtOH:AcAl ratio achieved from balancing dehydrogenation and coupling rates and (2) the different free energy changes for dehydrogenation of different alcohols. Based on this understanding, the theoretical butanol-butyraldehyde ratio would be ~62, fairly consistent with the ratio of ~55 observed at all conversions where butyraldehyde could be detected.

The distribution of alcohols as a function of conversion is shown in Figure 6.3. Butanols, which include 1-butanol, 2-buten-1-ols, and 3-buten-1-ol, are the most dominant alcohols below 50% conversion, above which hexanols and ethylbutanols become dominant. Ethylbutanols are produced in a slight excess *versus* hexanols at all conversions, consistent with previous reports.[2,5] Ethylhexanols are the major C_8 alcohols, produced either from the coupling of two butanols or of a hexanol nucleophile and an ethanol electrophile. 1-Octanol, on the other hand, can only be formed through the coupling of an ethanol nucleophile and a hexanol electrophile, thus the preferential formation of the branched C_8 alcohol is expected due to the low concentrations of 1-hexanol relative to 1-butanol.

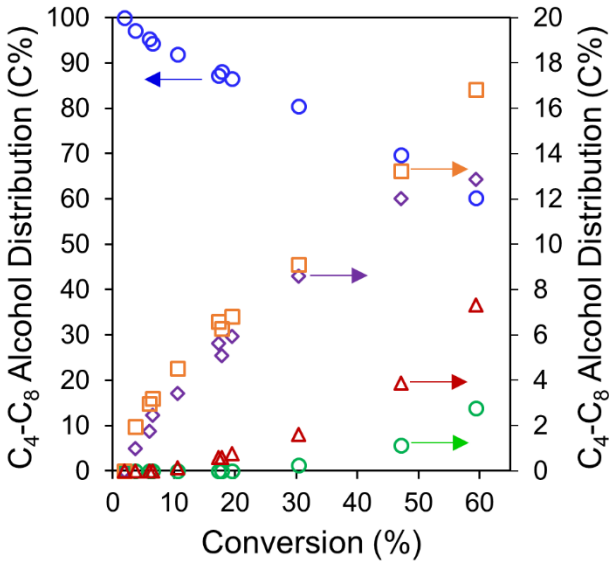

Figure 6.3 | **Alcohol distribution as a function of conversion.** Alcohols: (○) butanols, (◇) hexanols, (○) octanols, (□) 2-ethyl-1-butanols, (△) 2-ethyl-1-hexanols. Butanol values shown on left axis, all other alcohols correspond to values on right axis. Conditions: 350°C, 7.8 kPa ethanol, 93.5 kPa argon, 8.7-2102.0 s kg_{cat} $mol_{ethanol}^{-1}$.

As noted prior, the carbon-number distribution of the alcohols can often be described by step-growth kinetics—coupling wherein the rate constants of all coupling reactions are equal.[2,5] According to these kinetics, the alcohol distribution can be described by Equation 6.1 where y_n is the mole fraction of oligomer n and α is the alcohol oligomerization probability.

Equation 6.1 $$y_n = (1-\alpha)\alpha^{n-1}$$

By plotting $\log(y_n)$ *versus* $n-1$ the α value which describes the alcohol distribution can be obtained from the slope. This parameter increases linearly with conversion as shown in Figure 6.4. As noted by Moteki and Flaherty[2], α can be linked to conversion according to Equation 6.2. This should be taken as the maximum alpha value allowable by step-growth kinetics, since this assumes that EtOH is only consumed via alcohol coupling reactions.

Equation 6.2 $$\alpha_{max} = 1 - \sqrt{1-X}$$

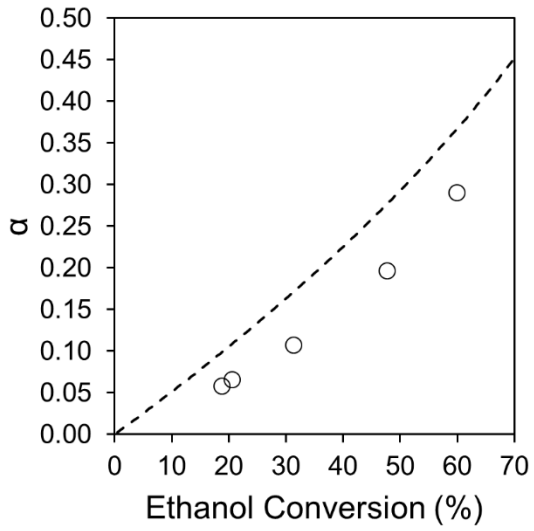

Figure 6.4 | **Step growth probability α as a function of ethanol conversion.** Circles show experimental data obtained at 350°C with 7.8 kPa ethanol in argon, dotted line shows maximum theoretical α in the absence of side-reactions.

The experimentally observed α values are consistently below α_{max}, which may be explained either by a deviation from step-growth kinetics or by the increasing prevalence of side reactions at elevated conversions. Determining which requires rigorously modeling side-reactions and how they are affected relative to coupling reactions by increasing conversions.

Side reactions become more prevalent at higher conversions as noted previously in Chapter 5. The resulting products generally consist of mono-enes formed from unimolecular dehydration, dienes presumably formed from Lebedev condensation, aromatics formed from oligomerization and cyclization of alkenals, and unidentified species which could not be confidently identified. Products which fall into this last category are broadly distributed and generally suggested by GC MS to be highly unsaturated hydrocarbons and oxygenates presumably formed in the same manner as identifiable dienes and aromatics—through coupling reactions interrupted prior to alcohol formation. The FT-ICR-MS data shown previously in Figure S5.2 also support this assignment. Side-products can therefore be generally put into one of two categories: those which are formed through condensation reactions and those which are not. The former can be thought to share the

same rate-limiting formation step as alcohol coupling, while the latter form via different mechanisms entirely.

The general pathway for alcohol conversion over HAP can therefore be simplified according to Figure 6.5. A generic alcohol (alcohol 1) can either be dehydrated to a mono-ene (e.g. EtOH to ethylene) or reversibly dehydrogenated (e.g. EtOH to AcAl). The aldehyde undergoes deprotonation, which is generally considered to be the rate-limiting step in coupling. The resulting enolate then attacks another aldehyde (aldehyde 2) through aldol condensation to produce an alkenal. This is then hydrogenated (presumably via MPV transfer) to an alkenol. This may then undergo keto-enol tautomerization to an aldehyde and subsequent C=O hydrogenation[1] or direct C=C hydrogenation by surface H (not pictured).[2] The alkenol, aldehyde, and alcohol will be considered here as products of successful Guerbet coupling. The alkenal produced from aldol condensation can instead undergo further oligomerization reactions and a combination of dehydration and cyclization to form trienes and aromatics. Alkenols can also be dehydrated to form dienes through a Lebedev-type reaction scheme. All such products are described here as products of "interrupted coupling", or IC. This product grouping will be central to the development of a kinetic model discussed in further detail later.

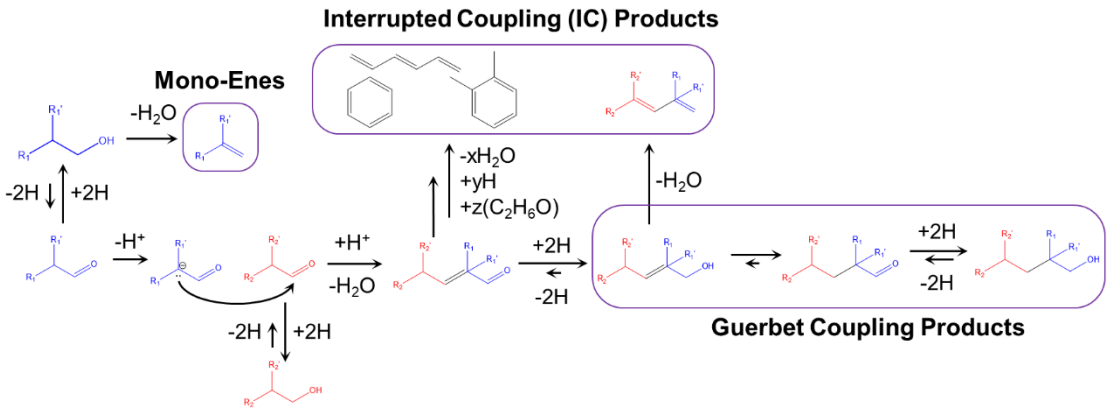

Figure 6.5 | **Alcohol conversion pathways over HAP.** An alcohol (1,blue) can either dehydrate to a mono-ene or dehydrogenate reversibly to an aldehyde. This aldehyde can then be deprotonated to attack an electrophile aldehyde (2,red) in concerted aldol condensation to produce an alkenol and water. Guerbet coupling products are then formed via a series of hydrogen transfer and isomerization reactions. Side reactions after the aldol condensation step instead lead to dienes, trienes, and aromatics, grouped here as "interrupted coupling" (IC) products.

6.3.2 Detrimental effects of water on selective ethanol coupling

The impact of water on reaction rates must be understood to properly model the kinetics as a function of conversion. Water was cofed with 7.8 kPa EtOH at partial pressures ranging from 0.3-3.0 kPa with the conversion maintained near 10% conversion by adjusting the EtOH contact time. Figure 6.5a shows that the EtOH coupling rate decreases with the addition of water rapidly at first and then more steadily past 1.2 kPa. Returning to a feed without water present fully restores catalytic activity. These results indicate that water-induced inhibition is due to site blocking rather than irreversible site reconstruction. These data also notably suggest that the amount of water produced by ~10% conversion is sufficient to decrease EtOH coupling rates by ~50%. Figure 6.5b shows that EtOH dehydration also decreases, though to a lesser extent than coupling. This discrepancy may be the cause for the increase in ethylene selectivity observed with increasing conversion. Figure 6.5c also shows that the fraction of EtOH coupling which goes to 1,3-butadiene rather than C_{4+} alcohols and aldehydes increases with increasing water content. This suggests that full alkenal hydrogenation is inhibited by the presence of water more-so than partial hydrogenation

and dehydration to form a diene. This would explain the increasing selectivity to IC products with increasing conversion. Altogether, these findings help to develop rate expressions which can be used to describe the rates of dehydration, Guerbet coupling, and IC as a function of conversion.

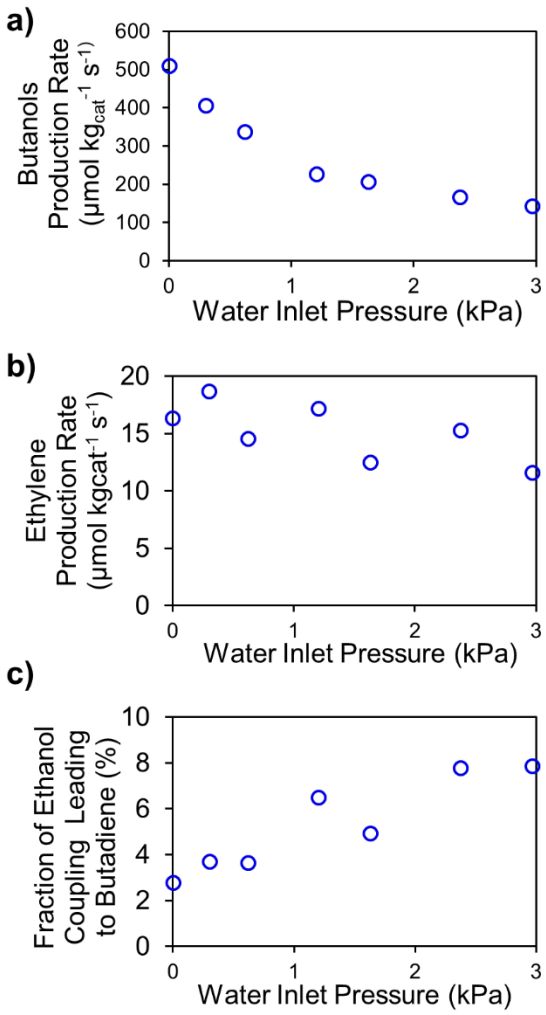

Figure 6.6 | **The impact of water feed content on ethanol conversion. a |** The apparent rate of ethanol coupling**. b |** The apparent rate of ethanol dehydration. **c |** The ratio of coupling through Guerbet *versus* Lebedev mechanisms. Conditions: 350°C, 7.8 kPa EtOH, 0.3-3.0 kPa water, balance argon (101.3 kPa total), 75-250 s kg_{HAP} mol_{EtOH}^{-1}.

6.3.3 Kinetic model description

The kinetic model described here is intended to describe the three main reactions occurring in alcohol conversion: dehydration (to mono-enes), Guerbet coupling (to alcohols, alkenols, and aldehydes), and IC (to dienes, trienes, and aromatics). A set of possible reactions based on previous

literature is proposed in Table S6.1. These serve as a guide for the generation of rate expressions. Dehydration is modeled assuming a first-order rate expression in which the reaction occurs on an acidic site of type A. The rate-limiting step is the C-O scission of an adsorbed alcohol. A rate expression can then be derived according to Equation 6.3 assuming that bound alcohols are in equilibrium with the gas phase. Here $k_{D,i}$ is the dehydration rate constant for alcohol i, $K_{ads,A,i_{alcohol}}$ is its adsorption constant to an acidic site, and $P_{i_{alcohol}}$ is its partial pressure. The most abundant surface intermediates are assumed to be alcohols and water, thus the summation $\sum K_{ads,A,j}P_j$ includes these species only.

Equation 6.3 $$r_{dehyd,i} = k_{D,i}K_{ads,A,i_{alcohol}}P_{i_{alcohol}}\left(\frac{1}{1+\sum K_{ads,A,j}P_j}\right)$$

The rate-limiting step for both Guerbet coupling and IC is assumed to be deprotonation of the nucleophile aldehyde. This is followed by coupling with an electrophile aldehyde via aldol condensation Applying the steady-state approximation on the concentration of the deprotonated aldehyde (i.e.$\frac{d\theta_{n_{aldehyde,deprot}}}{dt}\sim 0$) allows for the rate $r_{n@e}$ of a specific condensation event between nucleophile n and electrophile e relative to all other electrophiles e_i to be expressed according to Equation 6.4. Here $k_{dp,n}$ is the rate constant for deprotonation, θ_n is the fractional coverage of basic sites of type B by aldehyde n, θ_e is the same for the electrophile, $k_{n@e}$ is the rate constant of aldol condensation between the nucleophile and electrophile, and the summation $\sum k_{n@e_i}\theta_{e_i}$ is taken over all aldehydes e_i.

Equation 6.4 $$r_{n@e} = k_{dp,n}\theta_n\frac{k_{n@e}\theta_e}{\sum k_{n@e_i}\theta_{e_i}}$$

This rate expression ensures that the commonly-observed first order dependence of EtOH coupling on AcAl concentration is preserved. Since aldehydes are not observed at easily quantifiable levels, it is convenient to relate aldehyde surface coverages to the gas-phase pressures

of their respective alcohols. As discussed prior, the gas phase alcohol-aldehyde ratio is fairly constant past 5% conversion thus the two can be assumed to be pseudo-equilibrated. Alcohol condensation can therefore be modeled according to Equation 6.5. Here $k'_{dp,n}$ is an apparent deprotonation rate constant which formally includes a surface reaction rate constant, an aldehyde adsorption constant, and a constant relating the pressures of alcohol n and aldehyde n, $k'_{n@e}$ is the apparent condensation rate constant which formally includes similar constants for the electrophile species, and $\sum K_{ads,B,j}P_j$ is defined similarly for sites of type B as it was for sites of type A.

Equation 6.5 $$r_{n@e} = k'_{dp,n}P_{n_{alcohol}}\left(\frac{k'_{n@e}P_{e_{alcohol}}}{\sum k'_{n@e_i}P_{e_{i_{alcohol}}}}\right)\left(\frac{1}{1+\sum K_{ads,B,j}P_j}\right)$$

This expression formally represents the rate of alkenal formation. Following this, Guerbet coupling products are formed presumably through a series of base-catalyzed H-transfer and possibly isomerization reactions. IC instead results from reactions over different sites which are not inhibited in the same manner as base sites. For simplicity, these are assumed to experience no inhibition outside that of the initial deprotonation. Guerbet coupling and IC can therefore be modeled according to Equation 6.6 and Equation 6.7, respectively, where k'_G is an apparent rate constant leading to Guerbet coupling products and k'_{IC} is an apparent rate constant leading to IC products.

Equation 6.6 $$r_{n@e,GC} = k'_{dp,n}P_{n_{alcohol}}\left(\frac{k'_{n@e}P_{e_{alcohol}}}{\sum k'_{n@e_i}P_{e_{i_{alcohol}}}}\right)\left(\frac{1}{1+\sum K_{ads,B,j}P_j}\right)\left(\frac{k'_G\frac{1}{1+\sum K_{ads,B,j}P_j}}{k'_G\frac{1}{1+\sum K_{ads,B,j}P_j}+k'_{IC}}\right)$$

Equation 6.7 $$r_{n@e,IC} = k'_{dp,n}P_{n_{alcohol}}\left(\frac{k'_{n@e}P_{e_{alcohol}}}{\sum k'_{n@e_i}P_{e_{i_{alcohol}}}}\right)\left(\frac{1}{1+\sum K_{ads,B,j}P_j}\right)\left(\frac{k'_{IC}}{k'_G\frac{1}{1+\sum K_{ads,B,j}P_j}+k'_{IC}}\right)$$

All mono-enes are grouped by carbon number for simplicity. Alcohols, aldehydes, and alkenols are grouped by skeletal structure and will be henceforth discussed together as “alcohols”

unless stated otherwise. IC products will refer to all IC species or only dienes depending on the purpose of the modeling.

These rate expressions were evaluated for a set of 185 distinct alcohols undergoing 231 possible coupling reactions (462 in total for both Guerbet coupling and IC) allowing for all possible alcohols up to C_{14} to be formed as well a few up to C_{16}. Alcohols with branching at the α-carbon were allowed to act as electrophiles but not as nucleophiles, a notion previously discussed in Section 3.9. Differential material balances were automatically generated using an Excel file and MATLAB script for each species i as a function of contact time according to Equation 6.8. Here $\nu_{i,k}$ is the stoichiometric coefficient for species i in reaction k and the summation is taken over all 647 reactions explicitly modeled. τ is the contact time of the entire gas rather than EtOH only.

Equation 6.8
$$\frac{dP_i}{d\tau} = P \sum_k \nu_{i,k} r_k$$

These differential equations were solved in MATLAB using an ODE solver (ode23t) with inlet pressures and contact times provided as inputs. Specified kinetic constants were then fit to the experimental outlet pressures of specified products using a non-linear fitting algorithm (nlinfit). Initial guesses for these parameters were based on approximations from experimental extrapolations and were iteratively adjusted until the guesses and fits converged to two significant figures.

The main dataset used for fitting included 5 contact times from 8.7-87.6 s kg_{cat} mol_{EtOH}^{-1} with a 7.8 kPa EtOH feed, 3 other partial pressures of EtOH from 2-15 kPa at 35.0 s kg_{cat} mol_{EtOH}^{-1}, and 6 water cofeeds from 0.3-3.0 kPa with 7.8 kPa EtOH at contact times between 70 and 250 s kg_{cat} mol_{EtOH}^{-1}. EtOH conversion ranged from 3 to 12% for this dataset. First, outlet butanol pressures were fit by adjusting $k'_{dp,EtOH}$, $K_{ads,B,EtOH}$, and $K_{ads,B,water}$. All alcohols were assumed to possess the same adsorption, deprotonation, and coupling rate constants. This fitting was

initially performed in the absence of any side-reactions. The resulting fitted values were then fixed. Second, ethylene pressures were fit by adjusting $k'_{dehyd,EtOH}$, $K_{ads,A,EtOH}$, and $K_{ads,A,water}$. Third, the Guerbet coupling constant k'_G was fit to 1,3-butadiene pressures with k'_{IC} empirically fixed to 1. Butadiene was fit at this stage to ensure that the functional form of the IC rate expression was consistent with the data. Fourth, the dehydration constants for butanol were obtained from butanol feed data (collected from 5-15% conversion at various pressures ranging from 1.0-15.0 kPa). All higher alcohols were assumed to dehydrate with these kinetics. Fifth, all constants were refit in this order until full convergence was achieved for all parameters. The fits obtained at this stage are discussed below. The k'_G constant was then refit to account for all IC products. Since the specific identities of these species could not be fully determined, this parameter was fit against alcohol selectivities observed with a 7.8 kPa EtOH feed examined between 5 and 20% conversion.

6.3.4 Ethanol oligomerization modeling results: impacts of water on rates and selectivities

The parameters obtained initially for a model wherein dienes are the only IC products are provided in Table 6.1. Parity plots in Figure 6.7 show strong agreement between model-predicted and experimentally-observed pressures for the three species used in fitting (butanols, ethylene, and 1,3-butadiene). The competitive adsorption of water described by the model can therefore explain inhibition behavior. The parameters suggest that water binds to *B* sites with an adsorption constant approximately 15 times that of EtOH. These constants also suggest that water occupies more coupling sites than EtOH above 12% conversion and covers approximately 80% of the sites by 50% conversion, leaving less than 10% vacant (Figure S6.2). The adsorption constants for *A* sites are found to be lower than those for *B* sites. The lesser inhibition of dehydration sites compared to coupling sites therefore explains the increase in ethylene selectivity observed with increasing conversion. The same is true for butadiene formation; the increased propensity to produce IC

versus Guerbet products at higher conversions can be attributed to an inhibition of the Guerbet pathway without substantial inhibition of the IC pathway.

Table 6.1 | **Model parameters obtain from data fitting.** Uncertainties reflect the 95% confidence intervals on the fits.

Parameter	Model Value
k'_{dp} (mmol kg_{cat}^{-1} s^{-1} kPa^{-1})	0.350 +/- 0.062
$K_{ads,B,EtOH}$ (kPa^{-1})	0.286 +/- 0.022
$K_{ads,B,water}$ (kPa^{-1})	4.50 +/- 1.15
$k'_{dehyd,EtOH}$(mmol kg_{cat}^{-1} s^{-1} kPa^{-1})	0.00390 +/- 0.00159
$k'_{dehyd,ButOH}$(mmol kg_{cat}^{-1} s^{-1} kPa^{-1})	0.0101 +/- 0.0008
$K_{ads,A,EtOH}$ (kPa^{-1})	0.0490 +/- 0.0753
$K_{ads,A,ButOH}$ (kPa^{-1})	0.199 +/- 0.024
$K_{ads,A,water}$ (kPa^{-1})	0.314 +/- 0.186
k'_G (a.u.)	161 +/- 17

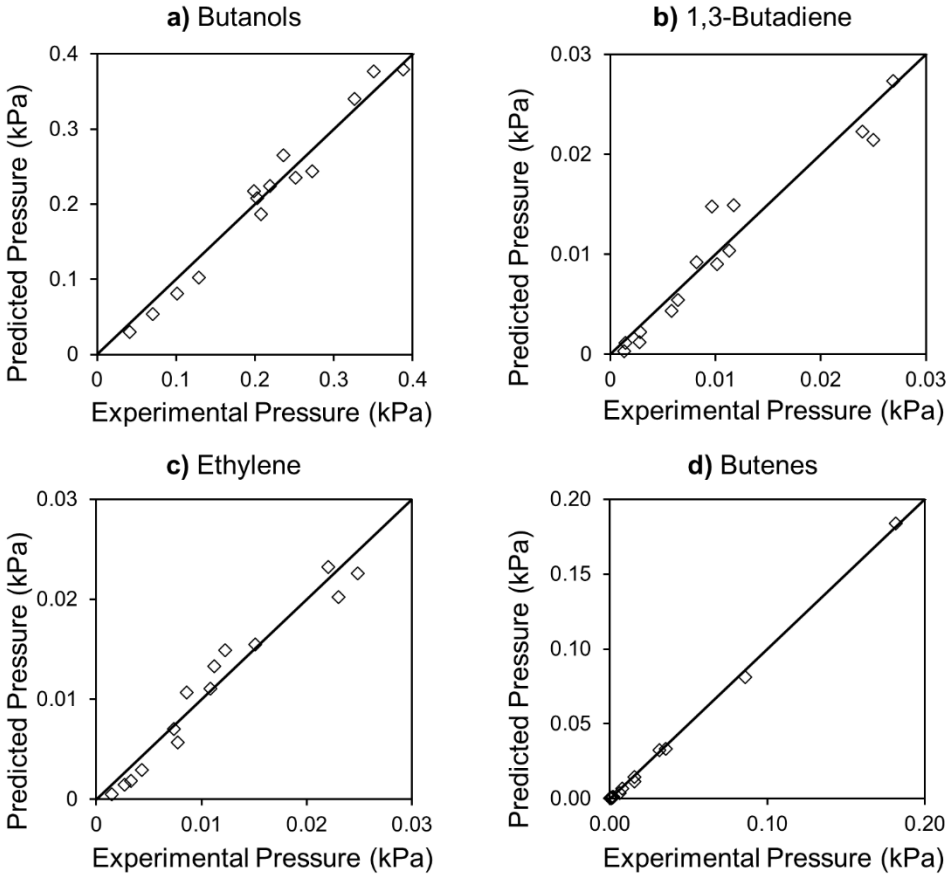

Figure 6.7 | **Parity plots comparing experimental and model-predicted pressures.** Model parameters provided in Table 6.1. Parity plots shown for the pressures of **a** | butanols, **b** | 1,3-butadiene, **c** | ethylene, and **d** | butenes.

In order to predict higher conversion behavior, the k'_G parameter was adjusted to fit the alcohol selectivites observed between 5 and 20% conversion. Error minimization was achieved with k'_G=48.3. This model was then used to predict the behavior observed at higher contact times up to the 2102 s kg_{cat} mol_{EtOH}^{-1} (the highest obtained experimentally) as shown in Figure 6.8. Here the experimental "effective" conversion and selectivities are reported as defined previously. The model accurately predicts conversion and alcohol selectivity at these conditions (Figure 6.8a), which required contact times 8x the highest used to generate the model. The inhibition behavior therefore can be used to reliably extrapolate low-conversion data to higher conversions where the chemistry can be used to produce C_{6+} alcohols. The full C_4-C_8 alcohol distribution is also accurately predicted at elevated conversions (Figure 6.8b). Given that the model assumes all deprotonation and coupling rate constants are equal, step-growth kinetics reliably describe the chemistry even in the presence of side-reactions. The main distinction between this model and true step-growth is the fact that α-branched alcohols are not allowed here to serve as nucleophiles. Slight reactivity differences may also be present, but they do not have a large impact on the product distributions examined here. Altogether, the strong agreement between model and experiment suggest that the model is a useful tool for predicting EtOH oligomerization behavior.

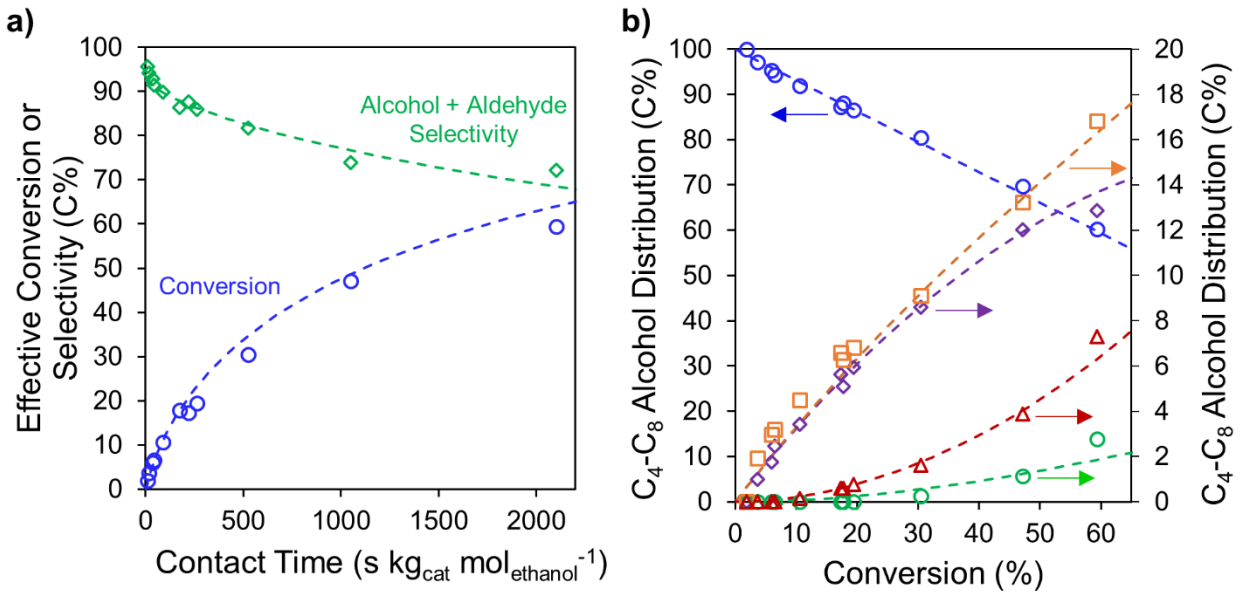

Figure 6.8 | **Comparison of experimental ethanol oligomerization with model predictions.** Experimental data shown as points, model data shown as dashed lines. **a** | Effective conversion (○) and alcohol + aldehyde selectivity (◇) as a function of contact time. **b** | Distribution of alcohols, alkenols, and aldehydes lumped together as "alcohols" according to skeletal structure: (○) butanols, (◇) hexanols, (○) octanols, (□) 2-ethyl-1-butanols, (△) 2-ethyl-1-hexanols. Experimental data collected at 350°C with 7.8 kPa ethanol in argon (101 kPa total).

6.3.5 Ethanol oligomerization model predictions: requirements to produce distillate-range alcohols

As noted in Chapter 5, EtOH conversions above 87% should yield distillate-range alcohols (average carbon number above C_{10}) if EtOH is solely converted through step-growth oligomerization. While our results will show that higher conversions are in fact required, this serves as a useful benchmark for discussion. Figure 6.9a predicts that a contact time of ~6,500 s kg_{cat}^{-1} mol_{EtOH}^{-1} is required to reach 87% conversion. For perspective, the average fermentation plant in the US (~80 MMgal EtOH $year^{-1}$) would therefore require nearly 1,430 metric tons of

catalyst. A methanol-to-olefins plant of a similar size would require only ~6 tons.[14] Development of more active catalysts or those which experience lesser inhibition by water may therefore be key to advancement of this EtOH oligomerization technology. If water-inhibition effects could be eliminated (i.e. no adsorption of water), the catalyst mass requirement would be reduced by 86% to 200 tons. Increasing catalytic activity is therefore still of great importance. Figure 6.9b shows that the alcohol selectivity decreases to only ~50% at 87% conversion. IC species produced at 39% selectivity are the main byproducts. Figure 6.9c shows that the average alcohol carbon number at this conversion is substantially lower than predicted, only about 6.9. As contact time increases, the carbon number reaches 8 around 10,900 s kg_{cat}^{-1} $mol_{ethanol}^{-1}$ (93.9% conversion), 9 around 15,750 s kg_{cat}^{-1} $mol_{ethanol}^{-1}$ (97.0% conversion), and finally 10 around 21,900 s kg_{cat}^{-1} $mol_{ethanol}^{-1}$ (98.6% conversion). At this point the alcohol selectivity is predicted to be only 23.0%. The model therefore suggests that single-pass ethanol oligomerization over HAP cannot be used at these conditions to selectively produce distillate-range alcohols. The byproduct hydrocarbons may still be useful for lighter fuels after hydrogenation, however. Co-production of gasoline hydrocarbons and distillate alcohols may be possible. Figure 6.9c shows that alcohol linearity (i.e. the mole fraction of alcohols which are linear rather than branched) decreases with conversion to 59% at 87% conversion. At

the alcohol carbon number targets of 8, 9, and 10, the alcohol linearities are 45.9%, 34.7%, and 24.3%, respectively.

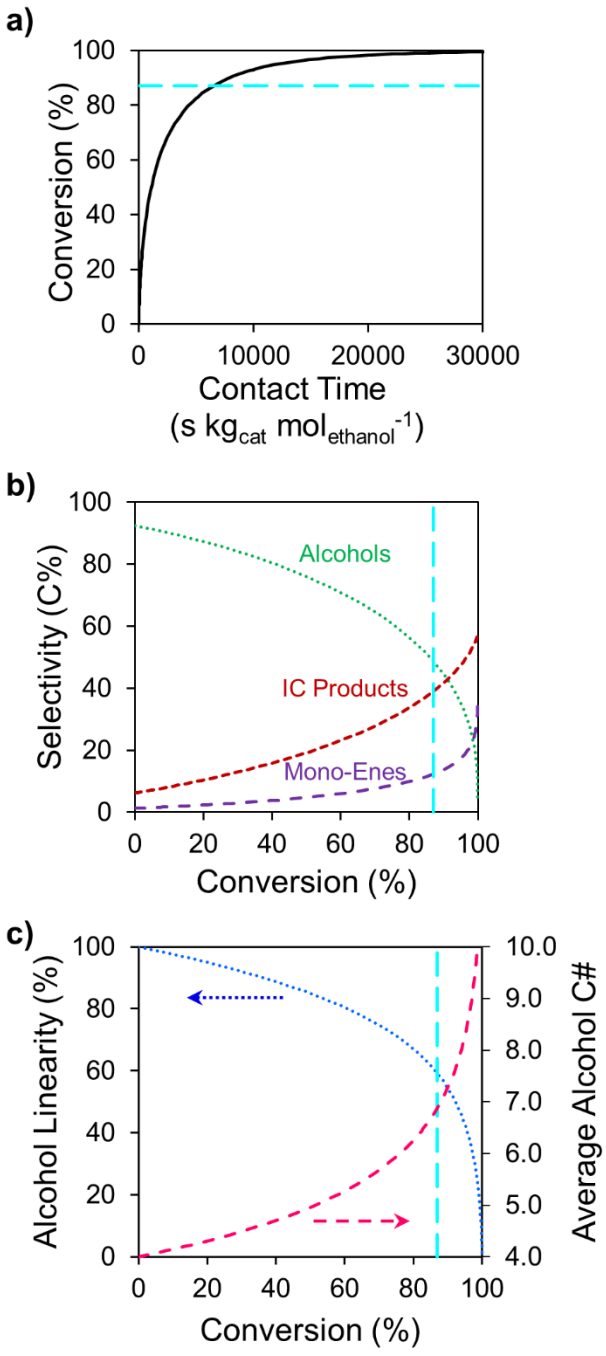

Figure 6.9 | **Model predictions for ethanol oligomerization over HAP.** The dashed teal line is at 85% conversion, the original distillate-range target. **a |** Ethanol conversion as a function of contact time. **b |** Selectivities to alcohols, mono-enes, and IC (interrupted coupling) products *versus* conversion. **c |** Alcohol linearity and average alcohol carbon number *versus* conversion.

The difficulty in producing heavy distillate-range alcohols is rooted in three phenomena: consumption of alcohols by side reactions, competitive adsorption by water, and the combination of step-growth kinetics and low branched-alcohol reactivity. Side reactions lead to lower alcohol pressures and in turn lower coupling rates. If side reactions are removed from the model, C_{10+} alcohol averages can be achieved past 11,900 s kg_{cat}^{-1} $mol_{ethanol}^{-1}$ (99.3% conversion), a 46% contact time decrease *versus* when they are present. Competitive adsorption of water instead limits rates by decreasing the surface concentrations of reactive intermediates without affecting gas-phase concentrations. If side reactions are kept in the model but competitive adsorption by water is removed, the minimum contact time required to achieve C_{10+} averages is only 1,340 s kg_{cat}^{-1} $mol_{ethanol}^{-1}$ (99.6% conversion), a 94% contact time reduction *versus* the original model. Removing inhibition also improves alcohol selectivity and therefore complicates a direct comparison of these two scenarios, but the results nonetheless suggest that inhibition plays a larger role in limiting the production of heavy alcohols than side reactions do. In both cases, the alcohol linearity is 29%. The third limitation regarding oligomerization kinetics is more complex. Since α-branched alcohols cannot couple in a nucleophilic role, their production slows overall coupling rates and leads to self-limiting condensation. These alcohols (e.g. 2-ethyl-1-butanol and 2-ethyl-1-hexanol) are produced when C_{4+} linear alcohols couple in the nucleophile role. In the step-growth model, substantial formation of these alcohols is unavoidable. The implications of deviating from step-growth can be understood using the kinetic model.

Limiting the formation of branched alcohols may be a strategy to improve ethanol oligomerization into the distillate range. Various catalysts (particularly Mg_xAlO_y systems containing transition metals) in the literature preferentially form linear alcohols,[15-17] but this notion has not received substantial attention. As shown in Equation 9, this preference can be defined

according to the rate expressions proposed here by dividing the rate of coupling between an ethanol nucleophile and a C_{4+} electrophile and the rate of coupling between a C_{4+} nucleophile and an ethanol electrophile. Two parameters can be defined which control this preference: the apparent nucleophilicity of ethanol relative to higher alcohols ($\eta = \frac{k'_{dp,Et}}{k'_{dp,C4+}}$) and the apparent electrophilicity of ethanol relative to higher alcohols ($\varepsilon = \frac{k'_{C4+@Et}}{k'_{Et@C4+}}$). This equation suggests that catalysts can promote linear alcohol formation if they provide either higher η or lower ε.

Equation 9 $$\frac{r_{linear}}{r_{branched}} = \frac{r_{Et@C4+}}{r_{C4+@Et}} = \frac{k'_{dp,Et}}{k'_{dp,C4+}} * \frac{k'_{Et@C4+}}{k'_{C4+@Et}} = \eta * \frac{1}{\varepsilon}$$

Figure 6.10a,b shows the effect of changing η on alcohol linearity and carbon number as a function of conversion when inhibition and side-reactions are removed from the model to avoid secondary effects. While increasing η increases alcohol linearity (Figure 6.10a), it does not help to produce higher alcohols. Figure 6.10b clearly shows that higher η will in fact lower the average alcohol carbon number in the products. This is because increasing η promotes butanol formation but not its consumption, which leads to product mixtures rich in butanol even at high conversions. While higher alcohols can be produced through cross-coupling of an ethanol nucleophile and higher alcohol electrophiles, ethanol will be the dominant electrophile present at most conversions if all alcohols have the same effective electrophilicities as assumed in this model ($k_{n@e}$=1).

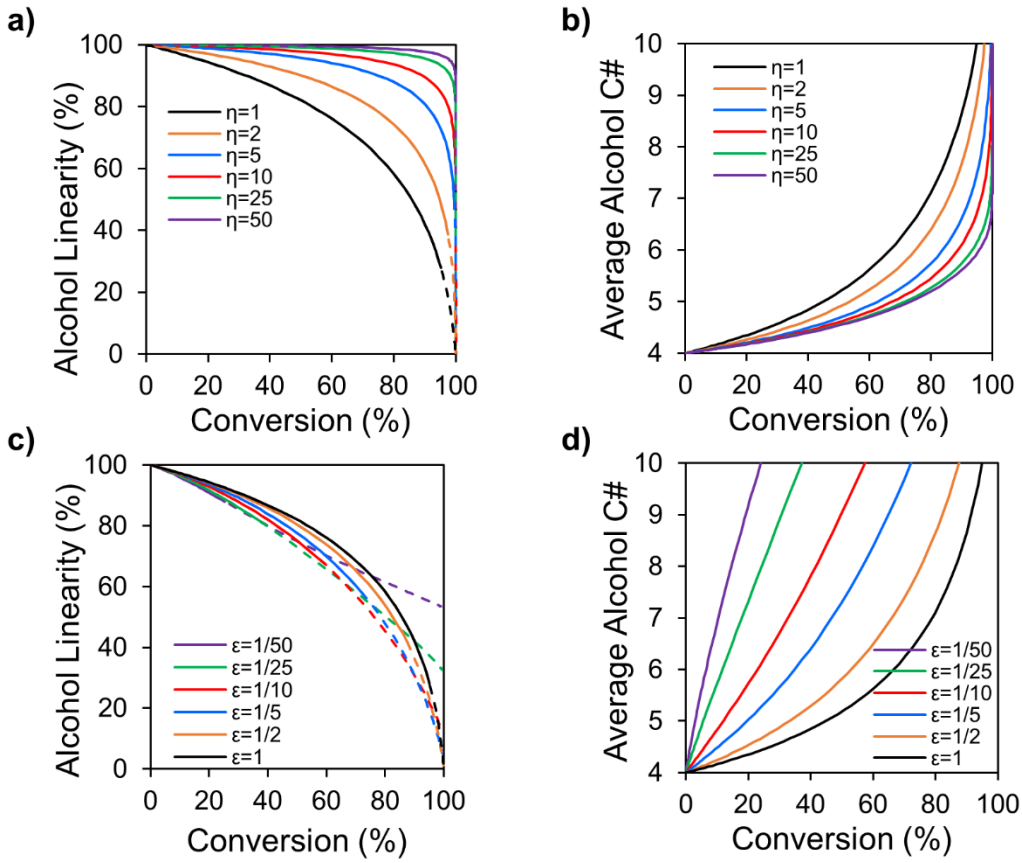

Figure 6.10 | **The impact of adjusting the relative effective nucleophilicity (η) or the relative effective electrophilicity (ε) of ethanol on alcohol distributions as a function of conversion.** a) Alcohol linearity at different η. b) Average product alcohol carbon number at different η. c) Alcohol linearity at different ε. d) Average product alcohol carbon number at different ε. The dashed lines on the linearity plots represent distributions where the average carbon number is greater than 10.

Decreasing ε has less of an impact on alcohol linearity (Figure 6.10c), though the actual trends are unclear. Linearity generally decreases from ε=1 to 1/10 before increasing at lower ε. On the other hand, the average carbon number increases strongly with decreasing ε such that ε=1/10 enables C_{10+} alcohol distributions to be achieved at as low as 60% conversion. The aberrant trends in the linearity plot are likely related to the heavy distributions producible at low conversions in concert with limitations from the model. The dashed lines represent distributions with above C_{10} averages where artificial limitations may manifest. These limitations appear since the alcohols modeled extend up to C_{20}, thus the alcohol distributions will be improperly truncated when

substantial amounts of C_{20} alcohols are anticipated. It is clear, however, that η and ε affect the alcohol distribution differently. Linear alcohols can be increased by increasing η while heavy alcohols can be best produced by decreasing ε. Understanding this difference is critical to catalyst development. For example, two catalysts may produce 1-hexanol and 2-ethyl-1-butanol at a 5:1 ratio at low conversions, but one may do so because η=5, ε=1 while the other may do so because η=1, ε=1/5. Depending on the goal of the ethanol oligomerization (i.e. producing linear alcohols or heavy alcohols), one of the two will likely be a more promising catalyst to study further. Combing these two changes (η=5, ε=1/5) allows for improvements in both linearity and carbon number, though a slight degree of offset is present. It is unclear how these parameters can be manipulated, though the systems studied by Jordison et al.[15] and Sun et al.[16] both appear to be more consistent with ε shifts based on the C_4:C_6 ratios observed.

Figure 6.11 additionally shows model predictions for the conversion of aqueous ethanol feeds. Enabling the use of sub-azeotropic ethanol feeds may be important to the economics of ethanol oligomerization. This may be particularly important if operating at low single-pass conversions which would necessitate that ethanol be separated from the product stream and recycled into the reactor. Figure 6.11a shows how added water decreases the alcohol selectivity for scenarios in which 10, 25, or 50% is the target conversion. Using feeds near the azeotrope at 5 wt% water decreases the alcohol selectivity at these conversions from 90, 86, and 77% to 81, 77, and 67%, respectively. Figure 6.11b shows the catalyst scale-up required to obtain these target conversions as more water is introduced into the feed. The amount of catalyst required to achieve these conversions with 5 wt% water in the feed increases by 120%, 85%, and 57%, respectively. The addition of water is therefore clearly detrimental to ethanol oligomerization. Stronger impacts

can be seen when operating with low-conversion targets because byproduct water is already produced in substantial amounts at elevated conversions.

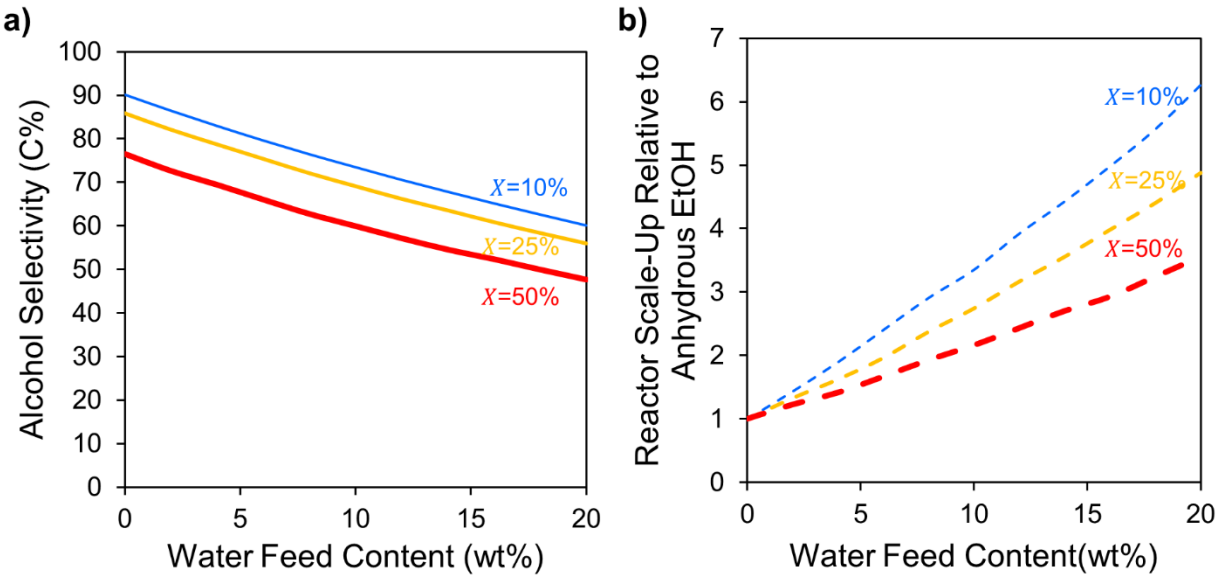

Figure 6.11. Model predictions for the conversion over aqueous ethanol over HAP. a) Alcohol selectivities predicted at 10, 25, and 50% conversion. b) Required scaling factors relative to anhydrous ethanol feeds to achieve 10, 25, and 50% conversion.

6.3.6 Higher alcohol conversion: oligomerization of single-components and ethanol co-feeds

Since this chemistry shows clear limitations in direct EtOH oligomerization to the distillate range, adding separations and recycles after the oligomerization reactor may be helpful in improving process economics. The conversion of higher alcohols was therefore examined either as single components or as co-feeds with EtOH. The alcohols studied included 1-butanol, 1-hexanol, and 2-ethyl-1-butanol.

Figure 6.12 shows the impact of increasing feed alcohol pressure on dehydration rate, coupling rate, and dehydrogenation rate for all alcohols. Langmuirian behavior is observed in all cases. Figure 6.12a shows that all alcohols dehydrate with similar rates. As noted prior in Table 6.1, however, butanol has a higher apparent dehydration rate constant. The rate is similar only because this rate constant if compensated by the stronger adsorption of butanol. Figure 6.12b

suggests that 1-butanol and 1-hexanol couple at similar rates much lower than EtOH. Model fits give lower apparent rate constants for coupling of these alcohols, inconsistent with findings of the EtOH oligomerization model. Ethylbutanol did not show any coupling activity. The dehydrogenation rate trends shown in Figure 6.12c may provide some insight into differences observed in linear alcohol coupling rates. AcAl production rates decline with increasing conversion, while butyraldehyde and hexanal increase before leveling out. Faster EtOH dehydrogenation rates would lead to coupling beginning at lower conversions, making EtOH coupling appear to be faster. Without deconvoluting dehydrogenation and coupling in the model, however, it is unclear what is responsible. Future studies may examine this in further detail.

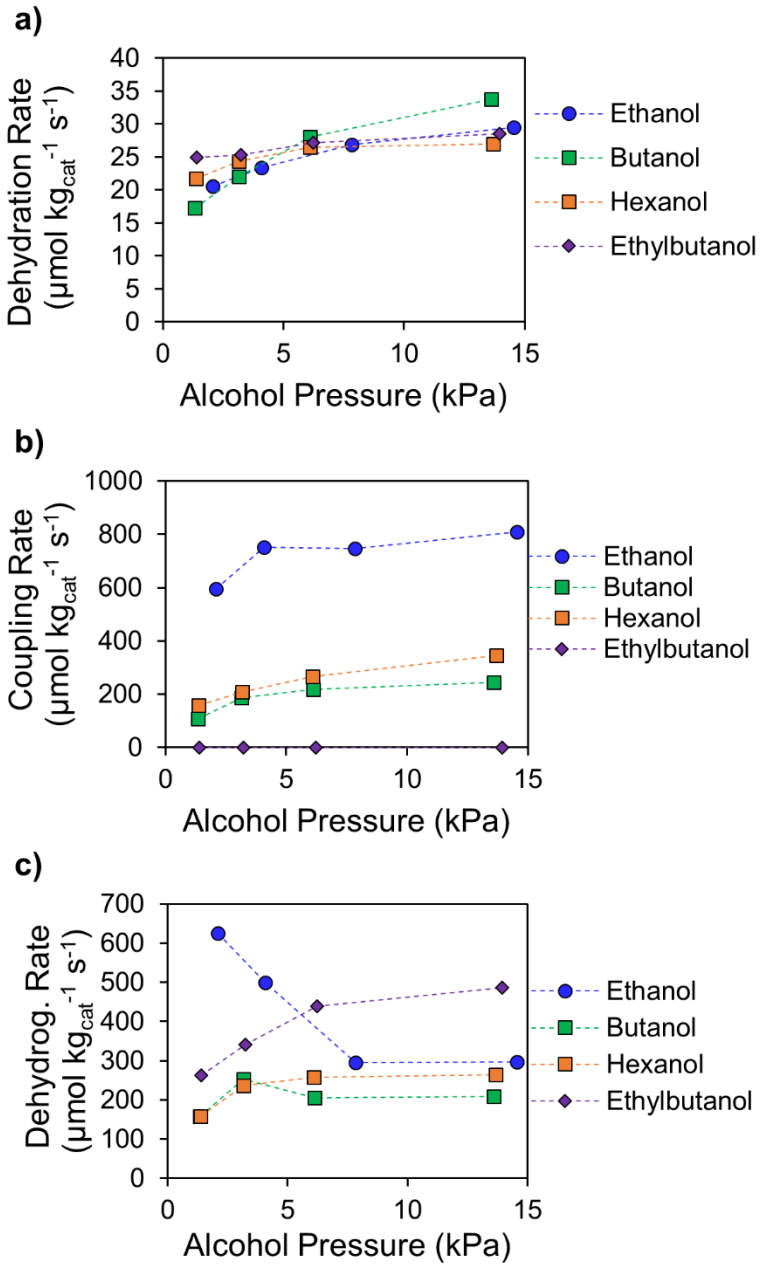

Figure 6.12 | **Coupling of single-alcohol feeds at varying partial pressures. a** | Dehydration rate based on C_n mono-ene production rates. **b** | Coupling rate based on C_{2n} alcohol/aldehyde production rates. **c** | Dehydrogenation rates based on C_n aldehyde production rates. n=carbon number of alcohol fed.

Co-feeding these alcohols with EtOH showed additional unexpected behavior. Adding 1-butanol to an EtOH feed linearly increased the production of 1-hexanol, 2-ethyl-1-butanol, and 2-ethyl-1-hexanol (Figure 6.13a). The hexanol rate increases more than the ethylbutanol rate,

suggesting that added butanol preferentially acts as an electrophile rather than as a nucleophile. Similarly, adding hexanol improves the rate of octanol formation more than ethylhexanol formation (Figure 6.13b). Adding 2-ethyl-1-butanol increases the formation of only one species which could not be positively identified via GC MS. Cross-coupling with an EtOH-derived nucleophile would produce 4-ethyl-1-hexanol while coupling with an EtOH-derived electrophile would produce 2,2-diethyl-1-butanol. This species elutes in the GC between 2-ethyl-1-hexanol and 1-octanol and is therefore more likely the former. This is also consistent with the notion that 2-ethyl-1-butanol cannot appreciably serve in a nucleophilic role. The promotion of linear alcohols *versus* branched alcohols is inconsistent with the EtOH oligomerization model since it suggests that either higher alcohols are poor nucleophiles or that they are good electrophiles (relative to EtOH). While some part of this may be related to the transient regime in the catalyst bed before alcohol-aldehyde pseudo-equilibrium is established, it may also imply that there exists an alternative coupling mechanism which involves direct coupling between an alcohol and an aldehyde. In prior literature such mechanisms have been mentioned with varying degrees of support. Moteki and Flaherty suggested that aldol condensation routes fully explain the behavior[2], while Ho et al. noted that alcohol-aldehyde coupling cannot be fully dismissed.[1] Meunier and coworkers alternatively concluded that aldol condensation is not relevant to EtOH coupling, proposing that either alcohol-alcohol or alcohol-aldehyde coupling is actually the dominant coupling mechanism.[7,8] If the alcohol serves in an electrophilic role in aldehyde-alcohol coupling, a slowly-dehydrogenating alcohol may serve primarily in this role when cofed with EtOH. Such behavior cannot be accounted for in the present model. Nonetheless, it may have important implications on performing EtOH oligomerization with the addition of separation/recycle loops. If co-feeding higher alcohols with EtOH promotes the formation of linear alcohols, distillate-range

alcohol production may be more feasible. Modeling this behavior would require a more fundamental understanding of the low-conversion transient regime which remains poorly understood.

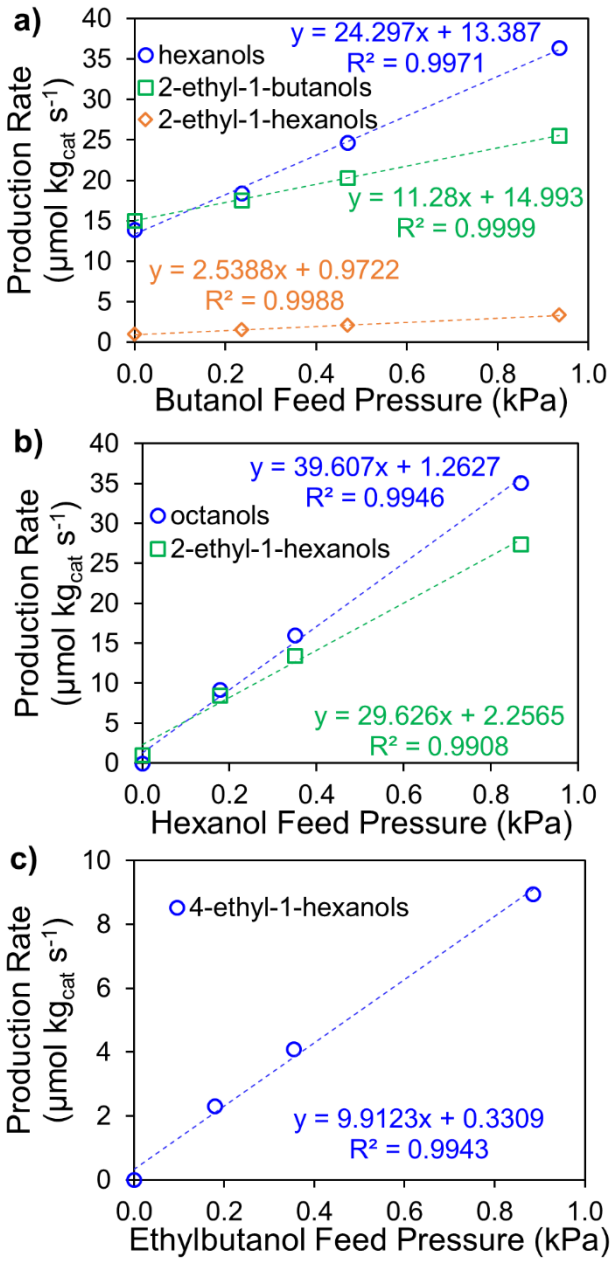

Figure 6.13 | **Impact of higher alcohol co-feeds with ethanol on cross-coupling rates. a** | Rates of 1-hexanol, 2-ethyl-1-butanol, and 2-ethyl-1-hexanol as a function of 1-butanol feed pressure. **b** | Rates of 1-octanol and 2-ethyl-1-hexanol as a function of 1-hexanol feed pressure. **c** | Rate of 4-ethyl-1-hexanol formation as a function of 2-ethyl-1-butanol feed pressure. Ethanol feed pressure kept constant at 7.84 kPa with contact time of ~218 s kg_{cat} μmol_{EtOH}^{-1}.

6.4 Conclusions and Future Directions

We have developed a kinetic model based on experimental data over a wide range of contact times which elucidates the causes of changing rates and selectivities observed with increasing ethanol conversions. This model explicitly evaluates rate expressions for alcohol dehydration to mono-enes, alcohol coupling to higher alcohols and aldehydes, and interrupted alcohol coupling to dienes and aromatics. The decrease in alcohol coupling rates observed with increasing conversion can be attributed to competitive adsorption with water. This inhibiting effect is much less pronounced for dehydration and additionally leads to an increased probability that alcohol coupling interruption occurs as conversion increases. By accounting for these behaviors, it can be shown that modified step-growth kinetics wherein α-branched alcohols cannot serve as nucleophiles describe both the carbon number and branching of alcohols in the products. This allows for the accurate prediction of high-conversion behavior and additionally allows for modeling of aqueous feeds to be performed. These results generally suggest that direct oligomerization of ethanol to distillate-range alcohols over HAP cannot be performed selectively due to the high contact times required. The introduction of higher alcohols into the feed leads to aberrant behavior which cannot be described by this model, likely in part because the model lumps alcohol dehydrogenation into coupling rate constants for simplicity. Future efforts should be aimed at modeling the low-conversion transient regime prior to the establishment of alcohol-aldehyde pseudo-equilibria. This as well as the investigation of distinct alcohol-aldehyde cross-coupling mechanisms may help to explain the preferential action of co-fed alcohols as electrophiles rather than as nucleophiles. Promising new catalysts for ethanol oligomerization into the distillate range would also ideally promote the electrophilic action of higher alcohols over ethanol.

6.5 References

1 Ho, C. R., Shylesh, S. & Bell, A. T. Mechanism and kinetics of ethanol coupling to butanol over hydroxyapatite. *ACS Catal.* **6**, 939-948, (2016).

2 Moteki, T. & Flaherty, D. W. Mechanistic insight to C–C bond formation and predictive models for cascade reactions among alcohols on Ca-and Sr-hydroxyapatites. *ACS Catal.* **6**, 4170-4183, (2016).

3 Hanspal, S., Young, Z. D., Shou, H. & Davis, R. J. Multiproduct steady-state isotopic transient kinetic analysis of the ethanol coupling reaction over hydroxyapatite and magnesia. *ACS Catal.* **5**, 1737-1746, (2015).

4 Hanspal, S., Young, Z. D., Prillaman, J. T. & Davis, R. J. Influence of surface acid and base sites on the Guerbet coupling of ethanol to butanol over metal phosphate catalysts. *J. Catal.* **352**, 182-190, (2017).

5 Tsuchida, T., Kubo, J., Yoshioka, T., Sakuma, S., Takeguchi, T. & Ueda, W. Reaction of ethanol over hydroxyapatite affected by Ca/P ratio of catalyst. *J. Catal.* **259**, 183-189, (2008).

6 Ogo, S., Onda, A., Iwasa, Y., Hara, K., Fukuoka, A. & Yanagisawa, K. 1-Butanol synthesis from ethanol over strontium phosphate hydroxyapatite catalysts with various Sr/P ratios. *J. Catal.* **296**, 24-30, (2012).

7 Scalbert, J., Thibault-Starzyk, F., Jacquot, R., Morvan, D. & Meunier, F. Ethanol condensation to butanol at high temperatures over a basic heterogeneous catalyst: How relevant is acetaldehyde self-aldolization? *J. Catal.* **311**, 28-32, (2014).

8 Meunier, F. C., Scalbert, J. & Thibault-Starzyk, F. Unraveling the mechanism of catalytic reactions through combined kinetic and thermodynamic analyses: application to the condensation of ethanol. *CR Chim.* **18**, 345-350, (2015).

9 Moteki, T., Rowley, A. T. & Flaherty, D. W. Self-terminated cascade reactions that produce methylbenzaldehydes from ethanol. *ACS Catal.* **6**, 7278-7282, (2016).

10 Scanlon, J. T. & Willis, D. E. Calculation of flame ionization detector relative response factors using the effective carbon number concept. *J. Chromatogr. Sci.* **23**, 333-340, (1985).

11 Ogo, S., Onda, A. & Yanagisawa, K. Selective synthesis of 1-butanol from ethanol over strontium phosphate hydroxyapatite catalysts. *Appl. Catal. A-Gen.* **402**, 188-195, (2011).

12 Young, Z. D. & Davis, R. J. Hydrogen transfer reactions relevant to Guerbet coupling of alcohols over hydroxyapatite and magnesium oxide catalysts. *Catal. Sci. Technol.* **8**, 1722-1729, (2018).

13 Yaws, C. L. *Chemical properties handbook*. (McGraw-Hill, 1999).

14 Tian, P., Wei, Y., Ye, M. & Liu, Z. Methanol to Olefins (MTO): from fundamentals to commercialization. *ACS Catal.* **5**, 1922-1938, (2015).

15 Jordison, T. L., Lira, C. T. & Miller, D. J. Condensed-phase ethanol conversion to higher alcohols. *Ind. Eng. Chem. Res.* **54**, 10991-11000, (2015).

16 Sun, Z., Couto Vasconcelos, A. s., Bottari, G., Stuart, M. C., Bonura, G., Cannilla, C., Frusteri, F. & Barta, K. Efficient catalytic conversion of ethanol to 1-butanol via the Guerbet reaction over copper-and nickel-doped porous. *ACS Sustain. Chem. Eng.* **5**, 1738-1746, (2016).

17 Pang, J., Zheng, M., He, L., Li, L., Pan, X., Wang, A., Wang, X. & Zhang, T. Upgrading ethanol to n-butanol over highly dispersed Ni–MgAlO catalysts. *J. Catal.* **344**, 184-193, (2016).

6.6 Supplemental Information

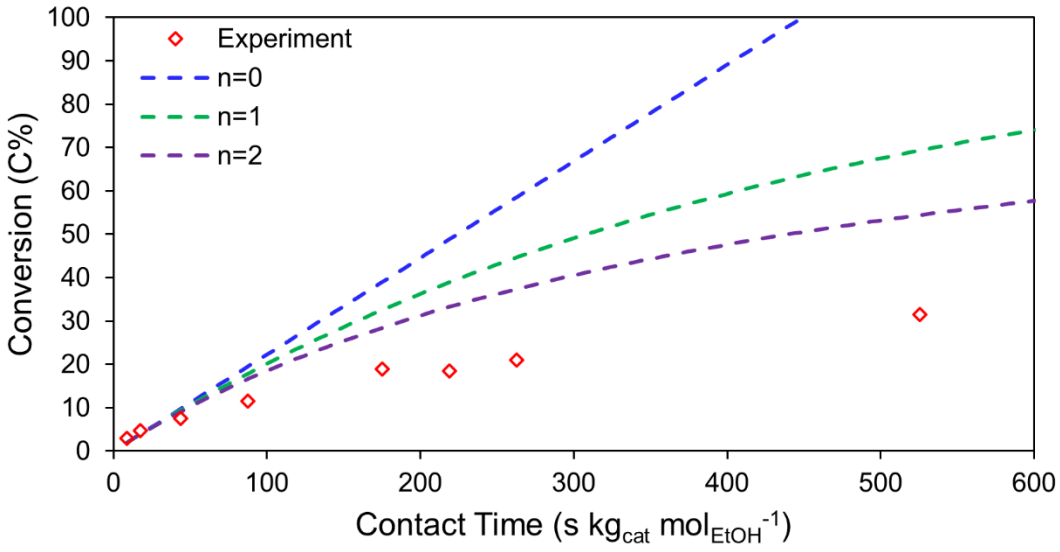

Figure S6.1 | **Conversion *versus* contact time as a function of the overall apparent rate order with respect to ethanol.** Experimental data points shown in diamonds. Dashed lines show approximate conversion expected when extrapolating form 3.0% conversion based on 0^{th}, 1^{st}, or 2^{nd} order rate expressions.

Table S6.1 | **Proposed set of reactions involved in alcohol conversion.** These equations rigorously allow for alcohol to be dehydrated to mono-enes, coupled to alcohols, or condensed to dienes. These reactions involve A sites (acidic), B sites (basic), C sites (H-accepting), and D sites (Lebedev-promoting). C and D sites are not explicitly involved in the generation of the rate expressions used in the model.

	Dehydration reactions	
1	$i_{alcohol} + *_A \longleftrightarrow i_{alcohol}\ *_A$	Alcohol adsorption to acid site (pair)
2	$i_{alcohol}\ *_A \rightarrow H_2O\ *_A + i_{mono-ene}$	Alcohol dehydration (E2 mechanism)
3	$H_2O\ *_A \longleftrightarrow H_2O + *_A$	Water desorption from acid site
	Condensation reactions	
4	$n_{alcohol} + *_B \longleftrightarrow n_{alcohol}\ *_B$	Nucleophile alcohol adsorption to base site
5	$e_{alcohol} + *_B \longleftrightarrow e_{alcohol}\ *_B$	Electrophile alcohol adsorption to base site
6	$n_{alcohol}\ *_B + 2\ *_C \longleftrightarrow n_{aldehyde}\ *_B + 2H\ *_C$	Nucleophile dehydrogenation, surface-mediated
7	$e_{alcohol}\ *_B + 2\ *_C \longleftrightarrow e_{aldehyde}\ *_B + 2H\ *_C$	Electrophile dehydrogenation, surface-mediated
8	$n_{aldehyde}\ *_B \longleftrightarrow n_{aldehyde} + *_B$	Nucleophile aldehyde desorption from base site
9	$e_{aldehyde}\ *_B \longleftrightarrow e_{aldehyde} + *_B$	Electrophile aldehyde desorption from base site
10	$n_{aldehyde}\ *_B \rightarrow n_{aldehyde,deprot}\ *_B$	Nucleophile deprotonation (rate-limiting)
11	$n_{aldehyde,deprot}\ *_B + e_{aldehyde}\ *_B \rightarrow ne_{alkenal}\ *_B + H_2O\ *_B$	Aldol condensation
13	$ne_{alkenal}\ *_B + i_{alcohol}\ *_B \longleftrightarrow ne_{alkenol}\ *_B + i_{aldehyde}\ *_B$	Alkenal C=O hydrogenation, MPV
14	$ne_{alkenol}\ *_B + 2\ *_C \rightarrow ne_{alcohol}\ *_B + 2H\ *_C$	Alkenol C=C hydrogenation, surface mediated
15	$ne_{alcohol}\ *_B \longleftrightarrow ne_{alcohol} + *_B$	Product alcohol desorption from base site
16	$H_2O\ *_B \longleftrightarrow H_2O + *_B$	Water desorption from base site
17	$ne_{alkenol}\ *_B \longleftrightarrow ne_{alkenol} + *_B$	Alkenol desorption from base site
18	$ne_{alkenol} + *_A \longleftrightarrow ne_{alkenol}\ *_A$	Alkenol adsorption to acid site
19	$ne_{alkenol}\ *_A \rightarrow H_2O\ *_A + ne_{diene}$	Alkenol dehydration (E2)
20	$2H\ *_C \longleftrightarrow H_2\ **_C$	H-H recombination
21	$H_2\ **_C \longleftrightarrow H_2 + 2\ *_C$	H_2 desorption

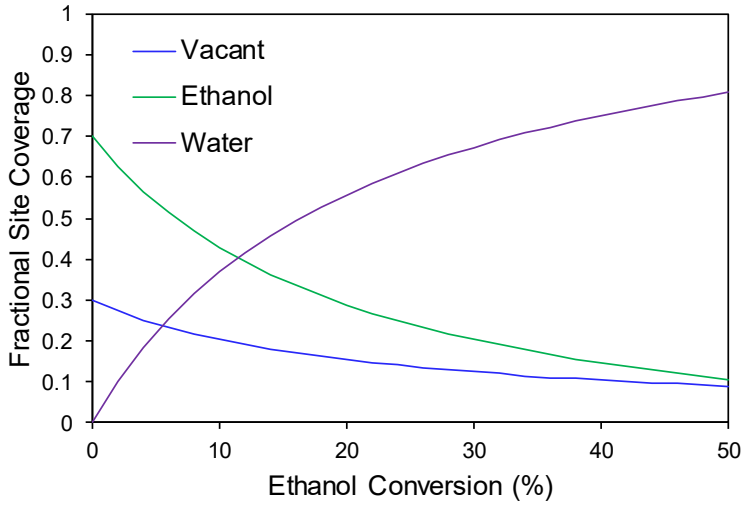

Figure S6.2 | **Fractional occupation of coupling sites by ethanol and water.** Coverages based on the adsorption constants provided in Table 6.1.

Chapter 7. Conclusions and Future Directions

7.1 Summary of dissertation contents

In this dissertation, two different biomass-to-distillate fuel platforms were analyzed: the sugar-mediated mono-oxygenate platform and the ethanol platform. In Chapter 2, the performance of a low-cost Co/TiO_2 catalyst for sorbitol hydrodeoxygenation to monofunctional oxygenates was discussed.[1] This catalyst enabled production of these species at up to 56 C% yield, higher than those achieved with costly noble-metal catalysts. FT-ICR-MS also provided possible evidence of oligomer formation which had not previously been documented. Irreversible deactivation of the catalyst is still prevalent, however, and higher yields are likely required for such a process to be economical. Chapter 3 discusses the possibility of using EtOH as a platform molecule for distillate fuel synthesis, critically assessing how different chemistries can be combined in new ways to achieve this goal.[2] The findings described here are intended to help direct future research in rational directions to continue advancing ethanol-to-distillate conversion to the commercial scale. Chapter 4 details our findings in using Cu-doped AlMgO and AlCaO catalysts prepared via an emulsion-mediated synthesis for ethanol coupling.[3] Our findings provide insights into how the gas phase can be manipulated to promote selective coupling. However, these catalysts are limited by fairly low coupling selectivities (<55%) and inhibition by products which made achieving conversions above 35% on the lab scale challenging. Chapter 5 details the use of calcium hydroxyapatite (HAP) to catalyze ethanol coupling.[4] While higher selectivities can be achieved, coupling rates and selectivities decrease with conversion, limiting selective oligomerization (>80%) to at most 40% conversion. We then showed that bimolecular dehydration can be used to selectively convert the resultant C_4-C_8 alcohol mixtures to high-cetane diesel ethers. A process was devised which can produce these ethers in addition to jet-range paraffins at overall yields above 80%. Chapter 6

discusses a kinetic model which describes ethanol oligomerization over HAP, clarifying the origins of the limitations observed in the prior chapter. Inhibition by water is responsible for the decline in both conversion rates and alcohol selectivities. In the absence of this inhibition, however, the underlying step-growth kinetics in addition to the low reactivity of branched alcohols in coupling reactions leads to carbon number limitations preventing distillate-range alcohol production even at extreme contact times. The model additionally shows that distillate-range alcohols could be most effectively produced using catalysts which depress the electrophilic activity of ethanol relative to higher alcohols.

7.2 The sorbitol platform: recommendations for future research

Future research focused on advancing the sorbitol platform is three-fold: understanding the initial deoxygenation reactions involved in sorbitol conversion, understanding the effect of di-functional species in the subsequent upgrading to fuels, and understanding the factors controlling deactivation of a SMSI-stabilized catalysts. Carbon efficiency is often more important to economics than catalyst cost, thus achieving high yields should be the first priority for the technology. The major challenge with optimizing mono-functional yields is the vast number of pathways by which sorbitol can be converted. If sorbitol simultaneously undergoes dehydration and retro-aldol condensation, for example, sorbitan and glycerol hydrodeoxygenation must be optimized in tandem, and these have very different deoxygenation requirements. Improving C_4-C_6 mono-oxygenate production therefore requires that sorbitol is pushed down a small number of initial pathways, which then allows for the subsequent deoxygenation steps to be controlled more easily. Balancing subsequent deoxygenation to avoid yielding both di-functional oxygenates and hydrocarbon will still be complex. If the di-functional species can also be upgraded to distillate fuels, however, this hydrodeoxygenation step may be optimized more easily. After monofunctional

yields are improved, an important next goal is to reduce catalyst costs. It is unclear whether deactivation of the Co/TiO_2 catalyst used here occurred before or after the reversal of the SMSI film. Factors such as temperature, H_2 pressure, H_2O pressure, and the presence of certain oxygenate functionalities may be important to maintaining such films. Understanding these phenomena may place constraints on the utilization of SMSI to stabilize base metals for aqueous-phase biomass conversions. The role of the $Co\text{-}TiO_x$ interfacial sites produced via SMSI is also unclear and is worth further investigation.

7.3 The ethanol platform: recommendations for future research

To generally advance the use of ethanol as a distillate fuel platform molecule, more focus should be put into how chemistries can be combined and how separation/recycle loops influence process economics. This would help to better understand the true potentials of different pathways.

Current directions in ethanol-to-distillate conversion mainly rely upon olefin oligomerization technologies, especially for the production of jet fuels. Future work in this area should focus on understanding how product linearity can be manipulated so that both highly-branched jet fuels and minimally-branched diesel fuels can be produced. It is unclear whether these hydrocarbons will provide any operational advantage over conventional fuels, however, thus a better understanding how oxygenates may improve combustion may be important to producing performance-advantaged fuels from biomass. If such advantages exist, bringing the fuels to market may be easier to motivate. The impact of branching on ether cetane and the extent to which C_8 ethers can be blended into diesel fuels are particularly important considerations for furthering the research described in this dissertation. Whether jet fuel can contain oxygen also remains a question. While we have stated that jet fuel must theoretically comprise molecules with C:O ratios of 16:1 or greater, the origins of this metric are unclear.

Implementing fuels derived from ethanol oligomerization will require the development of novel catalytic systems which can promote the formation of linear alcohols. As noted in Chapter 3, catalysts which rely upon transition metals to mediate H-transfers often do promote the formation of linear alcohols. The Cu/AlMgO catalyst we investigated in Chapter 4 did in fact produce C_6 alcohols which were nearly 80% linear. Understanding the aspects which control this linearity are important, as is understanding how to obtain higher alcohol selectivities at lower contact times. This will require a combination of accelerating reaction rates, decreasing inhibition, and decreasing side-reactions to enable operation at higher temperatures where rates are inherently faster. Operating aldol condensation without C=O saturation may also be a viable pathway that should received further attention. These systems may be easier to optimize than Guerbet coupling due to the complexities related to H-transfers in mediating alcohol-aldehyde equilibria.

7.4 Comparisons of the ethanol and sorbitol platforms and new concepts for their integration

Both the ethanol and sorbitol platforms have their merits. Sorbitol is already close to the distillate range with its six carbon atoms and can be produced in the absence of the carbon losses. Hydrodeoxygenation to mono-oxygenates is difficult to perform selectively, however. Fermentative ethanol synthesis on the other hand is necessarily accompanied by carbon losses, but can be converted in subsequent steps with higher selectivities. The extensive commercialization of ethanol production at large volumes is very appealing since it removes several barriers which other biomass-to-distillate processes may face. The ethanol platform generally appears to be more promising for these reasons.

Sorbitol and ethanol may also be converted together. Other work in the Huber group[5] has explored the decomposition of biomass in supercritical methanol over $Cu_xMg_yAlO_z$ materials, reminiscent of those used in ethanol coupling. This process produces higher alcohols by

depolymerizing cellulose, catalyzing retro-aldol condensation, and growing the resultant C_2-C_4 species via methanol incorporation. The final alcohol products do not undergo appreciable deoxygenation and therefore can be isolated. Sorbitol was found to act similarly. While this rigorously requires consumption of methanol, it may overall offer a more selective pathway for converting sorbitol (or other sugar alcohols and sugars) to mono-functionals. The methanol utilized in the process may also be at least partially replaced by ethanol, which can simultaneously undergo oligomerization via Guerbet pathways. Ethanol may not incorporate into the retro-aldol products as effectively as methanol, but it likely shows some activity. The resulting C_{4+} alcohol mixtures could then be valorized by the bimolecular dehydration process proposed here in order to produce diesel ethers. Any secondary alcohols formed from sorbitol conversion are more likely to undergo unimolecular dehydration, but the resulting olefins can be converted via oligomerization to make jet fuels.

7.5 References

1 Eagan, N. M., Chada, J. P., Wittrig, A. M., Buchanan, J. S., Dumesic, J. A. & Huber, G. W. Hydrodeoxygenation of Sorbitol to Monofunctional Fuel Precursors over Co/TiO2. *Joule* **1**, 178-199, (2017).

2 Eagan, N. M., Kumbhalkar, M. D., Buchanan, J. S., Dumesic, J. A. & Huber, G. W. Chemistries and processes for the conversion of ethanol into middle-distillate fuels. *Nature Reviews Chemistry* **3**, 223-249, (2019).

3 Petrolini[†,] D. D., Eagan[†,] N., Ball, M. R., Burt, S. P., Hermans, I., Huber, G. W., Dumesic, J. A. & Martins, L. Ethanol condensation at elevated pressure over copper on AlMgO and AlCaO porous mixed-oxide supports. *Catal. Sci. Technol.* **9**, 2032-2042, (2019).

4 Eagan, N. M., Moore, B. M., McClelland, D. J., Wittrig, A. M., Canales, E., Lanci, M. P. & Huber, G. W. Catalytic synthesis of distillate-range ethers and olefins from ethanol through Guerbet coupling and etherification. *Green Chem.* **21**, 3300-3318, (2019).

5 Galebach, P. H., McClelland, D. J., Eagan, N. M., Wittrig, A. M., Buchanan, J. S., Dumesic, J. A. & Huber, G. W. Production of Alcohols from Cellulose by Supercritical Methanol Depolymerization and Hydrodeoxygenation. *ACS Sustain. Chem. Eng.* **6**, 4330-4344, (2018).